ANALYTICA CHIMICA ACTA

International monthly devoted to all branches of analytical chemistry
Revue mensuelle internationale consacrée à tous les domaines de la chimie analytique
Internationale Monatsschrift fur alle Gebiete der analytischen Chemie

ELSEVIER SCIENTIFIC PUBLISHING COMPANY

AMSTERDAM

Anal. Chim. Acta, Vol. 78, No. 1, 1–240, August 1975

Published monthly

ANALYTICA CHIMICA ACTA

Publication Schedule for 1975

Vol. **74,** No. **1**	January 1975	
Vol. **74,** No. **2**	February 1975	**(completing Vol. 74)**
Vol. **75,** No. **1**	March 1975	
Vol. **75,** No. **2**	April 1975	**(completing Vol. 75)**
Vol. **76,** No. **1**	May 1975	
Vol. **76,** No. **2**	June 1975	**(completing Vol. 76)**
Vol. **77**	July 1975	**(complete in one issue)**
Vol. **78,** No. **1**	August 1975	
Vol. **78,** No. **2**	September 1975	**(completing Vol. 78)**
Vol. **79**	October 1975	**(complete in one issue)**
Vol. **80,** No. **1**	November 1975	
Vol. **80,** No. **2**	December 1975	**(completing Vol. 80)**

Subscription price for 1975 (covering Vols. 74–79): Dfl. 570.000 plus Dfl. 54.00 postage, US$ 265.53 inclusive of postage. Subscribers in the U.S.A. and Canada receive their copies by airmail. Additional charges for airmail to other countries are available on request. For advertising rates apply to the publishers.

Subscriptions should be sent to:
Elsevier Scientific Publishing Company, P.O. Box 211, Amsterdam, The Netherlands.

GENERAL INFORMATION

Languages

Papers will be published in English, French or German.

Detailed information

Authors should consult Vol. 73, p. 435 for detailed instructions. Reprints of this information are obtainable from Dr. Macdonald or from: Elsevier Editorial Services Ltd., Mayfield House, 256 Banbury Road, Oxford (Great Britain).

Submission of papers

Papers should be sent to:

PROF. PHILIP W. WEST,
Coates Chemical Laboratories,
College of Chemistry and Physics,
Louisiana State University,
Baton Rouge 3,
La. 70803 (U.S.A.)

or to:

DR. A. M. G. MACDONALD,
Department of Chemistry,
The University,
P.O. Box 363
Birmingham B15 2TT (Great Britain)

Reprints

Fifty reprints will be supplied free of charge. Additional reprints (minimum 100) can be ordered at quoted prices. They must be ordered on order forms which are sent together with the proofs.

PRINTED IN THE NETHERLANDS

Pharmaceutical applications of Thin-Layer and Paper chromatography

edited by **KAREL MACEK.** *Medical Faculty, Charles University, Prague*

1972, xvi + 744 pages, Dfl. 250.00
ISBN 0-444-40939-4

Chromatography is the most widely used modern procedure in analytical chemistry today. With an increasing awareness of the importance of the applications of paper and thin-layer chromatography in the fields of pharmaceutical research, production and control, it has become necessary to survey the possibilities of these methods with their associated literature, and to present this information in a useful form.
With this in mind, the editor provides an introduction to the techniques, the evaluation, and the applications of paper and thin-layer chromatography. Selected procedures such as the preparation of samples, detection methods, choice of solvent systems and sorbents, and the principles of quantitative analysis, are discussed generally and the book is richly tabulated. An appendix outlines the preparation of more than 150 detection reagents. On the basis of these data, readers with an understanding of the principles of the techniques described can solve any analytical problems they may encounter in drug analysis.

CONTENTS: Introduction. Techniques of paper and thin-layer chromatography. Radioactive compounds. Combination of TLC and PC with other chromatographic techniques. Combination of PC and TLC with some spectroscopic methods. Identification of organic compounds by PC and TLC. Documentation of chromatograms. Laboratory for PC and TLC. The tasks of paper and thin-layer chromatography. Synthetic drugs. Steroids. Cardiac glycosides and their genins. Saponins. Peptide and protein hormones. Alkaloids. Vitamins. Antibiotics. Plant extracts. Auxiliary compounds. Investigation of the fate of drugs. Detection reagents. Author index. Subject index. List of substances chromatographed.

CONTRIBUTORS: V. Betina, J. Davídek, I. M. Hais, K. Hiller, J. Janák, G. Katsui, B. P. Lisboa, M. Luckner, K. Macek, L. Nover, V. Rábek, G. Székely, H. D. Woitke.

Elsevier

BOOK DIVISION, P.O. Box 211
AMSTERDAM - THE NETHERLANDS

181Ea

ANALYTICA CHIMICA ACTA
Vol. 78 (1975)

ANALYTICA CHIMICA ACTA

International monthly devoted to all branches of analytical chemistry
Revue mensuelle internationale consacrée à tous les domaines de la chimie analytique
Internationale Monatsschrift für alle Gebiete der analytischen Chemie

ELSEVIER SCIENTIFIC PUBLISHING COMPANY
AMSTERDAM

Anal. Chim. Acta, Vol. 78, No. 1, 1–240, August 1975

PRINTED IN THE NETHERLANDS

Analytica Chimica Acta, 78 (1975) 1–62

THE DETERMINATION OF NITROGEN-15 BY EMISSION AND MASS SPECTROMETRY IN BIOCHEMICAL ANALYSIS: A REVIEW

R. FIEDLER and G. PROKSCH

I.A.E.A. Laboratory, A-2444 Seibersdorf (Austria)

(Received 16th May 1974)

INTRODUCTION

Tracer methods have become a standard technique in agricultural, biological, chemical and medical research. The quantitative evaluation of results is based on the isotope dilution law which says that in a system in equilibrium, the ratio of tracer to carrier isotope is constant (apart from the "isotope effects" which in the case of nitrogen-15 are considered to be negligible for most purposes).

The tracer is frequently a radioactive isotope and the determination of the ratio of tracer to carrier in a sample from the system requires two independent measurements, i.e. determination of the amount of radioactive elements with suitable detection equipment such as a G.M. counter, liquid scintillation counter, etc., and chemical determination of the amount of carrier element in the system. The ratio of the radioactive to the inactive element is usually referred to as the specific activity.

Nitrogen unfortunately does not have a radioactive isotope of sufficiently long half-life to enable radioactive tracer experiments of reasonable duration to

be performed; the radioactive isotope with the longest half-life, nitrogen-13, has a half-life of only 10 min. To carry out tracer experiments with nitrogen, one must therefore work with the stable enriched isotope nitrogen-15. This has the advantage that the experiments are not limited in time as they are in the case of radioactive tracers; but it has the disadvantage of requiring a more complicated detection method. In nature, nitrogen is a mixture of two stable isotopes, ^{14}N and ^{15}N, with a natural abundance of the latter of 0.366 atom% ± 1.5% relative (see p. 57). Several techniques (see p. 55) make it possible to enrich the nitrogen in ^{15}N. One of the commonest methods is based on isotope exchange between ^{15}NO and $H^{14}NO_3$ in solution, the heavy isotope being enriched in the nitric acid. By recycling, as much as 99.5% ^{15}N can be obtained.

Normally the $^{14}N/^{15}N$ ratio of a system is determined by means of mass spectrometric or emission spectrometric techniques on nitrogen gas generated from the sample. The number of ^{15}N atoms in the total amount of nitrogen atoms in percent is called the atom-% or % abundance. When the ^{15}N % abundance of natural nitrogen, i.e. 0.366%, is subtracted from the ^{15}N % abundance of the sample, the ^{15}N atom-% excess is obtained, and this is analogous to the specific activity of a radioactive system. In contrast to radioactive detection equipment, which assesses the radioactive isotope only, both mass and emission spectrometry determine the $^{14}N/^{15}N$ ratio in one operation.

Principle of detection

The ^{14}N and ^{15}N atoms in the gas are paired to form the nitrogen molecules $^{14}N_2$, $^{14}N^{15}N$ and $^{15}N_2$ which can be written as $^{28}N_2$, $^{29}N_2$ and $^{30}N_2$ (see p. 57).

Both mass and emission spectrometric methods provide output signals which are proportional to the number of the three types of molecules. In any nitrogen gas mixture, the ^{15}N % abundance can be derived from the formula

$$\frac{^{30}N+\frac{1}{2}\,^{29}N}{(^{28}N+^{29}N+^{30}N)} \times 100$$

which represents the ratio of the nitrogen-15 atoms to the total number of nitrogen atoms expressed in %. When the values for the output signals of a mass or emission spectrometer corresponding to ^{28}N, ^{29}N and ^{30}N are substituted into the above equation, the ^{15}N % abundance of the sample is obtained.

If equilibrium exists between the ^{28}N, ^{29}N and ^{30}N molecules according to $^{28}N + {}^{30}N \rightleftharpoons 2\,{}^{29}N$, it becomes unnecessary to measure the output signals of the three nitrogen molecules; only the ^{28}N and ^{29}N signals need be measured (usually by measuring the height of the peaks from a recorder connected to the spectrometer). The ^{15}N % abundance can then be calculated from the equation:

$$^{15}N\ \%\ \text{abundance} = \frac{100}{2R+1}$$

where $R\ (= h^{28}N/h^{29}N)$ is the ratio of peak heights found for ^{28}N and ^{29}N. For the derivation of this equation as well as the theoretical background, see p. 58.

Principles of conversion to nitrogen gas

The conversion of organically and inorganically bound nitrogen to nitrogen

gas can be made by two different methods.

The first method is based on digestion of the sample in sulfuric acid with additives such as hydrogen peroxide or a suitable catalyst, i.e. one of the many modifications of the Kjeldahl method[1]. Organic and inorganic nitrogen is converted to ammonia which is recovered by steam-distillation of the acid mixture after addition of excess of sodium hydroxide. The ammonia gas can be trapped in hydrochloric acid solution, and the excess of acid back-titrated with sodium hydroxide for determination of the total nitrogen content. The titrated solution can then be acidified with hydrochloric acid and evaporated to a small volume. By means of the so-called Rittenberg technique, the ammonia in the extract is oxidized by sodium hypobromite to nitrogen gas, which can be admitted to a mass spectrometer to determine the $^{14}N/^{15}N$ ratio.

The second method involves dry combustion of the organic and/or inorganic nitrogen-containing compounds with copper oxide or copper in the presence of lime. This modified Dumas reaction results in the complete oxidation of ammonia to nitrogen and reduction of nitrogen compounds to nitrogen gas. Calcium oxide is also added to absorb the water and carbon dioxide which are usually formed simultaneously. There are many ways in which the Dumas reaction can be carried out; detailed descriptions of the techniques are given later. An advantage of the Dumas procedure is that all the bound nitrogen can be converted to gas and the pressure measured, so that the total nitrogen content of the sample and the isotope ratio can be readily determined on the same sample.

In practice, it is also possible to combine the two methods, e.g. by preparing Kjeldahl extracts, and then converting the ammonia to nitrogen gas by the Dumas reaction instead of the Rittenberg reaction.

Although the principles of gas preparation for emission and mass spectrometry are identical, the actual procedures differ considerably, because the quantity of gas required for mass spectrometry is of the order of 30 μg–3 mg of nitrogen, whereas emission spectrometry requires only 0.2–10 μg. Problems of contamination of a sample with nitrogen from chemicals, air, filter paper, adsorption of nitrogen on the glass walls, *etc.*, may be important when quantities as small as a few micrograms of nitrogen are involved.

Principle of mass spectrometry

A mass spectrometer designed for gas analyses essentially comprises 5 units (Fig. 1): (1) an inlet system for the introduction of nitrogen gas; (2) an ion source

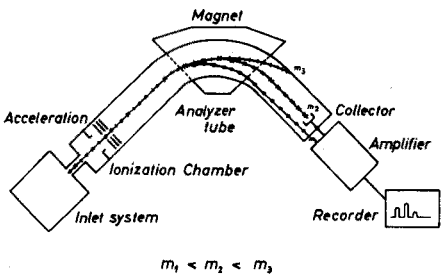

Fig. 1. Block diagram of a mass spectrometer.

where the nitrogen molecules, bombarded with electrons, become charged and accelerated; (3) a magnetic field in which the charged molecules are separated into different paths according to their momentum; (4) a collector placed at the end of the flight tube where the molecules discharge, and the discharge currents are amplified; and (5) a recorder which registers the amplified discharge currents as peaks as the mass range is scanned. The heights of the peaks are proportional to the amounts of the three molecules in the gas mixture. By simply measuring the heights, the ^{15}N % abundance can be determined.

Although the principle is simple, the practice of mass spectrometry is complicated. The whole system must be maintained under high vacuum, and the electric and electronic components must be highly stabilized. Artefacts can be produced easily when such instruments are not supervised by highly qualified personnel.

Principle of emission spectrometry

An external energy source can be used to bring the nitrogen molecules to an excited state. When the excited molecules return to the ground state, the energy difference is emitted as electro-magnetic radiation of specific energy. There is a small difference in the wavelengths of the light emitted by the excited ^{28}N, ^{29}N and ^{30}N molecules. When the emitted light is resolved by a monochromator, the light intensity corresponding to the three nitrogen molecules can be measured. The recorded peak heights allow the ^{15}N % abundance to be calculated in a similar way to mass spectrometry.

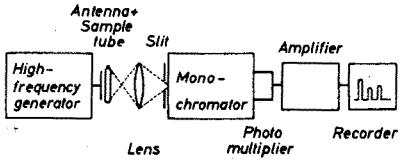

Fig. 2. Block diagram of a set-up for the emission spectrometric ^{15}N determination.

An emission spectrometric nitrogen detection assembly consists of the following units (Fig. 2): (1) a micro-wave (high-frequency) power generator for the excitation (electrodeless discharge) of the nitrogen gas in the sample tube; (2) a device for transferring the power from the generator to the nitrogen gas; (3) a monochromator which resolves the light of different wavelengths and with which it is possible to scan; and (4) a photomultiplier, amplifier and recorder which convert the light quanta to electrical signals to provide measurable peaks for the calculation of ^{15}N abundance.

Emission spectrometry is simpler than mass spectrometry from a technical point of view. No high vacuum is required and the instrument can be installed and supervised by any experienced analyst.

SAMPLE PREPARATION AND VACUUM TECHNIQUES

For the determination of $^{14}N/^{15}N$ ratios, it is necessary to convert all the nitrogen atoms in the sample to a single compound. For both mass spectrometry and emission spectrometry, nitrogen gas is preferred for the following reasons. First,

it is much easier to generate nitrogen from different inorganic and organic compounds or matrices than NO, NO_2 or NH_3. When nitrogen is produced as the gas, it is easily separated from the remainder of the sample. Secondly, nitrogen is inert with respect to all materials normally involved in mass and emission spectrometry. Thirdly, the interpretation of the isotopic data is simple as there are no interferences from other elements. In the case of NO, for example, the mass spectrometric peak of $^{14}N^{17}O^+$ would be identical with that of $^{15}N^{16}O^+$.

Since the amount of nitrogen required for mass spectrometry is about 100 times more than that required for emission spectrometry, sample preparation differs considerably in practice although the principle remains the same.

During an analysis, no dilution of the ^{15}N in the sample with atmospheric nitrogen should occur. Because air contains 78% N, the sample conversion must be done in vacuum. The vacuum necessary is of the order of 10^{-2}–10^{-5} mm Hg, depending on the amount of nitrogen involved and on the magnitude of the memory effect arising from adsorption of nitrogen on the walls of the container. The degree of cleaning or desorption of the gas sample containers of the molecular layers of nitrogen adsorbed on the walls is important, as is the exchange of molecules between gaseous and adsorbed phases.

The chemical part of the analysis introduces similar problems, e.g. nitrogen impurities in chemicals which are not detectable or hardly detectable by normal chemical methods can also dilute the nitrogen in the sample. Many of these problems are associated with the vacuum part of the analysis, and therefore some fundamental aspects of high-vacuum techniques are briefly outlined in the next section.

Vacuum techniques

Vacuum techniques are an integral part of the preparation of samples for mass spectrometric and emission spectrometric determinations of ^{15}N abundance in gas samples. High-vacuum techniques are also involved in the operation of mass spectrometers.

Figure 3 shows the working region of different kinds of vacuum pumps (1 torr being a pressure equivalent to 1 mm of mercury).

Pumps. Mechanical rotary pumps[3] are used for the range between atmospheric pressure and 10^{-2} torr for single stage or 10^{-3} torr for 2-stage pumps. They are mainly used as forepumps for diffusion or similar pumps, because the latter do not function at atmospheric or near atmospheric pressures. The rotary pump consists of a solid cylindrical housing (stator). The rotor, mounted eccentrically in the stator, sweeps the gas in the volume between it and the stator from the inlet to the exhaust port (Fig. 4). By rotation, the volume behind the vane increases and the gas from the vacuum system can move into this volume. When the vane has passed the inlet port, the gas becomes compressed (decrease of volume) and is pushed through the discharge valve and the oil to the discharge port.

Two-stage pumps (compound pumps) are normally used in which two chambers are arranged in series within the same housing. In the presence of condensable vapours, the compound pump produces a better end vacuum than the single pump.

The rotary pump is also a compressor, and therefore any condensable gases present, *e.g.* water and volatile organic compounds, may be condensed during the

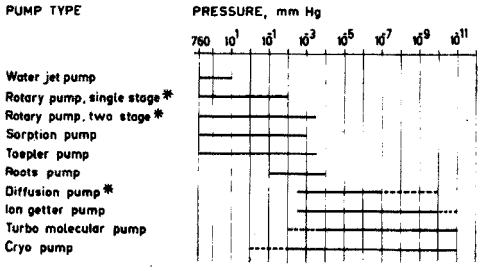

Fig. 3. Working region of different vacuum pumps. Only the asterisked types are used in vacuum lines for sample preparation.

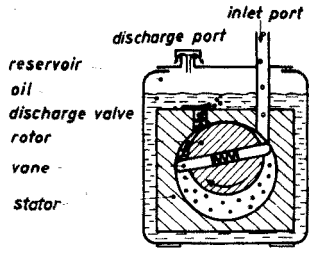

Fig. 4. Cross-section of a rotary pump.

pumping. To minimize the loss of pumping speed by mixing of the pump oil and condensable products, a gas ballast valve is built in; this lets some air in when the vane has passed the inlet slit. Because of the higher pressure the discharge valve opens earlier than it would do under normal conditions. The compression ratio (without valve $1:10^3$, with valve approximately $1:10$) decreases and the impurities do not condense. The end vacuum reached by a pump with gas ballast valve is a little lower than that of a pump without it.

Diffusion or vapour stream pumps[4] utilise mercury or special oils. The liquid is evaporated and the vapours stream downwards from one or more jets (Fig. 5). The vapours strike the cooled walls of the pump, condense and flow back to the boiler. The pumping action of a diffusion pump is caused by the vapour jet stream which transfers momentum to the gas molecules which have to be pumped out of the vacuum system. Usually the gas is compressed by a number of successive jet streams before it is finally evacuated by a rotary pump.

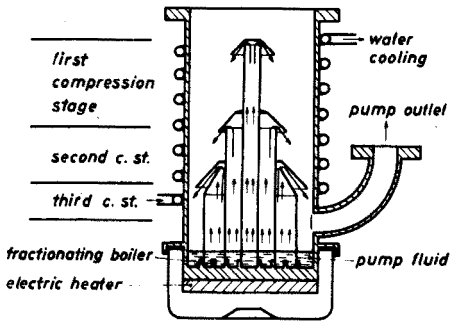

Fig. 5. Cross-section of an oil diffusion pump.

TABLE I

VAPOUR PRESSURE OF MERCURY AT VARIOUS TEMPERATURES

Temp. (°C)	−180	−78	0	20	100	200
Torr	negligible	$3 \cdot 10^{-9}$	$2 \cdot 10^{-4}$	10^{-3}	$2 \cdot 10^{-1}$	17

Oil pumps are mostly used with a water-cooled baffle which holds back most of the oil particles of the pump fluid from the vacuum system. Vapour pressures of mercury at different temperatures are shown in Table I.

Traps and baffles[5]. A trap consists of a system of cooled walls or plates placed near the vacuum pump, and serves to reduce the vapour pressure, e.g. to condense the vapours that might migrate from the pumping liquid to the vacuum system. As can be seen from Table I, the mercury diffusion pump alone does not produce a high vacuum, because of the relatively high vapour pressure of mercury at room temperature. A cooling trap near the pump decreases the vapour pressure, thus obtaining a higher vacuum.

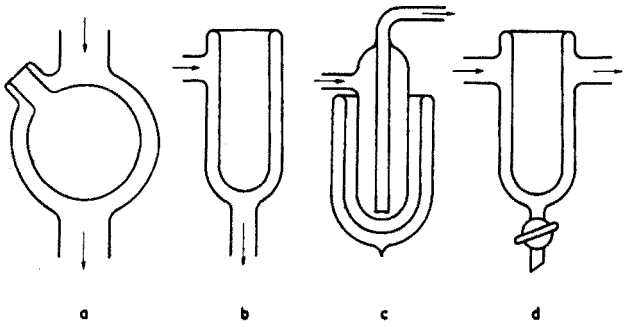

Fig. 6. Different types of cooling traps.

Figure 6 shows different types of traps, mainly made of glass. Types (a) and (b) are normally used with diffusion pumps, and (c) and (d) with rotary pumps. When liquids have to be degassed and the space above them evacuated, type (d) is ideal, as at the end of the process the ice can be melted from the cold finger and the liquid removed through the stopcock placed at the bottom.

Baffles work similarly but the condensate is returned to the boiler of the pump, reducing the fluid consumption; they are therefore mostly used in connection with diffusion pumps. Figure 7 illustrates a water-cooled baffle.

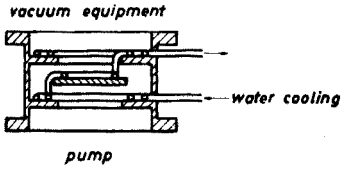

Fig. 7. Cross-section of a water-cooled baffle.

Measurement of vacuum (vacuum gauges). Many different vacuum gauges exist, each based on a different principle and applicable only to certain pressure ranges. Figure 8 shows the pressure regions where the different types of gauge apply.

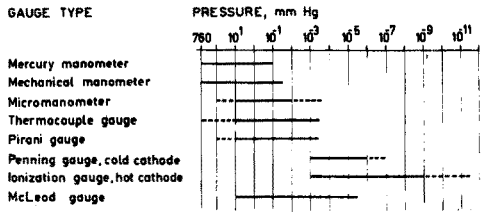

Fig. 8. Working region of various gauge types.

The working principle of a mechanical low-pressure manometer is based on the deformation of a metal sheet or diaphragm, when subjected to a certain pressure or vacuum on one side. The pressure can be indicated in two ways: (i) by mechanical transfer of the bending of the diaphragm; or (ii) by electrical transfer, where the diaphragm acts as the varying part of the capacitor[6]. The pressure range of type (i) is 760–0.5 torr. Different instruments have different working scales (0–760, 0–100, 0–50, 0–20) where one can distinguish 2, 1, 0.2 and 0.05 torr, respectively. Such gauges measure pressures well down to 1 torr (but lose accuracy below this) and are used, for example, for the preparation of gas mixtures. With type (ii), called a micro-manometer or diaphragm-type micro capacity torr meter, one can differentiate types for measuring pressures in the ranges from 0–50 or 0–20 torr with an accuracy of $\pm 1 \cdot 10^{-3}$ torr. There also exist types with a range up to 10^{-3} torr, used mainly to measure the vacuum in the inlet system of a mass spectrometer. Both types (i) and (ii) measure the total pressure, the sum of all gas and vapour pressures.

Thermal conductivity gauges operate on the principle of heat loss from a filament where the heat loss is pressure-dependent. The rate of heat loss from a filament of certain materials depends on the thermal conductivity of the surrounding gas. Normally these gauges are calibrated for air, and calibration curves are necessary for other gases. Gauges based on this principle are the Pirani and the thermocouple gauges.

In the Pirani gauge[7,8], a heated filament with a large temperature coefficient of resistance in the evacuated chamber forms part of a Wheatstone bridge arrangement. The change of the resistance, according to the conductivity of the gas and its pressure, is proportional to the pressure change. In the thermocouple gauge[9,10], a thermocouple is connected to a heated filament and the temperature changes are measured by means of a voltmeter.

Both types, the Pirani and the thermocouple gauge, are calibrated by the manufacturer for dry nitrogen, which is also valid for air; for all other gases calibration curves are required. The pressure range is from atmospheric pressure to 10^{-3} torr. The range from 760 torr to 1 torr, which is not of great interest in vacuum technique, is not very accurate, but there are special instruments available in which the pressure range from 100–1 torr is relatively accurate.

Ionization gauges[11] are based on the principle that the number of ions formed by collision between the residual gas molecules and bombarding electrons, emitted from a filament, is measured. The ionization gauge is used below 10^{-3} torr, as only then is the number of ions formed directly proportional to the pressure. One can distinguish two basic types: (i) one with hot filament (thermionic emission) and (ii) the cold cathode (vacuum discharge) gauge.

The hot filament gauge, is built similarly to a normal triode valve. The electrons produced by a directly heated filament pass through a grid and then produce ions by collision; the ions are corrected by the anode and measured by a voltmeter. The pressure range for the triode type is 10^{-3}–10^{-7} torr. The modification of Bayard and Alpert[12] extends the measurable pressure range to 10^{-11} torr.

In the Philips or Penning Gauge (cold cathode gauge)[13], the electrons produced by a high-voltage discharge are forced to travel in the form of a spiral by a magnetic field before moving towards an anode. The high-voltage discharge current is measured with an ammeter which can be calibrated in pressure units. The discharge works in the range $5 \cdot 10^{-6}$–$5 \cdot 10^{-2}$ torr.

All compression manometers are based on Boyle's law. A gas or vapour with a pressure P in a given volume V is compressed, by mercury, to a smaller volume v, which is usually the volume of a calibrated capillary. The pressure p in the smaller volume v is $p = P \cdot V/v$. The distance from the top of the capillary to the mercury level is a measure of the volume, and the volume is a measure of the vacuum, when the mercury level in the communicating container is at the same height as the top of the capillary. The distances in the capillary can be calibrated so that the pressure can be read directly. The McLeod gauge[14] is based on this principle.

Most of the compression gauges are similar in design. They are mostly used in simple vacuum work, as they are cheaper than the other gauges mentioned. The pressure range of the different compression gauges is $10^{-3} - 100$ torr, depending on the construction. The precision is not very high, except for the McLeod precision type[14]. For most purposes, in the range 10^{0}–10^{-3} torr, a compression gauge is sufficiently precise. All compression gauges measure the total pressure, i.e. the sum of all gas and permanent vapour pressures.

Materials. Materials used in vacuum techniques should have the following characteristics: vacuum tightness, low degassing rate, machinability, and chemical inertness. Materials which fulfil these demands are some metals, glass, ceramics and elastomers. Degassing rate can be defined by the amount of gas released per second per cm^2 of the surface of a material (in cm^2) under vacuum conditions.

The preferred metals are steel, stainless steel, copper and aluminium. Steel is generally coated with nickel to decrease the degassing rate and protect it against corrosion. Copper is seldom used because it is rather soft and not so easy to machine. It is used only in the form of long tubing for connections. The harder copper alloys like bronze are more frequently used. Brass is easy to machine but can only be used after coating with nickel because of its high degassing rate. For rough vacuum devices, special aluminium alloys are used, but equipment for high-vacuum work can also be made of such alloys.

In spite of some disadvantages the best metal for vacuum techniques is still stainless steel. It has a very low degassing rate, and low porosity, and it is inert to weak acids which facilitates cleaning. Moreover, as it is easily polished, thus reducing the real surface area, high vacuum is more readily obtained.

All the materials can be machined relatively easily and can be soldered and welded. For the welding of vacuum equipment experience is necessary. The normal method for welding stainless steel is with an argon arc. Argon is used to cover the hot area to keep oxygen away which could burn the material and cause the weld never to become vacuum-tight.

Glass is predominantly used for most vacuum apparatus. The advantages of glass are its transparency, low degassing rate, electrical insulating property, and chemical inertness. Many glass parts for vacuum apparatus are available in different forms and sizes commercially. With some experience in glass blowing, such parts can be easily built together.

At the present time Pyrex glass (80.5% SiO_2, 12.9% B_2O_3, 3.8% Na_2O, 2.2% Al_2O_3 and 0.4% K_2O). is preferred for glass blowing.

As will be shown later, vacuum leak detection and repair is easier for glass than for metals.

Ceramics, mainly alumina (Al_2O_3) and steatite ($MgSiO_3$), are used for isolating electrical connections through metallic parts of vacuum equipment.

Elastomers are often used for demountable seals. Synthetic rubbers are available in many variations and can also be applied for high-vacuum lines. Fluorinated elastomers like Viton, Vel-F or Fluorel are preferred because of their better degassing properties.

Construction principles and sealing problems. In principle, in all vacuum work, pipes and connections should be made as short as possible. It is advantageous to minimize the number of seals because each seal may become a source of leakage. The amount of welding should be also kept to a minimum for similar reasons. Tubing of too small diameter (d) decreases the velocity of gas flow or diffusion by a factor proportional to d^3. A construction plan of the vacuum apparatus should always be made before the prefabricated parts are ordered. This may save time and money in many cases, *e.g.* if the space for the vacuum system is small or limited by various factors.

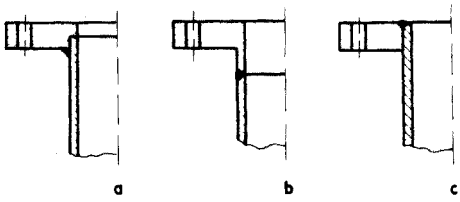

Fig. 9. Construction principles for welding.

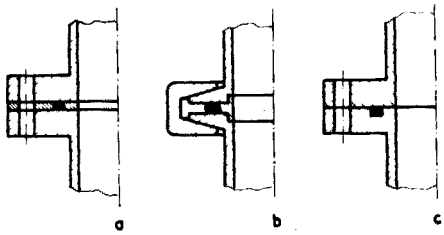

Fig. 10. Sealing of flanges.

All parts which are in contact with the vacuum should have a very smooth surface and all mechanical work must be done carefully.

With regard to welding and sealing, Figs. 9 and 10 give a number of examples of the ways in which a pipe may be welded to a flange. In case (c) (Fig. 9) a weld is shown which has to be machined on a lathe to obtain a smooth surface on the flange. Figure 10(a) and (b) illustrates sealed flange connections to flanges without

an 0-ring groove: (a) shows an 0-ring placed between an aluminium spacer; (b) shows nearly the same principle but the two flanges are held together with a clamp ring. Figure 10(c) shows a flange connection with an 0-ring in a groove.

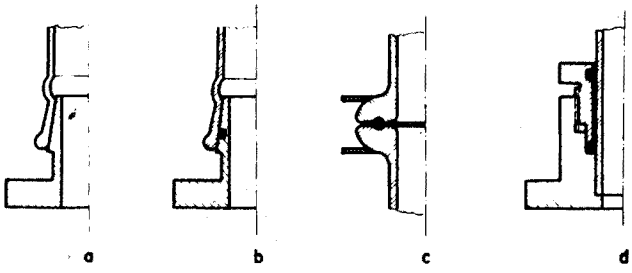

Fig. 11. Metal–glass joints.

A big problem is to join metal to glass. Figure 11 shows some possibilities for the solution of this problem. Figure 11(a) shows an example where the metal and the corresponding glass conical joints are sealed vacuum-tight by means of high-vacuum grease. Figure 11(b) is similar to (a) but the grease is replaced by an 0-ring. Figure 11(c) is a special 0-ring joint where the glass and metal parts are equal in size and are held together by clamps. Figure 11(d) shows a system where an 0-ring is pressed onto the wall of the glass tube with a screw, sealing it tightly; the second 0-ring above serves only for centering the system.

Another solution for the glass-metal joint is the Kovar–Pyrex seal, which is however expensive compared with other types of seals. Figure 12 illustrates how such a seal can be constructed. Kovar, an alloy of Co, Ni and Fe, can be welded to any steel or stainless steel part. The type of connection that is chosen depends on the purpose for which it is required. The Kovar Pyrex seal is, for instance necessary, for the connection of the glass inlet system to the ion source of a mass spectrometer.

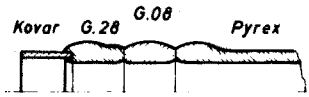

Fig. 12. Tubular seal between Kovar and Pyrex glass. G.28 and G.08 are special glasses to obviate the problems of the different thermal expansion of Kovar and Pyrex.

One construction element often used is the bellows. It is not only in use for valves but also to reduced vibrations. For example, a bellows is necessary between a rotary pump and the vacuum line. Bellows can be made of stainless steel or tombac, the latter being a copper alloy.

The symbols used for later vacuum diagrams are given in Fig. 13.

Leak detection. One of the greatest problems of vacuum technique is to ensure that the equipment is vacuum-tight. Experience has shown that a system is vacuum-tight when the degassing and the leak rates are between 10^{-5} and 10^{-6} torr l s^{-1}. An example is given to indicate how this can be measured.

A vacuum device of 1-l volume was evacuated for 4 h, which degassed the inner surfaces; this was assisted by heating the system with a hair dryer (an insulated resistance wire wound around the system and heated serves the same purpose). The

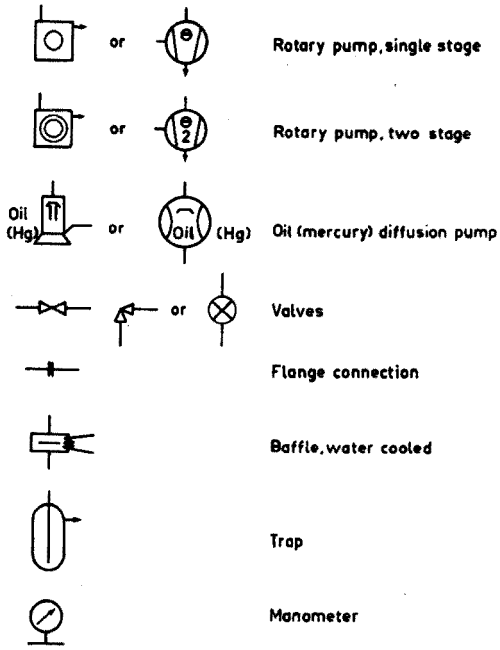

Fig. 13. Symbols for vacuum diagrams.

device was isolated, after cooling, from the pump by closing the main taps. Next the pressure change was determined per time unit. In the present case, a pressure change from $1 \cdot 10^{-3}$ torr to $2 \cdot 10^{-3}$ torr was registered in 120 s. The following calculation gave a value which could be compared with 10^{-5}–10^{-6} torr l s^{-1}.

$$\frac{\text{difference in vacuum} \times \text{volume}}{\text{time}} = \frac{1 \cdot 10^{-3} \times 1}{1.2 \cdot 10^{2}} = 8.4 \cdot 10^{-6} \text{ torr l s}^{-1}.$$

The vacuum system could be considered tight for most purposes. When the result is higher than 10^{-5} torr l s^{-1}, a leak is indicated. Leak detection methods are different for glass and for metals. In both cases, however, the valves, stop-cocks, joints and seals should be checked first. When no leak can be found, the search must be continued.

For glass apparatus, the Tesla coil or high-frequency leak detector is very useful. By spraying the glass surface with the spark emitted from the electrode, a discharge can be observed inside the system. When the spark reaches a micro hole in the glass, it goes through this hole into the vacuum system. The leak can at first be closed with Picein or other special vacuum waxes and later closed properly by glass blowing. If still no vacuum is obtained, more leaks must be present.

For metallic systems, leak detection is more difficult because the Tesla coil cannot be used. One method is to spray acetone stepwise over the surface of the system. A rapid change in the reading of a thermocouple or Pirani gauge, indicates that acetone has penetrated the leak. Here also Picein or special vacuum wax can be used for closing the leak.

Another method of detection in metallic systems is the halogen leak detector,

which also uses the indication of a Pirani or thermocouple gauge. Instead of acetone, a gas, often Freon, is used as described above. As Freon is heavier than air, the search should start at the lowest part of the apparatus to prevent an incorrect indication of a leak when the gas moves downwards past the leak.

The best but also the most expensive way is by means of a small mass spectrometer, called a helium leak detector. Here the vacuum system to be investigated is connected to the ion source of the mass spectrometer and the mass range of the instrument is adjusted for helium. Helium is used as its content in air is very low. By means of a gas pistol, the system is treated with a stream of helium; the top part is treated first because helium is lighter than air. The indication not only shows the location of the leak but also the rate of leakage, when the system is calibrated by a standard or reference leak.

The conversion of nitrogen compounds to nitrogen

The method for the conversion to nitrogen gas should be generally applicable to all kinds of compounds and materials; it should be as simple as possible and should involve a minimum of time and manpower. The possibility of dilution by cross-contamination, which would alter the ^{15}N abundance of a sample, must be minimal. Sub-sampling errors can be prevented by using well mixed, finely ground material. Three different methods for the conversion are available, i.e. the Kjeldahl–Rittenberg, the modified Dumas, and a combination of Kjeldahl and Dumas methods.

The Kjeldahl–Rittenberg method. This method was introduced by Rittenberg[2] in 1948. The Kjeldahl method was used to convert the sample nitrogen to ammonia which was distilled into hydrochloric or sulfuric acid. After concentration of the acid distillate, the ammonia was oxidized to nitrogen with an alkaline solution of sodium hypobromite in vacuum. The following steps are necessary for the analysis:

(1) digestion of the sample with concentrated sulfuric acid;
(2) separation of the ammonia by distillation after addition of alkali;
(3) determination of the ammonia by back-titration, colorimetry *etc.*;
(4) acidification;
(5) evaporation to a small volume;
(6) oxidation of the ammonia to nitrogen.

A detailed account will be given of each of these steps in the succeeding sections. Modifications of the method, e.g. micro or sub-micro analyses of nitrogen by diffusion techniques[15] or determination of ^{15}N in different chemical forms separately, will be included. Sources of contamination and their elimination will be mentioned at the end of the corresponding analytical step.

Generally, in view of the potential inhomogeneity of agricultural samples, it is advantageous to use a sub-sample which is as large as possible. More sample than is actually required for the ^{15}N analysis decreases the sub-sampling errors and reduces the possible dilution or cross-contamination from micro leaks or memory effects. For the digestion, quantities sufficient for triplicate isotope analysis are normally used. For the oxidation process an aliquot or the total amount of extract can be used since in this step the ammonia salt or nitrogen gas is taken from a uniformly distributed sample and no sub-sampling error can arise.

Digestion. The digestion method includes the conversion of organically and inorganically bound nitrogen in the sample to ammonia by boiling with sulfuric

acid. Although the Kjeldahl method[1] has been used for about 90 years and several hundreds of papers on the technique have been published, there is still no universally accepted digestion method. The best compromise seems to be to adapt the digestion technique to the nature of the sample material. Several attempts have been made to decrease the digestion time required for quantitative reaction: pretreatment of the sample, and addition of salts to increase the boiling point of the digest, catalysts, and oxidizing agents (other than the permanganate suggested by Kjeldahl) have been examined.

Pretreatment is necessary for nitrates and nitrites, for compounds containing the pyridine heterocyclic ring, and for compounds such as lysine which when treated with concentrated sulfuric acid are converted to pyridine-like compounds. Nitrates must be reduced to ammonia with for example iron powder and acid; nitrites are first oxidized with, say, permanganate to nitrate and then treated as above[16]. Pyridine(which does not char with sulfuric acid), and compounds forming it, must be first reduced; the addition of charring organic compounds such as dextrose also helps[17].

Potassium sulfate is generally used to raise the digestion temperature. Ogg and Willits[18] stated that the rate of digestion approximately doubles for each 10°C rise in temperature; but losses of ammonia occur[19] when the temperature exceeds 410°C. McKenzie and Wallace[20] found that a temperature of 422°C is suitable but this should only be reached after the fuming in the initial digestion period has stopped. Such conditions can be obtained with a ratio of 2.5 g of K_2SO_4 to 1.5 ml of sulfuric acid (1.66 g ml^{-1}). When an amount of 2 g ml^{-1} is used, there is still complete recovery of nitrogen with a digestion temperature of 390°C (lower than the boiling point of the mixture). Baker[21] stated that 1–2 g/ml could be safely used with a temperature of 410°C.

The well known catalysts are selenium, mercury(II) oxide and copper sulfate. Although copper sulfate is the least effective, it is still in use. Mercury(II) is very effective but mercury–ammine complexes may be formed unless, sodium sulfide or thiosulfate is added along with alkali after the digestion to precipitate mercury as a black sulfide which does not combine with ammonia. Osborne and Wilkie[22] found mercury(II) to be the best catalyst for protein digestion. Middleton and Stuckey[17] recovered the total nitrogen from nicotinic acid by using mercury(II) oxide, and McKenzie and Wallace[20] obtained complete recovery from tryptophan by using a higher boiling point mixture made by addition of potassium sulfate and mercury(II) to the sulfuric acid. Perrin[23] showed that with a higher than normal HgO concentration, the nitrogen could be recovered completely after a total digestion time of 15–20 min from resistant compounds such as nicotinic acid, tryptophan and other nitrogen-containing substances. Baker[21] found no effect of mercury(II) on the decomposition of ammonia such as that caused by selenium, but a marked one on the digestion of nicotinic acid, the recovery from which was satisfactory above 390°C.

Selenium alone does not always result in complete recovery of sample nitrogen, probably because of decomposition of ammonia. However, Patel and Sreenivasan[24] stated that selenium could be used without causing losses of ammonia if the digestion was completed within a short time. This confirmed by Middleton and Stuckey[17] but Baker[21] found unsatisfactory recoveries caused by losses of nitrogen when

selenium was applied above 387°C. The use of selenium seems justified only when the heating is not continued after decolorization of the sulfuric acid and when it is known that this is sufficient to give quantitative recovery of ammonia. A mixture of selenium and mercury(II) oxide at 365°C is said[21] to result in maximal recovery of nitrogen.

Of all the oxidizing agents tested, hydrogen peroxide has been found to be the best[25]. McKenzie and Wallace[20] developed a semimicro and micro Kjeldahl method which was used for the complete digestion of tryptophan (98–99% recovery). The method involved 20 additions of 0.05 ml of 30% hydrogen peroxide at 120–140°C (decomposition temperature of H_2O_2) to the digest.

Depending on the amount of sample, the Kjeldahl digestion can be divided into three types: macro, semimicro and micro. In principle, the digestion proceeds more rapidly when small sub-samples are used. The macro method is used when only relatively large samples can be guaranteed to be homogeneous. Kirk[26] used 1–2 μg of nitrogen for ultramicro Kjeldahl work with the same precision as the macro method. In this method, complete recovery of nitrogen was easier to obtain than with larger samples. McKenzie and Wallace[20] recommended the use of 0.2–2 mg N per sample, and Baker[21] 5 mg. The use of microgram samples or less naturally only makes sense when it is possible to distil quantitatively such small amounts of nitrogen as ammonia. This was first demonstrated in 1933 by Conway[15], who found that diffusion techniques are a more satisfactory means than distillation of removing ammonia from a micro Kjeldahl digest. Kirk[26] removed the ammonia (4–20 μg) from the digest by a combination of boiling and aeration. Later, amounts of nitrogen of the order of 0.1 μg (ref. 27) and 0.5 μg (ref. 28; with 1% accuracy) were handled by applying a vacuum diffusion technique[25,29].

It is important to control the consumption of sulfuric acid, otherwise the boiling point will increase when the digest becomes clear if potassium sulfate is used, and losses of nitrogen may occur. The amount of acid needed for a particular compound can be calculated by the method of Middleton and Stuckey[17]: "The amount of acid required for any compound is readily calculated from its molecular formula by deducting from the latter the elements of ammonia and carbon dioxide (or water) corresponding to the number of atoms of N and O respectively. Any other elements present may be allowed for in a similar manner, *e.g.* sulphur when combined with 0 as in sulphonic acids, may be taken as converted to sulphur dioxide. while sulphur in a sulphide group is assumed to be eliminated unoxidized. In the cases of salts of alkali metals, allowance should be made both for the additional acid used in forming the sulphate and for the extra alkali sulphate present. By the subtaction of these elements of ammonia, water, carbon dioxide, sulphur dioxide, HCl, sulphur, sodium etc., from the formula there is left a residual formula containing C and H." The factor used in the calculation depends on the C/H ratio of this residual formula, and is taken from Table II, which also gives the general values for carbohydrates, fats and proteins, and factors for zinc for use when it is added in the determination of nitrogen present as nitrate. The acid consumption per gram is then equal to

$$\frac{\text{residual formula weight}}{\text{molecular weight}} \times \text{factor}$$

and the amount of acid in ml to be added for a particular assay is then equal to

6+(acid consumption per gram × weight of substance taken). Actually, great accuracy is not generally required in the calculation of the factor, and the total volume of acid need not be measured with an accuracy greater than, say ±0.25 ml. For ill-defined samples, Table III gives some indication of sulfuric acid requirements.

TABLE II

FACTORS FOR CALCULATING ACID CONSUMPTION

1 g sample	*ml sulfuric acid allowed*
CH_2	11.4
CH	10.2
$C_{1.5}H$	9.9
C_2H	9.6
$C_{2.5}H$	9.4
C_3H	9.3
C_4H	9.1
C	8.9
carbohydrate	4.0
fat	9.7
protein	4.9
Zn	0.8
Na	1.2
K	0.7
salicylic acid	5.5

TABLE III

AMOUNTS OF SULFURIC ACID NEEDED FOR VARIOUS MATERIALS DURING KJELDAHL DIGESTION[30]

Material	*Acid consumption (ml 18 M H_2SO_4/g material)*
Soil organic carbon	10.0
Soil organic matter	5.8[a]
Al_2O_3	1.6
Fe_2O_3	1.04[b]
Clay	0.6
$CaCO_3$	0.6
Silt	0.3
Sand	0
Salicylic acid	6.8
$Na_2S_2O_3 \cdot 5\,H_2O$	0.6
Reduced iron	1.5[b]

[a] Calculated from organic carbon value on assumption that soil organic matter contains 58% carbon.
[b] Calculated on assumption that digestion product is iron(III) sulfate.

Example: Sulphathiazole $C_9H_9O_2N_3S_2 = 255.3$. Subtract 3 NH_3, SO_2, S (one S atom is not linked to 0), leaving $C_9 = 108$. Then the acid consumption is $108/255 \times 8.9 = 3.8$ ml g^{-1}.

Distillation. After digestion the ammonia is liberated by addition of an alkali.

Distillation can be carried out normally or by steam-distillation. Steam-distillation has the advantage that "bumping" is prevented in the presence of precipitates in the extract. The type of distillation apparatus chosen depends on personal choice. In some cases, the Kjeldahl flask itself can be incorporated into the set-up; others prefer to transfer the extract to a separate distillation flask. The size of the apparatus of course depends on the sample size used.

Hoskins[31] developed an inter-changeable macro- and semimicro apparatus. Bremner[30], Kirk[25], McKenzie and Wallace[20], and many other workers, have developed different types of steam-distillation apparatus.

The receiving liquid of the distillation is normally boric acid but for mass- and emission spectrometry isotope determination, hydrochloric or sulfuric acid is preferable. The smaller solubility product of the borates causes them to precipitate when the solution is evaporated to a small volume for the determination of $^{14}N/^{15}N$ ratio, and also losses of ammonia can occur[32].

The actual determination of ammonia is normally done by titration or colorimetry[30]. In case of separation by diffusion techniques, capillary burettes are however necessary for the titration.

For the determination of $^{14}N/^{15}N$ ratios in distillates, interferences are introduced in the normal Kjeldahl analysis. These may originate from foreign sources or from the samples themselves. The foreign sources normally dilute the % ^{15}N whereas the ^{15}N content of other samples may cause cross-contamination. The causes of interference with the $^{14}N/^{15}N$ ratio determinations, associated with digestion and distillation, are:

(i) dilution or contamination from outside sources, such as absorption of ammonia or amines from the air, nitrogen impurities in the chemicals, and the nitrogen content of the indicator;

(ii) cross-contamination from poorly cleaned laboratory equipment, especially the distillation apparatus;

(iii) losses of nitrogen by incomplete conversion to ammonia of certain resistant nitrogen-containing compounds or groups; this gives rise to false % ^{15}N values.

In order to prevent interference from contamination the following rules should be observed.

(a) The laboratory atmosphere must be free of ammonia and amine vapours; no bottle or container of such liquids should be stored in the working area where ^{15}N preparation work is done. Only pure chemicals (p.a., M.A.R.) should be used. The acids (sulfuric and standard) must be always kept in tightly stoppered bottles to prevent absorption of ammonia or amines.

The dilution of ^{15}N from a sample by nitrogen from chemicals in a normal preparation procedure has been found to be of the order to 2% (ref. 33). Proksch[34] obtained a % ^{15}N abundance value by the Kjeldahl–Rittenberg procedure which was 2% lower than the value obtained by direct combustion by a modified Dumas method. This was attributed to nitrogen impurities in the chemicals which were not detectable by normal chemical methods. The proper choice of an indicator must also be considered from this point of view. Dilution of the % ^{15}N can occur because of the nitrogen content of the indicator. This is especially important in the case of emission spectrometric determination of ^{15}N where only very small samples

are necessary and the amount of sample nitrogen may be of the same order of magnitude as the indicator nitrogen. The often-used Tashiro indicator (0.2% methylene blue solution in 95% ethanol and 0.2% methyl red solution in 95% ethanol[20]) contains so much nitrogen that it may dilute the % ^{15}N of the sample to half of its value, as has been reported by Faust[35]. Faust, however, found no release of nitrogen from the Tashiro indicator during distillation or Conway diffusion and no decomposition with alkaline hypobromite solution when the extract was oxidized after titration and evaporation. It is also of importance to have the end-point of the titration in the acid region to prevent losses of ammonia at the end of the titration.

TABLE IV

CROSS-CONTAMINATION IN THE DISTILLATION APPARATUS

Investigator	*First distillation*		*Second distillation*[a]			*Nitrogen retention*	
	amount N (mg)	*% ^{15}N sample*	*amount N (mg)*	*% ^{15}N sample*	*% ^{15}N distillate*	*(μg)*	*(%)*
Bremner[30] (1965)	1	30	1	0.366	0.396	1	0.1
Faust[35] (1969)	0.5	55	0.05	0.366	2.05	1.6	0.3
Hüser[33] (1963)	3	48.2	3	0.362	0.704	22	0.7
Hüser[33] [b]	5	96.5	5	0.362	0.374	2.7	0.05

[a] 2nd distillation follows immediately after the first one.
[b] Steaming for 1 h after the first distillation.

(b) All equipment must be cleaned with detergents or acids. The cleaning of the distillation apparatus is not easy and even steaming for several minutes may not be sufficient to remove all the nitrogen which is adsorbed on the glass walls and tubes. The degree of cross-contamination which can arise has been investigated by several authors and is illustrated in Table IV. This Table shows that cross-contamination becomes appreciable when samples with large differences in % ^{15}N abundance or total nitrogen content are distilled one after the other. This cross-contamination may be prevented by distilling 10–20 ml of ethanol between samples[36].

(c) Incomplete digestion or losses of ammonia during the digestion can be prevented by choosing a suitable digestion method. When selenium is used as a catalyst or potassium sulfate for raising the temperature, a too long digestion time or overheating should be avoided. The combination of adequate digesting agents, catalysts, temperature and time of digestion has to be established for each particular kind of material, e.g. seeds, leaves, roots *etc.*

The oxidation of ammonia to nitrogen gas[2,37]. The oxidation of ammonia produced by the Kjeldahl digestion to nitrogen by means of hypobromite takes place in an alkaline medium in an evacuated container. The reaction proceeds according to the reaction

$$2\,NH_3 + 3\,OBr^- = N_2 + 3\,H_2O + 3\,Br^-$$

Hypobromite is a rather unstable compound and the reagent should be kept in a strongly alkaline medium, stored in a refrigerator. Hüser *et al.*[38] found that the full oxidizing power lasted only one week, but it is said to be possible to keep the solution for 6 months without too much loss of oxidizing power[36]. The freshly prepared solution develops some oxygen but this stops after a few days. To inhibit the formation of oxygen during the oxidation of ammonia, potassium iodide can be added[39] but this does not prevent it completely[40]. In addition to oxygen, N_2O is also formed[41,42] especially with freshly prepared hypobromite solutions. NO^+, which is formed from N_2O during ionization, interferes with ^{15}N measurements[43] in the mass spectrometric analysis and a liquid-nitrogen trap should be built into the inlet system of the mass spectrometer or in the transfer line for the preparation of the emission spectrometric discharge tubes, where N_2O is readily frozen out.

Bromine may also be formed in the solution. After the titrimetric determination of ammonia, the solution should be acidified to prevent ammonia losses. If too great an excess of hydrochloric or sulfuric acid is used, bromine may be formed according to the reaction

$$Br^- + OBr^- + 2\,H^+ = H_2O + Br_2$$

The excess of acid should not be higher than 0.35 ml of 0.1 *N* HCl or H_2SO_4[36].

Normally 0.5–2 mg of nitrogen is sufficient for the routine mass spectrometric determination of ^{15}N. In principle, twice the minimal amount of nitrogen required for the analysis of the isotopic ratio should be used in order to reduce the influence of cross-contamination and/or dilution from micro-leaks. The optimal amount of nitrogen is determined by the volume of the inlet system of the mass spectrometer and the Rittenberg vessel. For emission spectrometric analyses (where about 1/100th of the amount of nitrogen needed in mass spectrometry suffices) 0.1–0.3 ml of solution containing 0.03–0.1 mg NH_4–N is placed in a smaller Rittenberg vessel. Here again, the optimal and the minimal amounts of nitrogen are determined by the volume of the transfer line and discharge tube. There are several different types of Rittenberg vessels in use, as illustrated in Figs. 14 and 15. In operation, an amount of solution necessary to obtain the optimal nitrogen gas pressure is added to one arm of the Rittenberg vessel; into the other one the required amount of alkaline hypobromite solution is pipetted.

The preparation of the alkaline hypobromite solution is as follows[36]. Dissolve 200 g of sodium hydroxide in 300 ml of water and cool the solution in ice. Transfer

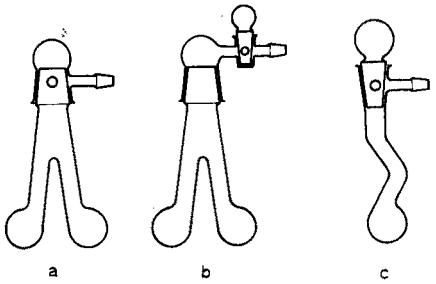

Fig. 14. Different types of Rittenberg vessel. This Figure shows 3 Rittenberg vessels used for mass spectrometry which can be rotated on the vacuum line without taking them off. (a) Recommended by Bremner[30], (b) recommended by Balestrieri[40], (c) recommended by Smith *et al.*[44].

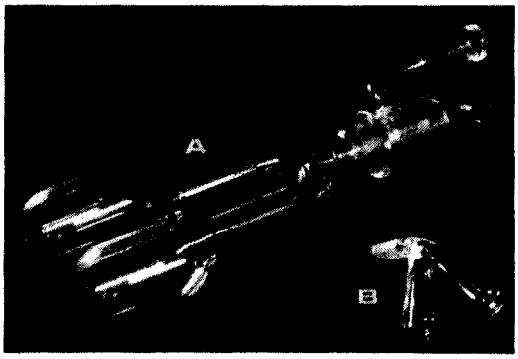

Fig. 15. Two Rittenberg vessels used in the IAEA Laboratory: (a) for mass spectrometry; (b) for emission spectrometry[45] with an extremely small volume.

half of the cooled solution to a 500-ml wide-mouth Erlmeyer flask, immerse the flask in crushed ice and add 60 ml of bromine over a period of 30 min. Stir the solution vigorously during the addition of bromine and regulate the rate of addition in such a way that the temperature of the solution does not exceed 5°C. When the addition of bromine has been completed, add the remainder of the alkaline solution and after stirring the mixture for a few minutes, stopper the flask and place it in a refrigerator for 4–6 days. Remove the precipitate of sodium bromide which forms during this period by filtration under suction through a glass-fiber filter, and dilute the filtrate with an equal volume of a solution prepared by dissolving 2 g of potassium iodide in 1 l of water. Store the hypobromite–iodide solution in a tightly stoppered bottle in a refrigerator. Care should be taken during preparation and storage of the reagent to protect it from atmospheric CO_2. One ml of this solution will oxidize 5–6 mg of ammonia to nitrogen, and the reagent will retain its activity for at least 6 months if stored in a refrigerator.

Samples for mass spectrometry are normally prepared on a separate vacuum line, whereas samples for emission spectrometry are prepared on the same line on which the electrodeless discharge tube is cleaned, filled and sealed off.

In case of mass spectrometry, the Rittenberg flasks are closed with the upper cap with high-vacuum grease. For this purpose the conical joint is greased with 4 lines of grease[46] every 90°, and the cap is heated with a hair dryer to about 40°C and then pressed on the joint so that all enclosed air bubbles are removed. The side-arm must correspond with the outlet in the ground joint so that the inside of the vessel is open to the air. When the grease has cooled the vessel can be attached to the line. The vacuum line needed for mass spectrometric analysis consists of a rotary pump and a liquid air trap with a stopcock (to allow drainage of water when the ice collected in the trap has melted after sample preparation[47]). The line has 4–6 arms for fitting the Rittenberg vessels and a vacuum meter, see Fig. 16. A diffusion pump is not required as the pressure in the line is determined by the vapour pressure of the solutions in the Rittenberg vessel. The stopcocks of the flasks, preferably made of Teflon (greaseless), are opened partially to the vacuum which removes the dissolved air from the solutions. Soon after this is complete, the liquid starts to boil. When boiling stops and the liquids freeze, the stopcocks are

opened fully for 8 min. Now the container is closed by turning it through 180°. Once the ice has melted, the reaction is started by transferring the sample into the alkaline hypobromite solution by tilting the vessel. Care should be taken to transfer the sample and not the hypobromite solution because the reaction must take place in alkaline medium. When the reaction is complete (30 s), the mixture is frozen with liquid air, the Rittenberg vessel is connected to the inlet system of the mass spectrometer and the gas is allowed to flow in. The freezing should be done carefully in order to avoid cracking the glass. Freezing should start at the bottom to enable the ice and the upper liquid to expand to the upper part of the arm. Experience has shown that about 2% of the vessels crack during routine operation.

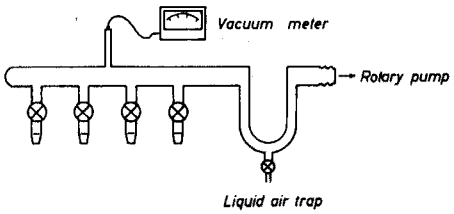

Fig. 16. Scheme of a vacuum line for the preparation of nitrogen gas samples by the Rittenberg method.

The same procedure is followed in the case of sample preparation for the optical ^{15}N determination[45]. The smaller Rittenberg vessel (Fig. 15b) is, however, not removed from the vacuum line, and mixing is performed by rotating the vessel; the gas is then allowed to flow over liquid air traps into the precleaned discharge tubes (see p. 23).

The possible sources of contamination which may occur during oxidation are:

(i) air leak in the Rittenberg vessel;

(ii) bad vacuum from a leak in the line;

(iii) cross-contamination from the walls of the Rittenberg vessels. Contamination can be easily prevented by careful checking of the greased ground joint, control of the vacuum during the analysis, and steaming of the Rittenberg vessel or washing with acids.

Preparation of the electrodeless discharge tube. The discharge tube required for emission spectrometry should have the following properties:

(i) it should be highly transparent for ultraviolet radiation as the spectral bands used for the analysis are in this region;

(ii) the softening point should be high because any adsorbed gases must be removed by heating; if the Dumas method is used to convert the sample nitrogen to nitrogen gas, the temperature of the mixture during combustion may be as high as 700–800°C;

(iii) as the tube is used only once, the price should be as low as possible.

There are three types of sample tubes in use at the present time (Fig. 17).

(a) Figure 17, B, shows a Uviol glass tube[45]. Uviol has a transmittance of 90% for a 1-mm thickness for radiation of 300 nm. The sample tube has a volume of about 2 ml. Because of the restriction in the middle with a wall thickness of 0.25–0.3 mm, an intense discharge is obtained concentrated around the restriction. The tube is connected to the vacuum line, as suggested by the supplier, by means of black

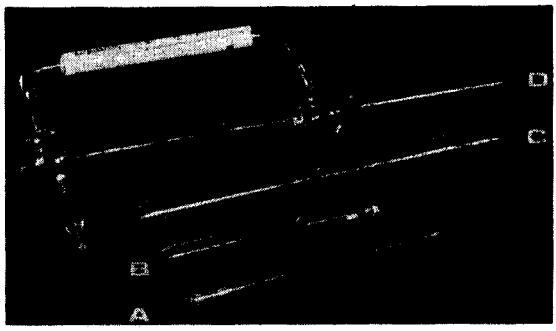

Fig. 17. Sample tubes: (a) electrodeless discharge tube made from quartz tubing; (b) electrodeless discharge tube made from Uviol or hard glass; (c) Pyrex glass tube used for the modified Dumas method in mass spectrometric sample preparation; (d) standard discharge tube for the calibration curve (Statron).

vacuum wax. The softening point of Uviol is 470°C.

(b) Hard glass tubes are the same shape and size as those of Uviol. Hard glass (Pyrex, Rasotherm *etc.*[45]) has a transmittance of 8% at 300 nm for a thickness of 10 mm. The thickness of the glass at the restriction is also 0.25–0.3 mm which is sufficient to allow enough ultraviolet radiation to pass through. The connection to the vacuum line is the same as in the case of Uviol. The softening point is 570°C. By using a grating monochromator which has a higher luminosity (spectral luminous efficiency) than prism instruments, the loss of light intensity caused by absorption in comparison to Uviol can be compensated.

Fig. 18. Teflon 0-ring joint with a cross-section of the joint with an inserted quartz tube.

(c) Figure 17A shows a quartz tube[48]. The quartz tubes have 100% transmission at 290–300 nm for a 1-mm thickness; the tubes have an internal diameter of 2 mm and a length of 100 mm, and the wall thickness is 2 mm. The volume is about 0.2 ml. Care must be taken in handling the quartz because, for example, each fingerprint which is not washed off with alcohol will carbonize on heating the tube; this makes the quartz milky and less transparent to the ultraviolet radiation. The connection of the tube to the vacuum line can be made by means of a Teflon 0-ring joint (see Fig. 18), as can the Uviol and hard glass tubes if suitably sized joints are available. Before the tube is connected to the vacuum line, it must be cleaned of all inorganic and organic compounds especially those which contain nitrogen. This is done by washing the tubes with acid and baking them in a furnace at a temperature of 50°C lower than the softening point of the glass. To avoid subsequent contamination, the tubes should be kept dust-free in a desiccator. As the amount of sample nitrogen in the discharge tubes is of the order of 1–10/μg, nitrogen still adsorbed on the walls of the tube can dilute the nitrogen of the sample significantly; Table V, prepared by Faust[49], demonstrates this point.

TABLE V

DILUTION OF THE SAMPLE ^{15}N CONTENT CAUSED BY IMPROPER TUBE CLEANING AND BY NON-DEGASSING OF CHEMICALS.

(% dilution of the sample % ^{15}N abundance)

Sample-N amount μg	*by not heating out the tube (%)*	*by not heating out the chemical (%)*[a]
20	5	3
10	—	13
5	—	17

[a] See Preparation of sample for emission spectrometry.

In addition to nitrogen, CO_2, water, oxygen and other gases which are present in the laboratory atmosphere must be removed from the tube as they can disturb the discharge. If CO_2 is present, it decomposes to form CO under the influence of the high-frequency discharge. CO has a spectral band near that of $^{14}N/^{15}N$ so that the $\%\ ^{15}N$ value will apparently be too high. When the level of $\%\ ^{15}N$ abundance of

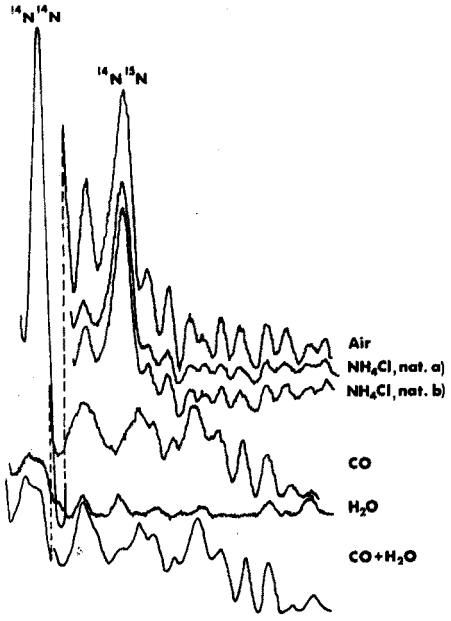

Fig. 19. Spectrum of N_2, CO and H_2O. This Figure explains why traces of CO_2 which decompose under the influence of the high-frequency discharge to CO cause an apparently higher ^{15}N content. The 5 spectra were recorded between 299.6 and 297 nm on a Hilger–Watts Monospek 600. Air: filled at 5 torr into the tube, recorded at 1–50. NH_4Cl natural abundance (a): 2–3 torr N_2, burned with CaO and CuO as one briquet[48], recorded at 1–50. NH_4Cl natural abundance (b): 2–3 torr N_2 burned with CaO and CuO separated[50], recorded at 1–50, thus yielding a purer background spectrum. CO (identical with the spectrum of a CO_2 filled tube): filled at 1 torr, recorded at 1–10. H_2O: filled at 10 torr contains traces of CO_2 which were not removed even after 5-min boiling in vacuum. $CO+H_2O$: obtained by geometric addition of the water and CO spectrum. It can be seen that the $^{14}N^{15}N$ band is lifted by a greater extent than the $^{14}N_2$ band thus increasing apparently the ^{15}N content.

the sample is below 1% this effect can be significant; Perschke *et al.*[50] found ^{15}N values which were 5–10% too high because of this effect (see Fig. 19). Traces of water cause an unstable discharge and if more than a half-volume of water vapour is present in the tube, the discharge will extinguish immediately after ignition[51]. Oxygen does not affect the discharge below 15% by volume of the nitrogen, as it is removed together with the other gases during the procedure[51].

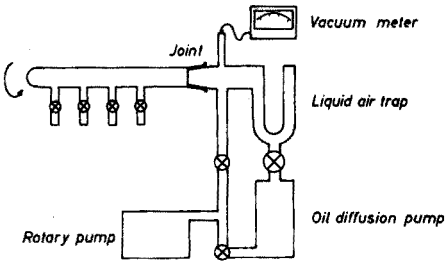

Fig. 20. Block diagram of a high-vacuum line for the preparation of electrodeless discharge tubes.

A block diagram of the high-vacuum line for the preparaton of the tubes is shown in Fig. 20; the system is similar to the preparation line of a NOI-4 ^{15}N Analyzer. After the tubes have been cleaned in the muffle furnace, the residual adsorbed gases are removed by connecting the sample tubes to the high vacuum line (better than 10^{-4} mm Hg) and heating them with a hand torch at a temperature at which the glass starts to soften (a small deformation can be observed). For Uviol and hard glass, treatment with a Tesla coil (leak detector) after the heating out releases the remainder of the adsorbed gases. This is not necessary for quartz because of the higher baking temperature which can be reached without danger of collapse. After cooling, the nitrogen gas from the Rittenberg vessel is allowed to flow into the tube via a liquid air trap which should remove all water. However, micro ice crystals can be carried along with the gas stream and enter the discharge tube. A similar effect has been observed in mass spectrometry[52]. In order to remove this water, an activated calcium oxide briquet, identical to the briquet used for the Dumas method (see p. 26) is added to the tube before it is mounted on the high-vacuum line[53].

The pressure of nitrogen in the sample tubes is normally adjusted to 3–5 torr. Although the light intensity of the discharge is highest at a pressure of 1.5 torr[54], the discharge lasts longer when more introgen is present, and a more stable discharge is obtained at 3–5 torr. This happens because the high-frequency discharge must provide enough energy for the ionized gas molecules to become implanted in the glass on collision with the walls; at very low filling pressures, the amount of nitrogen in the tube decreases very rapidly, which causes instability and rapid dying out of the discharge. After being filled, the tubes are sealed off by hand torch and heated in a furnace at 500°C for 2 h (430°C for Uviol) to complete the lime–water reaction. On cooling, the gas can be analysed for its ^{15}N content.

The preparation of standard discharge tubes. Emission spectrometric curves of the optical signal against ^{15}N content must be prepared and regularly checked against standard discharge tubes filled with gas whose ^{15}N abundance has been estabilished by mass spectrometry. Clearly, the discharge of such tubes should be

stable over long periods and their % ^{15}N content should correspond to the mass spectrometric value, *i.e.* there should be no dilution from residual traces of nitrogen from the walls and carbon dioxide should be absent. They can be prepared as follows: nitrogen of appropriate ^{15}N enrichment is prepared from a suitable source. A sample is taken for mass spectrometric measurement and the remainder is used to fill a discharge tube (containing a calcium oxide briquette) on the normal tube preparation line. The tube walls are heated with the hand torch and treated for 2–3 min with a spark from a Tesla coil to equilibrate the last traces of nitrogen and impurities on the walls with the sample gas. On cooling, the surface will be coated with a layer of sample gas which will not dilute the standard material. Then the gas is pumped out of the tube, which is immediately thereafter filled again with 3–5 torr of the nitrogen gas. The tube is then sealed off and is heated for 2 h at 430°C for Uviol, or 500°C for hard glass, to remove any carbon dioxide or water from the surface before the actual analysis is made. When this technique is used, the standard tubes obtained will provide at least 5 h of discharge[53,55].

Modified Dumas method. The original Dumas method[56] involved the oxidation of organic material with copper oxide in an atmosphere of carbon dioxide which is then passed through a strong potassium hydroxide solution. All elements present (*e.g.* C, H, N, Cl, S, O, P, *etc.*) are converted to forms which either react with copper oxide or are very soluble in strong alkali solution, except nitrogen, the volume of which is measured at the end of the reaction. This method has been used in many modifications for determinations of organically bound nitrogen.

In the modified Dumas method, organic matter is oxidized with copper oxide and the generated gases, except for nitrogen, are absorbed by calcium oxide. For nitrates and nitrites, it is necessary to replace part of the copper oxide by copper, to reduce these salts to nitrogen. The reaction is carried out in vacuum in a closed tube[34,48–50,57]. The Dumas method involves less preparation time and manpower than other methods since only two working steps are involved. As each sample is contained in a separate tube and the amount of chemicals involved is smaller than for the Kjeldahl–Rittenberg process, dilution and cross-contamination risks are smaller. Samples may be in the form of organic or inorganic compounds, and all kinds of biological material, including Kjeldahl concentrates, can be treated.

Preparation of samples for mass spectrometry [34,58,60]. Finely powdered dry material or an extract evaporated to dryness is filled into a Pyrex glass tube of about 6-ml volume (see Fig. 17(c)). The tubes are pre-cleaned by preliminary heating at 500°C for 3 h together with copper oxide (and copper when nitrate is present) and freshly prepared calcium oxide (activated by heating to 1000°C). The amount of sample should correspond to 0.5–5 mg of nitrogen. The amounts of copper oxide and calcium oxide should correspond to about twice the quantities theoretically needed for oxidation and absorption, respectively, in order to ensure complete conversion of sample nitrogen to nitrogen gas. For example, 0.15 g of plant material ground to 200–300 mesh and mainly composed of $(CH_2O)_x$, requires 0.8 g of copper oxide for oxidation and 0.75 g of calcium oxide for absorption of water and carbon dioxide, so that actually 1.6 g of oxidant and 1.5 g of lime should be placed in the tube, which is then connected to the vacuum line. This consists of no more than a rotary pump, a liquid air trap and a vacuum gauge with a meter (Fig. 21).

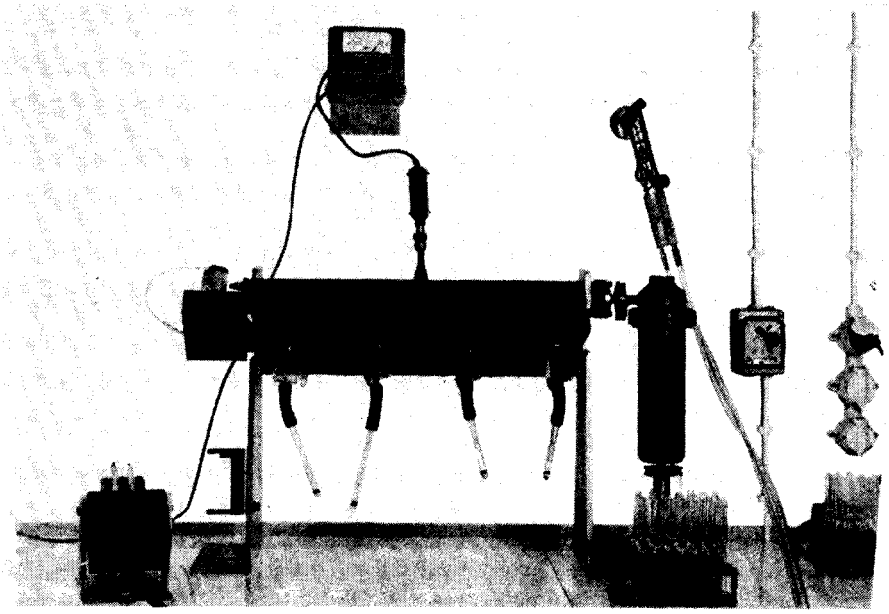

Fig. 21. Preparation line for mass spectrometric samples following the modified Dumas methods.

In the absence of samples, the line should have an end vacuum of about $5 \cdot 10^{-3}$ torr. The tubes are evacuated for 5–15 min until a pressure of $5 \cdot 10^{-4}$ or 10^{-2} torr is attained. The time required and the magnitude of the end vacuum depend on the vapour pressure of the particular kind of sample. Inorganic and organic compounds with low vapour pressure are ready within 5 min at a vacuum of 10^{-2} torr, whereas plant material needs 15 min for a final vacuum of $5 \cdot 10^{-2}$ torr. The tube is then sealed off with a hand torch and the top of the tube is annealed for about 2 min to prevent cracking from tensions in the relatively thick glass. The contents of the tube are carefully mixed before combustion in a muffle furnace, in which the tubes are placed in a horizontal position for at least 3–4 h. When the samples have cooled to room temperature, they can be introduced into the inlet system of the mass spectrometer, which should contain a liquid air or nitrogen trap.

The temperature of combustion is very important, as naturally the rate of reaction increases with increasing temperature. The maximal temperature is, however, limited by the properties of the glass of the sample tube. Above 570°C Pyrex becomes plastic and may explode because of the gas pressure inside the tube. The sample can be safely heated up to 570°C provided that the temperature control of the oven is satisfactory and no temperature gradients greater than 5°C occur; samples should be placed on an asbestos plate in the centre of the oven. When the temperature cannot be controlled to at least ± 5°C, which is normally the case for ovens working at such temperatures, 550–560°C is safer. It is also advisable to check the oven temperature with an additional thermocouple placed in the same region as the samples. Although only 70–80% of the sample nitrogen is converted to nitrogen gas for plant material (though 85–90% can be achieved by careful mixing),

the $^{14}N/^{15}N$ ratios obtained after combustion at 550–560°C for 3–4 h agree satisfactorily with those obtained by the Kjeldahl–Rittenberg method. In work on grain analysis, a check was made in which the $^{14}N/^{15}N$ ratios (about 2% excess ^{15}N) from grain burned to yield 70–80% of the total nitrogen, agreed completely with the ratios obtained from a combustion in which there was a 97% recovery of nitrogen.

The use of special glasses, such as Supremax or Pyrex 1720 with softening points as high as 650°C, has more disadvantages than advantages: Supremax glass is about three times as expensive as Pyrex and the necessary glass-blowing technique is more complicated since the glass has to be carefully and slowly heated to the working temperature to prevent breaking. The glass tends to react with lime, which results in cracks when the tubes are cooled afterwards. Pyrex 1720 is about 16 times more expensive to the authors than normal pyrex and tubes of the required dimensions are not all readily available commercially. The use of quartz is even more costly; and it reacts with lime above 600°C and cracks owing to the formation of calcium silicate.

Preparation of samples for emission spectrometry[48–50,53,59]. Since much less material is required for emission spectrometry measurement than for mass spectrometry, the direct conversion of nitrogen from a sample should be done only when no subsampling error will be introduced. As the nitrogen content of the sample should yield a pressure of 3–5 torr in the discharge tube, it is necessary to know the approximate content of the sample to at least $\pm 20\%$. If homogeneity cannot be guaranteed at the sample size rquired for this method, it is necessary to take a much larger amount, convert it to nitrogen and take an aliquot.

The appropriate amount of sample in solution or suspension is placed in a quartz capillary (1.5 mm o.d. and 0.8–0.9 mm i.d.), dried at 40–50°C, and inserted into the discharge tube together with a 7–10 mm long copper oxide wire (1–2 mg) and a calcium oxide briquette (3 mg CaO). To prevent mechanical disintegration of the briquette when it absorbs water, CO_2, HCl, *etc.*, it should be briquetted[59] with alumina in a 1:1 mixture by applying a pressure of about 10 kg cm^{-2}. The discharge tube is cleaned by heating with a hand-torch under high vacuum conditions as described on p. 23. The copper oxide in the tube is heated simultaneously but only to a maximum temperature of 650°C, otherwise oxygen will be released. Calcium oxide has to be activated by pre-heating to 1000°C to decompose any $CaCO_3$; if it is not heated adequately, samples with a ^{15}N abundance below 1% may yield 5–10% (relative) high spectral values owing to interference by carbon dioxide. During the baking-out process of one end of the tube, the sample-holding capillary is moved to the cool end to prevent destruction of the sample while heating; when the other end of the tube is heated, the sample is moved to the end already baked out. After the tube has cooled and been sealed off with the hand torch, the sample is burned at 850°C for 30 min. In the case of hard glass tubes, activation of the CuO and CaO can only be made at about 500°C because of the softening of the glass. The final combustion temperature for Pyrex is 560°C and for Uviol 440°C, heating being continued for 4 h in both cases.

During the preparation, combustion and storage of samples, contamination may occur by incomplete oxidation to nitrogen, air leaks during sealing, combustion or storage, and release of nitrogen from CuO and CaO when these chemicals and the tube walls have been insufficiently degassed.

With this method, the isotope ratio can be determined in 1–2 μg of nitrogen. When smaller quantities of nitrogen are used, however, the discharge either does not occur or it is of such short duration that sensitivie measurement is impossible. This is due to the relatively fast removal of the nitrogen molecules from the gas phase and implantation in the walls of the tube under the influence of the electrodeless discharge. However, these difficulties can be to some extent overcome by adding certain noble gases to the tube; isotopic ratios can then be determined on samples down to 0.2 μg of nitrogen[48].

All the noble gases sustain a discharge in the plasma of small amounts of nitrogen, but to different extents. The two extremes, helium and xenon, however, are the most interesting. In the presence of xenon, the nitrogen discharge is relatively weak (the ionization potential of xenon is lower than that of nitrogen) but lasts a relatively long time. In the presence of helium, the nitrogen discharge is very intense, but lasts no longer than with nitrogen alone. These results can be interpreted as meaning that xenon is adsorbed on or implanted in the quartz walls more readily than nitrogen and hinders the uptake of the nitrogen. Helium which is not readily taken up by the quartz does not delay nitrogen adsorption, but as its ionization potential is higher than that of nitrogen, it intensifies the nitrogen spectrum by a process of energy transfer. It is therefore advantageous to use both properties to give better nitrogen discharge conditions. Merely coating the walls of the tube with adsorbed xenon and using a helium–nitrogen gas mixture is insufficient, as the discharge last only about 3 min, but adding 2% by volume of xenon to the helium (in addition to the xenon coating of the tube) enables the discharge to be measured for 10–15 min which is adequate. The following procedure was therefore developed.

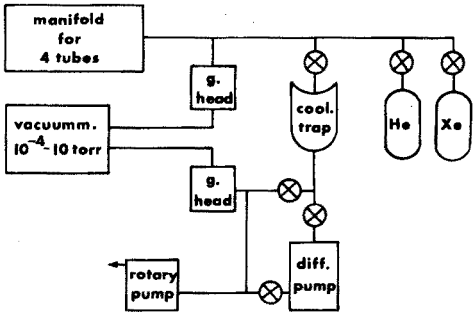

Fig. 22. High-vacuum line for the preparation of electrodeless discharge tubes with noble gas.

The high-vacuum line used is shown in Fig. 22. After removal of adsorbed gases from the walls of the quartz discharge tube, degassing of copper oxide and activation of calcium oxide by heating with a hand torch, about 5 torr of xenon is introduced into the tube. The tube is flamed for about 5 min and cooled to room temperature. During this treatment, remaining traces of impurities on the walls exchange with the xenon which itself becomes adsorbed. At the same time, the chemicals are treated in the same way as the glass walls; the temperature for copper oxide should not excced 650°C. The capillary holding the sample is always moved to the cool part of the tube to prevent disintegration of the sample. The xenon still remaining in the gas phase is pumped out and 10 torr of helium mixed

with 2% xenon is introduced. The tube is sealed off and the sample combusted. When this method is used, the $^{14}N/^{15}N$ ratio can be determined in as little as 0.2 μg of nitrogen.

Total nitrogen determination before mass spectrometric isotope detection[60,61]

In the modified Dumas method, if it is assumed that the total nitrogen in the sample is converted to nitrogen gas and all other gases formed are absorbed by the lime, the pressure of the nitrogen can then be taken as a measure of the total nitrogen content of the sample. The tube has only to be crushed in an evacuated chamber of known volume and the pressure measured to obtain the nitrogen content of the sample.

This method works very well with inorganic and simple organic compounds but not with biological materials of a more complicated nature, e.g. plant material. For most biological samples, combustion is not complete. Tarry and carbonized products are formed around the sample particles especially with grain (starch) products because the combustion temperature of 570°C is relatvely low. The particles are coated with tarry material and the enclosed material remains unoxidized. Moreover, hydrocarbons are found in the gas phase after cooling. By more careful mixing of the copper oxide and plant material, the total nitrogen yield increases from 70–80% to 75–90%. This result confirms the findings of Simon *et al.*[62] that copper oxide at 650°C has too low a vapour pressure to oxidize organic material completely; only particles in close contact will be oxidized. In the IAEA laboratory a rotary sample holder has been developed; this can be inserted in the muffle furnace so that during the combustion sample particles have a better chance of coming in contact with the chemicals in the tube. On cooling, the rotation (about 10–15 r.p.m.) is continued to assist the rapid absorption of oxygen, water and carbon dioxide. Another advantage of this device is that the rotation evens out any temperature gradients, and an oven temperature of 570°C can be used without risking softening of the pyrex.

It has also been established that the replacement of 50% of the copper oxide by Cuprox results in a higher nitrogen conversion and a reduction in the hydrocarbon content of the gas phase. Cuprox consists of copper oxide containing platinum catalyst on alumina (Coleman reagent). Further improvements can be obtained by heating samples overnight at 570°C (12–15 h) and by adding more oxidizing power in the form of potassium perchlorate to the mixture; under such conditions, even starchy materials can be oxidized to an extent of 97–100%. Results with a relative standard deviation of ±3% were obtained, which is very similar to the deviation obtained by the Kjeldahl method on plant products[63]. Potassium perchlorate is preferred to other oxidants (*e.g.* PbO_2, MnO_2) as the AR grade contains only 0.0005% N impurity. It has previously been used successfully by Simon *et al.*[62] who oxidized organic material in milligram amounts (10–20 mg). Inorganic and simple organic compounds could be determined with a relative standard deviation of ±2% per single measurement.

Sample preparation[60]. A Pyrex ampoule (see p. 24) is filled with an amount of sample corresponding to 1–4 mg of nitrogen. Inorganic compounds are burned with 0.4 g of copper oxide (or 0.4 g of copper in the case of nitrates or nitrites) and 0.5 g of lime. Simple organic compounds like amino acids, pyridine, *etc.* are oxidized

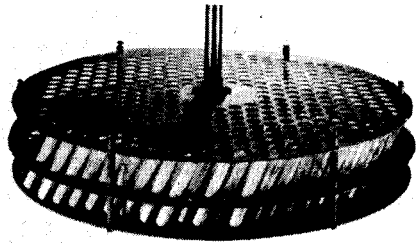

Fig. 23. Rotary device without cover plate.

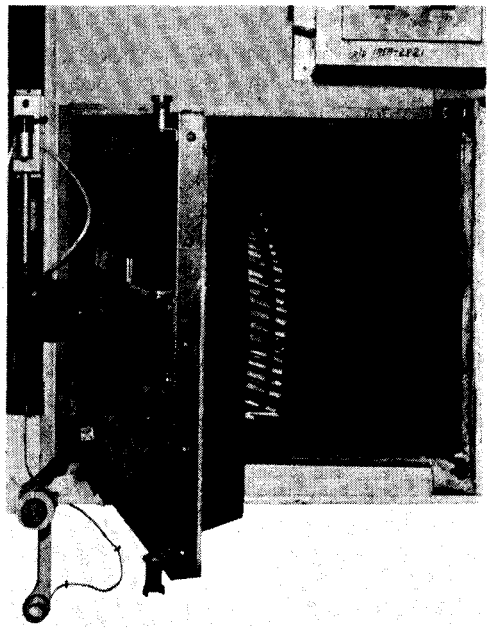

Fig. 24. Rotary device with the cover plate in the open furnace.

with 0.8 g of copper oxide–Cuprox mixture (1 : 1) and 0.8 g of lime. In the case of more complex matrices, such as straw, green plant material and grain, 0.15-g samples are oxidized with 1.6 g of CuO–Cuprox (1 : 1) and 1.5 g of lime. For straw and green material, 0.05 g of potassium perchlorate is added; for starchy material, 0.12 g should be used. The sample to be analysed is weighed into the tube but the other reagents can be added from measuring cups. The tubes and their contents are evacuated (see p. 000), and care must be taken to prevent loss of the sample particles with the air stream caused by opening the stopcock to the vacuum too quickly. After being sealed off, the tubes are placed in a rotary device (Fig. 23) and put into the oven (Fig. 24). Green plant material and straw are completely burned after 7 h but starch-containing samples such as grain need 12–16 h. The combustion temperature is always 570°C.

Pressure analysis. The pressure of the generated nitrogen gas is measured after the sample tube has been crushed in an evacuated chamber of known volume or a volume previously calibrated by nitrogen samples of known nitrogen content.

The inlet system of the mass spectrometer can be used for this pressure analysis. The pressure can be read from a mercury manometer normally connected to the inlet system, or by a membrane instrument or by capacity pressure-meter.

The sample tube is placed in the chamber, which is then evacuated, and the pressure is recorded after the tube has been crushed and the gas has expanded.

Mercury manometers have the disadvantage that false readings may be obtained when the glass surface becomes greasy or the mercury becomes oxidized. Moreover, the pressure must be within a previously known range (test range), otherwise the standard volume has to be corrected when an increase or decrease takes place owing to higher or lower pressure of the nitrogen samples in the standard volume.

A diaphragm manometer (p. 7) was found to be unsuitable because of non-linearity in the lower pressure range. A micro-manometer (capacity torr-meter) works with optimal accuracy only within a certain pressure range so that samples with a very low or high pressure have to be repeated using more or less material to obtain a suitable pressure; the pressure can be read directly or via a recorder.

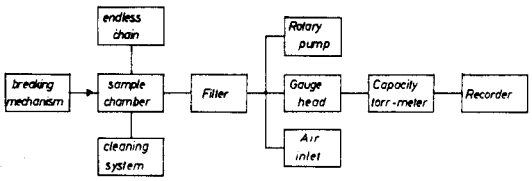

Fig. 25. Block diagram of the automated nitrogen analyzer.

In the IAEA laboratory, a special crushing device connected to the inlet system of the mass spectrometer is in use. Magazines with a capacity of 12 and 36 sample tubes are available. By rotating the magazine in the evacuated chamber one sample tube after the other can be crushed by an electro-magnetic driven metal bar. As the volume increases after each tube is crushed, a correction for each position has to be made. When a constant volume is desired, a system similar to that of the automatic nitrogen analyser can be adapted. This system has the disadvantage that after the crushing of each tube, the background has to be pumped down from atmospheric pressure.

The automatic nitrogen analyser consists of the following parts: sample changer (endless chain), sample chamber and breaking mechanism, vacuum system, filter and manometer, cleaning system, and control system (Fig. 25). The sample changer is an endless chain of open ended plastic tubes where 200 samples can be stored. It is driven stepwise by a latch mechanism and synchronous motor, over a hole in the base-plate which allows the glass tube containing the sample to fall into the sample chamber. This consists of an aluminium cylinder with two flaps at top and bottom, an ampoule breaking mechanism and a connection to the vacuum system. The vacuum connection leads through a filter chamber, provided with a sintered glass disc and quartz wool to a three-valve system, one controlling the evacuation of the chamber, one to return the chamber to atmospheric pressure and the third to control the connection to the manometer. The cleaning system ensures the removal of the broken ampoules and the residues of the combustion

mixtures, while the control system coordinates the different mechanical and electrical switching sequences. Figure 26 shows in a cycle diagram the different working steps of the instrument. The duration of one cycle is 4 min. One of the main design problems of the instrument was to solve the assembly of the three valve system, the filter chamber, the manometer and the sample chamber with a total volume of approximately 60 ml.

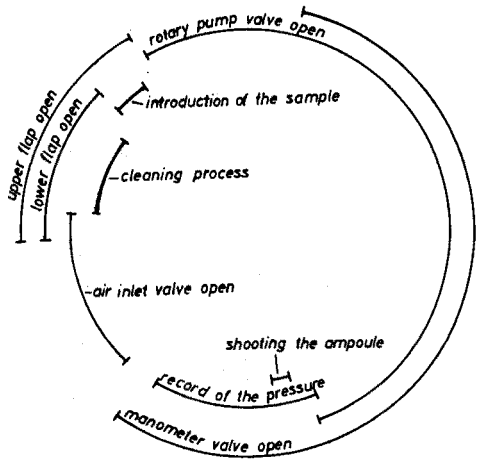

Fig. 26. The working cycle of the automated nitrogen analyzer.

The pressure measured is proportional to the nitrogen present in the sample. The total nitrogen can be calculated as follows:

$$\% \text{ N} = \frac{\text{amount of nitrogen}}{\text{amount of sample material}} \cdot 100 \tag{1}$$

or

$$\frac{K \times \text{pressure of nitrogen}}{\text{amount of sample material}} \cdot 100 \tag{2}$$

where K is a constant depending on the volume (about 60 ml) and the temperature of the system. The temperature and the volume can easily be kept constant, so that equation (2) can be used for the measurements when K is known. The manometer used has a working range of 0–50 mm Hg, and the recorder is best calibrated to give a 40-mm reading for 1 mg of nitrogen (50 mm Hg corresponds to a reading of 185 mm). Normally, 150 mg of sample material is used for the combustion. The maximum indication on the recorder allows the measurement of samples up to 4.6 mg of nitrogen or approximately 3% total nitrogen. For samples with higher total nitrogen amount, 120 mg or 100 mg of sample material is used so that 3.85% or 4.6% total nitrogen can be measured. Naturally for higher nitrogen contents, smaller samples can be used if homogeneity can be guaranteed.

MASS SPECTROMETRY

The various types of mass spectrometers are the single focusing, double

focusing, time of flight, cycloidal focusing and radio frequency (quadrupole) instruments. For work with nitrogen, a single focusing instrument is almost always used. The general principle has been outlined on p. 2.

The gas sample is introduced into the gas inlet system, where the pressure is reduced, the sample gas passes into the ion source, and the ions formed pass through accelerating slits and become an unresolved accelerated ion beam. In the magnetic field the ions travel in circular paths whose radii are functions of the ions mass charge ratio. The resolved beam is focused onto the detector and the discharge current is amplified and subsequently recorded.

During acceleration through a potential difference V, a kinetic energy eV is given to the ion. All ions having the same charge are accelerated to the same energy level. In a magnetic field with a direction of induction normal to the direction of motion, the ion beam will be deflected in circular paths.

The commonly used equation to describe the interaction is:

$$r = \frac{144}{B}\frac{MV}{n}$$

where r = radius of deflection in cm; M = mass of an ion in atomic numbers; V = voltage applied to the electrode of the ion source, in V; B = magnetic induction in gauss; and n = electronic charge of the ion.

Further information can be obtained in textbooks[64–73] or from some references[39,74,75].

Sample size

The sample size always depends on the volume of the inlet system and of the sample bottle. Examples for viscous and molecular inlet systems are given below.

Viscous inlet system. Volume of the sample bottle = 30 ml (V_b). Volume of the inlet system = 15 ml (V_{is}). Pressure in the inlet system after introduction of the gas sample = 40 torr (P_{is}). pV = constant (Ideal gas law)

$$V_b \cdot P_b = (V_b + V_{is}) \cdot P_{is}$$

Thus

$$P_b = \frac{(30+15)\cdot 40}{30} = 60 \text{ torr}$$

Recalculated to atmospheric pressure and at a temperature of 0°C, 60 torr in a volume of 30 ml gives

$$V_{atm} = \frac{V_b \cdot P_b}{P_{atm}} = \frac{30 \cdot 60}{760} = 2.37 \text{ ml}$$

Avogadro's law says that the volume of 28 mg of nitrogen is 22.4 ml at a temperature of 0°C and atmospheric pressure (760 torr).

$$\frac{22.4}{28} = 0.8 \text{ ml/mg } N_2$$

$$\frac{2.37}{0.8} = 2.95 \text{ mg } N_2$$

Thus, a minimum of 3 mg of nitrogen would be necessary for this type of inlet system.

Molecular inlet system. Volume of the sample bottle = 30 ml (V_b). Volume of the inlet system up to the standard volume = 90 ml (V_{is}). Volume of the reservoir = 3000 ml (V_r). Volume of the standard volume = 3 ml (V_{stv}). Pressure in the reservoir = 10^{-2} torr (P_r).

$$P_{stv} = \frac{V_r \cdot P_r}{V_{stv}} = \frac{3000 \cdot 10^{-2}}{3} = 10 \text{ torr}$$

$$P_b \quad \frac{(V_b + V_{is}) \cdot P_{stv}}{V_b} = \frac{(30+90) \cdot 10}{30} = 40 \text{ torr}$$

Recalculated to atmospheric pressure and a temperature of 0°C, 40 torr in a volume of 30 ml gives

$$V_{atm} = \frac{V_b \cdot P_b}{P_{atm}} = \frac{40 \cdot 30}{760} = 1.58 \text{ ml}$$

0.8 ml/mg N_2 (see above)

$$\frac{1.58}{0.8} = 2 \text{ mg } N_2$$

The ability to expand the standard volume more than once into the reservoir makes it possible to use only this 2 mg of nitrogen to obtain good conditions in the inlet system.

Techniques for sample introduction into the inlet system

When the digestion method is used for sample preparation, the Rittenberg flask may be utilized as sample bottle (Fig. 14). The ammonium salt solution is placed in one of the side arms, with the hypobromite in the other, and the liquids are mixed shortly before measurement; the ammonium salt solution should always be added to the hypobromite. During the reaction nitrogen is released. Then the liquid is frozen by immersion in liquid air, which reduces its vapor pressure and prevents unnecessary contamination of the sample. The gas is introduced into the inlet system. A cooling trap in the inlet system is required to remove the water vapor, which is always introduced in small quantities with the nitrogen. One disadvantage in using the Rittenberg flask as the sample bottle is that the storage of big bottles is very difficult and should only be done for short periods of time in a refrigerator. This kind of storage may cause trouble because the grease used for sealing becomes hard, which tends to destroy its vacuum properties.

The dry combustion method has the advantage that samples can be stored easily, and the chance that leaks will develop during storage is small. Figure 27 shows suitable sample bottles. The main problem with glass ampoules is how to destroy them under vacuum conditions; this may be done by different methods depending on the number of samples which have to be analyzed.

The sample ampoule (Figure 27a) should be used only when the number of samples is low, *i.e.* 10–20 analyses per day. The various methods for crushing the sample and passing the nitrogen gas into the inlet system are shown in Fig. 28; Fig.

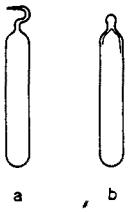

Fig. 27. Sample tubes for the modified Dumas method.

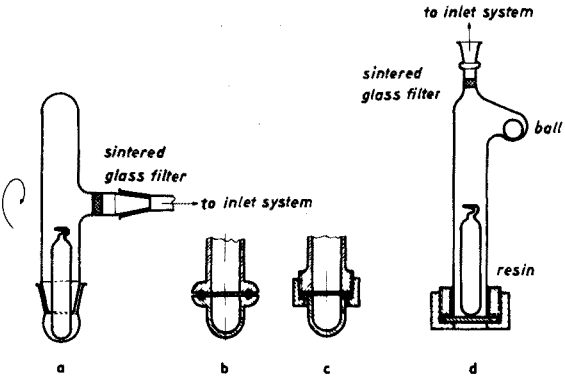

Fig. 28. Breaking devices for sample ampoules.

28(a) shows how the sample ampoule may be destroyed by turning the tube rapidly through 180°. The sintered glass filter is necessary to prevent dust particles of the sample from entering the inlet system. Figures 28(b) and (c) show other possibilities for breakage. Grease is used to make the vacuum seals in Fig. 28(a), while the two other devices have greaseless glass joints. Another technique is shown in Fig. 28(d); a metal thread is connected by a two-component resin to the glass body of the valve, sealing being achieved by the resin and an 0-ring, and the system is closed by a metal plate at the bottom; the iron ball is then moved by a magnet to break the ampoule.

The need to analyze a large number of samples led to the development[60] of a special device (Fig. 29) for breaking the ampoules shown in Fig. 27(b). The cylindrical magazine (1) holds 36 ampoules (2), and rests on the chamber base (3), which is covered with Teflon foil (4) for ease of rotation. The chamber base is inserted from below into the chamber (5) and fixed by a bayonet lock. A pin (6) makes it possible to turn the magazine in 36 steps. The rotary transmission is sealed by two Simmer rings (7). The piston (8), sealed by two Simmer rings (10), is impelled by an electro-magnet (9) at the ampoule to break it, and the gas is released. The gas then passes through the filter chamber (11) where quartz wool (12) and a sintered glass disc (13) prevent dust particles from entering the inlet system of the mass spectrometer. The sample cylinder is moved from one position to the next by a synchronous motor (14), connected to the semi-automatic inlet system. Figure 30 shows a semi-automatic inlet system. The ampoule-breaking device can also be used with manual operation.

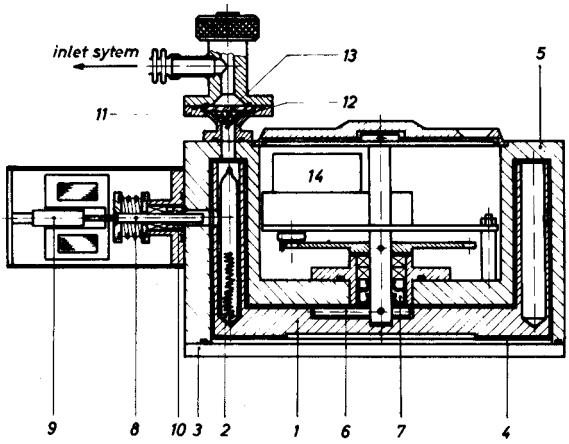

Fig. 29. Cross-section of a multiple gas–sample holder for the inlet system of a mass spectrometer.

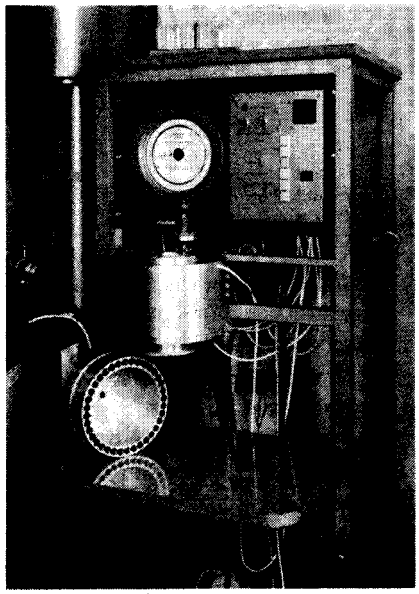

Fig. 30. Semi-automatic inlet system with a multiple gas sample holder.

When intensities must be measured at more than one m/e position, scanning is necessary. Scanning can be done by varying the accelerating voltage of the lens system of the ion source; for instruments with a permanent magnet, this is the only technique available to focus more than one m/e onto the collector; increasing values of m/e are focussed as the source accelerating voltages decrease. If an electromagnet is used, the accelerating voltage can be kept constant and sweeping can be done by changing the magnetic field by varying the coil current of the magnet; m/e increases with increasing magnetic field. A typical scan for enriched nitrogen is shown in Fig. 31. Scanning is mainly done when a single collector is used as detection unit. For a double collector system or a photoplate, the accelerating voltage and the magnetic coil current are kept constant.

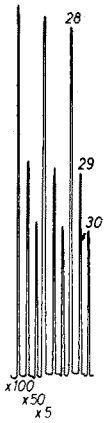

Fig. 31. Typical scan of enriched nitrogen.

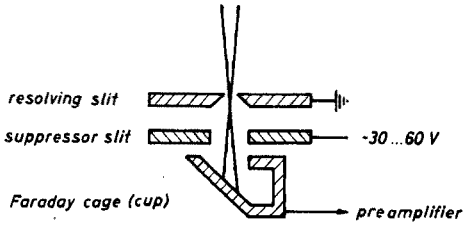

Fig. 32. Single collector.

Single collectors. The single collector (Faraday cup collector) is commonly used. Figure 32 shows the principle. The ion beam passes through the slit of the earthed resolving slit; frequently, the slit width can be varied to ensure good resolution for higher m/e values. The ion beam passes to the suppressor slit and is collected in the Faraday cup. The charge of the ion beam is amplified by a preamplifier and a normal d.c. amplifier. The suppressor slit is kept at a potential of -30 to -60 V to ensure that no secondary electrons ejected from the collector are recollected, which would result in too large an ion current. The signal from the d.c. amplifier is recorded as a measure of the intensity of the beam at the m/e value collected. At $m/e=28$, the beam can contain CO and C_2H_4 as well as nitrogen, hence the background must be measured before the sample is introduced; this allows the unwanted components of $m/e=28$ to be corrected for, provided that they are not present in the sample. Figure 33 illustrates the mass spectrum of a nitrogen sample. The different m/e values of ions likely to be encountered in an analysis of nitrogen gas are shown in Table VI.

The calculation of the nitrogen-15 atom-% from this information is described in Appendix 2.

During successive measurements of one sample, the intensity of the peaks decreases steadily. In order to allow for this decrease, the nitrogen-15 %-abundance can be calculated as follows: by means of a straight edge, successive peaks of 28, 29, and 30 are connected, and the peak heights are measured as shown in Fig. 34. In this way the measurements correspond to peak heights, where each isotope was measured at the same time.

TABLE VI

POSSIBLE *m/e* VALUES IN ANALYSIS OF NITROGEN

m/e	*ion*	*m/e*	*ion*	*m/e*	*ion*
12	$^{12}C^+$	16	$^{16}O^+$, $^{16}O_2^{2+}$	30	$^{15}N_2^+$
14	$^{14}C^+$, $^{14}N^+$, $^{14}N_2^{2+}$	17	$^{16}OH^+$	32	$^{16}O_2^+$
14.5	$^{14}N^{15}N^{2+}$	18	$^1H_2{}^{16}O^+$	40	$^{40}Ar^+$
15	$^{15}N^+$	28	$^{14}N_2^+$, CO^+, $C_2H_4^+$	44	$^{12}C^{16}O_2^+$
		29	$^{14}N^{15}N^+$, HCO^+, $C_2H_5^+$		

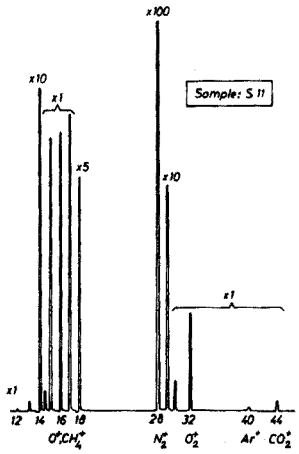

Fig. 33. Mass spectrum of an ashed plant material sample (modified Dumas sample).

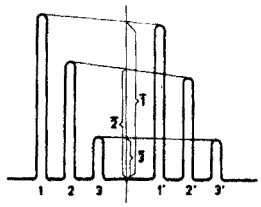

Fig. 34. Evaluation of measurements.

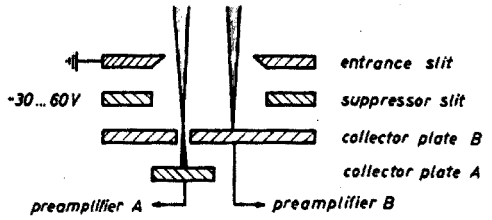

Fig. 35. Double collector.

Double collector. The double collector method normally requires a double inlet system to introduce alternately a standard and a sample to the ion source; the

principle is shown in Fig. 35. The ion beam of the isotope with the lower intensity is focused on collector plate A, while the ion beam of the other isotope is focused on plate B. The discharge of each beam is transferred to the corresponding preamplifier and d.c. amplifier. For measurement, the output signal of amplifier B is reduced by means of a decade potentiometer until the full signal of amplifier A has the same value; a galvanometer or recorder may be used to check the balance of the two signals, the deflection of a decade potentiometer being proportional to the percentage abundance. If the difference between the ratio of a standard and the sample is very small, it can be read directly on the recorder, but if the deflection is more than full scale, a change of one or more decades may be required to obtain a reading on-scale. In any case, calibration for this deflection is necessary; this is shown in Figure 36.

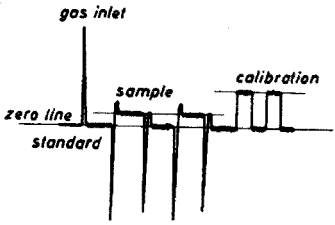

Fig. 36. A double collector measurement.

The principal advantages of the double collector method are that samples with very small differences in isotopic ratio can be measured much more precisely than with a single collector, and that fluctuations in the ion source can be compensated for, because all isotopes of interest are measured at the same time.

EMISSION SPECTROMETRY

The determination of the $^{14}N/^{15}N$ ratio by emission spectrometry is based on an isotope effect, *i.e.* the mass of the molecule affects the wavelength of emission lines, in this case in the ultra-violet region. The necessary excitation is usually provided by high-frequency discharge. The gas is enclosed in an electrodeless discharge tube and is excited by an external source (microwave or high-frequency power generator in combination with its electrode, antenna or resonant cavity). As the nitrogen for analysis is in a small closed tube, the amount needed for the analysis can be as low as 1–10 μg. Since the excitation is in almost all cases non-destructive, the analysis can be repeated many times. The emitted radiation is resolved in a monochromator and the light intensities corresponding to the different wavelengths are detected by a photomultiplier and amplifier system and finally recorded. The intensities of certain lines of the three different nitrogen molecules ^{14}N–^{14}N, ^{14}N–^{15}N and ^{15}N–^{15}N are used as a measure of their relative concentrations.

The sample size of the order of 1–10 μg can be further reduced to 0.2 μg with the aid of noble gases (see later). It is therefore possible to determine the ^{15}N content of very small amounts of nitrogenous material, *e.g.* spots of chromatograms (paper, thin layer, columns *etc.*), fractions separated by amino-acid analyzers and electrophoresis apparatus, or small individual samples (seeds, excised organs of small animals etc.).

The cost of adequate emission spectrometric ^{15}N detection equipment is about 1/3 to 1/2 of the cost of the mass spectrometer. However, as the analysis is carried out on μg amounts, interference from all kinds of contamination during the different steps is a major problem.

The standard deviation involved in emission spectrometry is $\pm 3\%$ for a single measurement, which is higher than for mass spectrometry where it is only about 0.5%. However, the sampling error of most biological samples exceeds 3%, so that the precision of the emission spectrometric method is generally adequate.

The emission spectrometer can therefore have two different purposes: (i) as an alternative to the more expensive mass spectrometer; and (ii) for the isotope analysis of samples available in μg amounts only.

Theory of molecular spectra

Isotopic analysis is possible by emission spectroscopy because isotopic atoms and molecules differ slightly in their respective energy levels.

An atom can incorporate energy by raising one or more electrons to a higher energy state, *i.e.* to a shell more remote from the nucleus. This absorbed energy will differ from one isotope to another and when the electron returns to the former energy state(s), the energy difference is emitted in the form of electro-magnetic radiation of distinct wavelength, thus forming an atomic or line spectrum where each line corresponds to a discrete energy difference. The energy difference for identical transitions of isotopes amounts to some hundredths of a nanometer.

With molecules, and only di-atomic ones will be considered here, there are five ways in which energy can be incorporated[76], but only three are of interest for the present spectroscopic purpose, namely, electronic energy, vibrational energy, and rotational energy.

The incorporation of energy may be by

(i) raising one or more electrons to a higher orbital similar to the case of atoms,

(ii) increased vibration (oscillation) of the two atoms along the inter-nuclear axis, and

(iii) increasing the rotation of the molecule around an axis passing through the center of gravity perpendicular to the inter-nuclear axis.

Each energy change involved in the present process can be explained by a combination of these three kinds of energy storages.

A transition between two electronic states including the vibrational transitions would show a line spectrum as in case of atoms, but superimposed in each vibrational transition are all allowed rotational levels which have much smaller energy differences. The whole constitutes an electronic band spectrum, though not every band is equally probable, so that some are more intense than others. Each band therefore represents a transition from a vibration state in the excited electronic state to one in the ground state with its associated allowed rotational transitions. In the case of nitrogen, the O–O band has the greatest intensity (Fig. 37) in the band system of the electronic transition $C(^3\Pi_u)$–$B(^3\Pi_g)$ (also called 2nd positive group)[77].

A band observed with a normal instrument shows one end sharply defined and more intense and the other more diffuse and of lower intensity, called the band head and band shade respectively. Bands are said to be shaded or degraded to the

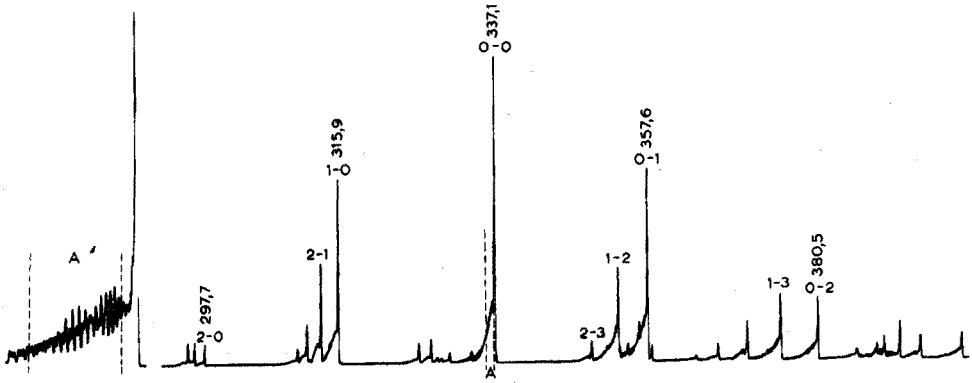

Fig. 37. The nitrogen spectrum between 400 and 290 nm recorded with a Hilger–Watts Monospek 600 (slit widths 0.06 nm, slit heights 1 mm, scanning speed 2.5 nm min^{-1}). (A) shows the rotational lines of the shade when the resolution is increased by reducing the slit width (slit widths 0.015 mm, slit heights 1 mm, scanning speed 0.25 nm min^{-1}).

infrared or ultraviolet, the latter being the case with nitrogen. With higher resolution, 2 or 3 series of rotational lines called R, Q and P branches can be observed.

The mass difference between isotopic molecules manifests itself mainly in the vibrational and rotational energies (as moments of inertia are involved) and the corresponding wavelengths of the emitted light. The isotope shift for an O–O vibrational transition is zero or small (in the case of nitrogen-14–14 and nitrogen-14–15 it is only 0.011 nm) but the difference becomes greater with increasing order of the vibrational transition. At the same time the intensities of the bands decrease rapidly, so that a compromise must be made between increasing isotope effect and decreasing intensity. In the case of nitrogen, the 2–0 transition at 297.7 nm for $^{14}N_2$ has been generally chosen[51,78–81]. This transition has the additional advantage that there are no interfering bands from impurities except for carbon monoxide which has one at 297.6 nm[82].

If the same electronic transition probabilities are assumed for the isotopic molecules, the intensities of the band heads (P-branch) can be used as a measure of the isotopic molecular concentrations. Of course, the rotational bands also exhibit isotope effects so that the isotopic bands differ slightly, but these effects only influence very precise evaluations. The wavelengths of the band heads of the three isotopic molecules of nitrogen are 297.7 nm for $^{14}N_2$, 298.3 nm for $^{14}N^{15}N$ and 298.9 nm for $^{15}N_2$.

The $^{14}N/^{15}N$ ratio determination by emission spectrometry with electrodeless discharge tubes

The excitation of nitrogen gas by electrodeless discharge by means of microwaves (high frequency). For the necessary excitation, the gases in a closed system were originally excited in Geissler tubes, but these tubes are inefficient and quite complicated and costly to prepare. The most convenient method is the electrodeless discharge where gases are excited by microwaves in the MHz frequency range. Microwave discharge has found increasing application, as this discharge source has

many attractive characteristics: (i) it can produce a high degree of ionization, dissociation and excitation without undue heating of any background gas; (ii) no electrodes are necessary so that the reaction tubes are free from contamination and less subject to damage; (iii) the source has no dangerous high-voltage contacts.

High frequencies from 13 to 2450 MHz have been used and there are different opinions about the best frequency. Broida and Chapman[83] stated that 150 MHz allows a wider pressure range for the nitrogen gas. Leichnam and Capitini[84] found, when working with atomic spectra with some thousand MHz, a high background, broader lines and self-absorption. By lowering the frequency to a few hundred MHz the discharge operates at lower temperatures and pressures, and the disadvantages of the higher frequency decrease or even disappear. The advantage of using 2450 MHz for excitation is the longer life of the discharge by reducing "clean-up". This phenomenon is explained by the fact that the excited gas molecules strike the discharge tube walls with sufficient velocity to become fixed in or to the wall, but this is less pronounced at the higher frequencies, because of the shorter travel length of the molecule.

Microwave power generators specially designed for the excitation of nitrogen have a fixed frequency as well as a fixed power output, such as the IAEA-generator 100 MHz and 50 W[51], the Statron 27 MHz and 60 W[82], and the JASCO 13 MHz and 50 W.

Commercially available microwave generators all have a frequency of 2450 MHz and an adjustable power supply which has the advantage that operation at lower power increases the discharge lifetime of the tube. It was found[55] that with the cavities or antenna which will be mentioned later, 5–10 W is the minimum requirement to maintain the discharge, but a higher power (10–20 W) is adequate for a stable emission of radiation. Further increases of power above this level cause the plasma to expand into the discharge tube without a significant increase of the light intensity. To obtain optimal conditions in the case of a cavity (*i.e.* minimum reflected power from the cavity), a reflected power meter built into the generator is an advantage.

The transfer of microwave power from the generator to the sample is made by a coaxial cable connected to an antenna or resonant cavity or by electrodes built into the generator. The discharge tube is merely placed in a suitable position close to the electrodes (normally 2) and the power switched on.

The ideal device for the transfer of power is a cavity (also called a discharge, gas or resonant cavity or cavity resonator). The types recommended are the Evenson cavity with 1/4 wave and the Broida cavity with 3/4 wave, both at 2450 MHz. The latter should yield a more stable discharge[85,86].

When the tube is introduced into the cavity, the geometry and so the electric field change; in order to regain standing waves, the cavity must be tuned by turning the adjusting screws. In the case of the Broida cavity, some difficulties were experienced in starting the discharge and in tuning[55]; this could be eliminated by small alterations and then the tubes could be run at 20 W instead of 40 W[55].

An important point is the cooling of the plasma. Because of the heating during the excitation, a widening of the lines or bands occurs, causing poorer resolution. In addition, if a relatively stable temperature is maintained by the regulation of the cooling air, the pressure of the gas in the tube is kept constant, which increases the stability and lifetime of the discharge. In the case of nitrogen,

the tube is cooled preferably to such an extent that its outside wall at the height of the plasma does not heat above 50–60°C[55 80]. When the tube is not cooled, an apparent decrease of the % ^{15}N may be observed[87], which may be due to desorption or diffusion of the gas through the hot walls, as it is difficult to distinguish the effects[80].

Isotope detection by the emission spectrophotometer. Emission spectrophotometers are more suitable than emission spectrographs for ratios above hundred[88], which require a long and difficult measurement; the ratio for naturally occurring nitrogen with its ^{15}N isotope is 135.6. The development and evaluation of the photographic plates is also time-consuming.

The components of an emission spectrophotometer which are of importance in $^{14}N/^{15}N$ measurements are as follows[82,89]. Monochromator: The ability of a monochromator to resolve radiation of different wavelengths may be expressed in terms of the reciprocal dispersion. The maximum reciprocal dispersion which allows a sufficient resolution of the relevant lines of the nitrogen isotope spectrum is about 3.5 nm mm^{-1} at a wavelength of 298 nm. With this low resolution, the ^{15}N abundances must be calculated by means of a calibration curve made with standards of known ^{15}N % abundance (see below). With a reciprocal resolution of 2 nm mm^{-1} or less, the line intensities can be measured directly as it is possible to make a reasonable interpolation of the background.

Monochromators with quartz or NaCl prisms or gratings are all suitable provided they have sufficient resolution. An old spectrograph can be converted to a spectrometer by substituting a photomultiplier, amplifier and recorder for the photographic plate and providing a mechanical scanning device. Such an instrument has been operated satisfactorily in the IAEA Laboratory for the past 5 years[50,51]. A NaCl prism monochromator is cheaper than one with a quartz prism and is used in the commercially available Statron ^{15}N analyzer[53,82,90]; the crystal inside the monochromator must, of course, be kept dry. Grating monochromators have the advantages that dispersion is linear, that the luminosity is about 20 times higher, because of the shorter path length of the light beam and lower absorption by the ruled surface than by the prism and that the optical system is simpler. This usually results in a lower price for a grating with the same reciprocal dispersion as a quartz prism monochromator. The monochromator should have an automatic scanning device with a speed of 0.5–1.5 nm min^{-1}.

Another factor which can reduce the cost of a grating monochromator is that a diffraction grating, unlike a prism, also gives second order, third order, *etc.*, spectra depending on the grating. The wavelength of the higher order spectra will appear at wavelengths (λ) following the equation

$$p_1\lambda_2 = p_2\lambda_1$$

where p is the order of the spectrum. Thus 600 nm of the second-order spectrum appears at 300 nm of the normal or first-order spectrum. At the same time the peaks (lines or bands) are resolved nearly twice as well as each wavelength is doubled. This means that a coarser (cheaper) diffraction grating can be used when second-order spectra are used, the same resolution of the peaks being obtained. A disadvantage is that the higher order spectra decrease in intensity with increasing order, but the second-order spectrum intensity is still high enough (0.5% of the first order) to obtain a good measurement, as the operating voltage of the photomultiplier,

the slit width and height can be increased. To eliminate interfering bands in the case of nitrogen at 600 nm, a band pass filter which absorbs 100% of the radiation in the vicinity of 600 nm and transmits not less than 90% at 300 nm, is placed between the light source and monochromator.

Theoretically, this allows monochromators with reciprocal dispersions up to 6–7 nm to be used for the ^{15}N measurement. Photomultiplier: As the bands of interest for nitrogen analysis are in the ultraviolet, the following types are suitable: RCA 1P28, C31025B; Hamamatsu R456, R446, R106; and EMI 9781B, 9783B. The high-voltage supply for the photomultiplier must be highly stabilized with a maximum of about 1500 V $\pm 0.001\%$ and 100 mA, as the photomultipliers have a maximum of about 1250 V. Amplifier: This can be a d.c. or a.c. instrument. The ratio of the highest and lowest sensitivity level for both types of amplifiers for the full scale must have a value of about 100 as the natural abundance of ^{15}N expressed by the ratio of $^{28}N_2/^{29}N_2$ is 135.6. For nitrogen, a d.c. amplifier is sufficient, as the bands of interest are in the ultraviolet and are not too much affected by naturally occurring radiation.

An a.c. amplifier provides greater versatility (for use in other types of analyses). If an a.c. amplifier is used, a modulator or a chopper (electronic or mechanical) is necessary. This has the advantage that only the modulated signals are amplified and all the others rejected (dark current of the photomultiplier, stray light etc.) yielding a background which is 100 times smaller than that obtained with a d.c. amplifier. For more sophisticated units, the modulator is provided with a synchronous reference signal which is capable of driving the reference of a lock-in amplifier, so that only the modulated light independent of the pre-selected frequency is amplified.

Recorder: This should have a chart width of 200, or better 250 mm, and a response time of 1 s, which will suffice to scan the monochromator with a speed of 0.5–0.7 nm min^{-1}. For a speed around 1 nm min^{-1}, a response time of 0.5 s is required. The chart speed must be around 10–20 mm min^{-1}.

All these units are easily available and can be built together without difficulty at about the same cost as that of a commercially available complete ^{15}N analyzer, with the advantage that the same equipment can be used for many other analytical purposes[112].

Measurement. The discharge or sample tube is inserted between the electrodes of the microwave power generator, its antenna or resonant cavity to excite the nitrogen gas sample. The air cooling is switched on, the high frequency applied and the discharge started with a spark from a Tesla coil. In case of a cavity, the maximal power uptake from the power source and the minimal reflected power can be obtained by tuning with the screws of the cavity.

The emitted radiation is focussed by means of a quartz lens onto the entrance slit of the monochromator. With an a.c. amplifier and a mechanical chopping device, the latter is placed immediately after the light source to ensure that only this specific light is modulated and later amplified.

As the wavelength calibration of a monochromator is not always exact, it is necessary to find the precise positions of the three bandheads of $^{14}N_2$, $^{14}N^{15}N$ and $^{15}N_2$. For this a standard sample of 20–50% ^{15}N abundance is used. With a d.c. amplifier, a standard sample of natural abundance is necessary to find the optimum between a strong signal of the weak $^{14}N^{15}N$ line and a low background of the

spectrophotometer. This can be obtained by adjusting the entrance and exit slit widths and heights, the high voltage of the photomultiplier and the amplification. Similarly, the optimal conditions for good resolution and strong signal must be established. For monochromators with a reciprocal dispersion of 2 nm mm^{-1} or less, the instrument must be adjusted for a strong signal with sufficient resolution that the correct ^{15}N abundances are obtained[55]; when the slits are too wide, the resolution can decrease to such an extent that the band heads of the isotopic nitrogen molecules influence each other, and low values for ^{15}N are then obtained.

The zero points of the amplifier and recorder are adjusted and the peak with the highest expected intensity is also adjusted to about 90% of the full scale deflection at the lowest possible sensitivity of the amplifier in order to keep the measuring error as small as possible. For the other peak, the optimal sensitivity must be determined. This selection of the sensitivity levels can be made by manual scanning or by test runs with automatic scanning.

The measurement, once started, can be repeated as long as the discharge continues but sometimes the number of replicates is limited by the tube life. If the tube is well prepared, the plasma has a pink colour. When the nitrogen pressure is above 5 torr, the colour of the plasma becomes whitish and the presence of water or carbon dioxide is indicated by a bluish white discharge. When the nitrogen pressure is too low, a weak cyclamen colour appears but changes rapidly to a weak or sometimes strong, red colour which can be attributed to the Palmer lines of hydrogen. In the latter case and in the case of too many impurities (H_2O and CO_2), the nitrogen bands disappear and often the discharge also ends.

Evaluation of the electronic–vibrational spectrum of ^{14}N and ^{15}N. The peak heights used as a measure for the relative concentrations of the nitrogen molecules are only part of the broad molecular band, *i.e.* the band head. As the bands in the monochromators used are not completely resolved, several corrections are necessary to obtain the true ^{15}N % abundance value. It is impossible to resolve the bands of the three nitrogen molecules completely, because when the reciprocal dispersion is decreased, the bands are resolved into their rotational fine structure lines. It can be seen from Fig. 38 that the rotational lines of the two different nitrogen molecules

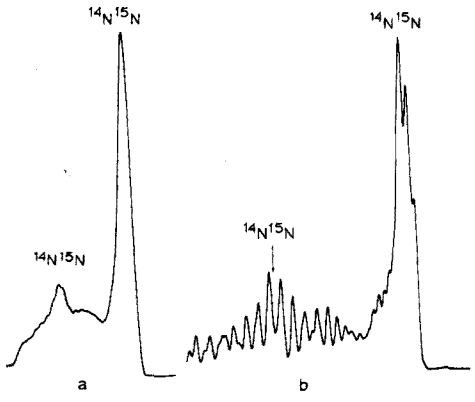

Fig. 38. Spectrum of a 96% ^{15}N abundance sample between 297 and 299 nm recorded with a Hilger–Watts Monospek 600. (a) Low resolution, slit width 0.05 mm, slit height 1 mm, scanning speed 0.5 nm min^{-1}. (b) High resolution, slit width 0.015 mm, slit height 1 mm, scanning speed 0.25 nm min^{-1}.

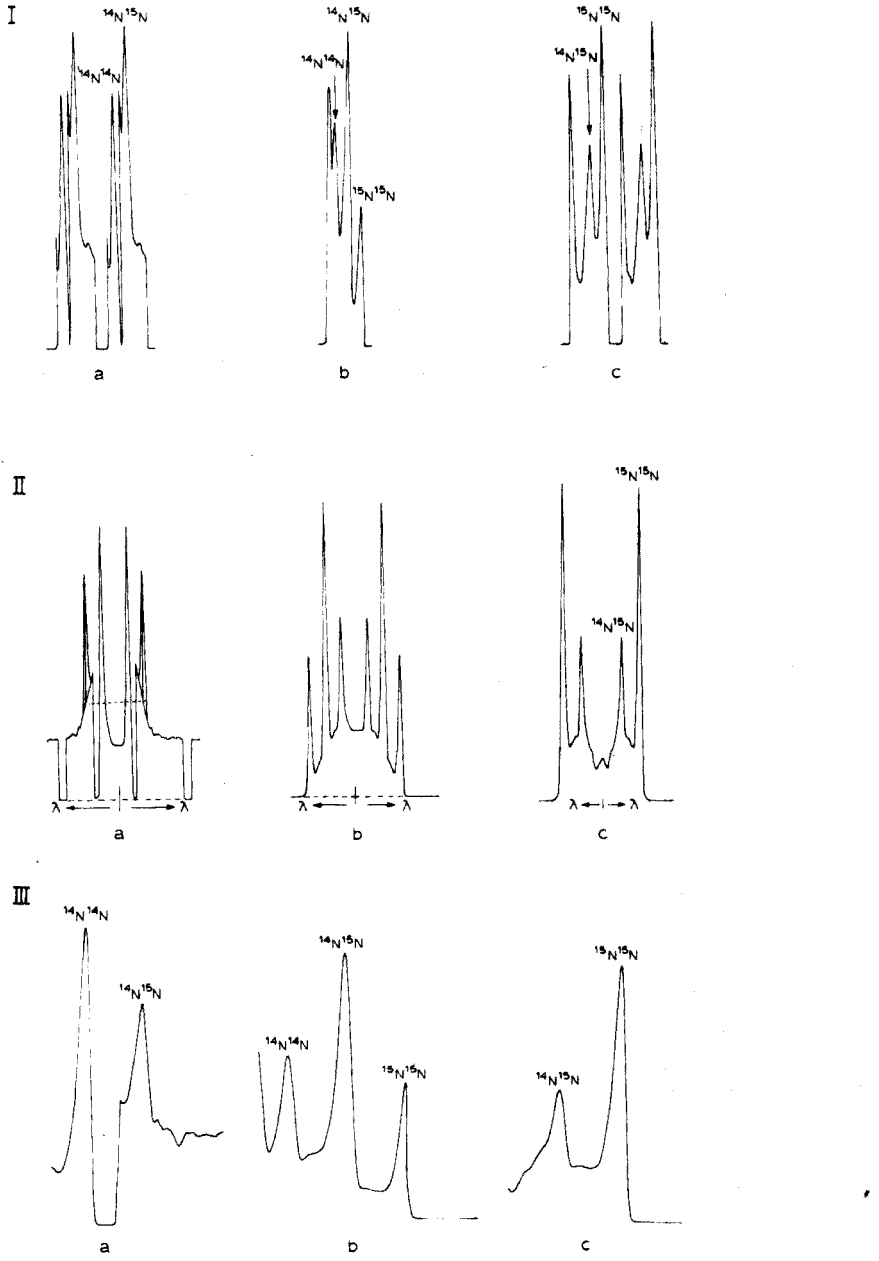

Fig. 39. Three samples (a) natural abundance nitrogen 1/50, (b) 52% abundance nitrogen 1/1, (c) 84% abundance nitrogen 1/1, measured with 3 different monochromators. (I) Mirror monochromator SPM 1 (Carl Zeiss Jena) with a reciprocal dispersion of 3.5 nm mm^{-1} with a NaCl Crystal UV 56 (NOI-4). (II) Hilger–Watts Quartz spectrograph E 724 adapted with a RCA 1 P28 photomultiplier[51] with a reciprocal dispersion of 2 nm mm^{-1}. (III) Hilger–Watts Monospek 600, 1200 lines/mm grating, blazed at 250 nm, adapted with a Hammamatsu R 446 photomultiplier.

overlap and may even coincide, thus producing similar difficulties with interpretation as with the bands.

The method of evaluation which must be applied depends on the reciprocal dispersion of the monochromator in use. When this is above 3 nm mm^{-1}, evaluation is made by means of a calibration curve; in the region of 2 nm mm^{-1} and better, the ^{15}N % abundance values can be calculated without calibration curves but with geometrical and arithmetrical corrections which are not possible for the poorer reciprocal dispersion spectra. An example of the results from three different spectrophotometers with different monochromators shows the differences in the recorded spectra (Fig. 39).

Evaluation when the reciprocal dispersion is about 3.5 nm mm^{-1}. The vertical heights of the peaks above the background are taken as a measure of the intensity of the bandheads, although one peak may be influenced by the presence of the others. The ^{15}N % abundance is calculated with these heights as described on p. 47, and the "apparent" ^{15}N values obtained are corrected by means of a calibration curve. This curve is prepared from standard discharge tubes of known ^{15}N % abundance, previously analysed mass spectrometrically and measured under the same conditions as the sample. At least one standard of similar ^{15}N % abundance as the sample should be measured on the same day as the sample. This method is with the Statron ^{15}N analyzer. The calibration curve is split up into four sections: 0.366–2.5%, 0.366–5%, 2.5–25% and 10–55%. Up to about 40%, the $^{28}N_2$ and $^{29}N_2$ peak heights are used for the calculation of the ^{15}N % abundance; above 40%, those of $^{29}N_2$ and $^{30}N_2$ are used.

It is necessary to investigate experimentally whether this method of evaluation or the following method should be used for instruments with monochromators with reciprocal dispersions between 3.5 and about 2 nm mm^{-1}.

Evaluation when the reciprocal dispersion is around 2 nm mm^{-1} or better (tested for 1.2 nm mm^{-1}). The peak heights measured can be used after geometrical or arithmetrical corrections for background in the normal formulae given on p. 47 to calculate the ^{15}N % abundance directly. Two effects are observed which make such corrections necessary.

(a) The band head or peak with smaller intensity sits on the shoulder of the following bigger one. This has noticeable effects when the intensity of the bigger peak is three times or more that of the smaller.

(b) The band shade influences the following band head or peak noticeably when the intensity of the preceding peak is 1/3rd or more of the following band head.

The interaction of these two effects on methods of determining peak height has been investigated empirically[55]. Sources of known ^{15}N content were analysed and the results evaluated by various methods. A method was considered acceptable if it gave results within $\pm 3\%$ of the true value. The limits given were chosen, as experience has shown that this standard deviation is an average over a long period of time. No one method of evaluation was satisfactory for the entire concentration range. Figure 40 shows examples of the evaluation methods.

0.366–3.8 ^{15}N % abundance (Fig. 40(a)): As a measure of the intensity of $^{28}N_2$, the vertical height above the background is taken, and for the $^{29}N_2$ the vertical height above the interpolated background of the shoulder of the $^{28}N_2$ peak.

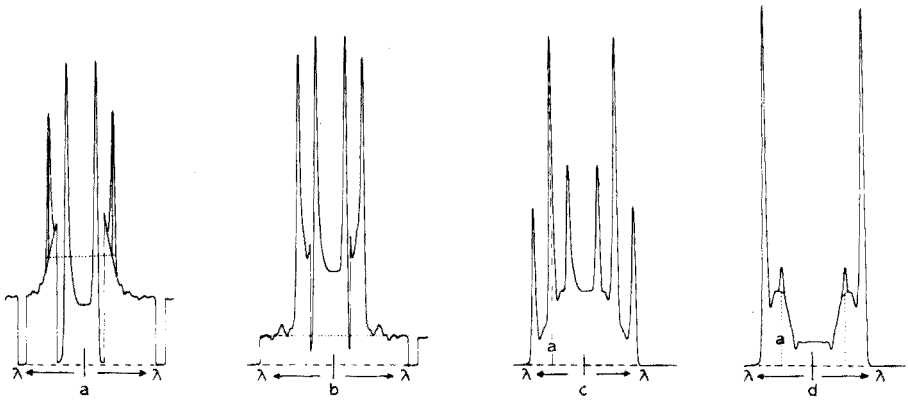

Fig. 40. Examples of the evaluation of the nitrogen spectra when the reciprocal dispersion of the monochromator is around 2 nm mm^{-1} or better. Spectra were recorded between 297 and 299 nm on a Hilger–Watts Quartz spectrograph E 724 converted to a spectrophotometer[51]. (a) Natural abundance: (----) background for $^{14}N_2$ peak; (· · · · ·) background for $^{14}N^{15}N$ peak; (——) interpolation of the background under the $^{14}N^{15}N$ peak. (b) 4.91% ^{15}N abundance: (----) background for $^{14}N_2$ peak; (· · · · ·) background for $^{14}N^{15}N$ peak. (c) 51.7% ^{15}N abundance: (——) background for $^{15}N_2$ peak, and $^{14}N^{15}N$ peak; (—a–) 20% correction for the $^{14}N^{15}N$ peak height from the $^{15}N_2$ peak. (d) 97% ^{15}N abundance: (----) background for $^{15}N_2$ and $^{14}N^{15}N$ peak; (· · a · ·) 20% of $^{15}N_2$ peak as a correction for the $^{14}N^{15}$ peak height.

Here the effect of the shoulder of the strong $^{28}N_2$ band head is dominant.

3.8–15 ^{15}N % abundance (Fig. 40(b)): The vertical height above the background for both $^{28}N_2$ and $^{29}N_2$ peaks can be used. Here the shoulder effect of the $^{28}N_2$ and the shading of the $^{29}N_2$ balance out. The $^{30}N_2$ peak, when detectable, can be estimated by the vertical height above the interpolated background of the shoulder of the $^{29}N_2$ peak, like the $^{29}N_2$ in the previous region.

15–45 ^{15}N % abundance (Fig. 40(c)): The vertical heights above the background of the $^{29}N_2$ and $^{30}N_2$ peaks are used. $^{28}N_2$ can be estimated, if required, by reducing the vertical height above the background of the $^{29}N_2$ peak by 20%. This corresponds to subtracting the contribution of the band shade of $^{29}N_2$ to the total height of the $^{28}N_2$ peak. As the $^{30}N_2$ band starts from the background it can be used even at this relatively low $^{30}N_2$ concentration together with the $^{29}N_2$ for the calculation of the ^{15}N % abundance. The shoulder effect of the $^{29}N_2$ and the shading of the $^{30}N_2$ balance out.

45–99.5 ^{15}N % abundance (Fig. 40(c),(d)): The vertical height above the background of the $^{29}N_2$ peak, reduced by 20% of the height of the $^{30}N_2$ peak, and the vertical height above the background of the $^{30}N_2$ peak are used. The band shade of $^{30}N_2$ raises the $^{29}N_2$ band head by 20% of the intensity of the $^{30}N_2$ band head.

Calculation of the ^{15}N % abundance. The calculation is made with the same formulae as in mass spectrometry. As the three isotopic molecules in the discharge are in equilibrium, only the 2-peak formulae are necessary for calculation of the ^{15}N % abundance.

In the range 0.366 to 14–15% ^{15}N the formula

$$\%\ ^{15}N = \frac{100}{2R+1} \text{ where } R = \frac{\text{intensity of 28}}{\text{intensity of 29}}$$

is adequate, but above these values the formula

$$\% \, ^{15}N = \frac{100}{R'+1} \text{ where } R' = \frac{\text{intensity of 29}}{2 \times \text{intensity of 30}}$$

should be used. Here as in the case of mass spectrometry, the peak height is a measure of the intensity, and the intensity is a measure of the relative concentration of the corresponding isotopic molecule.

The total intensity is obtained by multiplying the peak height by the sensitivity used: *e.g.*

$$R = \frac{18 \cdot 100}{14 \cdot 1}$$

where 18 is the peak height of the $^{28}N_2$, 14 is the peak height of the $^{29}N_2$, 100 is the sensitivity for $^{28}N_2$, and 1 is the sensitivity for $^{29}N_2$.

COMPLETE COURSE OF A MASS SPECTROMETRIC ANALYSIS

Kjeldahl–Rittenberg oxidation

A variation of the Kjeldahl method is chosen which is suitable for the material to be investigated. For example, for plant material by the method of McKenzie and Wallace[20]: 1 g of dried and finely ground (200-μm particle size) plant material is weighed into a 100-ml Kjeldahl flask, 6 ml of concentrated sulphuric acid is added, and the contents are mixed so that all material is in contact with the acid. The flask is placed on a hot plate which prevents the development of too much foam. After 10 min, when the liquid is uniformly black and the upper part of the flask is washed clean by the refluxing acid, the flask is removed and when cooled to 120–140°C, 30% hydrogen peroxide is added dropwise until the decomposition of the peroxide stops. The contents are then heated again. When the sulphuric acid starts boiling, the process is repeated until the digest becomes colourless and remains in this state. After cooling, 50–60 ml of distilled water are added together with a boiling bead and 1–2 drops of the Tashiro indicator. Then *ca.* 5 ml of 50% sodium hydroxide solution are poured carefully down the side of the flask to form a layer under the extract. The flask is connected to a distillation apparatus and shaken, and if an alakline medium is established, which is shown by the colour of the indicator, the distillation is started. If not, further alkali must be added. When the water starts condensing at the highest point of the distillation system, a further 10 min is allowed. Then the receiving flask is lowered and the distillation is continued for a further 3 min. The receiving liquid is 0.1 *N* or 0.05 *N* HCl or H_2SO_4; the normality depends on the amount of nitrogen in the sample and the accuracy of the analysis. After each distillation the apparatus should be cleaned by distilling 10–20 ml of ethanol to prevent cross-contamination. When the titration is finished, with the Tashiro indicator or another changing in the acidic pH range, the solution is acidified with 2–3 ml of 0.1 *N* HCl or H_2SO_4 and evaporated to about 5 ml to yield a nitrogen concentration of 1–6 mg ml^{-1}.

The Kjeldahl extract can of course be replaced by any other type of ammonia-separating reaction, *e.g.* from a Devarda distillation or from a process which separates ammonia only from specific nitrogen-containing groups.

For the Rittenberg reaction, 1–2 ml of the extract is pipetted into one arm of the Rittenberg vessel (Fig. 15) and 2 ml of alkaline sodium hypobromite solution (p. 19) in the other. The cap of the Rittenberg vessel is heated to about 40°C (with a hair dryer) and the male joint is greased with 4 parallel lines of high-vacuum grease along the joint. Then the cap is pressed firmly on the joint until the last air bubble has left the soft grease between the glass joints. During this operation the arm of the cap is held so that the inside of the container is aerated. After the grease has cooled, the vessel is connected to the preparation vacuum line, vacuum grease being used. The stopcock is opened slightly to reduce the pressure over the solution which allows the dissolved air to escape. Later, when the liquid starts boiling under reduced pressure and when the residue has cooled (by loss of heat of evaporation), the stopcock is opened fully. Normally after 10 min the extract is frozen, and the vessel under the cap is closed by twisting the container 180°; the stopcock of the vacuum line is also closed. The Rittenberg vessel is removed, the ice melted and the nitrogen gas generated by letting the extract flow into the alkaline sodium hypobromite solution, so that during the reaction, the medium is alkaline. After freezing out the liquid, which is divided again into the two limbs, the gas can be introduced into the inlet system of the mass spectrometer, or can be used to fill a discharge tube for emission spectrometric determination.

Introduction into the mass spectrometer. The Rittenberg vessel is hooked to the glass joint connection of the inlet system of the mass spectrometer while the two limbs are kept in liquid air. The air from the Rittenberg arm and joint is pumped out through the inlet system firstly by the preliminary vacuum pump and then by high vacuum. The measurement of background in the mass spectrometer at mass 28 (*i.e.* $^{14}N_2$) is started, until a value of 0.2–1% of full scale (depending on the accuracy required) has been reached. The needle valve between the inlet system and the mass spectrometer is closed and the nitrogen gas from the Rittenberg vessel is introduced into the inlet system by opening the Rittenberg flask (twisting the vessel under the cap by 180°). By carefully opening the needle valve, the nitrogen gas flows through a liquid air trap into the ionization chamber. Whether or not a reservoir which ensures a constant gas flow into the ionization chamber, should be used, depends on the precision needed for the analysis. Normally, a total volume of 0.5–1.5 l is suitable between the needle valve and ionization chamber. The use of a reservoir will affect the pumping time and therefore also the time required between two samples to obtain the desired background. The nitrogen gas is introduced until the recorder covers about 90% of the scale width at the lowest sensitivity step. Then the needle valve and the stopcock of the inlet system are closed. The next sample can then be connected, provided that the construction of the inlet system allows the removal of air without affecting the measurement of the sample in the other part of the inlet system. When the measurement is finished, the needle valve is opened and the gas of the sample that has just been measured is removed together with the remainder of air of the next sample, until the required background is established.

Modified Dumas method with a biological sample or its extract

Direct method. The finely ground sample (particle size around 200 μm) with approximately 0.5–4 mg of nitrogen is filled into a pyrex glass tube (see p. 17).

About a 100% excess amount of copper oxide and Cuprox (a 1:1 mixture) and calcium oxide (freshly heated to 1000°C) are added and the tube is connected to the vacuum line. In the case of plant samples, *ca.* 0.15 g of sample together with 1.6 g of CuO and 1.5 g of CaO are placed in the pyrex tube. The stopcock is opened carefully to prevent losses of the finely powdered material; the cover of the heavy inorganic layers on the sample material helps in this respect. After 5 min the stopcock is opened fully and pumping is continued for about 10 min. The tubes are sealed off at the restricted part with a two-flame hand torch; a single flame hand torch is more difficult to work with as the tubes collapse quite quickly and leakage has to be prevented. The combustion particles are then thoroughly mixed and the tube placed horizontally in the muffle furnace or in the rotary device mentioned (see p. 29). The optimal temperature is 570°C but when the temperature in the furnace cannot be kept constant, 560° or even 550°C is adequate. After 3–4 h at this temperature, the tubes are ready for analysis.

Combustion of an extract. A Kjeldahl extract or other type of extract (1–2 ml) containing sufficient nitrogen (0.5–4 mg) is placed in a pyrex glass tube (p. 17) and dried. The extract is dried at 100°C for aqueous solutions or at 85°C for alcoholic solutions. If the material might decompose at such temperatures, a vacuum desiccator or vacuum drying oven at a suitable temperature should be used.

The amounts of chemicals needed for the combustion are: for inorganic compounds, 0.4 g CuO and 0.5 g CaO; for organic compounds, 0.8 g CuO–Cuprox 1:1 and 0.8 g CaO. Nitrates or nitrites require reduction with 0.4 g of copper; 0.1 g of copper oxide is added to provide any oxidation necessary. The evacuation takes 5–7 min in this case and because of the absence of dust, the stopcock can be fully opened immediately. The tube is then sealed off and the contents mixed as soon as possible. The tube is placed in a horizontal position in a furnace and heated at 550–570°C (for 3 h). After cooling, the tube can be crushed to release the nitrogen gas for mass spectrometric analysis or a sub-sample may be used to fill the discharge tube for emission spectrometric analysis.

Introduction into the mass spectrometer. The sample tube is inserted into a crushing device which is part of the inlet system of the mass spectrometer. Multi-sample crushing devices have been developed capable of taking up to 36 samples (p. 34). The crushing device should be capable of being opened and cleaned well to remove glass splinters, chemicals, dust and ash from the previous samples. Care must be taken that any O-rings are cleaned and put back correctly to ensure a vacuum-tight seal. The sample tubes are placed into the numbered holes of the magazine which is inserted into its chamber. After closing by means of screws, the chamber is pumped out until the required background is reached. Then the needle valve between the sample holding device and the inlet system is closed and the tube crushed. By opening the needle valve, nitrogen is introduced into the mass spectrometer as described above. With a single-sample crushing device, this procedure must of course be repeated for every sample.

Mass spectrometric evaluation

As already described, the inlet system and the ion source of the mass spectrometer must be evacuated to check the background on *m/e* 28. The mass range of the instrument is adjusted for *m/e* 28 and the indication on the recorder checked. This

should be of the order of no more than a few % of the possible maximum. The sample gas is then slowly introduced until the recorder shows 90% f.s.d. The next step is to change the magnetic field or high voltage depending on the construction of the instrument, in order to carry out mass-scanning. During the scanning, the sensitivity of the recorder may have to be changed by attenuation or a similar device. For normal agricultural work, two full scans over the area of interest suffice, one scan being a complete record of all isotope peaks of interest. For standards and reference samples, 10 scans are made and the mean value calculated. After the measurement is finished, the inlet system and ion source of the instrument must be evacuated in preparation for the next sample. In the meantime, the calculation and evaluation of the records can be made. Figure 34 shows how the peaks of the different isotopes are evaluated; in all cases, two corresponding peaks are connected and the heights measured. To compensate for any variation during the measurement, the peak height measurement is done at one location. The peak heights have to be multiplied by the appropriate attenuation factor and substituted into the formulae on p. 58 for calculation of isotopic abundances. In the case of standard samples, the evaluation should be made from 10 scans, from which the standard deviation can be calculated.

Total nitrogen determination prior to mass spectrometric nitrogen-15 analysis

The preparation is the same as described above for the direct modified Dumas method or for combustion of an extract; the amount of sample must be known either by weighing, or for extract analysis, by pipetting a known aliquot into the tube. The amounts of chemicals needed (added with measuring cups) for combustion are:

for inorganic material, 0.4 g CuO (Cu for nitrates) and 0.4 g CaO;

for organic compounds, 0.8 g CuO–Cuprox (1 : 1) and 0.7 g CaO;

for material of complicated organic matrix (plant), 1.6 g CuO Cuprox (1 : 1), 1.5 g CaO and 0.05 g $KClO_4$;

for starch-containing material, *e.g.* grain, 1.6 g CuO–Cuprox (1 : 1), 1.5 g CaO and 0.12 g $KClO_4$.

After careful evacuation, the tube is sealed off and the contents are well mixed (vibrating mixer). The tube is placed in a rotary device for 7 h at 570°C. For starch-containing material, the combustion time should be 12–15 h.

For pressure analysis, the sample tube is broken after introduction into the crushing device and the sample nitrogen is allowed to expand as far as the needle valve of the inlet system. Pressure, room temperature and position of the sample (in the case of the special crushing device) are recorded, for calculation of the total nitrogen content of the sample.

COMPLETE COURSE OF AN EMISSION SPECTROMETRIC ANALYSIS

Kjeldahl–Rittenberg oxidation (diffusion technique)

When enough material is available, a normal semi-micro or micro Kjeldahl can be done (see above). The chemicals used must be checked for nitrogen impurities in order to correct for the blank. When an ultramicro Kjeldahl digestion has to be done, the interference of nitrogen impurities may be considerable. These impurities

can only be detected by means of isotopic dilution analysis, and the modified Dumas technique is preferable for such extremely small quantities of nitrogen, as contamination from chemicals is usually less than in the Kjeldahl method.

Diffusion methods may involve preliminary digestion of the sample to form ammonia or simply diffusion when nitrogen is already present as ammonia. As for the ultramicro Kjeldahl method, the chemials must be as free of nitrogen impurities as possible or the amounts of the impurities must be known quantitatively.

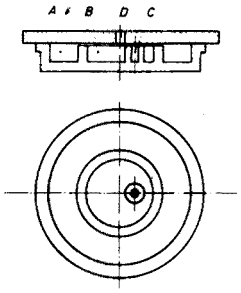

Fig. 41. Perspex Conway dish with an extremely small chamber (c).

For example, in the determination of amide–nitrogen from neutral amino acids, the paper strips from the electrophoresis containing neutral amino acids and amides are cut into small pieces and put into small glass tubes with 2 ml of 1.75 *M* sulfuric acid. These tubes are sealed like ampoules and heated in boiling water for 5 h to hydrolyse the amide[25,26]. After cooling, the ampoule is opened and the contents transferred to a Conway dish with a very small chamber (Fig. 41). For small volumes, the sample is added to compartment B, into which is poured 2 ml of 40% (w/v) sodium hydroxide through hole D, which is then quickly and tightly closed by a rubber stopper. Compartment C contains 30 μl of (1+9) hydrochloric acid, and on standing overnight, preferably slightly below room temperature, ammonia diffuses into C where it is trapped as ammonium chloride[91,92]. This solution can then be analysed for ^{15}N. Larger samples can be added to chamber A while B contains hydrochloric acid.

When enough sample is available, the Rittenberg reaction is carried out as described on p. 48. To ensure that all the dissolved air is removed during the evacuation on the preparation line, the solution in the 2 limbs is frozen out again with liquid air, after the ice formed during the evacuation on the preparation line for mass-spectromtric samples has been melted. Then the vessel is connected to the high-vacuum preparation line. For the emission spectrometric determination, the line is evacuated to 10^{-4}–10^{-5} mm Hg; the ice is melted and the reaction is made. This can be done, depending on the type of Rittenberg vessel, either directly on the line or after closing the cap and removing it from the line. If the container is removed, the air in the arm of the Rittenberg vessel must be pumped out after connection to the line. The gas is led into the precleaned discharge tube *via* a liquid air trap.

For small amounts of sample, the smaller type of Rittenberg vessel can be used; this takes 0.1–0.2 ml solution in each limb. The amount of nitrogen should be 50–300 μg depending on the volume of the transfer tubing of the vacuum line. As the Rittenberg vessel used in this process stays on the vacuum line, the removal

of air is made by freezing the liquid, pumping out the remaining gas, allowing the liquid to thaw and then repeating the cycle 3–4 times. The liquids are then mixed and after release of the nitrogen, frozen out, and the nitrogen gas is filled into a precleaned discharge tube at a pressure of 3.5 mm Hg. The pressure is regulated with a stopcock and indicated by a vacuum meter. When no pressure gauge is available, the amount of nitrogen formed must correspond, after expansion into the discharge tube, to a pressure of 3–5 torr which means that the amount of nitrogen in the extract has to be known to $\pm 20\%$.

The nitrogen gas can also be produed by a Dumas method as described above and the discharge tubes can be filled if a suitable crushing device is connected to the high-vacuum preparation lines. Before the tubes are connected to the vacuum line, they should be numbered and heated for 3 h to reduce the amount of absorbed gas on the surface. With Uviol glass, a temperature of 420°C can be used, with pyrex or Rasotherm, *etc.* 500°C, and with quartz 800°C. The tubes should be stored in a desiccator before connection to the vacuum line with black wax or by means of an 0-ring joint. If traces of water could reach the discharge tube (even when protected by a liquid air trap), a calcium oxide briquet of 2–3 mg should be introduced into the tube, before connection to the vacuum line. When evacuated, the tube is heated with a hand torch (oxygen–methane) until softening point of the glass is reached. After cooling, the nitrogen gas is expanded into the tube to give a pressure of 3–5 torr. The tube is then sealed off and is ready for analysis. When calcium oxide is used, it should be heated as high as possible (1000°C) immediately before addition to the tube, which is then sealed off, and placed in a furnace for 1–2 h at a temperature 20°C below the softening point of the material used, to ensure reaction with any water vapour. After 12 h (overnight), the tube is ready for analysis.

Modified Dumas method on the sample or its extract

For preparation of the discharge tube, the extract of a sample, its solution or suspension, is placed in the capillary of known volume so that after the combustion, the nitrogen content corresponds to 3–5 mm Hg of nitrogen in the discharge tube. For 0.25-ml quartz tubes 1–3 μg of nitrogen is necessary, and for 2.5-ml Uviol or pyrex glass tubes 7–15 μg of nitrogen necessary. The sample in the capillary is dried at 40–50°C on a hot plate with a plate for holding the capillaries slightly above the heater. The capillary with the dried sample inside is then inserted into the upper part of the discharge tube together with a copper oxide wire (1–2 mg) and 3–6 mg of a lime–alumina (1 : 1) briquet. The tube is connected to the high-vacuum line in a horizontal position and evacuated. The lower part of the tube is heated with the hand torch as described above, and after cooling, the capillary only is moved by tapping to the tip of the tube by turning the "comb" on which the tubes are connected to an angle of about 30° to the horizontal. Then the upper part which holds the CaO and CuO is heated to activate these reagents. If quartz tubes are used, the copper oxide is heated to a dark cherry red (600°C) and the lime to a bright white (1000°C). The lime should not be heated from below where the briquet touches the quartz walls but from the other three sides, in order to prevent reaction of the CaO with the silia. If hard glass is used, the temperature necessary for the degassing is limited by the softening point of the material; here treatment with a

Tesla coil for about 30 s helps to release residual adsorbed gases. After cooling, the chemicals are tapped down to the capillary and the tube is sealed off.

When the sample contains less than 1 μg of nitrogen, the following method should be applied. After degassing by heating the walls of the tube with a hand torch, 5 torr xenon is introduced, and the tube is heated again to a temperature near the softening point. After cooling, when the xenon has partly adsorbed onto the tube walls, the remainder is pumped off. This treatment should also be carried out, as described previously, in two steps, *i.e.* the lower part of the tube without sample and reagents is heated, the sample capillary is moved to the far end, and then the upper part with the chemicals is heated so that the sample in the capillary is not destroyed. Next a mixture of helium with 2% xenon to a pressure of 8–12 torr is introduced, and the tube is sealed off and ignited. The combustion temperatures and times are: 850°C for 30 min for quartz tubes; 550°C for 3 h for hard glass; and 450°C for 4 h for Uviol. After 12 hours of storage at room temperature, the tube is ready for analysis.

Measurement, evaluation and calculation

The electronic equipment is switched on 1 h before the measurement is started. For routine purposes, the apparatus should be left switched on except for the high-frequency generator which should be switched on 15 min before commencement of operations.

The discharge tube is inserted between the electrodes of the generator antenna or resonant cavity, the air cooling is started, and the discharge is ignited with a Tesla coil. With a resonant cavity, the tuning is done by means of the adjustable tuning stub for minimal reflected power. When the power in the generator is adjustable, about 50–100% more power is used during the analysis than the minimum necessary to maintain the discharge. The emitted light is focussed onto the entrance slit of the monochromator; after this, only minor corrections need be made for successive samples. Next, the wavelength of the peak (band head) with the highest expected intensity (normally that of ^{14}N) is selected and the recorded signal is adjusted so that about 90% of the scale of the recorder is covered. This can be done by changing the high tension of the photomultiplier, or the sensitivity range of the amplifier. The sensitivity for ^{14}N should be set as low as possible. The amplification step for the other peaks is selected by hand scanning or after test runs, and the instrument is then ready for operation. If the discharge cannot be initiated the sample must be reprepared; this may be necessary because of impurities, air from a leak, or the pressure of the nitrogen being too high. In the last case, the sample tube can be sealed by dipping one end of the tube with the capillary and chemicals in liquid air, shielding it with an asbestos plate and melting off above the plate. The cooling results in adsorption of the nitrogen gas in the cold tip, and reduction of pressure in the upper part where discharge will take place.

Several scans can be made for the measurement depending on the precision required for the result. To level out the instability between two or more measurements, the peaks and their baselines are connected, and the height of both peaks needed for the calculation are measured at one time, at one vertical chosen in the middle of the two measurements.

APPENDIX 1

The separation of nitrogen-15

Nitrogen-15 is separated either by physico-chemical methods or by chemical exchange processes. The physico-chemical methods are based mainly on gaseous diffusion, the best known one being the thermal diffusion method of Clusius[78,93–95]. Other diffusion processes also allow separation but for the large scale separation of nitrogen-15, only chemical exchange processes are practical.

The chemical excange processes which can be used are:

(a) $^{15}NH_3(g) + {}^{14}NH_4^+(sol) = {}^{14}NH_3(g) + {}^{15}NH_4^+(sol)$

(b) $^{15}NO(g) + H{}^{14}NO_3(aq) = {}^{14}NO(g) + H{}^{15}NO_3(aq)$

and in both cases, nitrogen-15 concentrates in the solvent phase. Process (a)[96,97] and process (b)[98–102] have been studied by many workers. Laroche and Combelles[103] applied the latter process industrially. The method is a counter current one in which the liquid phase, aqueous nitric acid, flows down a column and interacts with a rising gaseous atmosphere of nitric oxide. The nitric oxide is produced at the bottom in a boiler by the action of sulphur dioxide on the nitric acid:

$$2\,HNO_3 + 3\,SO_2 + 2\,H_2O = 3\,H_2SO_4 + 2\,NO\,.$$

In operation, the overall effect is of ^{15}N transport down the column since it concentrates in the nitric acid phase. By arranging several columns in a series cascade, such that a smaller second column operates on the product from the first *etc.*, much higher concentrations can be secured in shorter times than are possible if only one size of column is used throughout. With this metod concentrations of more than 95% ^{15}N abundance can be obtained.

Nitrogen-15 chemistry

Research with ^{15}N is facilitated by some characteristics of ^{15}N chemistry[87]. Nitrogen does not easily exchange with nitrogenous compounds; thus there are fewer problems than when, for example, deuterium or ^{18}O are used, when atmospheric humidity must be excluded, or exchange with the oxygen of glass at elevated temperature must be considered. All compounds can be produced and stored under normal conditions without exchange with atmospheric nitrogen. Many organic compounds can be produced easily directly or through very few intermediates from a few inorganic compounds such as ammonia, nitrous acid and nitric acid or their salts.

For the preparation of ^{15}N-labelled compounds, ^{15}N-enriched nitric acid is neutralized with potassium carbonate. By reducing the nitrates and distilling off the ammonia, ammonium salts can be readily obtained. ^{15}N-Ammonium chloride is used to prepare urea and potassium phthalimide which are two base products for the preparation of organic compounds. The mixture of 80% NO and 20% NO_2 which is directly obtained from the production plants can be used to form ^{15}N-nitrite by bubbling the gas through a sodium carbonate solution at 0°C. Enriched nitrogen gas is made by reducing the oxides with copper at 700–800°C.

The preparation of fertilizers or standards by dilution method

Dilution should only be done in cases where there is not an adequate supply of

standard or fertilizer of suitably low enriched material. The reason is that low enriched material is cheaper per gram of nitrogen-15 than the higher enriched material; in addition, the man power involved in the dilution has to be considered.

The dilution of the enriched material with a compound of the same constitution but with nitrogen of lower enrichment or natural abundance can be achieved by mechanical mixing or by dissolution.

Mechanical mixing of the enriched and natural material should only be done when the particle sizes and specific gravity of the components are very similar, for although the components are of the same chemical constitution, the physical properties can vary, one for example being crystallized and the other an amorphous precipitate or composed of smaller or bigger crystals which could cause component separation of the mixture with time and movement. Normally, a dilution by mechanical mixing of 1 : 1 is the maximum that should be considered and further dilution should be done by dissolving. As an aid to ensure that the distribution of the two components is uniform, one compound can be coloured with a little dye which can also be added as a powder before mixing.

For the dissolution method, the two components are dissolved in the amount of solvent needed to obtain a clear solution at about the boiling point. In most cases, water will be the solvent and the amount which dissolves at 95–100°C is used. When all has dissolved, the solvent is evaporated with stirring, until the crystallized product starts bumping when the container is cooled with ice or water to room temperature or a little below (5–10°C) while stirring in order to obtain a fine crystalline product. When the differences in the solubilities at room and boiling temperatures are small, further precipitation can be obtained by lowering the solubility by addition of a solvent in which the ^{15}N-labelled compound is insoluble but which is miscible with the solvent. In case of water, acetone and methanol are most effective. The precipitate is separated on a filter funnel, sucked dry, dried, and then powdered either in the open laboratory, or in a drying or vacuum drying cabinet. The filtered solution can be concentrated by evaporation of the solvent until the compound precipitates again. This process is repeated until the whole amount of labelled compound is recovered.

APPENDIX 2

Nomenclature for the ^{15}N concentration

The concentration of ^{15}N is usually expressed as atom-% ^{15}N or ^{15}N % abundance, thus:

$$\%\ ^{15}N = \frac{^{15}N}{^{15}N + ^{14}N} \times 100 \qquad (1)$$

Important for work with ^{15}N as a tracer is the ^{15}N % excess, or the ^{15}N % enrichment, which gives the % ^{15}N above the natural abundance 0.366% (see below):

$$\%\ ^{15}N \text{ excess} = \%\ ^{15}N \text{ abundance} - 0.366 \qquad (2)$$

In some catalogues the ^{15}N concentration is given in weight % (% w/w), which is different from the corresponding atom-% ^{15}N, so that recalculation is necessary. In calculating the % ^{15}N abundance or amount of ^{15}N in a compound, care should

be taken to correct the mole weight of the compound as illustrated in the following example:

Example: 1000 g $(^{15}NH_4)_2SO_4$ with 50% ^{15}N

	natural	50% abundance
Molecular weight of ammonium sulfate	132.16	133.15
Gram atom weight of N	14.007	14.53
% N total	21.19	21.78

If the amount of ^{15}N in 1000 g of the ammonium sulfate above is then calculated on the basis of the molecular weight of the natural ammonium sulfate for the weight-% and atom-% cases, the values in row A below are obtained. When the correct molecular and gram-atom weights are used, the values in row B are obtained. The differences, as can be seen, are significant.

	From (wt) %	From atom %	Difference
A (false)	105.9 g	109.6 g	3.7 g
B (correct)	108.9 g	112.7 g	2.8 g
Difference	3.0 g	3.1 g	

Natural abundance of nitrogen-15

The natural abundance of atmospheric nitrogen is 0.366 atom-% ^{15}N but not all nitrogen-containing compounds have this value[104,105]. Because of naturally occurring isotopic effects, some are enriched and some have a lower natural abundance ($\pm 1.5\%$)[106]. The following list shows some values which have been found for naturally occurring and manufactured compounds.

Hüser[33]: N_2 gas, Linde reinst -0.360; NH_4Cl -0.361.

Perschke[50], Fiedler[53]: N_2 gas, Linde reinst -0.360; $(NH_4)_2SO_4$ (Merck) -0.359.

Hoering[107]: white clover leaves -0.362, seaweed. Tokyo Bay -0.367. Matheron, impurity in 96% methane -0.361. Sal ammoniac, Mexico -0.369.

Bremner[108]: Grundy silt loam (virgin) -0.373.

Owens[109]: 8 soils investigated had a 0.005% higher abundance in ^{15}N than the atmospheric nitrogen.

Formation of the three isotopic molecules of N, and their distribution and equilibrium

Assuming that in a container ^{14}N and ^{15}N molecules are present in equal amounts, and that the binding probability is the same for each isotope, what types of isotopic molecules can be formed and in which proportion?

The reaction can be expressed by the equation

$$^{14}N_2 + {}^{15}N_2 \rightleftharpoons 2\ {}^{14}N{}^{15}N \tag{3}$$

and when equilibrium is established, the equation above must be valid. From this, the equilibrium constant, K_{eq}, is determined following the general rule of the Law of Mass Action:

$$K_{eq} = \frac{(^{14}N^{15}N)^2}{(^{14}N_2)(^{15}N_2)} = \frac{2^2}{1 \times 1} = 4 \tag{4}$$

That the equilibrium constant is 4 or has a different value can be easily checked by substituting the relative concentrations of the three molecules determined by mass or emission spectroscopy into the formula above.

Calculation of ^{15}N % abundance and derivation of various formulae

The ^{15}N concentration, as a percentage, is given by

$$\%\ ^{15}N = \frac{\text{all } ^{15}N \text{ atoms (in practice, all } ^{15}N\text{-containing molecules)}}{\text{sum of all N atoms (in practice, all N-containing molecules)}}$$

In the case of nitrogen gas, where the equilibrium

$$^{14}N_2 + ^{15}N_2 \rightleftharpoons 2\ ^{14}N^{15}N$$

exists, the $\%\ ^{15}N$ can be expressed as

$$\frac{^{15}N_2 + \frac{1}{2}\ ^{15}N^{14}N}{^{15}N_2 + ^{14}N^{15}N + ^{14}N_2} \tag{5}$$

In the numerator, only half the $^{29}N_2$ appears as only half of the molecule is ^{15}N.

When equilibrium is established, a formula using only the concentrations of two of the three molecules can be derived. This is possible because of eqn. (4), as shown in the following examples

(a) *The calculation of the $\%\ ^{15}N$ abundance from the $^{28}N_2$ and $^{29}N_2$ molecules.* From eqn. (4),

$$(^{15}N_2) = \frac{(^{14}N^{15}N)^2}{4(^{14}N_2)}$$

and when this introduced into eqn. (5), one obtains the formula[110,111]:

$$\%\ ^{15}N = \frac{100}{2R+1} \tag{6}$$

where $R = (^{14}N^{14}N)/(^{14}N^{15}N)$

Birkefeld *et al.*[111] give a table where R values and their corresponding $\%\ ^{15}N$ values are listed (up to 50% ^{15}N).

(b) *The calculation of the $\%\ ^{15}N$ abundance with the $^{29}N_2$ and $^{30}N_2$ molecular concentrations.* From eqn. (4),

$$(^{14}N_2) = \frac{(^{14}N^{15}N)^2}{4(^{15}N_2)}$$

which, when substituted into eqn. (5), yields

$$\%\ ^{15}N = \frac{100}{R'+1} \tag{7}$$

where $R' = (^{14}N^{15}N)/2(^{15}N_2)$.

Similarly, when substituting for $^{14}N^{15}N$,

$$\%\ ^{15}N = 100 \Big/ \left(\frac{^{14}N_2}{^{15}N_2} + 1\right)^{\frac{1}{2}} \tag{8}$$

It should be stressed that formulae 6, 7 and 8 can be used only when

equilibrium is established or accepted. With emission spectroscopy, equilibrium is established by the high-frequency source used to excite the nitrogen gas. In the case of mass spectrometry, the three peak formula (eqn. 5) must be used when the state of equilibrium is unknown and all three peaks can be measured with sufficient accuracy.

The authors are very indebted to Dr. H. Broeshart and Dr. G. B. Cook for their valuable suggestions.

SUMMARY

Methods for the establishment of $^{15}N/^{14}N$ ratios are reviewed. Mass spectrometric and emission spectrometric procedures are discussed in detail with particular reference to the analysis of biological materials. Some aspects of ^{15}N chemistry are also described.

REFERENCES

1 J. Kjeldahl, *Z. Anal. Chem.*, 22 (1883) 366.
2 D. Rittenberg, in D. W. Wilson, A. O. C. Nier and S. P. Riechman (Eds.), *Preparation and measurement of isotopic tracers*, Edwards, Ann Arbor, Mich., 1948, pp. 31–42.
3 G. Meyer, *Verh. Deut. Phys. Ges.*, 10 (1908) 753.
4 W. Gaede, *Ann. Phys. (Paris)*, 46 (1915) 357.
5 K. R. More, R. F. Humphrey and W. W. Watson, *Rev. Sci. Instrum.*, 8 (1937) 263.
6 D. Alpert, C. G. Matland and A. O. Coubrey, *Rev. Sci. Instrum.*, 22 (1951) 370.
7 M. Pirani, *Verh. Deut. Phys. Ges.*, 8 (1906) 686.
8 E. Warburg, G. Leithäuser and E. Johansen, *Ann. Phys. (Paris)*, 24 (1907) 26.
9 W. Rohn, *Z. Elektrochem.*, 20 (1914) 539.
10 E. Rumpf, *Z. Tech. Phys.*, 7 (1926) 224.
11 O. E. Buckley, *Proc. Nat. Acad. Sci. U.S.*, 2 (1916) 683.
12 R. T. Bayard and D. Alpert, *Rev. Sci. Instrum.*, 21 (1950) 571.
13 F. M. Penning, *Physica (Utrecht)*, 4 (1937) 71.
14 H. Mcleod, *Phil. Mag.*, 48 (1874) 110.
15 E. J. Conway, *Microdiffusion analysis and volumetric error*, Crosby–Lockwood, London, 2nd edn., 1947.
16 J. M. Bremner, in C. A. Black (Ed.), *Methods of soil analysis*, Amer. Soc. Agron., Madison, 1965 pp. 1179, 1238.
17 G. Middleton and R. E. Stuckey, *J. Pharm. Pharmacol.*, 3 (1951) 829.
18 C. L. Ogg and C. O. Willits, *J. Ass. Off. Agr. Chem.*, 33 (1950) 179.
19 G. R. Lake, P. McCutchan, R. van Meter and J. C. Neel, *Anal. Chem.*, 23 (1951) 1634.
20 H. A. McKenzie and H. S. Wallace, *Aust. J. Chem.*, 7 (1954) 55.
21 P. R. W. Baker, *Talanta*, 8 (1961) 57.
22 R. A. Osborne and J. B. Wilkie, *J. Ass. Off. Agr. Chem.*, 18 (1935) 604.
23 C. H. Perrin, *Anal. Chem.*, 25 (1953) 968.
24 S. M. Patel and A. Sreenivasan, *Anal. Chem.*, 20 (1948) 63.
25 P. L. Kirk, *Anal. Chem.*, 22 (1950) 354.
26 P. L. Kirk, *Mikrochem. Mikrochim. Acta*, 16 (1934) 13.
27 D. Brüel, H. Holter, K. Linderstrøm-Lang and K. Rözits, *Compt. Rend. Trav. Lab. Carlsberg. Ser. Chim.*, 25 (13) (1946) 289.
28 E. R. Tompkins and P. L. Kirk, *J. Biol. Chem.*, 142 (1942) 477.
29 J. Needham and E. J. Boell, *Biochem. J.* 33 (1939) 149.
30 J. M. Bremner, in C. A. Black (Ed.), *Methods of soil analysis*, Amer. Soc. Agron., Madison, 1965, pp. 1149–1178.

31 J. L. Hoskins, *Analyst*, 69 (1944) 271.
32 W. J. Wingo, O. L. Davis and L. Anderson, *Anal. Chem.*, 22 (1950) 1340.
33 R. Hüser, *Z. Anal. Chem.*, 197 (1963) 16.
34 G. Proksch, *Plant Soil*, 31 (2) (1969) 380.
35 H. Faust, *Optical spectroscopy techniques for ^{15}N assay*, presented at Research coordination meeting on recent development in the use of ^{15}N in soil-plant studies, Sofia, Bulgaria, December, 1969.
36 J. M. Bremner (1965), in C. A. Black (Ed.), *Methods of soil analysis*, Amer. Soc. Agron., Madison, pp. 1256–1286.
37 D. B. Sprinson and D. Rittenberg, *J. Biol. Chem.*, 180 (1949) 707.
38 R. Hüser, K. Habfast und M. Bradke, *Z. Anal. Chem.*, 176 (1960) 429.
39 A. P. Sims and E. C. Cocking, *Nature, London*, 181 (1958) 474.
40 C. Balestrieri, *Life Sci.*, 7 (1968) 269.
41 K. Clusius und G. Rechnitz, *Helv. Chim. Acta*, 36 (1953) 59.
42 J. B. Capindale and D. H. Tomlin, *Nature, London*, 180 (1957) 710.
43 P. F. Holt and B. P. Hughes, *J. Chem. Soc.*, (1955) 95.
44 J. H. Smith, J. O. Legg and J. N. Carter, *Soil Sci.*, 96 (1963) 313.
45 H. Faust, *Isotopenpraxis*, 1 (2) (1965) 62.
46 R. F. Glascock, *Isotopic gas analysis for biochemists*, Academic Press, New York, 1954.
47 A. S. J. Reid, G. L. Cumming and G. R. Webster, *Plant Soil*, 26 (1) (1967) 196.
48 G. B. Cook, J. A. Goleb and V. Middelboe, *Nature London*, 216 (1967) 475; *Anal. Chim. Acta*, 43 (1968) 229; V. Middelboe, *Appl. Spectr.*, 24 (1970) 608.
49 H. Faust, *Isotopenpraxis*, 3 (3) (1967) 100.
50 H. Perschke, G. Proksch, E. A. Kerö and A. Mühl, *Anal. Chim. Acta*, 53 (1971) 459.
51 J. P. Leichnam, V. Middelboe et G. Proksch, *Anal. Chim. Acta*, 40 (1968) 487.
52 I. Shatochin, Private communication, 1965.
53 R. Fiedler and G. Proksch, *Plant Soil*, 36(2) (1972) 377.
54 K. Sommer und H. Kick, *Z. Anal. Chem.*, 220 (1965) 21.
55 M. M. Ferraris and G. Proksch, *Anal. Chim. Acta*, 59 (1972) 177.
56 J. Dumas, *J. Pharm. Chim.*, 20 (1834) 144.
57 H. Günther, H. G. Floss und H. Simon, *Z. Anal. Chem.*, 218 (1966) 401.
58 W. Rolle, Kernenergie 5 (4) (1962) 403.
59 H. Perschke and G. Proksch, *IAEA-PL-341/16*, (1971).
60 R. Fiedler and G. Proksch, *Anal. Chim. Acta*, 60 (1972) 277.
61 R. Fiedler, G. Proksch and A. Koepf, *Anal. Chim. Acta*, 63 (1973) 435.
62 H. Simon, H. Daniel und J. F. Klebe, *Angew. Chem.*, 71 (1959) 303.
63 D. E. Uhl, E. B. Lancaster and Ch. Vojnovich, *Anal. Chem.*, 43 (1971) 990.
64 H. E. Duckworth, *Mass Spectrometry*, Cambridge University Press, London, 1958.
65 R. M. Elliot, *Advances in Mass Spectrometry II*, Pergamon, London, 1963.
66 H. Ewald und H. Hintenberger, *Methoden und Anwendung der Massenspektroskopie*, Verlag Chemie, Weinheim, 1953.
67 H. Ewald, *Massenspektrometrische Apparate* in S. Flügge (Ed.), *Handbuch der Physik*, Verlag–Springer, Berlin, 1956.
68 H. Kienitz, *Massenspektrometrie*, Verlag Chemie, Weinheim, 1968.
69 C. A. McDowell, *Mass Spectrometry*, McGraw–Hill, New York, 1963.
70 G. R. Rieck, *Einführung in die Massenspektroskopie*, Deutscher Verlag der Wissenschaften, Berlin, 1956.
71 J. Roboz, *Introduction to Mass spectrometry, Instrumentation and Techniques*, Wiley, New York, 1968.
72 F. P. Viehböck, in Linser and Kaindl's (Eds.), *Isotope in der Landwirtschaft*, Verlag–Parey, Hamburg, 1960.
73 J. Waldron, *Advances in Mass spectrometry*, Pergamon, London, 1959.
74 *Mass spectrometry in Physics Research, National Bureau of Standards Circular 522*, National Bureau of Standards, Washington, 1953.
75 A. O. Nier, *Rev. Sci. Instrum.*, 11 (1940) 212.
76 D. H. Whiffen, *Spectroscopy*, Camelot Press, London, 1966.
77 G. Herzberg, *Spectra of diatomic molecules*, van Nostrand, Princeton, New Jersey, 1950.
78 K. Clusius und E. W. Becker, *Z. Naturforsch. A*, 2 (1947) 154.
79 M. Hoch und H. R. Weisser, *Helv. Chim. Acta*, 38 (1950) 2128.

80 H. Hürzeler und H. U. Hostetler, *Helv. Chim. Acta*, 38 (1955) 1825.
81 L. I. Obolenskaya and N. T. Zhadkova, *Khim. Sel. Khoz.*, 1 (1964) 13.
82 G. Meier und G. Müller, *Isotopenpraxis*, 1 (2) (1965) 53.
83 H. P. Broida and M. W. Chapman, *Anal. Chem.*, 30 (1958) 2049.
84 J. P. Leichnam et R. Capitini, *Rapport CEA No. R-2428*, 1964.
85 G. B. Marshall and T. S. West, *Anal. Chim. Acta*, 51 (1970) 179.
86 C. Woodward, *Anal. Chim. Acta*, 51 (1970) 548.
87 K. Clusius, *Angew. Chem.*, 66 (17/18) (1954) 497.
88 A. I. Gorbunov and P. A. Sagorec, *Zh. Fiz. Khim.*, 29 (1955) 1442.
89 G. Meier, *Kernenergie*, 3 (9) (1960) 903.
90 L. Karlsson and V. Middelboe, *IAEA/SM-151/41*, 1972.
91 K. Kumasawa and S. Muhammad, *Soil Sci. Plant Nutr. (Tokyo)*, 18 (1972) 173.
92 K. Kumasawa and T. Yoneyama, *Plant Cell Physiol.*, 15 (1974) 655.
93 K. Clusius und G. Dickel, *Z. phys. Chem.*, 193 (1944) 274.
94 Gh. Vašaru, *Isotopenpraxis*, 4 (1968) 297.
95 W. M. Rutherford, W. J. Roos and K. J. Kaminski, *J. Chem. Phys.*, 50 (1969) 5359.
96 K. Clusius und E. Becker, *Z. phys. Chem.*, 193 (1953) 64.
97 H. G. Thode and H. C. Urey, *J. Chem. Phys.*, 7 (1939) 34.
98 W. Spindel and T. I. Taylor, *J. Chem. Phys.*, 23 (1955) 981.
99 D. Axente, Tr. Fodor, V. Mercea and M. Peculea, *Rev. Roum. Chim.*, 13 (1968) 707.
100 L. L. Brown and J. S. Drury, *J. Chem. Phys.*, 48 (1968) 1400.
101 M. Jeevanadam and T. I. Taylor, *Advan. Chem. Ser.*, 89 (1969) 119.
102 J. Mahenc et G. Pompidor, *Chim. Ind., Genie Chim.*, 99 (1968) 1137.
103 J. Laroche et R. Combelles, *FAO/IAEA Report, Technical meeting*, Brunswick, 1963, 423.
104 A. O. Nier, *Phys. Rev.*, 77 (1950) 789.
105 G. Junk and H. J. Svec, *Geochim. Cosmochim. Acta*, 14 (1958) 234.
106 A. Parwel, R. Ryhage and F. E. Wickman, *Geochim. Cosmochim. Acta*, 11 (1957) 165.
107 T. C. Hoering, *Science* 122 (1955) 1322; T. C. Hoering and H. E. Moore, *Geochim. Cosmochim. Acta*, 13 (1958) 225.
108 J. M. Bremner, H. H. Cheng and A. P. Edwards, *FAO/IAEA Report, Technical meeting, Use of isotopes in soil*, 1963, pp. 429–442.
109 L. D. Owens, *Soil Sci. Soc. Amer. Proc.*, 24 (1960) 372.
110 G. Haase, *Kernenergie*, 3 (9) (1960) 915.
111 H. Birkefeld, G. Haase und H. Zahn, *Massenspektrometrische Isotopenanalyse*, VEB Deutscher Verlag der Wissenschaften, Berlin (1962).
112 J. P. Leichnam, H. C. Figdor, E. A. Keroe et A. Mühl, *Int. J. Appl. Radiat. Isotop.*, 19 (1968) 235.

Analytica Chimica Acta, 78 (1975) 63–68

A NEW MEMBRANE ELECTRODE SYSTEM WITH IODIDE-SELECTIVE PROPERTIES

M. NOVKIRISHKA and R. CHRISTOVA

Department of Analytical Chemistry, University of Sofia, (Bulgaria)

(Received 20th November 1974)

Strongly basic anion-exchange resins selectively and irreversibly adsorb triiodide ions; placed into a moderately concentrated electrolyte solution, the triiodide-saturated resin neither exchanges with anions nor adsorbs iodine from the solution. Thus, the anion-exchange resin appears as a triiodide collector, in which the ratio of iodine to iodide is kept constant. Such a resin can be used in the preparation of a first-kind iodine electrode. In the fixed phase, the triiodide retains the same chemical and redox properties as in aqueous solutions. The interactions between the fixed I_3^-, I^- or I_2 and the ions in the solution affect the adsorption, and the triiodide-saturated resin selectively adsorbs iodide ions from the solution[1]. Such resin layers are shown here to be useful in the preparation of iodide-selective electrodes.

Membranes can be prepared from the anion-exchange resin Dowex 2-X8 with agar–agar as the binder, and located at the end of a glass tube; an electrolyte solution connects the membrane with a platinum wire[2]. The electrode reaction of the half-cell $(I_3^-, I^-)_r$ Pt is as follows:

$$(I_3^-)_r + 2e^- = 3(I^-)r$$

where the subscript r indicates the fixed phase. The equilibrium constant of the electrode reaction can be defined by the relationship: $K = (I^-)_r^3/(I_3^-)_r(e^-)^2$. The equation of the electrode potential then has the form:

$$E = E^\circ + \frac{RT}{2F} \cdot 2.303 \log [(I_3^-)_r/(I^-)_r^3)]$$

The electrode potential, measured against a saturated calomel electrode (SCE) in the presence of 0.01 *M* KNO_3 as electrolyte, was $+750 \pm 5$ mV. The potential remained the same when the KNO_3 solution was replaced by equimolar solutions of KCl, KBr or sodium acetate. Various samples of membrane electrodes prepared similarly possessed almost the same potential.

The potential of the electrode was influenced by the presence of iodide in the electrolyte solution into which the membrane and the platinum wire were immersed. The potential changes of the cell were proportional to the changes of iodide concentration so that the membrane could be used as an iodide-selective electrode.

EXPERIMENTAL

Preparation of resin

Some Dowex 2-X8 resin (20–50 mesh, stored in a humid state) was placed in a glass tube on a layer of glass wool, and activated by alternate washing with 2 *M* hydrochloric acid and 0.5 *M* sodium hydroxide until saturated. It was then washed with water until the eluate was neutral, and saturated with a solution containing 1 *M* potassium iodide and 0.1 *M* iodine[1]. The unadsorbed ions were then washed out, and the resin was dried in air and powdered in an agate mortar.

Preparation of Electrode

In order to function properly, the resin must be kept moist. The most suitable binder was agar–agar, in a 1:3 ratio to the resin. Agar–agar (0.3 g) was dissolved in 10 ml of water and 0.9 g of the air-dried resin and 0.1 g of potassium iodide were added; this mixture was poured into the wide part of a clean dry glass tube (Fig. 1) placed on a cover glass. The mixture reached a height of 1.2–1.3 cm by suction through the upper end of the narrower tube, and solidified after 10 min.

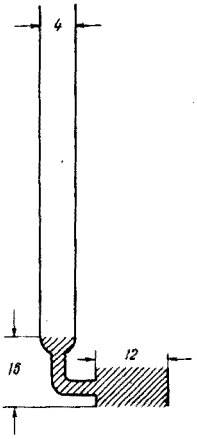

Fig. 1. Shape and dimensions (in mm) of the membrane electrode.

All the reagents were of guaranteed purity, and twice-distilled water was used.

Electrochemical cell

A specially prepared small saturated calomel electrode, immersed in 0.01 *M* KCl solution in the tall narrow arm of the glass tube was used as reference electrode. Both the membrane and the platinum wire were immersed in 0.01 *M* KNO_3 solution (Fig. 2). The experimental setup of this cell schematically is:

$$Hg \mid \tfrac{1}{2}Hg_2Cl_2 \parallel 0.01\ M\ KCl \parallel \text{membrane} \parallel 0.01\ M\ KNO_3 \mid Pt$$

The liquid-junction potential at the phase boundary between the membrane and the 0.01 *M* KNO_3 solution was low and constant. When iodide was present in the

KNO_3 solution, a potential difference was caused by adsorption of iodide at the membrane. The electrical resistance of the resin layer in the electrode was about 1 Mohm.

Measurements were made with a SP-2 pH meter and a Titrierautomat (AT-2; GDR). The total impedance of the two devices was 10^{11} ohms. The accuracy of the measurements, which were done with moderate stirring at constant temperature $25 \pm 0.2°C$, was ± 1 mV.

Response of the electrode

The e.m.f. was measured in solutions containing 10^{-7}–10^{-1} *M* iodide. The total ionic strength of the solutions was 0.01 (except at the highest concentration); KNO_3 was the supporting electrolyte. Iodide ions caused a decrease in the e.m.f. (Table I), the response being rapid and reversible; 20–45 s after the membrane electrode had been placed in solution, the e.m.f. reached a minimum value and

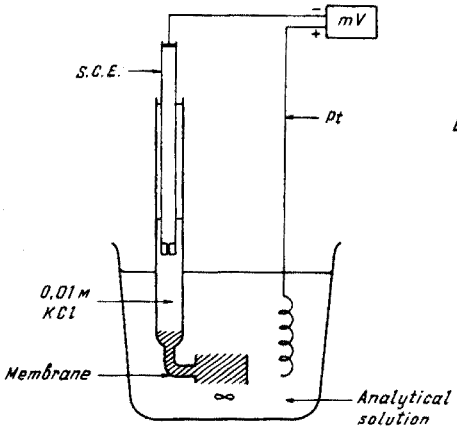

Fig. 2. The electrochemical cell.

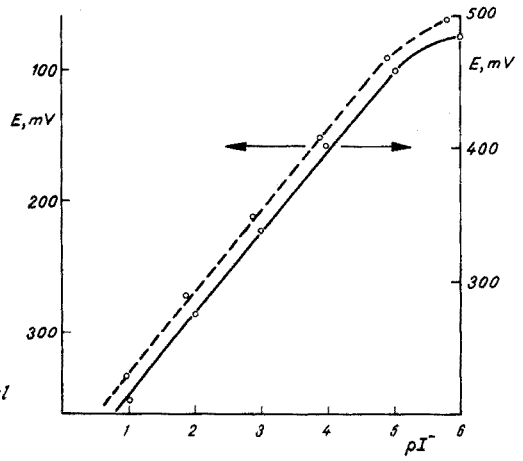

Fig. 3. The calibration plots for iodide activities. (—) Membrane electrode. (---) Radelkis iodide-selective electrode.

TABLE I

RESPONSE AND REPRODUCIBILITY OF THE ELECTRODE

pI^-	*E.m.f., mV*[a]			ΔE, *mV*			ΔE	$\Delta E - \Delta\bar{E}$		
	I	*II*	*III*	*I*	*II*	*III*		*I*	*II*	*III*
7	472	430	484							
6	480	480	491							
5	460	454	461	20	26	30	25	−5	−1	+5
4	400	399	404	60	55	57	57	+3	−2	0
3	339	335	343	61	64	61	62	−1	+2	−1
2	276	270	278	63	65	65	64	+1	+1	+1
1	210	212	210	66	62	68	65	+1	−3	+3

[a] Values for 3 different electrodes.

then slowly increased. The minimum value was taken as the correct one. The reproducibility of repeated measurements on the same solutions with the same electrode was ± 1 mV. The results obtained over several months with various specimens of membrane electrodes differed by only a few mV.

The calibration plot of the membrane electrode is compared with that of a Radelkis iodide-selective electrode in Fig. 3. It should be noted that, although the slopes appear very similar, one is negative and the other positive.

Conditioning of the membrane electrode

Good reproducibility was achieved only after careful conditioning, whether the electrode was newly prepared or used. For conditioning, the test solution in the cell was replaced by water which was stirred until the e.m.f. rose to about 500 mV; the water was then replaced by 0.01 *M* KNO_3 which was stirred until a constant e.m.f. of 510 mV$\pm$10 mV was achieved. If the steady state value was lower, the electrode was removed from the cell and dipped for 30 min in a solution containing 0.01 *M* I_2 and 0.1 *M* KI, after which it was washed with water and conditioned in KNO_3 solution as above. This conditioning was necessary before each series of measurements, but many samples could be analysed in a series provided that they were arranged in order of increasing iodide concentration.

The potassium chloride solution of the SCE was changed daily; the SCE was stored in a saturated KCl solution when not in use.

These membrane electrodes have been in use for more than two years, and if maintained properly as described above, do not change their characteristics for months.

TABLE II

SELECTIVITY COEFFICIENTS (K_{IN}) AND PERMISSIBLE CONCENTRATIONS OF INTERFERING IONS

Anions	K_{IN}	*Anions*	*Permissible concentration (M)*
Cl^-	$5\cdot10^{-5}$	NO_2^-	<0.01
Br^-	$5\cdot10^{-5}$	BO_3^{3-}	<0.005
NO_3^-	$5\cdot10^{-5}$	S^{2-}	None
CH_3COO^-	$5\cdot10^{-5}$		
SO_4^{2-}	0.2–1		
SCN^-	0.35–1		

Selectivity of the electrode

The influence of many anions was investigated, selectivity coefficients being determined by the separate solution and mixed solution methods[3] (Table II). Copper(II) and iron(III) did not interfere since they oxidized iodide only very slowly at pH 2–9. The selectivity for iodide over bromide was better then that obtained with AgI or AgI–Ag_2S electrodes[3]. Oxidants and reductants, such as arsenite, persulphate, hydrazine, hydroxylamine and thiosulphate, which affect the triiodide/iodide couple, cannot be tolerated.

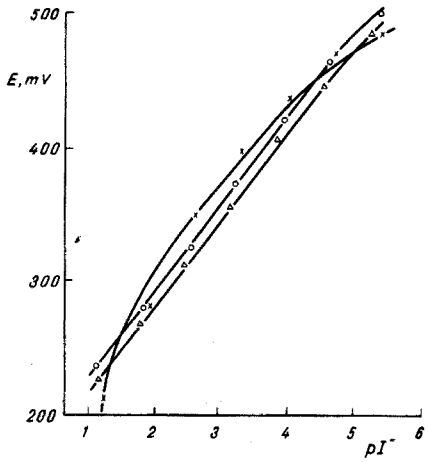

Fig. 4. Calibration plots at different ionic strengths: (○) 0.01; (△) 0.1; (×) 0.5.

Effect of pH and ionic strength

The response was unaffected by increase in ionic strength from 0.01 to 0.2 when KNO_3, KCl, KBr or sodium acetate was used as electrolyte, but at 0.5 curved calibration plots were obtained (Fig. 4).

The lower limit of pH was pH 2. At pH 1, reproducibility was poor owing to the rapid oxidation of iodide. The upper pH limit was about 8–9.

The mechanism of the electrode reaction

The function of the proposed membrane electrode can be explained as adsorption of iodide ions on the phase boundary, which causes a change in the relationship $(I_3^-)_r/(I^-)_r^3$. This was proved in tests with iodide-131. Several membranes were prepared in glass rings and dipped into solutions which contained different concentrations of potassium iodide and the same quantity of ^{131}I as iodide. After 1 min, the membranes were removed, washed with water and counted with a Geiger–Muller counter. The number of impulses was larger in the more concentrated solutions, being 1808 at pI^- 5, 2219 at pI^- 4, and 3478 at pI^- 3. The membranes were then washed with water as described above for conditioning, and the radiation was measured periodically. The radioactivity of the membranes initially decreased quickly, and then slowly to a small value. This indicates that the return of the electrode potentials to their initial value on conditioning must be due to desorption of iodide from the membrane surface.

RESULTS AND DISCUSSION

The novelty of the proposed electrode is the solid membrane which collects the iodine–iodide couple irreversibly.

The irreversible adsorption of triiodide ions by the anion-exchange resin can be explained by the formation of polyiodide complexes with the ionized groups of the resin. It is known[4] that triiodide forms polyiodide complexes with alkylammonium cations, the most stable being that formed with trimethylethyl-

ammonium ions $\{N(CH_3)_3C_2H_5\}I_9$; trimethylethylammonium is present in the Dowex 2 resin used. In the resin phase, the polyiodide complexes will be more stable because there the dielectric constant of the water is considerably lower[5]; thus other anions from the solution do not detectably displace triiodide which can be eluted only as hypoiodite with a solution of sodium hydroxide[6].

If the anion-exchanger is saturated with triiodide, only iodide ions are adsorbed. Other halides cannot be adsorbed, because only iodide participates in the complex-forming process with the exchange groups at the phase boundary.

The peculiar response of the membrane electrode is due to two processes: the adsorption of iodide at the phase boundary followed by diffusion inside the membrane. (Electrodes with very thin membranes have been prepared in order to study the diffusion).

The electrode proposed is easy to prepare and store; it is cheap and is not essentially damaged even when used in the presence of reductants which affect the triiodide–iodide couple.

The electrode was applied in the determination of iodide in sea water. The results compared with those obtained by the extraction–photometric method, showed deviations of 5% (relative) for contents of about $1 \cdot 10^{-4}$ *M*.

We are grateful to H. Albert and M. Yanakiev from the Faculty of Physics at the Sofia University for their assistance.

SUMMARY

The strongly basic anion-exchange resin Dowex 2 when saturated with triiodide and placed in a gel layer in a glass tube acts as an electrode for iodine, as does a platinum wire electrode. When the gel membrane is placed with a platinum electrode in an iodide solution, the anion-exchange resin adsorbs iodide selectively, and a decrease in the potential of the membrane electrode is caused. The arrangement can be used as an iodide-selective electrode, which shows a linear response over the pI^- range 1–5 and an excellent selectivity for iodide over other halides.

REFERENCES

1 M. Heuterbise and W. I. Ross, *Anal. Chem.*, 44 (1972) 596.
2 *Bulgarian Patent No. 18923*, June 25, 1972.
3 G. I. Moody and J. D. R. Thomas, *Selective Ion sensitive Electrodes*, Merrow, Watford, Herts, England, 1971.
4 A. A. Grinberg, *Introduction to the Chemistry of Complex Compounds*, Chimija, Leningrad, 1971 (Russ.).
5 J. Marinsky, *Ion Exchange*, Mir, Moscow, 1968 (Russian translation).
6 R. Christova and N. Gradinarova, *God. Sof. Univ., Khim. Fak.*, 65 (1970/1971) 1.

Analytica Chimica Acta, 78 (1975) 69–80

A PHOSPHATE-SELECTIVE ELECTRODE BASED ON IMMOBILIZED ALKALINE PHOSPHATASE AND GLUCOSE OXIDASE

G. G. GUILBAULT and M. NANJO

Department of Chemistry, University of New Orleans, New Orleans, Louisiana 70122 (U.S.A.)

(Received 27th January 1975)

Ion-selective electrodes are now available or can be constructed for a wide variety of ions. Many investigators have attempted to construct electrodes for phosphate ion[1–7]; however, all these electrodes have suffered serious interferences from common ions, such as chloride, nitrate and sulfate, and there is no report on a phosphate electrode which could be used for a practical assay of environmental and biological samples.

Another approach for a phosphate-selective electrode is the use of selective enzymes, that is, an enzyme electrode in which the enzyme catalyzes a reaction involving phosphate ion, and the reaction is followed electrochemically.

Weetall and Jacobson[8] have reported the spectrophotometric assay of phosphate ion based on a chromogenic substrate for alkaline phosphatase as follows:

$$\underset{\text{(colorless)}}{p\text{-nitrophenyl phosphate}} + H_2O \xrightarrow{\text{alkaline phosphatase}} \underset{\text{(yellow)}}{p\text{-nitrophenol}} + HPO_4^{2-} \qquad (1)$$

The presence of added inorganic phosphate in this reaction mixture causes a shift in the equilibrium between the substrate and the products, with a reduction in color production which is reciprocally proportional to the added inorganic phosphate.

The assay of sulfate has also been reported by the same investigators, with alkyl sulfatase instead of alkaline phosphatase[8].

It is difficult to design an electrode based on this reaction, since there is no electrochemical difference between the substrate and products. The same is true of other chromogenic substrates, such as *o*-carboxyphenyl phosphate[9] and sodium thymolphathalin monophosphate[10].

However, it was found possible to use a dual enzyme system for electroanalytical measurement of the alkaline phosphatase catalytic reaction as follows:

$$\text{glucose-6-phosphate} + H_2O \xrightarrow{\text{alkaline phosphatase}} \text{glucose} + HPO_4^{2-} \qquad (2)$$

$$\text{glucose} + O_2 \xrightarrow{\text{glucose oxidase}} \text{gluconic acid} + H_2O_2 \qquad (3)$$

When the glucose formed from glucose-6-phosphate is sensed electrochemically, it is possible to follow reaction (2), in which phosphate inhibition decreases glucose formation, thus lowering the response to the dual enzyme electrode.

This dual enzyme electrode was also found to be useful for the assay of

other oxyacids, such as arsenate, tungstate, molybdate and borate ions as well as for the substrate itself, glucose-6-phosphate.

EXPERIMENTAL

Immobilization of the dual enzymes

Alkaline phosphatase (100 mg; E.C., 3.1.3.1., Sigma, Type V, from chicken intestinal mucosa, 5 units/mg of solid) and glucose oxidase (100 mg; E.C., 1.1.3.4., Sigma, Type II, from *aspergillus niger*, 18 units/mg of solid) were dissolved in 5.0 ml of phosphate buffer (pH 7.8, 0.1 *M*), and then 10 drops of glutaraldehyde (Sigma, grade IV, aqueous 25% solution) were added to the mixture and stirred well. Next, the mixture was frozen by a dry ice–acetone coolant and kept in a refrigerator for one night.

The sponge-like copolymer was washed with phosphate buffer, and finally washed out by glycine buffer (pH 8.4, 0.1 *M*) to eliminate phosphate, and stored in a refrigerator until used.

Other combinations of the amounts of two enzymes, *i.e.*, glucose oxidase and alkaline phosphatase, with albumin as a matrix, did not give higher activity than that without a matrix.

Construction of the dual enzyme electrode

A platinum disc electrode (Beckman Model 39273) was used as the solid base electrode to sense the oxygen change. The procedure for the preparation of the enzyme electrode was as follows. The immobilized dual enzyme (dry weight, about 5 mg; 45 units of glucose oxidase and 13 units of alkaline phosphatase if there is no loss of activity during the immobilization process) was mounted on the surface of the platinum electrode and secured with a nylon net (Pharmacia Fine Chemicals, Inc., Piscatway, N. J., Nylon Screen No. 0670) and "O" rings. A cellophane sheet could be instead of nylon net, as in the case of a previous glucose electrode[11]. Then the electrode was stored in the buffer solution at room temperature (23°C).

Substrates

β-D-glucose-6-phosphate (monosodium salt; Sigma) was used without further purification. This substrate was confirmed not to be contaminated by glucose, by means of a glucose enzyme electrode[12].

A β-D-glucose (Sigma) was also used to test the dual enzyme function.

Buffers

Glycine buffer was prepared by adjusting the pH of a 0.1 *M* solution of glycine powder (Sigma) to pH 8.4. Tris-HCl buffer (pH 8.4, 0.1 *M*) was prepared from tris(hydroxymethyl)aminomethane (Sigma). Barbital buffer (pH 7.4, 0.05 *M*, with 0.1 *M* KCl) was made from 5,5′-diethylbarbituric acid (Sigma), the pH being adjusted with sodium hydroxide. All buffers contained 10 m*M* magnesium chloride as a cofactor for alkaline phosphatase.

Apparatus and procedures

A Heath polarograph system (Model EUA-19-2) was used as reported for ear-

lier electrodes[12,13]. The dual enzyme electrode together with a calomel electrode, was placed into a stirred buffer solution, and a potential of −0.6 V *vs.* SCE (where the current is proportional to the dissolved oxygen content) was applied. When the current reached a constant level, the phosphate solutions (0.01–1.0 ml) to be assayed were pipetted into the buffer solution (10.0 ml). About 1 min later, a certain amount of glucose-6-phosphate (*ca.* 35 m*M*, 0.5 ml) was injected into the sample–buffer mixture to initiate the reaction, and the initial rate of change in the dissolved oxygen limiting current was recorded, as well as the steady-state current. After the current had reached a steady state (1–2 min), the dual enzyme electrode was rinsed well with distilled water, and was dipped into a fresh buffer solution for 1 or 2 min to recover the dissolved oxygen level around the dual enzyme layer and to eliminate the remaining reactant, products and inhibitor, *i.e.*, phosphate ion.

All experiments were conducted at 30°C. The dual enzyme electrode could be used several hundred times for more than three months before it lost activity.

RESULTS AND DISCUSSION

Enzyme reaction—alkaline phosphatase

Alkaline phosphatase is a broad term associated with non-specific phosphomonoesterases with an optimal activity at alkaline pH as follows:

$$\text{orthophosphoric monoester} + H_2O \xrightarrow{\text{alkaline phosphatase}} \text{alcohol} + H_3PO_4 \quad (4)$$

Assays of alkaline phosphatase in serum and milk are one of the major subjects in clinical chemistry[14]. This enzyme has been reported as a zinc metal-enzyme and reacts with only orthophosphate to form a thermodynamically stable phosphoprotein[15–17]. The equilibria between inorganic orthophosphate (Pi) and alkaline phosphatase (E) can be represented as follows[16]:

$$E + Pi \underset{k_{-1}}{\overset{k_1}{\rightleftharpoons}} E \cdot Pi \underset{k_{-2}}{\overset{k_2}{\rightleftharpoons}} E\text{–}Pi + H_2O \quad (5)$$

The hydrolysis of phosphate ester (S) is expressed as follows:

$$E + S \underset{k'_{-1}}{\overset{k'_1}{\rightleftharpoons}} E \cdot S \xrightarrow{k'_2} E\text{–}P + Pi \quad (6)$$

The relationship at steady state has the Michaelis–Menten form for competitive inhibition as follows:

$$v = k'_3[E \cdot S] = \frac{k[E_0]}{1 + \dfrac{K_m}{[S]} + \dfrac{[Pi]}{[S]} \cdot \dfrac{K_m}{K_i}} \quad (7)$$

where K_m and K_i are the Michaelis–Menten and inhibition constants, respectively. In the presence of an excess Pi, eqn. (7) can be simplified as follows:

$$v = \frac{1}{[Pi]} \cdot \frac{kK_i[S][E_0]}{K_m} \quad (8)$$

At constant [S] and [E_0], the rate of reaction, v, is proportional to the reciprocal of Pi, and Pi can be estimated by the decrease of the original rate of the uninhibited reaction.

Enzyme reaction—glucose oxidase

The second step of enzymatic reaction is the oxidation of glucose to gluconic acid. As reported previously[11,13], glucose can be easily measured by an amperometric method, by means of a platinum electrode coupled with immobilized glucose oxidase at ± 0.6 V *vs.* SCE. This second reaction was found to have no interference from phosphate ion, and glucose oxidase did not oxidize the glucose ester, that is, glucose-6-phosphate. Since the formation of glucose in the alkaline phosphatase reaction builds up glucose inside the dual enzyme layer, and glucose oxidase has enough activity to oxidize glucose faster than its rate of formation, the total reaction rate will be determined by the first step, and phosphate ion can be measured by means of the oxidation of glucose.

This assumption was confirmed by the results that follow.

Electrode response to glucose-6-phosphate and glucose

Figure 1 shows the dual enzyme electrode response to substrate, glucose-6-phosphate (added at A). The current at -0.6 V *vs.* SCE, which is proportional to the amount of dissolved oxygen in the enzyme layer, decreased rapidly, and reached a steady state when the consumption of dissolved oxygen by the enzymatic reaction matched the supply of oxygen from the bulk solution to the enzyme layer by diffusion. This dissolved oxygen decrease could not be seen by the addition of

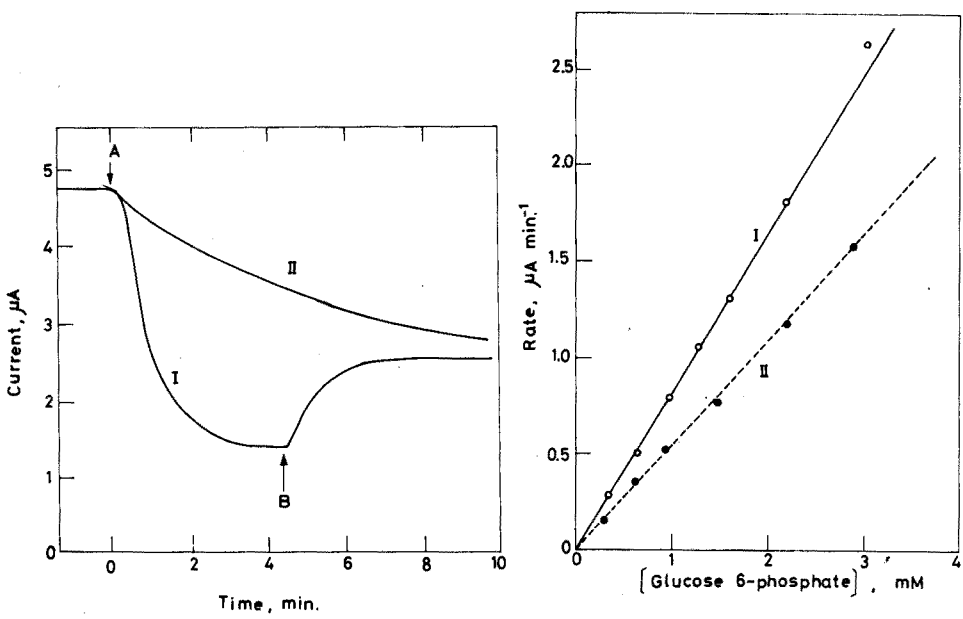

Fig. 1. Changes in the dissolved oxygen current during enzymatic reactions: 30°C; glycine buffer, 0.1 *M*; pH 8.4; -0.60 V *vs.* SCE. Curve I, 0.5 ml of glucose-6-phosphate (32 m*M*) added to 10.0 ml of glycine buffer (10 m*M* $MgCl_2$) at point A; 0.5 ml of 0.1 *M* phosphate solution added to this mixture at point B. Curve II shows the response when glucose-6-phosphate and phosphate are added at the same time (at A).

Fig. 2. Calibration curves for glucose-6-phosphate (I) without and (II) with phosphate ion: 30°C; glycine buffer, 0.1 *M*; pH 8.4; -0.60 V *vs.* SCE. I, no phosphate. II, 4.6 m*M* phosphate added.

glucose-6-phosphate to the glucose oxidase electrode, which indicates that glucose oxidase in the dual enzyme reacted only with glucose which was produced by the alkaline phosphatase catalytic reaction (eqn. (2)). At steady state, when phosphate ion, which was adjusted to the same pH as the buffer solution, was added at point B, an increase in the dissolved oxygen level was observed, indicating an inhibition[15] of the enzyme reaction by phosphate ion, with a consumption of less oxygen.

The addition of substrate and inhibitor at the same time resulted in a slower decrease of dissolved oxygen as shown in Fig. 1, curve II. In the case of a glucose oxidase electrode, the recovery of the dissolved oxygen level could not be obtained by the addition of phosphate ion. The same oxygen recovery in the dual enzyme electrode was observed in the presence of arsenate, molybdate, tungstate and borate solutions also.

One might question why the phosphate formed from the substrate during reaction (eqn. 2) did not affect the rate of recovery of the dissolved oxygen, by product inhibition of reaction (2), as added phosphate does in Fig. 1B. However, placement of the electrode in a glucose-6-phosphate solution for a long time (5 h) did not show self-inhibition by such buildup of phosphate in the enzyme layer, because of rapid diffusion of the small amount of phosphate produced to the bulk solution.

Figure 2 shows the calibration curves for glucose-6-phosphate, with and without phosphate ion added before injection of glucose-6-phosphate. In both cases, linear relationships were obtained and the same ratio of depression of the rate by

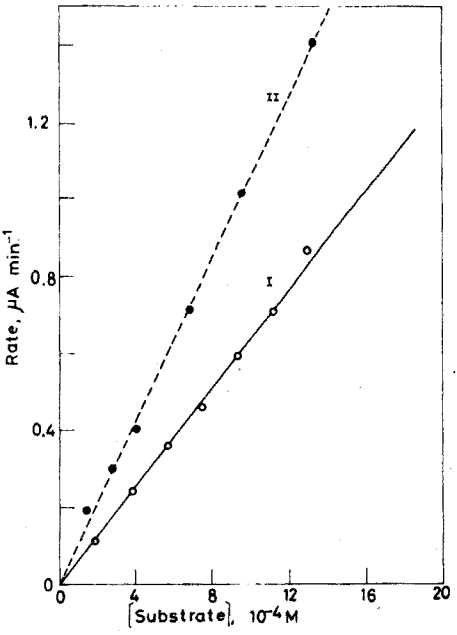

Fig. 3. Comparison of the response of the dual enzyme electrode to (I) glucose-6-phosphate, and (II) glucose: 30°C; glycine buffer, 0.1 *M*; pH 8.4; −0.60 V *vs.* SCE. A different electrode was used from that of Fig. 2.

phosphate ion was observed at each glucose-6-phosphate concentration. Relative standard deviations were 5.9% without phosphate and 3.6% with 1.0 m*M* phosphate added.

Glucose also reacts with glucose oxidase in the dual enzyme electrode and gave almost twice as high a rate as glucose-6-phosphate, as shown in Fig. 3. Thus, this dual enzyme electrode can be used for the assay of both substrates, in concentrations as low as $1 \cdot 10^{-4}$ *M*. Figure 3 also shows that the amount of glucose that diffuses into the enzyme layer from bulk solution is larger than that of glucose formed from the same amount of glucose-6-phosphate in the dual enzyme layer.

Effects of magnesium ion

Alkaline phosphatase has been known to require magnesium ion as a cofactor[17]. Figure 4 shows the effect of magnesium ion concentration on the rate. At the optimal magnesium concentration (10 m*M*) the reaction rate is 1.7 times faster than that without magnesium ion. Hence, all experiments were conducted, and all electrodes were stored, in a buffer solution which contained 10 m*M* magnesium(II).

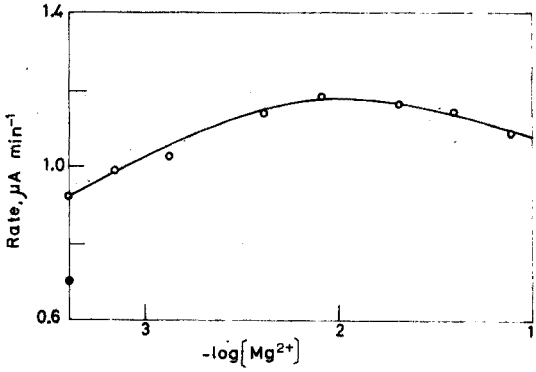

Fig. 4. Effect of magnesium ion: 30°C; glycine buffer, 0.1 *M*; pH 8.4; −0.60 V *vs.* SCE. Glucose-6-phosphate was kept constant at 0.85 m*M*. (●) No magnesium ion.

TABLE I

EFFECT OF ZINC AND CALCIUM IONS ON THE RESPONSE OF THE DUAL ENZYME ELECTRODE

$[Zn^{2+}]$ (*M*)	*Inhibition (%)*	$[Ca^{2+}]$ (*M*)	*Inhibition (%)*
$2.4 \cdot 10^{-4}$	0	$2.3 \cdot 10^{-4}$	0
$9.4 \cdot 10^{-3}$	18	$2.3 \cdot 10^{-3}$	0
$2.4 \cdot 10^{-2}$	66	$4.6 \cdot 10^{-2}$	7
$8.7 \cdot 10^{-2}$	100	$6.8 \cdot 10^{-2}$	8

The effects of other metal ions were also tested in barbital buffer solution. The results, shown in Table I, indicate a serious effect by an excess of zinc ion and slight effect by an excess of calcium ion. The normal levels of these ions in water would not pose an interference in phosphate assay. Solutions (1 m*M*) of copper, mercury,

lead and cobalt ions were also examined by the oxygen level recovery method (Fig. 1B); no interference on enzyme function was found.

Effect of pH on the electrode response

Since the enzyme electrode contains two enzymes, and the response rate is affected by the enzyme activity of both, the response of this dual enzyme electrode to glucose-6-phosphate should show a mixed pH profile. Alkaline phosphatase from chicken intestine has been reported[18] to show an optimal pH at 8–9, and glucose oxidase has an optimal pH at 5.5 (ref. 19).

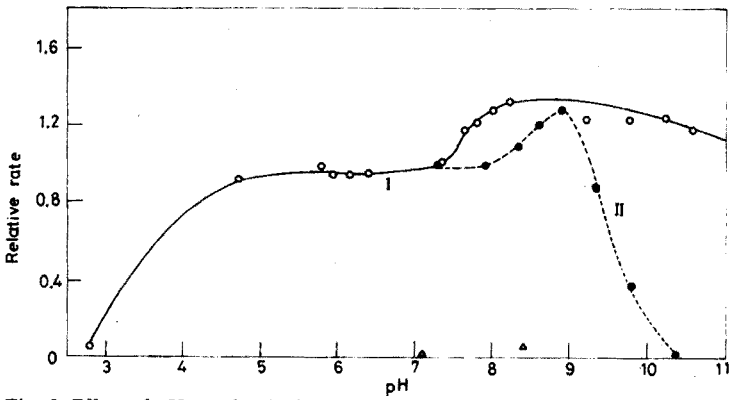

Fig. 5. Effect of pH on the dual enzyme electrode: 30°C; −0.60 V *vs.* SCE. I, Glycine buffer, 0.1 *M*; glucose-6-phosphate, 0.93 m*M*. II, Barbital buffer, 0.05 *M*, with 0.1 *M* KCl; glucose-6-phosphate, 0.57 m*M*. △ = Borate buffer, 0.1 *M*; glucose-6-phosphate, 0.93 m*M*.

Figure 5 shows the pH profile for the dual electrode, indicating an optimal pH around 9 in glycine and barbital buffers. However, the pH profile was not a typically shaped curve. At pH values lower than 9, the depression of activity was not as steep as on the alkaline side in glycine buffer. In the case of barbital buffer, which contained 0.1 *M* KCl, a different profile was observed on the alkaline side, owing to the stabilization of magnesium ion by chloride ion. At lower pH values, even at 5, the dual enzyme was still found to work well. The activity profile can be explained by a compensation in the activity of each enzyme and immobilization effects.

Borate buffer could not be used, since borate ion was found to inhibit the enzyme in the same way as phosphate ion.

The pH effect of phosphate inhibition must also be considered; pH 7.4 gave more sensitive results than pH 8.4, because of the greater K_i value at lower pH[17,20].

Calibration for phosphate ion

The depression of the rate with increase in phosphate concentration is shown in Fig. 6. Also, the reciprocal of the rate was found to be proportional to phosphate ion concentration added (in verification of eqn. (8)); measurement of phosphate ion by this method was found possible as low as $1 \cdot 10^{-4}$ *M*. In Fig. 7, another

calibration curve for phosphate is shown, based on the recovery of oxygen level by added phosphate after the attainment of a steady state (Fig. 1B). However, the oxygen recovery method, as can be seen from Fig. 1B, took a longer time than the decrease in oxygen level method (Fig. 1A) and also the current change was smaller.

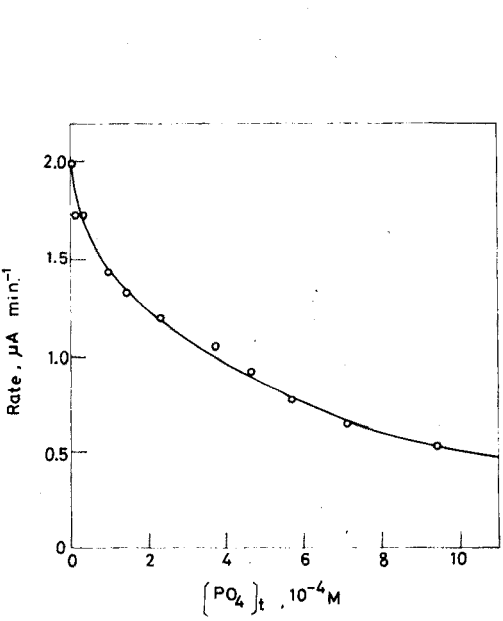

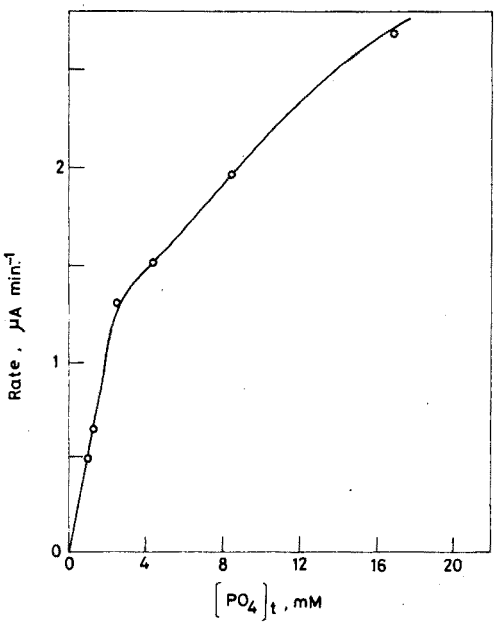

Fig. 6. Calibration curve for phosphate: 30°C; barbital buffer, 0.05 *M* with 0.1 *M* KCl, pH 7.4; −0.60 V *vs.* SCE; glucose-6-phosphate 1.78 m*M*.

Fig. 7. Calibration curve for phosphate using the oxygen recovery method. $T = 30°C$, barbital buffer 0.05 *M* with 0.1 *M* KCl, (pH 7.4). $E = -0.60$ V *vs.* SCE; glucose-6-phosphate 1.78 m*M*.

A change in slope of the calibration curve was observed above 2 m*M* phosphate (equivalent to the glucose-6-phosphate concentration), so that the method was not so sensitive to low phosphate concentration.

Effect of tris buffer

Tris buffer enhances the activity of alkaline phosphatase because of acceptance of phosphate ion by tris forming tris phosphate ester[21]. Figure 8 shows the effect of tris buffer on the phosphate inhibition of alkaline phosphatase activity at the same pH. As can be seen, about a one decade shift to lower sensitivity for phosphate was obtained because of this tris–phosphate reaction pathway, which enhanced the formation of glucose-6-phosphate.

Effect of ethanol

A more powerful phosphate acceptor than tris buffer is ethanol. Figure 9 shows the serious effect from the presence of ethanol. Curve I is the response of the dual enzyme electrode to glucose-6-phosphate as in Fig. 1; when ethanol was

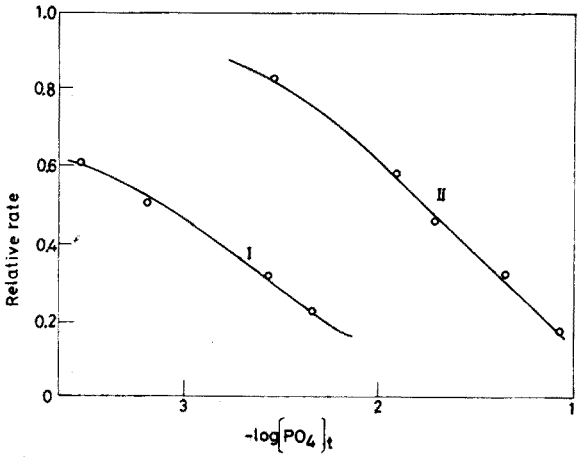

Fig. 8. Effect of tris-HCl buffer on the dual enzyme electrode response: 30°C; −0.60 V *vs.* SCE; glucose-6-phosphate, 0.93 m*M*. I, Glycine buffer, 0.1 *M*, pH 8.4. II, Tris/HCl buffer, 0.1 *M*, pH 8.4.

added at B, a rapid decrease of dissolved oxygen resulted. Curve II shows the response of the dual enzyme electrode to a mixture of substrate and ethanol. The rate was increased and also the steady-state current change caused by consumption of dissolved oxygen increased. This enhancement of the reaction reached up to a 180% increase of the initial rate (Table II). In the absence of glucose-6-phosphate, ethanol did not give any response to the dual enzyme electrode at first; however, several treatments of the dual enzyme electrode with ethanol solution caused a change of the electrode characteristics: namely, the dual enzyme electrode responded to ethanol faster than to glucose or glucose-6-phosphate (Table III).

This unexpected characteristic was found to be due to an alcohol oxidase impurity in glucose oxidase; this alcohol oxidase has been found during research

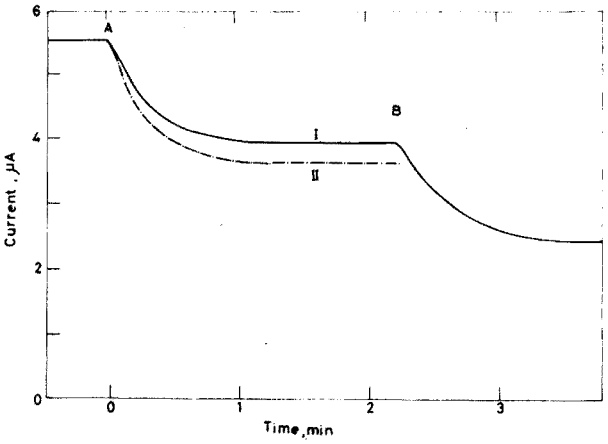

Fig. 9. Effect of ethanol on the dual enzyme electrode: 30°C; −0.60 V *vs.* SCE; barbital buffer, 0.05 *M* with 0.1 *M* KCl. I, Without ethanol, glucose-6-phosphate is added at A (11.8 m*M*, 0.5 ml) to 10.0 ml of buffer; at B absolute ethanol (1.0 ml) is added. II, The same amounts of glucose-6-phosphate and ethanol are added at A.

TABLE II

EFFECT OF ETHANOL ON THE DUAL ENZYME ELECTRODE RESPONSE

[EtOH] (M)	*Increase in rate (%)*
$3.2 \cdot 10^{-3}$	159
$1.1 \cdot 10^{-2}$	171
$5.5 \cdot 10^{-2}$	176

TABLE III

RESPONSE OF THE DUAL ENZYME TO GLUCOSE-6-PHOSPHATE, GLUCOSE AND ETHANOL

Substrate (M)	*Rate ($\mu A\ min^{-1}$)*		
	Glucose-6-phosphate	*Glucose*	*Ethanol*
$1.0 \cdot 10^{-4}$	0.65	1.10	3.85
$2.0 \cdot 10^{-4}$	1.33	2.05	6.43
$4.0 \cdot 10^{-4}$	2.60	3.41	9.91

on glucose oxidase[22]. The results in Table III indicate that this dual enzyme electrode could also be used for the assay of glucose-6-phosphate, glucose and ethanol.

Inhibition of alkaline phosphatase by oxyacids

One of the inhibitors of alkaline phosphatase is an oxyacid which can combine with the serine hydroxyl group, at the active center of the enzyme, to form esters; this results in an inhibition of the hydrolysis of substrate ester[17]. Figure 10 shows the effect of various oxyacids on the response of the dual enzyme electrode. The order of inhibition at pH 7.4 was found to be as follows: $WO_4^{2-} \geqslant AsO_4^{3-} \geqslant$

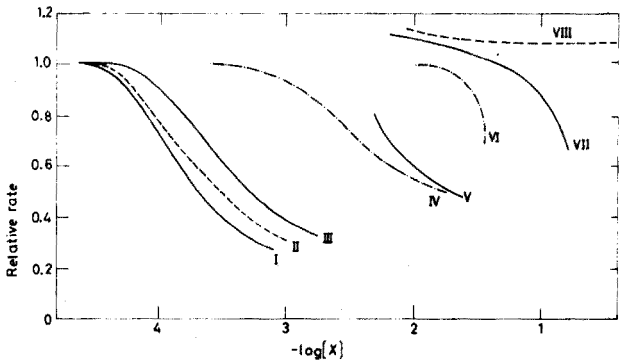

Fig. 10. Effect of various anions on the dual enzyme electrode. These inhibitors were added 2 min before the addition of glucose-6-phosphate. 30°C; −0.60 V *vs.* SCE; barbital buffer, 0.05 *M*, pH 7.4, with 0.1 *M* KCl. (I) Na_2WO_4, (II) NaH_2AsO_4, (III) NaH_2PO_4, (IV) Na_2MoO_4, (V) $Na_2B_4O_7$, (VI) EDTA, (VII) NH_4Cl, (VIII) NaOAc.

$PO_4^{3-} > MoO_4^{2-} > BO_3^{3-}$. Arsenite, had no effect on the enzyme activity up to 0.1 *M*, in contrast to arsenate.

As can be seen from Fig. 10, arsenate, tungstate, molybdate and even borate ions can be assayed as well as phosphate ion with the dual enzyme electrode. However, these mixtures could be separated and identified before measurement. In an assay for phosphate in rivers, streams or lakes, it is unlikely that any of these ions would be present to interfere.

The other common ions that exist in water solutions, such as chloride, nitrate and sulfate, which gave serious interferences on non-enzymatic ion-selective electrodes, did not show any effect up to 0.1 *M*. The buffer solution used has a relatively high concentration of potassium chloride (0.1 *M*) and also magnesium chloride (0.01 *M*). Bromide and iodide ions have no effect up to 0.1 *M*. The other possible inhibitors are reagents which can form complexes with the zinc in the enzyme protein resulting in the extraction of zinc from the enzyme or with magnesium ion used as a cofactor. As can seen in Fig. 10 (curve VI), EDTA interfered seriously above 15 m*M*, because of chelation of all the magnesium ion. Ammonium ion (curve VII) also affected the electrode response, but the effect was less than that of EDTA. Other inhibitors, like cyanide and high concentrations of heavy metal ions, were not tested. However, the addition of Mg–EDTA or Zn–EDTA could be helpful to protect the enzyme from serious denaturation by heavy metal ions.

The main disadvantage of the dual enzyme electrode is the difficulty in use in biological fluids which already contain glucose. In this case, the glucose in blood or biological fluid should be removed or measured before phosphate measurements. Another difficulty of this dual enzyme electrode could be possible inhibition and/or activation by other unknown chemicals in river water or biological fluids.

The dual enzyme electrode at present is not sensitive enough for assay of low concentrations of phosphate ion in river water; but the sensitivity for phosphate was found to depend on enzyme activity; namely, when the dual enzyme gave less response to glucose-6-phosphate, the sensitivity for phosphate was also less. It might be necessary to use more active enzyme or a more stable form and more substrate and possibly other oxygen-sensing devices, which could be used to make a more practical enzyme electrode for phosphate, and even sulfate, based on the same idea of a dual enzyme system.

Electrode stability

The daily response of the dual enzyme electrode to the substrate, glucose-6-phosphate, was observed during storage in buffer solution. Daily calibration was necessary, and the non-inhibition rate was compared with that of phosphate samples. After 3 months, the dual enzyme could still be used to measure phosphate over 10^{-4} *M*; even in solutions as low as pH 2.5 the enzymes remained active. After acidification, the enzymes recovered their activity reversibly. Even after EDTA treatment of the dual enzyme, the addition of zinc and magnesium ion could bring back some activity to the enzyme electrode.

The authors gratefully acknowledge the financial support of the Environmental Protection Agency (Grant No. EPA 800359) and the National Institutes of Health (Grant No. GM 17268). We would also like to thank Dr. S. S. Kuan for his helpful advice and suggestions.

SUMMARY

An enzyme electrode which senses oxygen consumption for the assay of phosphate ion (10^{-3}–10^{-4} *M*), was constructed by using two enzymes together:

$$\text{glucose-6-phosphate} \xrightarrow{\text{alkaline phosphatase}} \text{glucose} + \text{phosphate}$$

$$\text{glucose} \xrightarrow[O_2]{\text{glucose oxidase}} \text{gluconic acid} + H_2O_2$$

The competitive inhibition by phosphate ion added caused a smaller and slower oxygen consumption which could be detected by a platinum disc electrode at −0.6 V *vs.* SCE amperometrically. This dual enzyme electrode was also found useful for the assay of oxyacids other than phosphate, such as arsenate, tungstate, molybdate and borate.

REFERENCES

1 E. Pungor, K. Toth and J. Havas, *Mikrochim. Acta*, 4 (1966) 689.
2 G. Rechnitz, Z. F. Lin and S. B. Zamochnick, *Anal. Lett.*, 1 (1967) 29.
3 G. G. Guilbault and P. J. Brignac, Jr., *Anal. Chim. Acta*, 56 (1967) 139; *Anal. Chem.*, 41 (1969) 1136.
4 I. Nagelberg, L. Braddock and G. Barbero, *Science*, 166 (1969) 1403.
5 F. R. Shu and G. G. Guilbault, *Anal. Lett.*, 5 (1972) 559.
6 C. J. Coetzee and H. Freiser, *Anal. Chem.*, 40 (1968) 2071; 41 (1969) 1128.
7 M. Nanjo and G. G. Guilbault, *Anal. Chim. Acta*, in press.
8 H. H. Weetall and M. A. Jacobson, *IFS: Ferment. Technol. Today, Proc. IV*, (1972) 361.
9 H. Branderberger and R. Hanson, *Helv. Chim. Acta*, 36 (1953) 900.
10 A. V. Rou, *Clin. Chem.*, 16 (1970) 431.
11 G. G. Guilbault and G. J. Lubrano, *Anal. Chim. Acta*, 64 (1973) 439.
12 M. Nanjo and G. G. Guilbault, *Anal. Chim. Acta*, 73 (1974) 367; 75 (1975) 169.
13 M. Nanjo and G. G. Guilbault, *Anal. Chem.*, 46 (1974) 1769.
14 *Sigma Tech. Bulletins. No. 85, No. 104, and No. 104 M*; Sigma Chemical Co., St. Louis, Missouri, U.S.A.
15 L. Engstrom and G. Agren, *Acta Chem. Scand.*, 12 (1958) 357.
16 A. Garen and C. Levinthal, *Biochim. Biophys. Acta*, 38 (1960) 470.
17 T. W. Reid and I. B. Wilson in P. D. Boyer (Ed.). *The Enzymes, Vol. IV*, Academic Press, New York, 3rd edn., 1973, p. 373.
18 G. Y. Shinowara, L. M. Jones and H. L. Reinhart, *J. Biol. Chem.*, 164 (1964) 32.
19 H. J. Bright and M. Appleby, *J. Biol. Chem.*, 244 (1969) 3625.
20 T. W. Reid, M. Paulic, D. J. Sullivan and I. B. Wilson, *Biochemistry*, 8 (1969) 3184.
21 J. Dayan and I. B. Wilson, *Biochim. Biophys. Acta*, 81 (1964) 620.
22 F. W. Janssen and H. W. Ruelius, *Biochim. Biophys. Acta*, 151 (1968) 330.

Analytica Chimica Acta, 78 (1975) 81–92

A POLAROGRAPHIC AND SPECTRAL STUDY OF SOME C- AND N-NITROSO COMPOUNDS

W. FRANKLIN SMYTH, P. WATKISS, J. S. BURMICZ and H. O. HANLEY
Chemistry Department, Chelsea College, Manresa Road, London SW3 6LX (England)
(Received 14th January 1975)

The N-nitrosamines are not only potent carcinogens, but have additional mutagenic, embryopathic and teratogenic actions. They are formed by the action of nitrite on secondary amines, and volatile members of the series are conveniently assayed by steam distillation followed by gas–liquid chromatography–mass spectroscopy in foods and alcoholic beverages[1]. The formation and possible harmful effects of other nitroso compounds, *e.g.* nitrosophenols, formed *in vivo*, have recently been discussed[2,3].

All nitroso compounds are polarographically reducible; the mechanism of the reduction of C- and N-nitroso compounds[4–6], and the application of sensitive polarographic methods to the assay of dialkyl-N-nitrosamines[7–10] have often been discussed.

A spectral and polarographic study of a range of structurally different C- and N-nitroso compounds is described in this paper, and the determination of traces of such compounds by differential pulse polarography is discussed.

EXPERIMENTAL

Apparatus

Ultraviolet spectra of solutions maintained at 20°C were recorded with a Perkin-Elmer double-beam Model 137 spectrophotometer; 1-cm silica cells were used. The instrument was flushed with dry nitrogen to eliminate stray absorption effects.

A P.A.R. Model 174 Polarographic Analyser, operated in the sampled d.c. and differential pulse modes, was used in conjunction with a micro Kalousek vessel with a saturated calomel electrode. The dropping mercury electrode had the following characteristics: outflow velocity $m = 1.73$ mg s^{-1}, drop time $t = 4$ s at the potential of the saturated calomel electrode and at a mercury pressure $h = 80$ cm in 1 *M* potassium chloride. For the analyser the controlled drop time was 1 s with a modulation amplitude of 100 mV.

Reagents

Samples of the nitroso compounds were either donated or obtained from chemical suppliers. Stock solutions of each compound (about 10^{-3} *M*) were prepared in AnalaR methanol and kept in the dark under refrigeration to minimize decomposition.

A stock Britton–Robinson buffer solution (pH *ca.* 2.0) which was 0.04 *M* in

boric acid, phosphoric acid and acetic acid, was prepared from AnalaR reagents. From this, buffer solutions of varying pH were prepared by suitable addition of 0.1 *M* sodium hydroxide.

Procedures

Solutions were prepared for spectrophotometry by diluting the appropriate amount of stock solution with the appropriate buffer to give a concentration of $5 \cdot 10^{-5}$ *M*. To extend the pH range studied at either end of the scale, 1 *M* HCl, 0.1 *M* HCl, 0.1 *M* NaOH, and 1 *M* NaOH were used. The pH range 1–13 was scanned from 200 to 390 nm for each compound in increments of 1-pH unit to determine the approximate position of each pK_a value by observation of spectral changes. The region around each pK_a value was then studied with buffers differing by increments of *ca.* 0.3-pH unit. The pK_a values were then evaluated from the Henderson equation. The scan speed was 8 min for the range, and the reference cell contained a blank of buffer solution with the same amount of methanol as the samples.

For polarography, 2 ml of a 10^{-4} *M* solution of the nitroso compound in the appropriate supporting electrolyte was de-aerated with nitrogen for 3 min, and the *i–E* curve was recorded at a rate of 10 mV s^{-1} and a modulation amplitude of 100 mV. The sampled d.c. and differential pulse modes were used.

Polarography was used to monitor the nitroso compound content of the aqueous phase (5 ml of $5 \cdot 10^{-5}$ *M* compound buffered at a particular pH in the solvent extraction procedures. The *i–E* curves were recorded before and after a 10-min shaking with 5 ml of the solvent. If the nitroso compound was completely extracted, the organic layer was separated, the solvent evaporated off and the residue made up to 5 ml in the appropriate supporting electrolyte for polarographic examination.

RESULTS

It is convenient to describe the results according to the structural class of the compounds studied.

Class A compounds

Five compounds were investigated: dimethyl-N-nitrosamine (I), N-nitroso-piperidine (II), dicyclohexyl-N-nitrosamine (III), N-nitroso-3-methylaminosulpholane (IV) and diisopropyl-N-nitrosamine (V).

All these compounds exist as neutral species in the pH range 2–14, and could be extracted into non-aqueous solvents such as dichloromethane in this pH range (*e.g.* 99% for N-nitrosopiperidine). The variation of u.v. spectra with pH showed only one pK_a value of the order of 0 ± 2 corresponding to the formation of the protonated N-nitrosamines. The variation of $E_{\frac{1}{2}}$ with pH showed a break from about 25 mV/pH to 110 ± 20 mV/pH in passing through this pK_a value, and pK_a values of the order of 7 ± 1 (illustrated by the disappearance of the reduction wave of the protonated form and the simultaneous appearance of the reduction wave of the neutral molecule) were observed. The reduction of the protonated form (at pH 5) was found[11] microcoulometrically to be a 4-electron process and that at pH 10 a 2-electron process. Polarography of these solutions

following 75% reduction of the electroactive species showed no new electroactive species, and the u.v. spectra showed no new bands. Logarithmic analysis, *i.e.* log $[i/(i_d - i)$ *vs.* E, of the polarographic waves of the class A compounds showed two linear portions in acidic media ($pK_a < pH < 5$) and one linear portion at pH 10–12. These observations are in agreement with the following scheme:

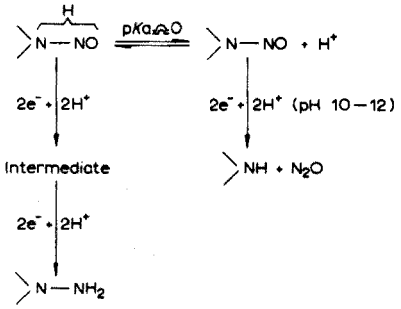

The final products of the electrolysis being those suggested previously[5,6]. The half-wave potentials of compounds I–V in solutions buffered at pH 2 were −0.90, −0.74, −0.75, −0.75 and −0.84 V *vs.* SCE, respectively. Differential pulse polarography of these compounds at pH 2 (and at pH 10–12) gave rise to very broad peaks (Fig. 1) with half-peak widths of the order 230 ± 20 mV. Dicyclohexyl-N-nitrosamine was the exception with a half-peak width of 160 mV. These peaks gave linear claibration plots of i_p *vs.* concentration in the range 10^{-4}–10^{-6} *M*. Below 10^{-6} *M* the peak disappeared into the supporting electrolyte decay curve. In order to test the possible selectivity, a mixture of $2.5 \cdot 10^{-4}$ *M* dimethyl-N-nitrosamine and $1.85 \cdot 10^{-4}$ *M* N-nitrosopiperidine was analysed, since these compounds had the greatest separation of $E_{\frac{1}{2}}$ values. The result (Fig. 1) showed incomplete resolution. More complicated mixtures would show even less resolution.

Class B compounds

Dibenzyl-N-nitrosamine (VI) and N-nitrososarcosinamide (VII) were examined as members of this class.

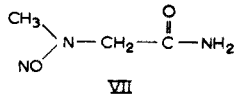

VII

The u.v. spectra of VI showed two changes with change of pH: the band at 235 nm in neutral solution ($\varepsilon = 1.22 \cdot 10^4$ l mol^{-1} cm^{-1}) moved to 244 nm ($\varepsilon = 1.62 \cdot 10^4$ l mol^{-1} cm^{-1}) in passing through the pK_1 value (0.7); and above pH 12 the 235-nm band moved to 225 nm ($\varepsilon = 1.72 \cdot 10^4$ l mol^{-1} cm^{-1}). Application of the Henderson equation gave a pK_2 value of 13.7. The u.v. spectra of VII also showed two changes with changing pH: the 232-nm band in neutral media ($\varepsilon = 3.76 \cdot 10^4$ l mol^{-1} cm^{-1}) moved to 236 nm ($\varepsilon = 1.70 \cdot 10^4$ l mol^{-1} cm^{-1}) below pH 1, the pK_1 value being 0; and this band moved to 241 nm ($\varepsilon = 0.37 \cdot 10^4$ l mol^{-1} cm^{-1}) above pH 12 ($pK_2 = 12.75$).

The variation of $E_{\frac{1}{2}}$ and i_{lim} with pH for 10^{-4} *M* solutions of VI and VII was rather similar to that of Class A compounds in acidic media. A 4-electron reduction wave was obtained for compound VI at pH 0–5 and for compound VII

at pH 0–7; this decayed to a 2-electron wave in both cases giving rise to pK_1 values of 7 for VI and 8.5 for VII. As for class A compounds, the $E_{\frac{1}{2}}$ value of the reduction wave corresponding to the neutral form was pH-independent. In the pH range 12–14, the 2-electron wave for VII gradually disappeared, confirming the existence of an acid–base equilibrium in alkaline media.

$E_{\frac{1}{2}}$ values were very similar to those of class A compounds over the whole pH range; for VI at pH 2, $E_{\frac{1}{2}} = -0.73$ V and for VII, $E_{\frac{1}{2}} = -0.81$ V. The half-peak widths were 170 ± 10 mV at pH 2 and pH 11. Calibration plots of i_p *vs.* concentration were linear down to 10^{-6} *M* for the 4-electron reduction at pH 2 or the 2-electron reduction at pH 11. At pH 8 in the sampled d.c. mode, compound VI caused a maximum on the reduction wave of the conjugate acid, which gave a sharp pre-wave on the differential pulse polarographic curve (Fig. 2). This phenomenon could be used for identification purposes. The effect was also observed for di-n-propyl-N-nitrosamine.

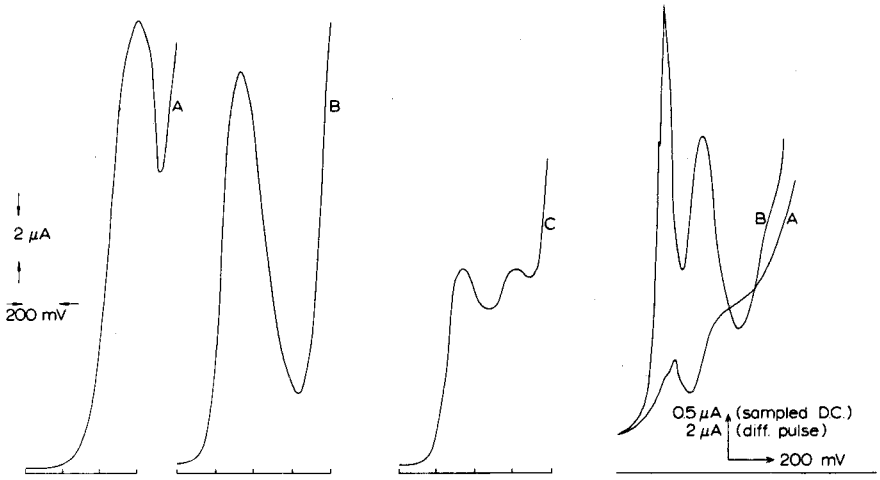

Fig. 1. Differential pulse polarograms of some aliphatic N-nitrosamines in Britton–Robinson buffer pH 5: A, dimethylnitrosamine $5 \cdot 10^{-4}$ *M*; B, N-nitrosopiperidine $3.7 \cdot 10^{-4}$ *M*; C, equivolume mixture of A and B. Instrumental conditions: scan speed $1 mVs^{-1}$; droptime 1s; modulation amplitude 50 mV.

Fig. 2. Polarograms of 10^{-4} *M* dibenzyl-N-nitrosamine in Britton–Robinson buffer pH 8: A, sampled d.c. mode; B, differential pulse mode. Instrumental conditions: scan speed $10 mVs^{-1}$; drop time 1s; modulation amplitude 100mV; starting voltage −1.0 V.

The following scheme is suggested for compounds of class B.

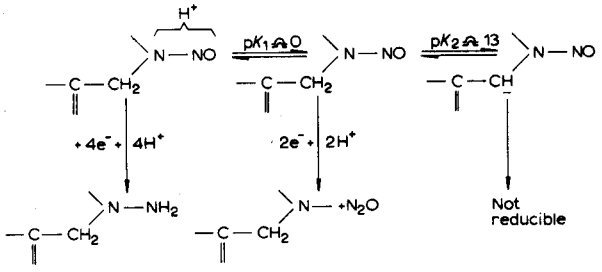

Class C compounds

Although it is generally admitted that diphenyl-N-nitrosamine (VIII) is not carcinogenic, N-methyl-N-nitrosoaniline (IX) does possess such properties. N-Nitrosamines with at least one phenyl group conjugated to the N–NO moiety were therefore studied to see if there were any polarographic differences that could be used to differentiate class C compounds from those of classes A and B.

Both VIII and IX protonate in acidic media with pK_1 values of -2.0 and 0.25, respectively. The absorption maxima of the neutral forms lie at 294 nm ($\varepsilon = 1.16 \cdot 10^4$ l mol^{-1} cm^{-1}) and 268.5 nm ($\varepsilon = 0.88 \cdot 10^4$ l mol^{-1} cm^{-1}), respectively, and that of the protonated form of IX occurs at 267.5 nm ($\varepsilon = 0.73 \cdot 10^4$ l mol^{-1} cm^{-1}). No spectral changes were observed in alkaline media pH 12–14. The two compounds showed similar polarographic behaviour, giving rise to a 4-electron reduction at pH 0–5 and a 2-electron reduction at pH 9–12. The pK_1' values were 7.0 for VIII and 7.4 for IX. The $E_{\frac{1}{2}}$ values were -0.6 V for VIII and -0.38 V for IX, which are considerably separated from those of classes A and B. Differential pulse polarograms of these compounds at pH 2 showed well-defined peaks, with half-band widths of 85 mV and 70 mV for VIII and IX, respectively, which were well separated from the supporting electrolyte decay wave; calibration plots were linear down to $5 \cdot 10^{-8}$ *M*. The corresponding waves at pH 11 showed a similar separation in reduction potentials (-0.95 V for VIII and -0.73 V for IX) but the peak heights were one-third of those at pH 2 and were also broader.

The following scheme is suggested to represent the spectral and polarographic behaviour of compounds of class C.

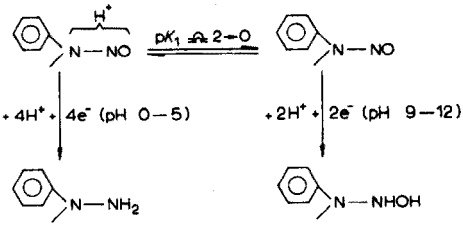

These N-nitrosamines conjugated to phenyl groups go through hydroxylamine intermediates in the reduction process in acidic media[4], so that the 2-electron reduction in alkaline media probably corresponds to reduction to the hydroxylamine which in the unprotonated state will not be reduced further. The shapes of the waves obtained in the sampled d.c. anddifferential pulse modes were quite different from those of classes B and C, which suggests a different reduction mechanism over the whole pH range. Logarithmic analysis of the waves for VIII confirmed this[11].

Class D compounds

The three compounds studied under this heading were ethylmethyl-N-nitrosocarbamate (X), N-methyl-N-nitrosourea (XI) and N-methyl-N-nitroso-N'-nitroguanidine (XII), all of which have powerful carcinogenic and mutagenic properties.

The spectrum of X in the pH range 0–14 did not change ($\varepsilon = 0.1 \cdot 10^4$ l mol^{-1} cm^{-1} at 244 nm, $0.09 \cdot 10^4$ at 265 nm (shoulder), and $0.009 \cdot 10^4$ at 370 nm),

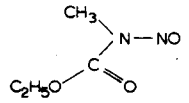

(X)

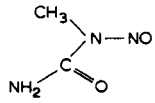

(XI)

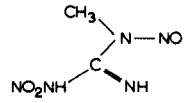

(XII)

whereas XI had two absorbing forms corresponding to the protonated N–NO moiety ($\varepsilon = 1 \cdot 10^4$ l mol^{-1} cm^{-1} at 225 and 242 nm, and $0.2 \cdot 10^4$ at 350 nm) and the neutral species ($\varepsilon = 2 \cdot 10^4$ at 233 nm). This corresponds to a pK_1 value of 2.0. Dichloromethane extracted the neutral form of XI with 60% efficiency and that of X with 95% efficiency. Compound XII, however, had four different absorbing forms in the pH range 0–14 corresponding to the dication, monocation, neutral

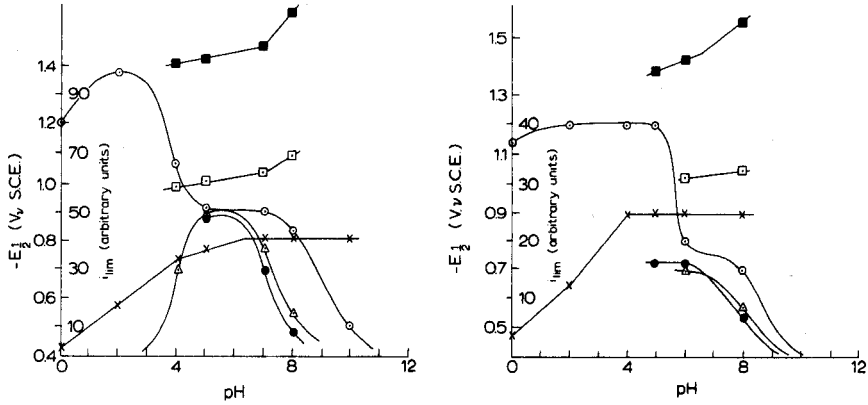

Fig. 3. The variation of $E_{\frac{1}{2}}$ and i_{lim} with pH for ethylmethylnitrosocarbamate, (○) i'_{lim}, (△) i''_{lim}, (●) i'''_{lim}, (×) $E'_{\frac{1}{2}}$, (□) $E''_{\frac{1}{2}}$, (■) $E'''_{\frac{1}{2}}$.

Fig. 4. The variation of $E_{\frac{1}{2}}$ and i_{lim} with pH for N-methyl-N-nitrosourea. (○) i'_{lim}, (△) i''_{lim}, (●) i'''_{lim}, (×) $E'_{\frac{1}{2}}$, (□) $E''_{\frac{1}{2}}$, (■) $E'''_{\frac{1}{2}}$.

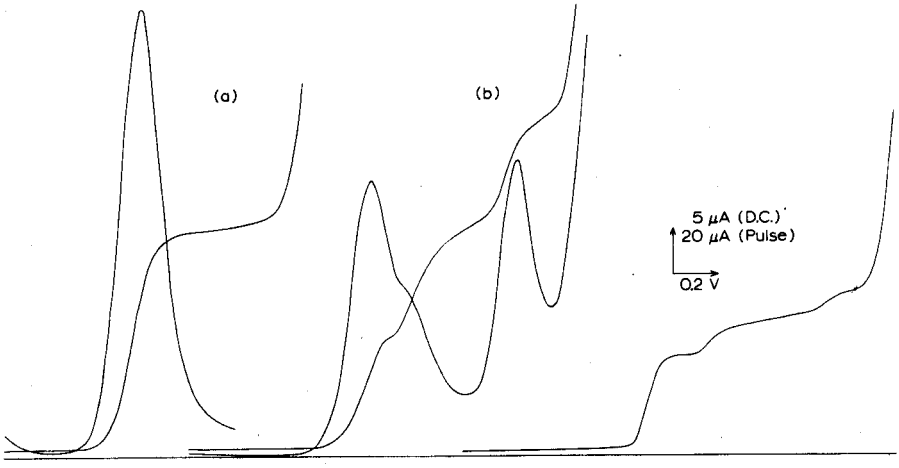

Fig. 5. Sampled d.c. and differential pulse polarograms of 5.10^{-4} *M* ethylmethylnitrosocarbamate in BR buffers. (a) pH 2.0; (b) pH 5.0; (c) pH 8.0. Instrumental conditions: scan speed 10 mVs^{-1}, drop time ls, modulation amplitude 100 mV, starting voltage OV.

species and monoanion. The wavelengths of maximal absorption occurred at 267 nm ($\varepsilon = 1 \cdot 10^4$) l mol^{-1} cm^{-1}), 273 nm ($\varepsilon = 1.15 \cdot 10^4$), 268 nm ($\varepsilon = 1.0 \cdot 10^4$) and 263 nm ($\varepsilon = 0.75 \cdot 10^4$), respectively, and application of the Henderson equation gave pK_a values of 1.0, 7.3 and 11.3. This compound was compared with diphenylguanidine which gave two pK_a values at approximately 1 and 12, which suggests that the pK_a value at 7.3 for XII corresponded to the loss of a proton from the N–NO moiety.

The *i vs.* pH and $E_{\frac{1}{2}}$ *vs.* pH plots are shown in Fig. 3 for compound X and Fig. 4 for compound XI; clearly, the polarographic behaviour of these two compounds is similar. In acidic media (pH 0–4 for XI and pH 0–3 for X) a 4-electron reduction wave is observed (*i'*) which, at higher pH values, decays to a 2-electron wave with the simultaneous appearance of two further waves (*i''* and *i'''*), both corresponding to 2-electron processes. These decay to zero by pH 8–9. The main wave (*i'*) is constant in height (X, pH 5–8; XI, pH 6–8) and then disappears gradually up to pH 10. The decay of wave *i'* is not connected with an acid–base equilibrium but corresponds to decomposition, since compounds X and XI showed no u.v. spectra above pH 10. This behaviour is illustrated in Fig. 5 for ethylmethyl-N-nitrosocarbamate at pH 2, 5 and 8; differential pulse polarograms are also given. The peaks are broad with half-peak widths of about 200 mV but the polarogram shows the characteristic three-peak pattern of X and XI at intermediate pH values. The following scheme illustrates these spectral and polarographic results for X and XI.

The sampled d.c. polarographic waves for N-methyl-N-nitroso-N'-nitroguanidine (XII) are given in Fig. 6 for the pH range 0–12. The differential pulse polarogram for pH 2 is also given and shows a characteristic three-peak pattern

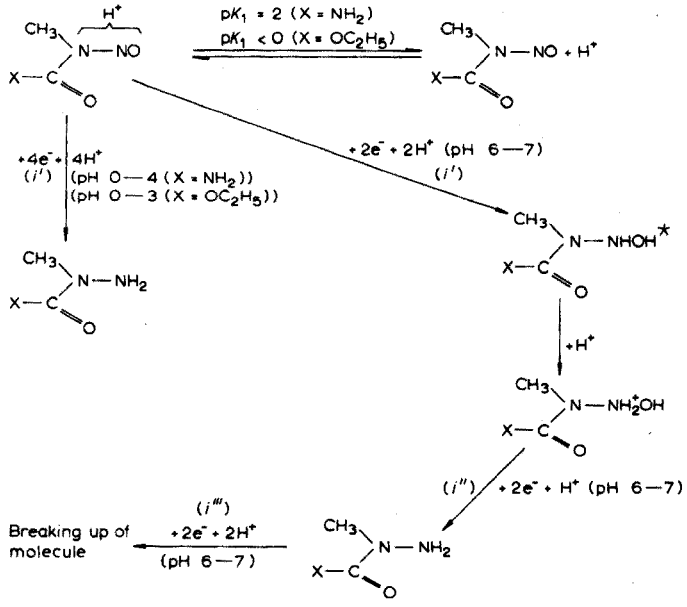

(* This is only reduced in the protonated form, hence the decay of *i''* and *i'''* with p$K' \simeq 7.5$.)

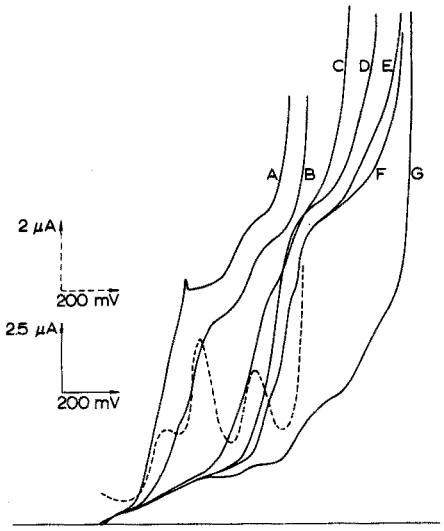

Fig. 6. Variation of wave shape with pH for 10^{-4} *M* N-methyl-N-nitroso-N'-nitroguanidine, (A) pH 0, (B) pH 2.0, (C) pH 4.0, (D) pH 6.0, (E) pH 8.0, (F) pH 10.0, (G) 12.0 (All Britton–Robinson buffers.) Instrumental conditions: scan speed 10 mVs^{-1}, sampled d.c. mode, drop time 1s, starting voltage 0 V. (Dotted line is the differential pulse polarogram at pH 2.0.)

with half-peak widths of about 80 mV. In the pH range 0–6 there was a 3-wave pattern, the first two together representing a 4-electron process and the third a 2-electron process. At pH 8–10 these three waves virtually united and, by pH 12, all the waves had decayed to a small fraction of their original height. This behaviour suggests that at pH 0–6, the first two waves correspond to the 4-electron reduction of the =N–NO moiety, which occurs more easily than that of any of the other nitrosamine compounds already studied in this paper, and that the third wave corresponds to the 2-electron reduction of the azomethine group. It is suggested that the grouping $=N–NO_2$ is electroinactive in acidic media (compare with dimethylnitramine in Fig. 8). The reaction mechanism has not been ascertained in alkaline media.

Class E compounds

Figure 7 shows the differential pulse polarograms of 10^{-4} *M* solutions of several aromatic C-nitroso compounds and illustrates the existence of large and very sharp peaks (half-peak width *ca.* 50 mV) at pH 10, and the absence of analytically usable peaks at pH 2. Unfortunately, the peaks occur at approximately the same potential for *o*- and *p*-nitroso compounds, thus endowing this very sensitive polarographic method for aromatic C-nitroso compounds with little selectivity. Since nitrophenols have been detected in some foods along with nitrosophenols[12], differential pulse polarograms of *p*-nitrophenol were recorded in pH 2 and pH 10 buffers. In contrast to *p*-nitrosophenol, *p*-nitrophenol gives its largest and sharpest peak in pH 2 buffer, the half-peak width being 100 ± 10 mV ($E_p = -0.23$ V).

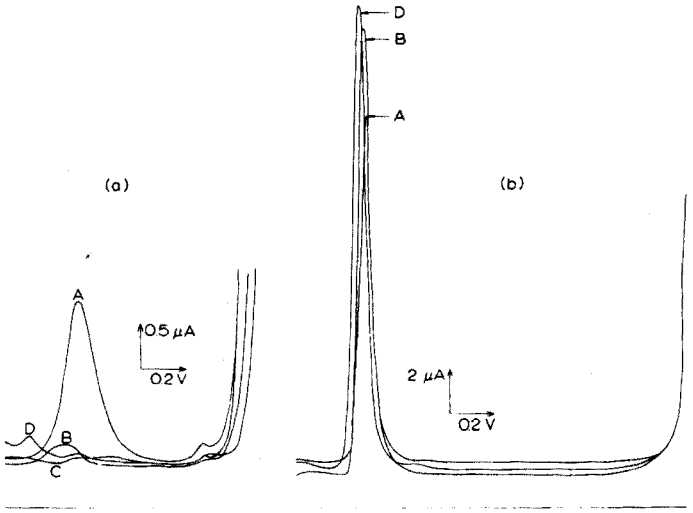

Fig. 7. Differential pulse polarograms of 10^{-4} *M* solutions of some C-nitroso compounds in Britton–Robinson buffers: (a) pH 1.8, (b) pH 10.0. (A) *p*-nitrosophenol, (B) N,N′-diethyl-p-nitrosoaniline, (C) 4-nitroso-phenazone, (D) 2-nitroso-1-naphthol. Instrumental conditions, scan speed 5 mVs^{-1}, drop time 1 s; modulation amplitude 50 mV, starting voltage 0 V.

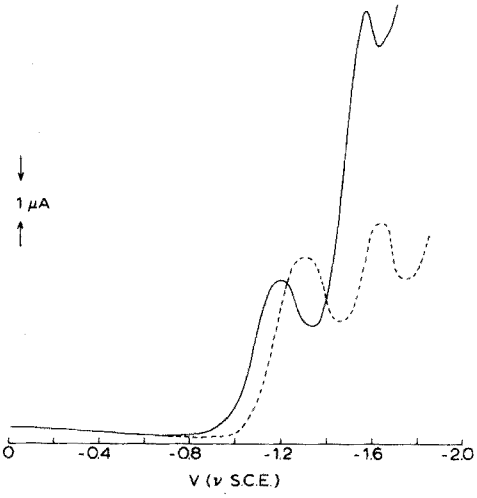

Fig. 8. Differential pulse polarograms of 10^{-4} *M* dimethylnitramine Britton–Robinson buffer, pH 7.4 (...) Britton–Robinson buffer pH 11.0 (no wave in Britton–Robinson buffer, pH 1.8).

ANALYTICAL APPLICATIONS

Since the class A compounds give differential pulse peaks with the greatest half-peak widths, several attempts were made to decrease the width of these peaks in order to obtain some measure of selectivity. Pulidori *et al.*[5,6] have stated that the 4-electron reduction of these compounds is complicated by adsorption effects, whereas the 2-electron reduction in alkaline media is not. However, the differential

pulse polarograms at pH 10–11 showed that the peak height decreased by about three times but the half-peak width did not alter. Because the peak was further removed from the supporting electrolyte decay in alkaline media, the detection limit was about the same (*i.e.* about 10^{-6} *M*) as that in acidic media where the peaks came much closer to the decay wave.

N-Nitrosamines have been converted to N-nitramines for other analyses such as gas chromatography, either by the use of oxidizing agents such as peroxytrifluoroacetic acid and hydrogen peroxide or by exposure to u.v. light[13]. Since it was expected that the nitramines would be electroactive, differential pulse polarograms were recorded for dimethylnitramine at different pH values (Fig. 8). The compound gave two peaks in alkaline media, but both were as broad as those of the parent N-nitrosamine and of no greater analytical utility.

Attempts to improve the selectivity by heating were also made. Solutions in a micro Kalousek cell with a mercury pool reference electrode were heated to 80°C and the differential pulse polarograms compared with that recorded at 25°C for N-nitrosopiperidine. The peak height increased by a third and the peak potential moved slightly towards more positive potentials but the half-peak width remained the same.

TABLE I

DIFFERENTIAL PULSE POLAROGRAPHIC DATA FOR NITROSO COMPOUNDS

(The waves underlined are recommended for analytical purposes.)

Compound	*pH 2.0*		*pH 10.0*	
	E_p	$i_p(\mu A)$	E_p	$i_p(\mu A)$
Group A				
N-Nitrosopiperidine	<u>−0.75</u>	1.5	−1.35	0.75
Dimethyl-N-nitrosamine	<u>−0.87</u>	2.0	−1.55[b]	0.75
Group B				
Dibenzyl-N-nitrosamine	—	—	−1.35	0.65
N-Nitrososarcosinamide	—	—	−1.35	0.50
Group C				
Diphenyl-N-nitrosamine	−0.6	2.5	<u>−0.95</u>	0.50
N-Methyl-N-nitrosoaniline	−0.65	3.0	<u>−1.20</u>	1.00
Group D				
N-Methyl-N-nitrosourea	<u>−0.65</u>	1.5	—[a]	—[a]
N-Methyl-N-nitroso-N′-nitroguanidine	−0.28[b]	1.0	−1.1[b]	0.8
	<u>−0.40</u>	2.0	−1.28	1.2
	<u>−0.65</u>	2.5		
Group E				
p-Nitrosophenol	+0.13	0.5	<u>−0.39</u>	3.5
	−1.0	0.5	<u>−0.89</u>	2.0
			−1.08	1.5
p-Nitrophenol	−0.03	0.5		
	<u>−0.22</u>	3.0	−0.90	2.0
	<u>−1.0</u>	0.5	−1.08	1.5

[a] No wave observed.
[b] Shoulder.

Nitroso compounds (representative of groups A–E) were then subjected to differential pulse polarography at concentrations of 10^{-5} *M* at acidic pH (2.0) and alkaline pH (10.0). The results (Table I) showed that compounds belonging to groups A–D gave larger peaks in acidic media than in alkaline media. The peaks did not sharpen in moving from acidic to alkaline media, thus these substances are best determined in acidic media (*e.g.* pH 2.0). The sensitivity was about 10^{-6} *M* for groups A and B (where the reduction wave was close to the decay wave of the supporting electrolyte) and about 10^{-7} *M* for groups C and D. Group E compounds gave much sharper and larger peaks than any of the other nitroso compounds investigated; linear i_p–concentration relationships were obtained down to $5 \cdot 10^{-8}$ *M*. *p*-Nitrosophenol was best determined in pH 10 buffer and nitrophenol at pH 2.

Dichloromethane was found to be the most efficient solvent for extracting these nitroso compounds at pH 4 where all, except N-methyl-N-nitroso-N′-nitroguanidine, are neutral molecules. The percentage extraction for 10^{-5} *M* solutions varied from 60% (N-methyl-N-nitrosourea) to 100% (*p*-nitrosophenol). Selective solvent extraction could therefore be used to separate only N-methyl-N-nitroso-N′-nitroguanidine from the other nitroso compounds.

After solvent extraction of a mixture of nitroso compounds, representative of groups A–E, with dichloromethane, differential pulse polarography could distinguish between compounds of groups E and C, but not between compounds of groups A, B and D, unless the mixture contained only two such compounds. Other polarographically active substances are usually extracted from foodstuffs, *e.g.* heterocycles such as furfural, and these are generally reduced at reasonably negative potentials like the dialkyl N-nitrosamines. Accordingly, the present results indicate that the technique is best applied to nitroso compounds that are reduced at more positive potentials (*i.e.* more highly conjugated nitroso compounds), for these give rise to larger and sharper differential pulse polarographic peaks.

The authors wish to thank Dr. Lunt and Dr. Walters (B.S.M.I.R.A., Leatherhead) for the provision of the dialkyl and cyclodialkyl N-nitrosamines.

SUMMARY

A wide range of N-nitroso compounds was investigated polarographically and spectrophotometrically. In general, the =N–NO group is reduced in a 4-electron step in acidic media, which is most suitable for differential pulse polarographic analysis at the trace level. If the groups R and/or R′ attached to the nitrosamine group are saturated entities, then the resulting differential pulse polarographic peaks are broad and of little use in the resolution of mixtures. The limit of detection is of the order of 10^{-6} *M*. If R and R′ are unsaturated, the polarographic peaks are much sharper, mixtures can be resolved and the limit of detection is of the order of 10^{-7} *M*. C-Nitroso and C-nitro compounds are best determined by differential pulse polarography, because the waves are comparatively large and sharp, and because the reductions occur at relatively positive potentials where co-extractible interferences from foods, etc., will interfere to a minimal degree.

REFERENCES

1 P. Bogovski, R. Preussman and E. A. Walker (Eds.), *N-nitroso compounds, Analysis and Formation*, W.H.O. Publication, 1972.
2 B. C. Challis, *Nature (London)*, 244 (1973) 466.
3 M. E. Knowles, J. Gilbert and D. J. McWeeney, *Nature (London)*, 249 (1974) 672.
4 L. Meites, *Polarographic Techniques, Tables*, Interscience, 1965.
5 F. Pulidori, G. Borghesani, C. Bighi and R. Pedriali, *J. Electroanal. Chem. Interfacial Electrochem.*, 27 (1970) 385.
6 G. Borghesani, F. Pulidori, R. Pedriali and C. Bighi, *J. Electroanal. Chem. Interfacial Electrochem.*, 32 (1971) 303.
7 C. L. Walters, E. M. Johnson and N. Ray, *Analyst (London)*, 95 (1970) 485.
8 A. Malins, *J. Agr. Food. Chem.*, 18 (1970) 740.
9 D. Daiber and R. Preussman, *Z. Anal. Chem.*, 206 (1964) 344.
10 L. Sander, *J. Ass. Offic. Anal. Chem.*, 53 (1967) 269.
11 J. Springall and P. Watkiss, Analytical Report, Chelsea College, 1974.
12 M. E. Knowles, Private Communication, Chelsea College, December 1974.
13 R. W. Rivers, M. Sc. Dissertation, Chelsea College, 1973.

Analytica Chimica Acta, 78 (1975) 93–98

DOSAGE DE L'ISONIAZIDE, DU N-ACÉTYLISONIAZIDE ET DE L'ACIDE ISONICOTINIQUE PAR POLAROGRAPHIE À TENSION SINUSOÏDALE SURIMPOSÉE

J. J. VALLON, A. BADINAND et C. BICHON

Laboratoire Central de Biochimie A, Hôpital Edouard-Herriot, Place d'Arsonval, Lyon (France)
Laboratoire de Chimie Analytique, U.E.R. des Sciences Pharmaceutiques, 69003 Lyon (France)

(Reçu le 30 decembre 1974)

Les études pharmacocinétiques exigent la mise en oeuvre de méthodes spécifiques et assez sensibles pour mesurer des concentrations de médicaments et de métabolites de l'ordre du microgramme par millilitre. La fluorimétrie permet, le plus souvent, d'obtenir de très hautes sensibilités, mais avec souvent une faible spécificité et des risques d'interférences. Parmi les méthodes électrochimiques modernes, la polarographie à tension sinusoïdale surimposée offre l'avantage d'associer une sensibilité souvent élevée à une grande sélectivité lorsque les substances à doser ont des potentiels de demi-vague voisins, comme cela est le cas pour les molécules organiques d'une même série chimique. Nous avons appliqué cette méthode au dosage de l'isoniazide, de son dérivé N-acétylé et de l'acide isonicotinique, en vue de leur dosage dans les milieux biologiques.

De nombreuses méthodes ont été décrites pour le dosage de l'isoniazide (INH) et de ses métabolites. Les dosages microbiologiques, fondés sur l'inhibition de la croissance de *mycobacterium tuberculosis*[1] ont l'avantage d'être spécifiques de l'INH libre mais la mise en oeuvre de la méthode nécessite plusieurs jours et ne dose pas les métabolites. Parmi les méthodes chimiques, certaines évaluent globalement l'INH et ses métabolites; Maher *et al.*[2] dosent l'hydrazine libérée par hydrolyse acide de l'INH ou de ses dérivés. D'autres sont spécifiques de l'INH libre, telles que la colorimétrie à la vanilline[2] ou à l'acide 2,4,6-trinitrobenzène sulfonique[3], ou la fluorimétrie après action du bromure de cyanogène[4]. Enfin, certaines réactions sont spécifiques du N-acétylisoniazide (AcINH)[5]. Aucune méthode ne dose la molécule mère et ses métabolites avec suffisamment de sensibilité pour permettre d'atteindre les concentrations des milieux biologiques.

L'électroréduction des dérivés pyridiniques conduit à l'hydrogénation d'une double liaison du noyau sur le groupe azométhine[6] selon la réaction:

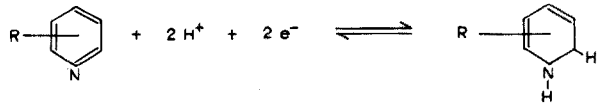

Les potentiels de demi-vague sont pH-dépendants: ils s'abaissent quand le pH augmente. Les substitutions sur l'hétérocycle, et en particulier sur l'azote intracyclique, modifient aussi les $E_{\frac{1}{2}}$. Les hydrazides à noyau pyridinique et leurs produits d'oxydation permanganique ont été récemment étudiés par polarographie

classique[7]. La polarographie à impulsions a permis aussi de doser l'acide 2-hydroxynicotinique et son métabolite dans le sang et l'urine[8]. Enfin, Bieder[9] a appliqué la polarographie à tension alternative surimposée à l'étude de l'élimination urinaire de l'éthionamide et du prothionamide.

Nous avons étudié successivement l'influence des paramètres électriques et des paramètres chimiques sur l'électroréduction de l'isoniazide (INH), de l'acide isonicotinique (INA) et du N-acétylisoniazide (AcINH).

PARTIE EXPÉRIMENTALE

Matériel et réactifs

L'étude a été faite sur un polarographe Tacussel PRG 3. Le débit du capillaire utilisé était de 95 mg min^{-1}.

Solution d'INH (100 µg ml^{-1}). On dissous 10 mg d'isoniazide Roche dans 100 ml d'eau distillée.

Solution d'acide isonicotinique. On oxyde 10 mg d'INH en solution dans 20 ml d'eau distillée par du permanganate de potassium 0,1 *N* jusqu'à coloration rose persistante; après un contact de 15 min, on décolore la solution par addition d'hydroxylamine à 1% dans l'eau distillée. On complète à 100 ml. La solution obtenue est à 100 µg ml^{-1} (exprimés en INH).

Solution d'acétyl-INH. On dissous 10 mg d'INH dans 0,5 ml d'anhydride acétique (Prolabo); après chauffage 5 min au bain-marie à l'ébullition, on complète à 100 ml avec de l'eau distillée. La solution obtenue est à 100 µg ml^{-1} (exprimés en INH).

Solutions tampon. Des solutions tampon de diverses molarités (1, 0,5, 0,1) ont été préparées par dilution de solutions molaires de phosphate disodique (pour des pH 5–8) ou d'acide citrique (pH 2–4); pour chaque dilution, le pH était ajusté à la valeur recherchée par addition d'acide chlorhydrique 12 *M* ou de soude 10 *M*, et vérifié au pH mètre.

Étude des paramètres chimiques

L'étude a porté sur les variations des potentiels de réduction, de l'intensité des pics polarographiques en fonction du pH et de la force ionique. Des quantités de 50 µg pour 5 ml de solution tampon ont servi aux essais. Les réglages de l'appareil, choisis à la suite d'essais préliminaires dans le tampon pH 6, étaient les suivants: étendue des potentiels explorés, −0,50 à −1,50 V *vs.* ECS; fréquence du signal alternatif, 120 Hz; amplitude du signal alternatif, 50 mV; angle de phase de détection, 0 grade; sensibilité de l'appareil, 1,25 µA/25 cm; hauteur du réservoir de mercure, 65 cm; écoulement du mercure, libre.

Variations du potentiel de demi-vague en fonction du pH. La figure 1 montre que les potentiels des pics polarographiques diminuent presque linéairement quand le pH augmente. L'acide isonicotinique est toujours réduit à un potentiel plus négatif que l'INH et l'AcINH. Pour ces deux derniers, les courbes sont presque confondues. Aux pH inférieurs à 8, l'INH présente un deuxième pic indiquant une réduction en deux étapes. Il apparait de façon nette que l'écart maximum entre les pics d'INH et d'AcINH est de 0,05 V, alors qu'il est environ de 130 mV entre l'INA et les autres dérivés.

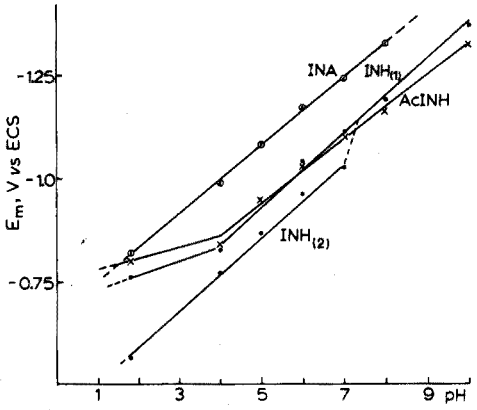

Fig. 1. Influence du pH sur le potentiel de pic.

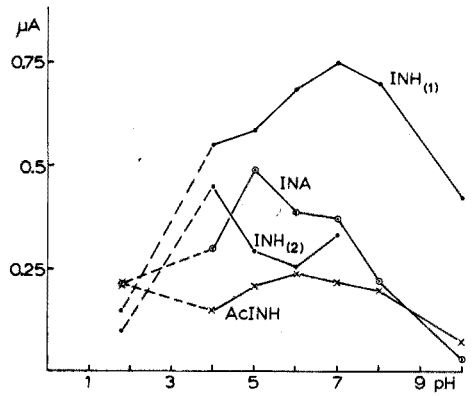

Fig. 2. Influence du pH sur la sensibilité. $INH_{(1)}$ et $INH_{(2)}$: première et deuxième vagues de l'isoniazide.

Ces observations montrent que, même en utilisant une amplitude faible de tension surimposée, il n'est pas possible de séparer les pics d'INH et AcINH, quelque soit le pH. On est donc conduit à envisager une différenciation des deux molécules grâce à leur oxydation différentielle en INA, comme nous l'avons fait par la suite.

Variations de la hauteur des pics avec le pH. La figure 2 montre l'influence du pH sur l'intensité du courant alternatif enregistré au sommet des pics. L'étude a été faite dans du tampon 0,5 *M*. L'intensité augmente avec le pH pour les trois composés, puis décroît. La zone de pH correspondant à la sensibilité maximum de détection varie avec chaque composé. Celle-ci est toujours plus élevée pour l'INH, faible pour l'AcINH et intermédiaire pour l'INA. Les sensibilités maximum sont obtenues à pH 7,0 pour l'INH, à pH 6,0 pour l'AcINH et à pH 5,0 pour l'INA.

Influence de la force ionique sur la sensibilité. Les pH 6, 7 et 8 ont été étudiés dans les tampons phosphate de molarité variable: 1 *M*, 0,5 *M*, 0,1 *M*. On constate que, quelque soit le pH, la sensibilité augmente quand la molarité croît de 0,1 *M* à 0,5 *M* et qu'elle baisse ensuite quand on atteint la valeur *M*. Dans la suite de notre travail, nous avons utilisé des tampons 0,5 *M* afin d'obtenir des sensibilités maximum et un pouvoir tampon efficace.

Étude des paramètres électriques

Des quantités de 50 µg de chacun des produits (exprimés en INH), en solution dans 5 ml de tampon 0,5 *M* à pH 6,0, ont servi à cette étude. Chaque essai était précédé d'un barbottage d'azote de 10 min.

Influence de la fréquence du signal alternatif. L'étude a été faite de 50 Hz à 400 Hz avec les réglages suivants: échelle des potentiels explorés, −0.8 à −1.5 V *vs.* ECS; hauteur de la colonne de mercure, 40 cm; fréquence de chute des gouttes, 1 goutte par s; amplitude du signal alternatif, 5 mV; angle de phase de détection, 0 grade; sensibilité de l'appareil, 250 nA/25 cm.

La fréquence donnant la sensibilité maximum de détection varie avec chaque

composé. La courbe de l'INH a un maximum à 140 Hz, celle de l'acide isonicotinique à 260 Hz, et l'AcINH à 120 Hz. Comme l'AcINH est détecté avec la sensibilité la plus faible, c'est la fréquence de 120 Hz qui a servi dans la suite de nos essais.

Influence de l'angle de phase de détection. La zône de -50 à $+50$ grades a été explorée avec les mêmes réglages que précédemment, à la fréquence alternative de 120 Hz. Avec un angle de phase nul, l'INH et l'INA sont détectés avec la sensibilité maximum. Le dérivé acétylé a un maximum vers $+20$ grades, mais sa sensibilité n'est abaissée que de 10% à 0 grade. Cette dernière valeur a été conservée par la suite, étant donné l'énorme avantage présenté par l'absence de courant capacitif à cette valeur.

Influence de l'amplitude du signal alternatif surimposé. L'amplitude de l'intensité alternative faradaïque est proportionnelle à l'amplitude de la tension alternative surimposée, mais la zone des amplitudes utilisables varie avec l'espèce électroactive. L'amplitude maximum de l'intensité alternative est obtenue avec un signal surimposé de 100 mV pour l'INH et l'AcINH. Pour l'INA, le maximum correspond à 60 mV car le pic correspondant se confond peu à peu avec la limite due au solvant quand l'amplitude augmente. Par contre, si l'on opère en milieu plus alcalin (pH 7,0), on constate que le maximum se situe là aussi à 100 mV.

En ce qui concerne l'influence de ΔE sur le pouvoir de résolution, nous avons constaté que, même aux faibles valeurs de ΔE, les pics de l'INH et de l'AcINH sont impossibles à individualiser par suite de l'existence d'un deuxième pic dû à l'INH aux pH inférieurs à 8,0. Il est donc plus avantageux d'utiliser une valeur ΔE de 100 mV dans les cas où la solution contient l'INH ou l'AcINH à l'état pur; on ne recherche alors pas un pouvoir de résolution très élevé; la sensibilité de détection se trouve beaucoup augmentée.

Influence des réglages du capillaire. L'intensité des courants faradaïques enregistrés dépend beaucoup du débit du capillaire et de la fréquence de chute des gouttes de mercure. Avec les réglages suivants (120 Hz, 50 mV; 0 grade) et une hauteur du réservoir de mercure à 50 cm, nous avons étudié l'influence de la fréquence de chute des gouttes. On constate que la sensibilité augmente quand la fréquence diminue de 5 gouttes par s à 1 goutte par s. Il conviendrait donc d'utiliser un écoulement libre du capillaire dans la mesure où la fréquence de chute des gouttes est un sous multiple entier de la fréquence de la tension alternative.

En ce qui concerne le débit du capillaire, la sensibilité est une fonction linéaire de ce débit. On aura donc intérêt à utiliser une colonne de mercure la plus longue possible.

Mise au point des dosages

À l'aide des résultats précédents, nous avons cherché à définir les conditions optimum pour détecter et doser les trois dérivés pyridiniques avec un maximum de sensibilité. Nous avons recherché, pour chaque molécule, le seuil de sensibilité et la linéarité des réponses en fonction des concentrations.

Dosage de l'INH. L'isoniazide est détecté avec un maximum de sensibilité à

pH 7,0 en tampon phosphate 0,5 *M*. Les réglages électriques les plus favorables sont: fréquence du signal alternatif, 140 Hz; amplitude du signal alternatif, 50 mV; angle de phase de détection, 0 grade variable; colonne de mercure, 70 cm; débit du capillaire, 95,18 mg min^{-1}; fréquence de chute des gouttes, 1 goutte par 4 s; vitesse de balayage de l'échelle des potentiels, 75 mV min^{-1}.

Une sensibilité meilleure serait obtenue avec une amplitude du signal alternatif de 100 mV, mais il n'est pas possible de dépasser 50 mV, étant donné l'amplitude élevée des oscillations au cours de la chute des gouttes. La sensibilité maximum de l'appareil utilisable dans ces conditions est de 1 nA cm^{-1}. La figure 3 (courbe B) montre l'enregistrement obtenu avec 0,2 μg d'INH par ml, le volume total de la cellule étant 5 ml: on constate que le signal obtenu est de 3 nA environ, soit une déviation de 3,5 cm.

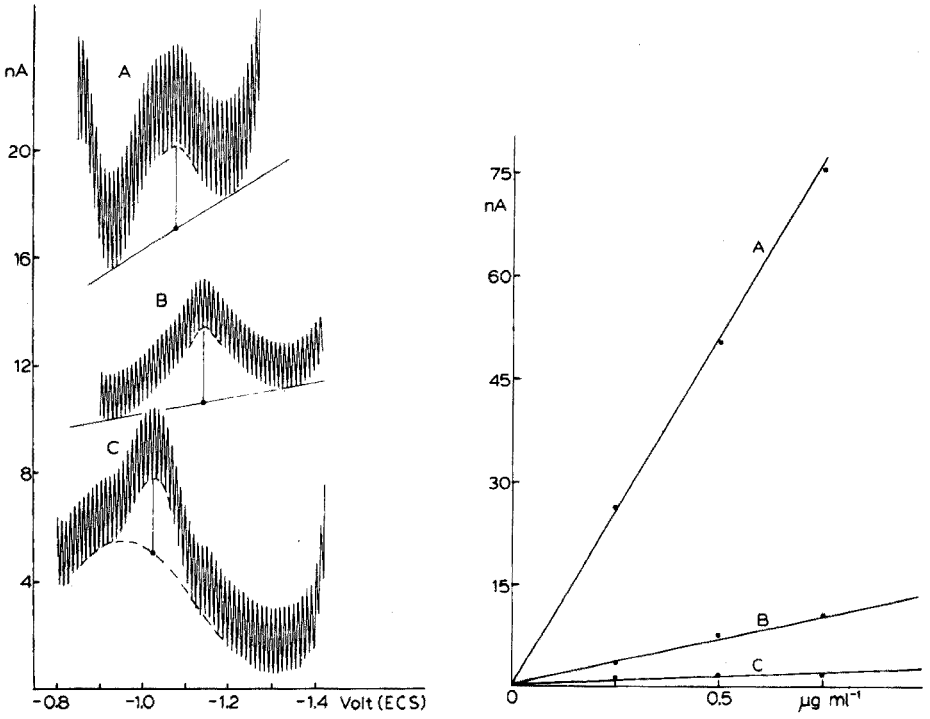

Fig. 3. Etude des limites de detection. (A) 0,03 μg d'acide isonicotinique par ml à pH 5,0 (angle de phase de détection, -10 grades). (B) 0,2 μg d'isoniazide par ml à pH 7,0 (angle de phase, -10 grades). (C) 1 μg d'acétyl isoniazide à pH 6,0 (angle de phase, $-7{,}5$ grades). Réglages de l'appareil: voir le texte.

Fig. 4. Courbes d'etalonnage de l'acide isonicotinique à pH 5,0 (A), de l'isoniazide à pH 7,0 (B), et de l'acétyl isoniazide à pH 6,0 (C).

La figure 4 montre la droite d'étalonnage obtenue. Le seuil de détection est donc environ de 0,2 μg ml^{-1}.

Dosage de l'AcINH. Le pH optimum pour ce dosage est 6,0 et la molarité 0,5 *M*. Nous avons utilisé les mêmes réglages que pour l'INH; en particulier, la

fréquence de 140 Hz et l'amplitude de 50 mV du signal alternatif modifient peu la sensibilité par rapport aux réglages optimum (110 Hz, 100 mV). La sensibilité choisie est identique.

La figure 3 (courbe C) montre que la concentration minimum décelable est de 0,5 μg ml^{-1} environ pour un signal de 3 nA. La Fig. 4 donne la droite d'étalonnage.

Dosage de l'INA. L'étude a été faite en tampon phosphate 0,5 *M* à pH 5,0 avec les mêmes réglages électriques. La Fig. 3 (courbe A) montre le signal obtenu avec 0,03 μg ml^{-1} soit 3 nA environ. La Fig. 4 donne la droite d'étalonnage.

CONCLUSION

La polarographie à tension alternative surimposée s'avère suffisamment sensible pour doser des concentration d'isoniazide et de ses dérivés (acétylisoniazide et acide isonicotinique) inférieures à 0,5 μg ml^{-1}. Elle permet ainsi d'atteindre les concentrations rencontrées dans les milieux biologiques au cours d'un traitement par l'INH. Nous avons entrepris l'application de la méthode à des dosages dans le sang et les urines en vue de la surveillance des thérapeutiques antituberculeuses, ainsi que pour la recherche du phénotype acétyleur de l'INH.

RÉSUMÉ

Les auteurs décrivent un dosage par polarographie à tension sinusoïdale surimposée de trois molécules pyridiniques: l'isoniazide (INH), le N-acétylisoniazide (AcINH), et l'acide isonicotinique (INA). L'étude des conditions de pH, de force ionique et des paramètres électriques a permis d'obtenir un seuil de détection égal à 0,5 μg ml^{-1} pour l'acétylisoniazide, à 0,2 μg ml^{-1} pour l'isoniazide et de 0,03 μg ml^{-1} pour l'acide isonicotinique.

SUMMARY

The a.c. polarographic determination of isoniazid (INH), N-acetylisoniazid (AcINH) and isonicotinic acid (INA) is described. Under the optimal conditions of pH, ionic strength and electrical parameters, the limits of detection are 0.5 μg ml^{-1} for AcINH, 0.2 μg ml^{-1} for INH, and 0.03 μg ml^{-1} for INA.

BIBLIOGRAPHIE

1 J. N. Vivien, R. Thibier et A. Lepeuple, *Rev. Fr. Malad. Resp.*, 1 (5–6) (1973) 753.
2 J. R. Maher, J. M. Whitney, J. S. Chambers et D. J. Stanonis, *Amer. Rev. Tuberc.*, 76 (1957) 852.
3 L. C. Dymond et D. W. Russell, *Clin. Chim. Acta*, 27 (1970) 513.
4 J. H. Peters, *Amer. Rev. Resp. Dis.*, 81 (1960) 485.
5 P. Venkataraman, L. Eidus et S. P. Tripathy, *Tubercle, London*, 49 (1968) 210.
6 R. Pointeau et J. Bonastre, *Eléments de polarographie*, Masson, Paris, 1970.
7 F. Pellerin et H. El Makkawi, *Ann. Pharm. Fr.*, 30 (*3*) (1972) 187.
8 J. Arthur, F. de Silva, N. Strojny et N. Munno, *Anal. Chim. Acta*, 66 (1973) 23.
9 A. Bieder, *Actualités de Chimie Analytique—21ème série*, Masson, Paris, 1972, pp. 1–25.

Analytica Chimica Acta, 78 (1975) 99–106

THE DETERMINATION OF METALS IN PETROLEUM SAMPLES BY ATOMIC ABSORPTION SPECTROMETRY

PART I. DETERMINATION OF VANADIUM

G. ŠEBOR, I. LANG*, P. VAVREČKA**, V. SYCHRA and O. WEISSER

Department of Petroleum Technology and Petrochemistry, Prague Institute of Chemical Technology, 166 28 Prague 6 (Czechoslovakia)

(Received 6th February 1975)

The determination of vanadium in petroleum samples, which is of considerable importance in fuel analysis and technology, is rather troublesome. Modern instrumental techniques, such as x-ray spectrometry, emission spectrography, spark-source mass spectrometry, and particularly atomic absorption spectrometry (a.a.s.) and neutron activation analysis, have been used in recent years in attempts to solve this problem. However, most of these techniques (including a.a.s.) do not provide reliable and accurate results for vanadium, for a variety of different reasons.

It has already been shown that the determination of vanadium in fuel oils by atomic absorption spectrometry is not accurate, even when the procedure is standardized by means of organometallic standards dissolved in the same way as the samples in methyl isobutyl ketone (MIBK); neither evaluation from calibration curves nor the use of the standard addition technique provides satisfactory results[1,2]. Sugihara *et al.*[3] have stated that, because of strong matrix interferences, a.a.s. should not be used for the determination of vanadium and nickel in petroleum samples dissolved in organic solvents, but only as a means of studying matrix effects. These effects have also been reported by Smith *et al.*[4] to cause erroneous results for trace amounts of vanadium in petroleum products (samples and Conostan reference solutions dissolved in MIBK).

Von Lehmden *et al.*[5] have compared the results obtained by modern instrumental techniques in nine different laboratories for the determination of trace metals in fuel samples; they reported considerable differences in the analytical results for most elements, variations being often nearly one order of magnitude, in each matrix studied (coal, ash, fuel oil and gasoline). Other authors[6,7] have also reported that the results obtained for vanadium in fuel oils by a.a.s. can differ widely; tests in eight different laboratories showed values in the range 22.4–444 p.p.m. for a sample with an NBS certificate value of 315 ± 5 p.p.m. All these reports indicate that the sample matrix can have a decisive influence on the analytical results for trace metals.

In petroleum samples, vanadium is present in the form of organometallic complexes with porphyrins and with other organic compounds[8,9]. In the porphyrin

* Present address: Fuel Research Institute, Prague 9-Běchovice.

** Present address: Mining Institute of the Czechoslovak Academy of Sciences, Prague 8.

compounds, vanadium is bound by four nitrogen donor atoms, while in the non-porphyrin compounds nitrogen, oxygen and sulphur can all act as donor atoms in various combinations[10]. The non-porphyrin vanadium compounds present in petroleum samples are probably organometallic complexes with configurations of nitrogen, oxygen, and sulphur donor atoms analogous to those found in β-diketones, β-ketoimines, salicylaldimines, monothio- and dithio-β-diketones, mono- and dithiocarbamates, etc.[11-14].

In some recent papers dealing with a.a.s.[15-21], the different behaviour of various types of metal–organic compounds in analytical flames has been discussed. For some compounds, there was a marked dependence of the absorbance of the metal on the volatility of the compound; for several metals, the absorbance varied considerably according to the nature of the metal bonding. For example, Fujiwara *et al.*[22] have reported that the absorbance of cobalt(III) complexes in an air–acetylene flame depends on the type of the coordinated ligand atoms, *i.e.*, N, O, C, and S. Differences in absorption signals from various organometallic compounds were observed, particularly for transition metals (Fe, Co, Ni, Mn, Cr, Cu), but also for lead and tin.

Some attention has been paid to the behaviour of vanadium compounds, for which the similar effects would be expected because vanadium is a typical transition metal. Kashiki *et al.*[23,24] have established that the absorbance of vanadium (as well as of several other metals) determined in petroleum samples dissolved in MIBK depends strongly on the type of the metal bond. This dependence can be eliminated by the addition of halogens (particularly iodine) to the samples[23,24]. Some authors have shown that free bromine can cause structural changes in vanadylporphyrins[25-27]. Sugihara *et al.*[28] have reported that chlorine can release vanadium both from synthetic vanadylporphyrins and from vanadylporphyrins present in petroleum samples. However, these workers[3] have also reported that the a.a.s. determination of vanadium in several crude oil samples when 1-methylnaphthalene is used for dilution, shows no dilution effect; only the type and composition of the samples seemed to be important, and the matrix effects could not be interpreted.

In the work described here, the effects of using different organometallic compounds of vanadium—bis-(1-phenyl-1,3-butandione)oxovanadium(IV), vanadyl tetraphenylporphyrin and Conostan vanadium standard—for the preparation of vanadium reference solutions for the direct determination of vanadium in petroleum samples diluted with xylene, are described. It is shown that the vanadium bonding in the standards, as well as the sample matrix, can cause significant errors.

EXPERIMENTAL

Apparatus

All measurements were carried out with a Varian-Techtron model AA-5 atomic absorption spectrometer equipped with an AB-50 burner for a nitrous oxide–acetylene flame. A shielded vanadium hollow-cathode lamp (A.S.L.) was used as a primary line source. Other experimental conditions were as follows: analytical line 318.4 nm; spectral bandwidth 0.33 nm; lamp current 6 mA; nitrous oxide flow rate 5.8 l min^{-1}; acetylene flow rate 3.4 l min^{-1}; rate of solution aspiration 2.0 ml min^{-1}; height of observation 0 mm (just above the burner top), or in some cases

2 or 6 mm. Non-specific absorption was measured under identical conditions by using a hydrogen hollow-cathode lamp.

Reagents

Stock solutions of bis-(1-phenyl-1,3-butandione)oxovanadium(IV) (VOBA) containing 100 μg V ml^{-1} were prepared as suggested by Isbell *et al.*[29], and described, *e.g.*, by Dean and Rains[30]: 0.07674 g of dried VOBA (Alfa Inorganic) was dissolved in 30 ml of xylene with addition of 10 ml of ethylhexanoic acid, 5 ml of acetylacetone, and 2 ml of dimethylaniline: acetylacetone and dimethylaniline were used in place of the 6-methyl-2,4-heptandione and bis(2-ethylhexyl)amine, respectively, recommended previously. The mixture was heated on an electric plate with vigorous stirring; when all the material had dissolved, the solution was cooled, transferred to a 100-ml volumetric flask and diluted to the mark with xylene.

Stock solutions of vanadyl tetraphenylporphyrine (VOTPP) containing 30 μg V ml^{-1} were prepared by dissolving 0.0400 g of the compound in 30 ml of hot xylene; after cooling, the solution was transferred to a 100-ml volumetric flask and diluted to the mark with xylene. VOTPP was prepared and characterized by the methods described earlier[31].

Stock solutions of Conostan vanadium standard (Continental Oil Company) containing 30 μg V ml^{-1} were prepared by dissolving 0.6 g of the standard (concentration, 5000 μg V ml^{-1}) in 100 ml of xylene.

A 10000-p.p.m. potassium standard stock solution was prepared by dissolving 5.3 g of potassium cyclohexanebutyrate (Alfa Inorganic) in 30 ml of hot xylene; after cooling, the solution was transferred to a 100-ml volumetric flask and then diluted to 100 ml with xylene[32].

Sample preparation

The effect of the vanadium bonding was studied with synthetic mixtures of the standards in xylene, as well as with real petroleum samples. The following petroleum samples were used: (1) a hydrogenated atmospheric residuum from Romashkino crude oil (U.S.S.R.); (2) a hydrogenated deasphaltisate from Romashkino atmospheric residuum; (3) asphaltenes from Romashkino crude oil; (4) an acetonitrile extract from Romashkino asphaltenes; (5) a vanadylporphyrin concentrate obtained by gel chromatography of sample 4.

An appropriate amount of the sample—but not more than 1 g per 10 ml of xylene—was dissolved with slight heating in xylene: after cooling the solution was diluted to a definite volume.

As the determination of vanadium in aqueous solution is usually done in the presence of an ionization suppressor (potassium) when a high-temperature nitrous oxide–acetylene flame is used, all measurements with xylene solutions were performed both with and without the addition of potassium.

RESULTS

Reference solutions (30 μg V ml^{-1}) prepared from VOBA, VOTPP, and Conostan vanadium standard were used to study the dependence of the vanadium absorption signal on the height of measurement in the nitrous oxide–acetylene

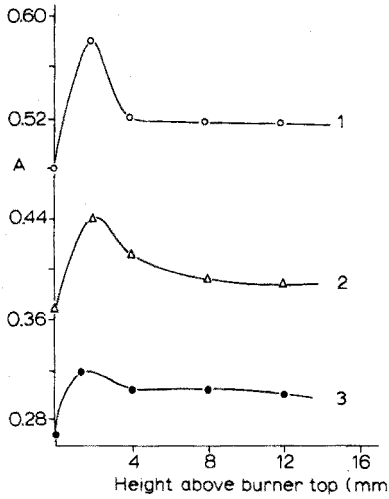

Fig. 1. Nitrous oxide–acetylene flame profiles for vanadium reference solutions (30 μg V ml^{-1}) prepared from different organometallic compounds: (1) VOTPP; (2) VOBA; (3) Conostan.

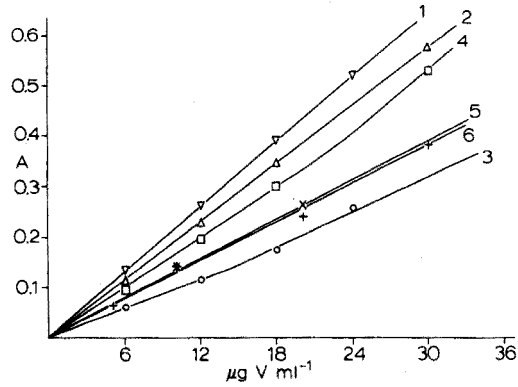

Fig. 2. Calibration curves for vanadium obtained with reference solutions prepared from different organometallic compounds, 1, VOTPP+K; 2, VOTPP; 3, VOBA+K; 4, VOBA; 5, Conostan+K; 6, Conostan.

flame. Flame profiles are shown in Fig. 1. For all the organometallic compounds studied, the profiles exhibited a maximum at a height of 2 mm.

For the experimental conditions described above, with an observation height of 2 mm, calibration curves were constructed by using reference solutions prepared from all the organometallic compounds studied (Fig. 2). These curves were then used to evaluate the vanadium concentrations in xylene solutions of real petroleum samples measured in the presence and in the absence of potassium. The results are listed in Table I.

TABLE I

VANADIUM CONTENT IN XYLENE SOLUTIONS OF PETROLEUM SAMPLES[a]

(All results are given in μg ml^{-1})

Sample	*Without K*			*With K (2000 μg ml^{-1})*		
	A	*B*	*C*	*A*	*B*	*C*
1	10.5	12.5	15.9	10.4	20.6	17.4
2	9.5	11.4	14.4	9.3	19.0	15.5
3	7.5	8.9	11.4	8.6	18.0	14.3
4	4.7	5.8	7.1	4.9	10.7	7.9
5	3.8	4.6	5.8	2.3	5.1	3.8

[a] A—VOTPP reference solutions; B—VOBA reference solutions; C—Conostan reference solutions.

VOTPP, VOBA, and petroleum samples 1 and 3 were used to examine a standard addition technique. In the case of organometallic standards, additions of

6,12 and 18 μg V ml^{-1} prepared from one organometallic reference solution were added to the reference solutions (6 μg V ml^{-1}) prepared from a second organometallic standard. With actual petroleum samples, amounts of x, $2x$, and $3x$ of either the VOBA or the VOTPP reference solutions were added to the sample solution containing a known amount of vanadium (x). Results were obtained for solutions containing potassium (2000 μg K ml^{-1}) as well as without potassium, at observation heights of 0, 2 and 6 mm (Table II); the standard addition plots for an observation height of 2 mm are shown in Figs. 3 and 4. No non-specific absorption was observed in any case.

DISCUSSION

The slopes of the calibration graphs show clearly that reference solutions containing the same concentration of the metal but prepared from different organometallic compounds give different absorption signals, the differences being more pro-

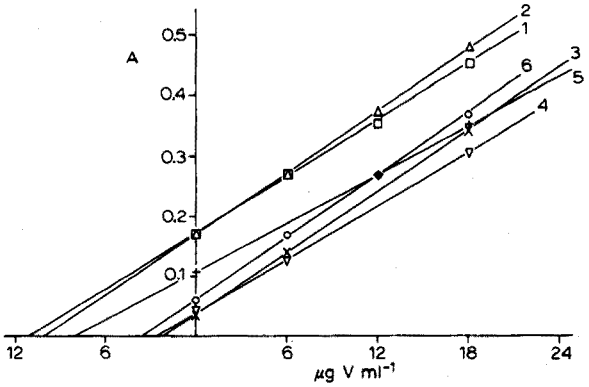

Fig. 3. Plots for the standard addition technique in the absence of potassium. 1, sample 1+VOTPP; 2, sample 1+VOBA; 3, sample 3+VOTPP; 4, sample 3+VOBA; 5, VOTPP+VOBA; 6, VOBA+VOTPP.

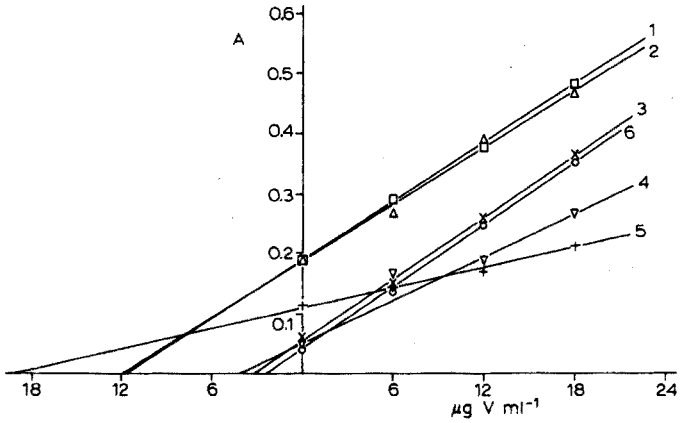

Fig. 4. Plots for the standard addition technique in the presence of 2000 μg K ml^{-1}. 1, sample 1+VOTPP; 2, sample 1+VOBA; 3, sample 3+VOTPP; 4, sample 3+VOBA; 5, VOTPP+VOBA; 6, VOBA+VOTPP.

TABLE II

VANADIUM CONTENTS IN XYLENE SOLUTIONS OF ORGANOMETALLIC STANDARDS AND IN PETROLEUM SAMPLES DETERMINED BY THE ADDITION TECHNIQUE

(All results are given in $\mu g\ ml^{-1}$)

Sample	*Without K* *Height of observation (mm)*			*With K (2000 $\mu g\ ml^{-1}$)* *Height of observation (mm)*		
	0	*2*	*6*	*0*	*2*	*6*
VOBA + VOTPP	3.4	4.6	4.0	2.3	2.1	2.2
VOTPP + VOBA	7.6	6.7	8.0	19.0	17.5	20.2
1[a] + VOBA	9.5	9.4	10.1	11.8	11.4	10.3
1 + VOTPP	10.8	9.8	9.9	11.2	10.6	11.9
3[a] + VOBA	2.5	2.8	2.3	4.6	2.8	2.2
3 + VOTPP	2.1	2.8	2.2	3.2	2.4	2.6

[a] Vanadium content determined after mineralization: sample 1, 10.8 $\mu g\ ml^{-1}$; sample 3, 1.9 $\mu g\ ml^{-1}$.

nounced for higher vanadium concentrations.

The function of potassium as an ionization suppressor in the determination of vanadium, when both elements are present as organometallic compounds in xylene solutions, is debatable. In the case of VOTPP, the addition of potassium increases the atomic absorption signal of vanadium, whereas with VOBA, the absorption signal is significantly decreased. Reference solutions prepared from the Conostan vanadium standard gave almost the same results whether or not potassium was present.

The increase in the vanadium signal for VOTPP indicates suppression of an ionization interference by potassium. But the results obtained for the other two standards tend to suggest that some "complexes" of potassium are formed with the vanadium compounds present in the sample solutions (with different thermal stabilities), and that the ease of vanadium release from these "complexes" is the decisive factor for the magnitude of the vanadium atomic absorption signal.

The content of vanadium determined in actual petroleum samples is therefore dependent on the type of organometallic compound used for the preparation of the reference solutions. The calibration curves show that, in the absence of potassium, the lowest results are obtained when VOTPP reference solutions are used, whereas the highest results correspond to the use of Conostan reference solutions. In the presence of potassium (2000 $\mu g\ K\ ml^{-1}$), all the samples studied give higher absorption signals than in the absence of potassium. Thus, the effect of potassium in real samples is analogous to that on VOTPP. In practice, this means that the vanadium sample signal evaluated from a calibration curve constructed from VOBA reference solutions gives results significantly higher than those evaluated from VOTPP calibration. Vanadium contents evaluated from Conostan reference solutions lie between these two values.

Since the increase in the vanadium atomic absorption signals of VOTPP reference solutions and real sample solutions in the presence of potassium is practically the same (with one exception), nearly identical results for the vanadium contents in real samples are obtained from the VOTPP calibration curves whether the measurements are made with or without potassium. Evaluation from the Conostan

calibration curves, where the absorption signal is hardly affected by potassium, leads to slightly higher values for the vanadium contents of real samples, because the magnitude of the sample signal changes in the presence of poassium. The most significant differences between the results—both with and without potassium—were observed when VOBA reference solutions were used.

The results evaluated by the standard addition technique confirmed those obtained from calibration curves. Additions of VOTPP to a solution of VOBA result in higher vanadium absorption signals than those obtained for additions of VOBA, *i.e.* the vanadium content determined is lower than the expected value. As a corollary, addition of VOBA to a solution of VOTPP leads to higher determined vanadium values than expected. The presence of potassium in the solution analyzed causes further deviations because potassium affects the signals of the two reference solutions differently. Thus, when VOBA and VOTPP were used together, the results by the standard addition technique never corresponded to the expected vanadium concentration of 6 μg ml^{-1} (Table II).

The application of the standard addition technique to the petroleum samples (1 and 3) showed that the effect of the vanadium bonding in the reference solution is less pronounced than in the case of solutions containing only pure compounds. This is probably due to the additional effect of the complex sample matrix. It can be assumed that the results obtained for vanadium contents in real samples are influenced by the sum of different effects arising from the type of the organometallic compound used for calibration and from matrix effects. More general conclusions will be possible only after the effects have been observed on larger numbers of petroleum samples of different character.

SUMMARY

Some atomic absorption characteristics of xylene solutions of Conostan vanadium standard, bis-(1-phenyl-1,3-butandione)oxovanadium(IV), and vanadyltetraphenylporphyrin in a nitrous oxide–acetylene flame were compared. Errors arising when these different organometallic compounds are used for standardization in the determination of vanadium in xylene solutions of various petroleum samples are discussed. The accuracy of the determination of vanadium in petroleum samples is affected both by the type of vanadium bonding in the standard organometallic compound and by the matrix of the sample.

REFERENCES

1 J. A. Bowman and J. B. Willis, *Anal. Chem.*, 39 (1967) 1210.
2 R. M. Yutkevich and V. M. Minut, *Khim. Tekhnol. Topl. Masel*, 17 (1972) 54.
3 J. M. Sugihara *et al.*, *Amer. Petrol. Inst., Res. Project*, 60 (1972) 35.
4 A. J. Smith, J. O. Rice, W. C. Shaner, Jr. and C. C. Cerato, *Amer. Chem. Soc., Div. Petrol. Chem., Prepr.*, 18 (1973) 609.
5 D. J. von Lehmden, R. H. Jungers and R. E. Lee, Jr., *Anal. Chem.*, 46 (1974) 239.
6 R. H. Filby and K. R. Shah, *Role of Trace Metals in Petroleum*, in press.
7 P. D. LaFleur and D. J. von Lehmden, *Symposium on Trace Analysis of Coal, Fly Ash, Fuel Oil and Gasoline, Research Triangle Park, N.C.*, May 1973.
8 T. F. Yen, L. J. Boucher, J. P. Dickie, E. C. Tynan and G. B. Vaughan, *J. Inst. Petrol.*, 55 (1969) 87.

9 J. M. Sugihara, J. B. Branthaver, G. Y. Wu and C. Weatherbee, *Amer. Chem. Soc., Div. Petrol. Chem., Prepr.*, 15 (1970) C5.
10 T. F. Yen, E. C. Tynan, G. B. Vaughan and L. J. Boucher, *Amer. Chem. Soc., Div. Fuel Chem. Repr.*, 11 (1967) 264.
11 L. J. Boucher, E. C. Tynan and E. C. Yen, *Inorg. Chem.*, 7 (1968) 731.
12 L. J. Boucher and T. F. Yen, *Inorg. Chem.*, 7 (1968) 2665.
13 L. J. Boucher and T. F. Yen, *Inorg. Chem.*, 8 (1969) 689.
14 F. E. Dickson, C. J. Kunesh, E. L. McGinnis and L. Petrakis, *Anal. Chem.*, 44 (1972) 978.
15 D. Trent, *At. Absorption Newslett.*, 4 (1965) 348.
16 G. R. Supp, I. Gibbs and M. Juszli, *At. Absorption Newslett.*, 12 (1973) 66.
17 G. N. Freeland and R. M. Hoskinson, *Analyst (London)*, 95 (1970) 579.
18 F. R. Hartlage, Jr., *Anal. Chim. Acta*, 39 (1967) 273.
19 B. W. Bailey and Fa-Chun Lo, *Anal. Chem.*, 44 (1972) 1304.
20 D. R. Bryant and A. R. Hodges, *Anal. Chem.*, 44 (1972) 405.
21 V. S. Sastri, C. L. Chakrabarti and D. E. Willis, *Can. J. Chem.*, 47 (1969) 587; *Talanta*, 16 (1969) 1093.
22 K. Fujiwara, H. Haraguchi and K. Fuwa, *Anal. Chem.*, 44 (1972) 1895.
23 M. Kashiki and S. Oshima, *Bunseki Kagaku*, 20 (1971) 1398; *Anal. Chim. Acta*, 55 (1971) 436.
24 M. Kashiki, S. Yamazoe and S. Oshima, *Anal. Chim. Acta*, 53 (1971) 95; 54 (1971) 533; *Maruzen Sekiyu Giho*, (1972) 54; (1971) 88.
25 W. W. Howe, *Anal. Chem.*, 33 (1961) 255.
26 M. Blumer and W. W. Howe, *Anal. Chem.*, 33 (1961) 1288.
27 M. F. Millson, D. S. Montgomery and S. R. Brown, *Geochim. Cosmochim. Acta*, 30 (1966) 207.
28 J. M. Sugihara, J. F. Branthaver and K. W. Willcox, *Amer. Chem. Soc., Div. Petrol. Chem., Prepr.*, 18 (1973) 645.
29 H. S. Isbell *et al.*, *Nat. Bur. Stand. (U.S.), Monograph No. 54*, 1962.
30 J. A. Dean and T. C. Rains, *Flame Emission and Atomic Absorption Spectrometry, Vol. 2*, M. Dekker, New York, 1971, p. 331.
31 P. Vavrečka, G. Šebor, I. Lang and O. Weisser, *Riv. Combust.*, in press.
32 G. E. Peterson and H. L. Kahn, *At. Absorption Newslett.*, 9 (1970) 71.

Analytica Chimica Acta, 78 (1975) 107–113

EMISSION SPECTROGRAPHIC DETERMINATION OF TRACE ELEMENTS IN AIRBORNE PARTICULATE MATTER COLLECTED ON GLASS FIBER FILTER

AKIYOSHI SUGIMAE

Environmental Pollution Control Center, Osaka Pref. 1-chome, Nakamichi, Higashinari-ku, Osaka (Japan)

(Received 11th November 1974)

Various filters, such as glass fiber, cellulose, and membrane filters have been used for the collection of airborne particulate matter. Although glass fiber filters contain high concentrations of metallic impurities, they have been frequently used because of their high collection efficiencies and low flow resistance. Emission spectrography has also been employed advantageously for the determination of trace elements in airborne particulate matter[1–14]. Spectrographic analysis[4] of airborne particulate matter collected on glass fiber filters is commonly accomplished by ashing organic matter in the sample either in a muffle furnace at 500°C or with a low-temperature asher, dissolving the residue in acid, concentrating, and analyzing the solution by d.c. arc excitation. However, the sample preparation steps are time-consuming and are liable to contamination and loss of sample constituents. Moreover, all the elements in airborne particulate matter are not necessarily dissolved in the acid. Elements such as lead, zinc, copper, and cadmium react with the glass during dry ashing at high temperature, forming acid-insoluble metal silicates[15]. A reduction of sample handling between the actual sample procurement and the electrode preparation would be advantageous from the standpoints of reduced errors and speed. Direct discharge of the airborne particulate matter collected on the filter should solve these problems. Various techniques have been reported for the direct analysis of cellulose and membrane filters[3,7–9]. However, information on the direct analysis of the airborne particulate matter on glass fiber filters is limited. The author[14] has described a technique for the direct analysis of glass fiber filters, in which sample disks punched from the filter are packed in a boiler cap electrode and d.c. arc excitation is used for the determination of volatile elements such as arsenic, antimony, cadmium, copper, lead, and zinc. The technique is suitable only for extremely volatile elements. The detection limit of elements of a more refractory nature can be lowered by direct striking of the discharge on the glass fiber filter packed in the electrode. However, the discharge is fairly erratic and glass formation in the electrode hinders volatilization of elements, Moreover, an excessive SiO band spectrum is observed.

In the method here described, the glass fiber filter on which airborne particulate matter has been collected is directly decomposed with sulfuric acid-hydrofluoric acid in the crater of shallow cupped electrode. Silica is expelled as silicon tetrafluoride; a spectroscopic buffer (a mixture of calcium fluoride and graphite powder) is added to the residue which remains in the crater, and the electrode is

subjected to d.c. arc excitation. The method is precise and useful for the determination of trace elements in airborne particulate matter.

EXPERIMENTAL

Apparatus and reagents

A Shimadzu 1.7-m Ebert grating spectrograph (type GE-170) with 1,200 lines per mm grating, and a reciprocal linear dispersion of 0.48 nm mm^{-1} in the first order was used. A Shimadzu Modular-source (type 280000) was used for direct current excitation; the unit has an output of 5, 10, and 15 A at 220-V d.c. Spectral line density was measured with a Nippon Jarrell-Ash microphotometer (type JM-3).

A low-temperature asher (Trapelo LTA-504) was used for oxidation of organic matter.

An electrode waterproofing solution was prepared by dissolving 1 g of paraffin in analytical-grade benzene and diluting with benzene to 100 ml.

A stock solution of internal standard elements was prepared by dissolving 0.100 g of high-purity indium metal and 0.500 g of high-purity cobalt metal simultaneously in a minimum volume of nitric acid and diluting to 1 l with distilled water. An internal standard solution was prepared by diluting a portion of the stock solution to 10 times its volume with distilled water.

Each stock solution of beryllium, cadmium, chromium, copper, iron, lead, manganese, nickel, tin, and vanadium was prepared by dissolving a weighed portion of the high-purity metal or salt in a minimum volume of nitric acid and diluting to volume in a volumetric flask. Requisite amounts of the solutions were then mixed and diluted with distilled water to make a series of standard solutions. The amounts were based on the estimated amounts of the elements in airborne particulate matter and the desired ranges to be covered. Each standard solution also contained 10 μg In ml^{-1} and 50 μg Co ml^{-1}.

A spectroscopic buffer was prepared by mixing thoroughly 1 part of high-purity calcium fluoride and 5 parts of high-purity graphite powder (National Carbon SP-2).

All other chemicals were commercially available and of reagent-grade.

Collection procedure

Airborne particulate matter was collected on a glass fiber filter (Whatman GF-A, 47 mm in diameter) in a filter holder (Sartorius SM 162 12). The filter holder was placed in a sampling location, and connected by plastic tubing to a vacuum system. Air was drawn through the filter at a flow rate of 30 l min^{-1} for 7 days. Before and after the collection of airborne particulate matter, the filter was weighed, so that the weight of the particulate matter was known. The atmospheric concentration of the airborne particulate matter could be calculated by dividing the weight by the air volume sampled.

Procedure

Warm the preformed graphite electrodes (Hitachi NE-1208, ASTM S-4) for 10 min at 80°C. Briefly immerse the crater portion of each electrode in waterproofing solution and then oven-dry for a few minutes. By means of a circular steel cutting

die, punch sample disks (4 mm diameter) out at random from the sample filter, which has been previously ashed with a low-temperature asher for 3 h to burn off airborne organic matter. Pack the disks in the crater of the waterproofed electrode. The total charge in the electrode is usually 4 disks, representing 4.00% of the total airborne particulate matter collected. On the sample disks, add 1 drop of methanol to distribute the internal standard solution (20 μl), which is then added, evenly in the electrode, from a micropipette. Evaporate the solution to dryness in an oven, and add 10 μl of concentrated sulfuric acid and 20 μl of hydrofluoric acid (48%) carefully to decompose the sample disks. Place the electrode under an infrared lamp, and heat until white fumes are evolved. Add another 20 μl of hydrofluoric acid, and heat to fumes of sulfur trioxide. The elements in the residue are then left as the sulfates in the electrode.

If the estimated amounts of the elements in the residue lie below the limits of determination, another 4 disks may be decomposed in the electrode. Caution must be taken to prevent the solution from boiling and splattering in the electrode while heating. After the electrode has cooled in a desiccator, fill the crater 1/3 full with about 8 mg of spectroscopic buffer (weighing is not necessary) and pack down.

Prepare standard electrodes in the same manner by packing blank filter disks in the electrode, adding 20 μl of the standard solution on the disks, decomposing the disks with sulfuric acid–hydrofluoric acid, and adding the spectroscopic buffer.

TABLE I

SPECTROGRAPHIC CONDITIONS

Excitation source	10-A d.c. arc
Sample electrode	Hitachi NE-1208 (ASTM S-3)
Counter electrode	Hitachi CTE-2001 (0.18-in. diameter, pointed)
Analytical gap	3 mm
Preburn time	None
Exposure time	50 s
Slit width	10 μm
Step filter	3 step filter (Transmission: 4, 20, 100%)
Film	4 × 10-in. Kodak SA-1

Discharge the electrodes so prepared under the conditions given in Table I. Construct working curves and determine the amounts of the elements in the sample disks in the usual fashion. A list of analytical line pairs and working ranges is given in Table II. The atmospheric concentrations of the analytical elements are determined from a knowledge of the filter area and the volume of air sampled.

RESULTS AND DISCUSSION

Choice of electrode

Wide ranges of type and size of electrode were investigated to improved sensitivity and precision. When a large electrode (10-mm internal diameter, 4.0-mm depth; walls 1.0 mm thick) was used, and sample disks of 10 mm in diameter were packed in the electrode, increased sensitivity was obtained. The electrode could be used for the detection of low concentrations. However, the discharge was erratic and

TABLE II

ANALYTICAL LINE PAIRS AND CONCENTRATION RANGES

Analytical line pair	*Range*	
	Amount of element (μg/electrode)	*Atmospheric concentration[a] (μg m^{-3} air)*
Be I 2348.610 Å[c]/Co I 2521.363 Å[c]	0.004–0.4	0.00033–0.033
Cd I 2288.018 Å[d]/In I 3039.356 Å[c]	0.04–4	0.0033–0.33
Cr I 2986.473 Å[c]/Co I 3044.005 Å[c]	0.02–2	0.0017–0.17
Cu I 3273.962 Å[b]/On I 3039.356 Å[c]	0.04–4	0.0033–0.33
Fe I 2929.008 Å[b]/Co I 3044.005 Å[c]	4–400	0.33–33
Mn I 3044.567 Å[c]/Co I 3044.005 Å[c]	0.2–20	0.017–1.7
Ni I 3050.819 Å[c]/Co I 3044.005 Å[c]	0.02–2	0.0017–0.17
Pb I 2614.178 Å[c]/In I 3039.356 Å[c]	0.2–20	0.017–1.7
Sn I 3034.121 Å[c]/In I 3039. 356 Å[c]	0.02–2	0.0017–0.17
V I 3060.460 Å[c]/Co I 3044.005 Å[c]	0.02–2	0.0017–0.17

[a] Based on an air volume sampled of 300 m^3.
[b] Spectrum at 4% transmittance part of step filter.
[c] Spectrum at 20% transmittance part of step filter.
[d] Spectrum at 100% transmittance part of step filter.

the precision was unsatisfactory. A deep electrode (Scribner–Mullin carrier type) produced a smooth burning arc, but bad background characteristics militated against accurate and precise results at low concentrations. Moreover, selective volatilization of elements was enhanced very markedly. A shallow cratered electrode (4.6-mm internal diameter, 1.6-mm depth; walls 0.8 mm thick) provided adequate sensitivity and satisfactory precision. Improvement of arc-burning characteristics also resulted from undercutting the electrode.

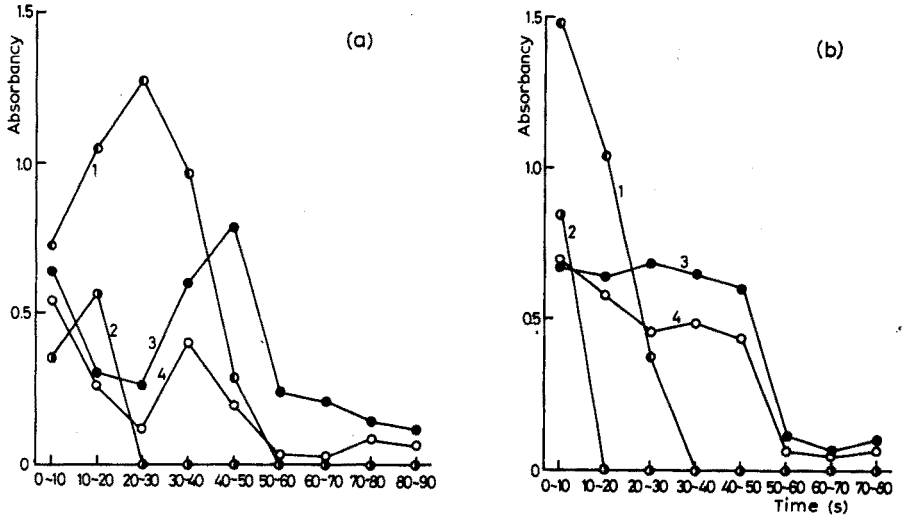

Fig. 1. Moving plate study for sample buffered with (a) sodium fluoride–graphite and (b) calcium fluoride–graphite. (1) Sn I 3034.121 Å; (2) Pb I 2614.178 Å; (3) Cr I 2986.473 Å; (4) Mn I 3044.567 Å.

Spectroscopic buffer

Sodium fluoride–graphite and calcium fluoride–graphite mixtures were chosen as possible spectroscopic buffers. Figure 1 shows a moving plate study for chromium, lead, manganese, and tin for samples buffered with the sodium fluoride–graphite and calcium fluoride–graphite mixtures. The time interval of the plotted points is 10 s. When the sodium fluoride–graphite mixture was used, each element volatilized very selectively. The volatilization sequence of the analytical elements was in the following order: cadmium and lead; copper and tin; manganese; beryllium, chromium, iron, nickel, and vanadium. Lead, tin, manganese, and chromium served as representative examples. Lead was totally volatilized in the first 20 s of the discharge, but the maximum intensity for the other elements was emitted after the arc had been burning for some time. The maximum intensity of chromium was reached after volatilization of the sodium buffer. Cyanogen emission and background, which were low at first because of the presence of the sodium, increased sharply during the late arcing time. In the sample buffered with calcium fluoride–graphite, the period of the volatilization of the elements was appreciably shortened; selective volatilization was reduced, the elements were almost volatilized in 50 s or less, and the line intensities of all the elements were enhanced. Blank glass fiber filters contain various metallic impurities, such as sodium, potassium, calcium, aluminum, and barium, at elemental concentrations greater than 1%. The sample is self-buffered, in the sense that it contains the alkali metals, but when samples were arced without the spectroscopic buffer, the discharge was erratic. A moving plate study indicated that all the analytical elements were completely volatilized after 20 s; and the line intensities were considerably smaller in the unbuffered sample than in the sample buffered with the calcium fluoride–graphite mixture. Moreover, excessive background was observed. Maximal sensitivity (line to background ratios) was obtained for a 50-s exposure with no preburn by using the calcium fluoride–graphite mixture as the spectroscopic buffer.

It is well known that selective volatilization is decreased if all elements are converted to volatile compounds, such as fluorides and chlorides. In the method. the sample glass fiber disks are decomposed with sulfuric acid–hydrofluoric acid in the electrode, and all elements are present in the residue as the involatile sulfates. However, the spectroscopic fluoride buffer is present in the electrode, so that on addition of nitric acid to the buffer, the constituents in the electrode are treated with hydrofluoric acid produced by hydrolysis. No appreciable difference was observed when the elements were converted from the sulfates to the fluorides.

Matrix effects

Matrix effects of increasing increments of the residue on the volatilization pattern of the elements determined were examined. For this investigation, the procedure for the decomposition of the sample disks was repeated, and 8 or 12 disks were decomposed in the electrode. When the sodium fluoride–graphite mixture was added to the residue, volatilization of the elements determined tended to be delayed as the amount of the residue increased. When the calcium fluoride–graphite mixture was used, the volatilization patterns remained uniform even if the amount of the residue was increased to the equivalent of 12 filter disks. Results indicated that the calcium fluoride–graphite mixture acted to maintain the normal excitation

temperature of the arc and so to offset matrix effects.

Interelement effects in spectrography are well known, but it was not expected that any element would be present in the airborne particulate matter itself in excessive amounts, hence no attempt was made to study such effects.

Choice of internal standard

Several factors must be considered when internal standard elements are selected. The nature of the volatilization under the discharge is important in controlling the precision. The rates at which the internal standard and the elements determined are volatilized should be very similar. Such elements as cadmium, copper, lead, and tin, which can be classified in the volatile group, were totally volatilized in the first 30 s or less of the discharge. The volatilization of beryllium, chromium, iron, manganese, nickel, and vanadium was delayed and continued for 50 s. Indium was chosen as the internal standard for the volatile element group, and cobalt as the internal standard for elements of a more refractory nature. The volatilization behavior of the internal standard elements closely paralleled those of the elements determined. Moreover, both elements occurred in insignificant amounts in most samples of airborne particulate matter.

The blank of the glass fiber filter contained elements such as copper, iron, lead, and manganese, as the residual metallic impurity. Because these elements were normally present at high concentrations in sample filters, less sensitive analytical lines were selected for iron, manganese, and lead. For copper, the intensity of the sensitive line was reduced by 4% by the use of a step filter. Therefore, working curves did not show a toe effect at lower concentrations owing to the residual amount of the element in the glass fiber filter.

Accuracy and precision

The method was evaluated by analysing the sample spiked with known amounts of the elements to be determined. For this experiment, the sample disks, packed in the crater of the electrode, were spiked by adding dropwise the solution containing known amounts of the elements, and the spike sample was then analysed. The recovery of each element ranged from 89 to 130% (Table III).

TABLE III

RECOVERY OF ELEMENTS ADDED TO SAMPLE

Element	*Added (μg)*	*Found (μg)*	*Recovery (%)*
Be	0.10	0.093	93
Cd	1.0	1.3	130
Cr	0.50	0.59	118
Cu	1.0	0.89	89
Fe	100	120	120
Mn	5.0	5.5	110
Ni	0.50	0.58	116
Pb	5.0	5.4	108
Sn	0.50	0.46	92
V	0.50	0.53	106

TABLE IV

PRECISION

Element	*Concentration*[a] *($\mu g\ m^{-3}$ air)*	*s_r (%)*	*Element*	*Concentration*[a] *($\mu g\ m^{-3}$ air)*	*s_r (%)*
Be	0.0027	11.9	Mn	0.20	7.1
Cd	0.023	18.2	Ni	0.038	10.3
Cr	0.042	15.1	Pb	0.63	12.7
Cu	0.079	11.2	Sn	0.048	15.3
Fe	6.0	6.9	V	0.040	10.1

[a] Mean of 6 determinations.

Table IV shows the concentrations for the elements determined and the standard deviations which were generally below $\pm 18\%$, values which are acceptable for most air pollution requirements. If accuracy requirements are somewhat higher, it has been found that duplicate or triplicate exposures are adequate.

SUMMARY

An emission spectrographic method is described to determine the concentrations of beryllium, cadmium, chromium, copper, iron, lead, manganese, nickel, tin, and vanadium, in airborne particulate matter collected on a glass fiber filter. Sample disks punched out from the glass fiber filter are packed in a shallow cratered electrode; an internal standard solution containing indium and cobalt is added and the disks are decomposed with sulfuric acid–hydrofluoric acid. A calcium fluoride–graphite mixture is added as a spectroscopic buffer before d.c. arc excitation. The precision of the method is better than $\pm 18\%$.

REFERENCES

1 M. P. Brash, *Appl. Spectrosc.*, 14 (1960) 43.
2 R. L. O'Neil, *Anal. Chem.*, 34 (1962) 781.
3 G. V. Wheeler, W. A. Ryder and K. R. Arnold, *Appl. Spectrosc.*, 16 (1962) 17.
4 *Air Pollution Measurements of the National Air Sampling Network*, U.S. Dept. Health, Education, and Welfare, Public Health Service, Washington, D.C., 1962, p. 213.
5 R. G. Keenam and J. L. Hoez, *Amer. Ind. Hyg. Ass. J.*, 25 (1964) 254.
6 P. W. West, in A. C. Stern (Ed.), *Chemical Analysis of Inorganic Pollutants*, in *Air Pollution, Vol. II*, Academic Press, New York, 1968, p. 171.
7 D. W. Lander, R. L. Steiner, D. H. Anderson and R. L. Dahm, *Appl. Spectrosc.*, 25 (1971) 270.
8 N. L. Morrow and R. S. Brief, *Environ. Sci. Technol.*, 5 (1971) 786.
9 T. Hasegawa and A. Sugimae, *Bunseki Kagaku*, 20 (1971) 840, 1406; 22 (1973) 3.
10 A. Sugimae, *Bunseki Kagaku*, 22 (1973) 1350.
11 S. Imai, K. Ito, A. Hamaguchi, Y. Kusaka and M. Warashina, *Bunseki Kagaku*, 22 (1973) 551.
12 Y. Yamane. M. Miyazaki and H. Nakazawa, *Bunseki Kagaku*. 22 (1973) 1135.
13 A. Sugimae, *Anal. Chem.*, 46 (1974) 1123; *Appl. Spectrosc.*, 28 (1974) 458.
14 A. Sugimae, *Int. J. Environ. Anal. Chem.*, 3 (1974) in press.
15 T. Y. Kometani, J. L. Bove, B. Nathanson, S. Siebenberg and M. Magyar, *Environ. Sci. Technol.*, 6 (1972) 617.

Analytica Chimica Acta, 78 (1975) 115–120

THE DETERMINATION OF ZIRCONIUM AND ALUMINIUM IN ALLOYS SLAGS AND FUMES BY 14-MeV NEUTRON ACTIVATION ANALYSIS

D. M. BIBBY, B. T. EDDY* and D. C. G. PEARTON*

NIM-WITS Activation Analysis Research Group, Nuclear Physics Research Unit, University of the Witwatersrand, Johannesburg (South Africa)

(Received 7th January 1975)

Zirconium is used on an ever-increasing scale as a nuclear fuel-cladding material, because it combines a low thermal neutron cross-section with a high melting point and good corrosion resistance, and in extreme environments in the chemical industry, because it shows good resistance to corrosion by both acids and alkalis. Zirconium is a constituent of high strength alloys; its compounds are useful catalysts and the oxide is used in refractory ceramics.

In view of the major role played by zirconium in the nuclear industry for many years, it is surprising that nuclear methods of analysis have not been applied more widely to its determination. The use of fast neutron activation analysis (f.n.a.a.) appears to be limited to a brief mention by Broadhead *et al.*[1] despite the high sensitivity reported for zirconium[2]. The determination of aluminium by f.n.a.a. is straightforward, and has been investigated by many authors[3].

In the present work, some aluminium–zirconium alloys, slags and fumes have been analysed by f.n.a.a., and the results are compared with those obtained by chemical analysis.

TABLE I

NUCLEAR REACTIONS ON ALUMINIUM AND INTERFERING REACTIONS FROM ZIRCONIUM

Element	*Reaction*	*Isotopic abundance (%)*	*Half-life*	*γ-Ray energy (keV)*
Al	$^{27}Al(n,p)^{27}Mg$	100	9.5 min	845[a], 1015
	$^{27}Al(n,\alpha)^{24}Na$	100	15 h	1369, 2750
	$^{27}Al(n,\gamma)^{28}Al$	100	2.24 min	1780
Zr	$^{90}Zr(n,2n)^{89}Zr$	51.5	4.2 min	
	$\rightarrow\beta^+ + {}^{89m}Y$	—	16 s	908
	$^{94}Zr(n,p)^{94}Y$	17.4	20 min	919

[a] Analysis peak.

* On secondment from Analytical Division, National Institute for Metallurgy, Private Bag 7, Auckland Park, Johannesburg, (South Africa).

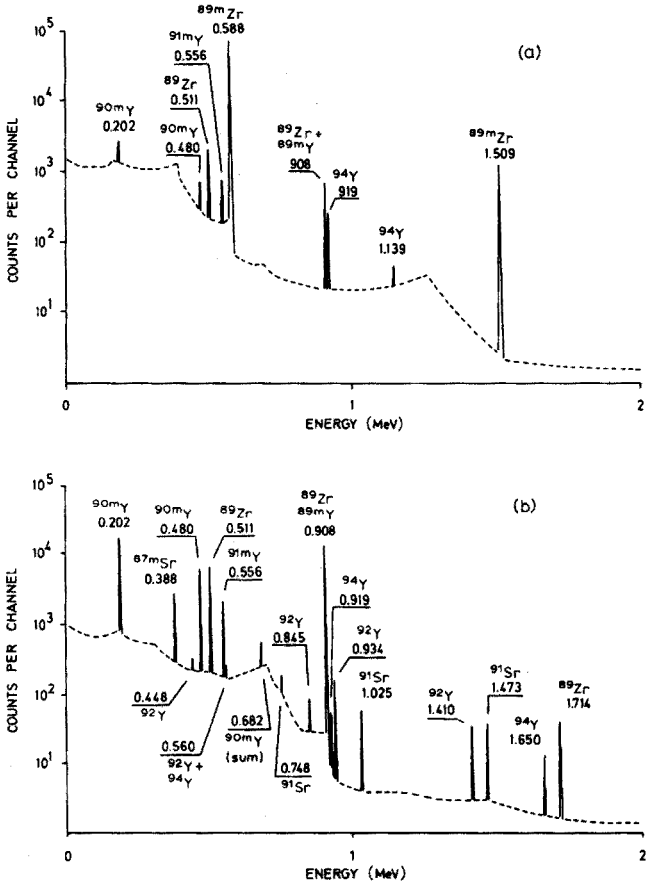

Fig. 1. Ge(Li) γ-ray spectra of 14-MeV neutron-irradiated zirconium: (a) irradiated 300 s, decay 100 s, count 300 s; (b) irradiated 300 s, decay 5000 s, count 5000 s.

TABLE II

14-MeV NEUTRON-INDUCED REACTIONS ON ZIRCONIUM

Reaction	*Isotopic abundance (%)*	*Half-life*	*Observed γ-ray peaks (keV)*
$^{90}Zr(n,2n)^{89m}Zr$	51.5	4.3 min	β^+, 588, 1508
$^{90}Zr(n,2n)^{89}Zr$	51.5	79 h	β^+, 1714
$^{89m}Zr \rightarrow {}^{89}Zr$	—		
$^{89}Zr \rightarrow \beta^+ + {}^{89m}Y$	—	16 s	908
$^{90}Zr(n,\alpha)^{87m}Sr$	51.5	2.8 h	388
$^{90}Zr(n,p)^{90m}Y$	51.5	3.1 h	202, 480, (682 sum)
$^{91}Zr(n,p)^{91m}Y$	11.2	50 min	556
$^{92}Zr(n,p)^{92}Y$	17.1	3.5 h	448, 560, 845, 934, 1410
$^{94}Zr(n,p)^{94}Y$	17.4	20 min	560, 919, 1139, 1650
$^{94}Zr(n,\alpha)^{91}Sr$	17.4	9.7 h	748, 1025, 1473

NUCLEAR DATA

The nuclear data used in the determination of aluminium are given in Table I, together with possible interfering reactions from zirconium for NaI(Tl) spectrometry. The 845-keV peak from ^{27}Mg was used to determine aluminium; the possible interferences were from ^{89}Zr and ^{94}Y. These interferences are discussed below.

Since little work has been reported previously on the determination of zirconium by f.n.a.a., the radioisotopes produced by fast neutron irradiation, and the γ-ray peaks which could be observed were investigated. A sample (15 g) of zirconium metal was irradiated in a flux of 10^9 n cm^{-2} s^{-1} for 300 s and counted after different decay times, using a 60-cm^3 Ge(Li) detector connected to an Intertechnique 4000-channel analyser. Isotopes were identified by a combination of half-life and γ-ray energy information. Typical spectra obtained after 1 min and 1 h are shown in Fig. 1. Table II lists the isotopes found by the above procedures, and the reactions producing them. All the peaks were identified readily from the literature[4,5], except the 682-keV peak; its half-life suggested that it was from the ^{90m}Y ($t_{\frac{1}{2}}$=3.1 h) isotope, which has a nuclear level at 682 keV, but no recorded direct transition to the ground state[4,5]. In order to investigate this peak in more detail, the ^{90m}Y isotope was produced from a sample of niobium oxide by the reaction ^{93}Nb(n,α)^{90m}Y. This route was chosen since virtually no other activity is produced from niobium, resulting in a far simpler γ-spectrum. The intensity of the 682-keV line, relative to the 480- and 202-keV lines, fell rapidly with distance from the detector, showing that it was a sum peak from the 202- and 480-keV lines. The estimated absolute activity from this line, if it does exist, must be less than 1%[5].

The reaction used for the determination of zirconium was: ^{90}Zr(n,2n)^{89m}Zr ($t_{\frac{1}{2}}$=4.3 min, E_γ=588 keV). Despite its poorer resolution, a NaI(Tl) detector was used for the quantitative work because of its high efficiency. Potential interfering γ-rays are those at 571 keV from ^{89}Zr($t_{\frac{1}{2}}$=79 h) and at 566 keV from ^{91m}Y($t_{\frac{1}{2}}$=50 min). However, these were minor peaks that did not give rise to measurable interferences in successive analyses.

The most serious problem involved a zirconium–aluminium mixture; the 588-keV peak from ^{89m}Zr was situated on the Compton edge of the 845-keV peak of ^{27}Mg produced from aluminium. A correction factor was, however, readily determined and applied to all samples analysed.

EXPERIMENTAL

Apparatus

The neutron generator was a Picker Nuclear Accelerator 1, operated to give *ca.* 10^{11} n s^{-1}. A pneumatic sample transfer system conveyed sample and monitor to a dual axis rotator for simultaneous irradiation, and to separate single axis rotators for counting. Two Bicron 125 × 125-mm NaI(Tl) detectors with resolutions of better than 8% for the 662-keV peak of ^{137}Cs were connected through Ortec 276 preamplifiers to Elscint CAV-N-4 amplifiers, modified to have a 0.4-μs time constant; their outputs were corrected for drift in the system by Canberra 1520 analogue stabilizers, set on either the 588-keV peak of ^{89m}Zr or the 845-keV

peak of ^{27}Mg, whichever was the more prominent. The monitor activity was measured with a Canberra 1431 S.C.A. and a Tennelec 546P scaler. γ-Ray analysis of the samples was carried out on an Intertechnique SA40 400-channel analyser with parallel printer output. Monitors of zirconium dioxide were prepared and irradiated simultaneously with the samples; correction for the zirconium activity will be more accurate than for the aluminium activity. However, since the irradiation time was short compared with the half-lives of ^{89m}Zr and ^{27}Mg, and the neutron output was relatively constant ($\pm 10\%$) over the irradiation time, significant errors in the aluminium determinations were not found.

Dead-time corrections were made by a modification of the method of Boloton *et al.*[6]. The output of the analogue stabilizer of the sample detection system was taken to a pulse-rate divider (1/32 for this work), and the divided pulses were used to trigger a BNC BH-1 long tail pulser. The long tail pulse, taken to the test input of the preamplifiers, appeared as a sharp peak in the γ-ray spectrum, whilst the simultaneous trigger output was taken directly to a scaler. The fractional live-time could then be determined from the ratio of the peak-area in the γ-ray spectrum to the number of trigger output counts. This gave a dead-time correction factor to compensate for isotopic decay during the counting time. Corrections were not applied to the monitor counts since the dead-time was expected to be very small and the count-rate was kept reasonably constant.

Sample preparation and density corrections

The samples (*ca.* 5 g) available for analysis, in the form of a coarse powder, were packed into 1.5-cm^3 polyethylene vials, which were fixed in position by spacers at the bottom centre of the standard 7.5-cm^3 polyethylene vials used as rabbits in the transfer system. Because of the unknown composition of the samples, the following empirical density correction factors were determined from a series of samples of different densities and known zirconium and aluminium contents: for ^{89m}Zr, exp $(-0.034\ M)$, and for ^{27}Mg, exp $(-0.022\ M)$, where M = sample mass.

Mutual interferences

With the NaI(Tl) detector, minor peaks from ^{89}Zr and ^{94}Y, at 908- and 919-keV respectively, interfered with the 845-keV peak of ^{27}Mg, while the 588-keV peak from ^{89m}Zr was situated on the Compton edge of the 845-keV peak of ^{27}Mg; the latter was the more serious, amounting to 7.25% of the 845-keV peak-area. The interference from zirconium was equivalent to 0.75% of the 588-keV peak-area. The 588-keV peak was therefore corrected for the ^{27}Mg contribution, and this corrected value was then used to correct the 845-keV peak.

Procedure

Samples were irradiated for 40 s, followed by a decay time of 100 s to allow ^{16}N (from any oxygen present) and ^{89m}Y activity to decay, and were then counted for 240 s.

RESULTS AND DISCUSSION

A Wang 600 calculator was programmed to integrate the peak-areas using

smoothed boundaries, to apply density corrections, to normalize the sample counts with respect to the monitor counts, to correct for mutual interferences, and to present the aluminium and zirconium concentrations in the sample.

TABLE III

PRECISION OF ALUMINIUM AND ZIRCONIUM DETERMINATIONS

	Aluminium	*Zirconium*
Number of determinations	11	11
Mean value (%)	48.6	51.1
Relative standard deviation (%)	1.7	1.8
Standard deviation from counting statistics only (%)	1.3	1.4

TABLE IV

COMPARISON OF RESULTS OBTAINED BY F.N.A.A. AND CHEMICAL ANALYSIS

Sample number	*No. of detns.*	*Zirconium*			*% Aluminium*		
		F.n.a.a.	*Chem.*	*%Δ*	*F.n.a.a.*	*Chem.*	*%Δ*
Alloys							
A1	2	54.8±1.0	55.5	−1.3	41.3±1.0	41.9	−1.5
A2'	4	52.5±0.5	52.2	+0.6	45.1±0.5	45.3	+0.5
A3	4	45.3±0.5	45.5	−0.4	48.3±0.5	51.2	−6.0
A4	2	60.6±0.5	60.6	0.0	34.3±1.0	34.5	−0.6
A5	6	49.2±0.5	51.2	−4.0	44.7±0.5	44.1	+1.4
A6	2	51.1±1.0	52.8	−3.5	43.4±1.0	42.6	+1.9
A7	2	54.6±1.0	54.0	+1.1	43.6±1.0	42.4	+2.8
A8	6	44.4±0.8	46.6	−5.0	50.3±0.5	49.1	+2.4
A9	3	57.8±1.0	58.6	−1.4	38.2±1.0	38.0	+0.5
A10	11	51.1±0.2	51.4	−0.6	48.7±0.2	48.6	+0.2
A11	2	82.0±2.0	80.3	+2.1	<1.5	3.75	—
A12	2	82.9±0.5	80.6	+2.9	<1.5	0.6	
						0.5	
Slags							
S1	1	29.3±0.5	28.4	+3.2	31.9	31.2	+2.3
S2	2	19.9±0.5	20.5	−2.9	27.8	27.8	0.0
Fumes							
F1	1	13.1	14.2	−7.7*	81.0	70.5	+15.0*
F2	2	<3	2.65	—*	80.0	74.2	+7.2*
		Av. % diff −0.6 excluding asterisked fume samples			Av. % diff = +0.06 excluding asterisked fume samples		

After the method had been developed, the precision was determined by analysing 11 samples of an alloy containing approximately equal amounts of zirconium and aluminium. The results, given in Table III, show that a precision close to that expected from counting statistics alone can be obtained.

The accuracy of the method is shown by a comparison of the values obtained by f.n.a.a. and by a wet chemical procedure, (Table IV). A comparison of the results obtained for alloys and slags shows no systematic errors, the average

deviations being −0.6% and +0.06% for zirconium and aluminium, respectively. The differences between the values obtained by the two methods are not significantly larger than the standard deviations obtained by repeated analysis. Discrepancies did occur, however, in the determination of aluminium in the fume samples, although the sum of the f.n.a.a. values for aluminium, zirconium and oxygen is close to 100%. The discrepancy may result from the difficulty of dissolving the fume samples completely for the wet chemical determinations. Thus the non-destructive f.n.a.a. method of analysis is preferable.

The limit of detection for zirconium in aluminium is 3–5%, because of the spectral interference from ^{27}Mg. The limit of detection of aluminium in zirconium is *ca.* 1%, because of the ^{89}Zr, ^{89m}Y and ^{94}Y isotopes produced from zirconium.

In practice, 10–12 samples can be prepared and analysed, in duplicate, in one man-day. This is more rapid than existing methods of analysis, particularly for refractory materials.

The authors thank Professor J. P. F. Sellschop, Mr. T. W. Steele and Mr. K. Dixon for their help and enthusiasm, for reading this paper critically, and for supplying the chemical data used; Mr. S. E. Rasmussen for suggesting the dead-time correction methods; and Dr. R. E. Robinson, Director-General of the National Institute for Metallurgy, for support and permission to publish this paper.

SUMMARY

Aluminium and zirconium have been determined in alloys, slags and fumes by 14-MeV neutron activation analysis. Nuclear reactions with zirconium have been investigated, and the radioisotopes produced by 14-MeV neutron activation have been determined. The results for alloys and slags agree well with those obtained by chemical methods; precisions of 1.8% were obtained in ideal cases. The neutron activation method is capable of analysing 10–12 samples, in duplicate, per man-day.

REFERENCES

1 K. G. Broadhead, D. E. Shanks and H. H. Heady, *Proc. Int. Conf. Modern Trends in Activation Analysis*, Texas A and M University, College Station, Texas, 1965, pp. 39–43.
2 M. Cuypers and J. Cuypers, *Gamma-ray Spectra and Sensitivities for 14-MeV Neutron Activation Analysis*, Texas A and M University, College Station, Texas, 1966.
3 R. Van Grieken and J. Hoste, *Annotated Bibliography on 14-MeV Neutron Activation Analysis*, Eurisotop Office Information Booklet No. 65, 1972.
4 C. M. Lederer, J. M. Hollander and I. Perlman, *Table of Isotopes*, Wiley, New York, 6th edn., 1968.
5 A. Hanser, *Nucl. Instu. Methods*, 107 (1973) 187.
6 H. H. Boloton, M. G. Strauss and D. A. McClure, *Nucl. Instu. Methods*, 83 (1970) 1.

Analytica Chimica Acta, 78 (1975) 121–127

THE DETERMINATION OF OXYGEN IN GERMANIUM BY ALPHA-PARTICLE ACTIVATION ANALYSIS

C. VANDECASTEELE* and J. HOSTE

Institute for Nuclear Sciences, Rijksuniversiteit Gent, Proeftuinstraat 86, B-9000 Gent (Belgium)

(Received 27th January 1975)

The presence of oxygen in germanium, even in minute concentrations, is believed to influence its properties. This is particularly important in the manufacture of high resolution Ge(Li) detectors by the lithium ion drift technique[1–4]. It has been proved that oxygen is responsible for at least some drift failures by forming lithium oxide complexes.

Most analytical methods for the determination of oxygen *e.g.* reductive fusion, infrared spectrometry and 14-MeV neutron activation, do not offer sufficient sensitivity to determine the lowest concentrations of interest and a more sensitive technique, such as charged particle activation analysis, is appropriate. So far, only helium-3 activation, based on the $O(^3He, nx)^{18}F$ reaction, has been applied to the determination of oxygen in germanium. The concentrations reported[5–7] are in the 3–300 ng g^{-1}, 100–500 ng g^{-1}, and 28–66 ng g^{-1} ranges, respectively, although results of up to 20 $\mu g\ g^{-1}$ have also been reported[8]. Giroux and Thomas[9] used the $O(\alpha, nx)^{18}F$ reaction, but the sensitivity of their technique was only 1 $\mu g\ g^{-1}$. It was therefore of interest to enhance the sensitivity obtainable with the latter nuclear reaction. The separation technique proposed by Giroux and Thomas[9] consisting of the selective removal of the interfering germanium, selenium, gallium and arsenic activities, was replaced by double distillation of fluorine as fluorosilicic acid followed by lead chlorofluoride precipitation to separate ^{18}F, produced from oxygen, from other activities. Yield determination was carried out by activation with a neutron source through the reaction $^{19}F(n, \alpha)^{16}N$.

When germanium is irradiated with 45-MeV α-particles, important activities of interfering isotopes are formed by the reactions given in Table I. This is shown in Fig. 1 by the Ge(Li) γ-ray spectrum of a sample measured 3 h after irradiation. The annihilation radiation emitted by the isotopes formed from germanium is about 10^5 times more intense than that from the ^{18}F, produced from 1 $\mu g\ g^{-1}$ of oxygen, 6 h after irradiation.

According to Giroux and Thomas[9], the spallation of germanium leading to ^{18}F should not be feared up to an α-energy of about 50 MeV.

EXPERIMENTAL

Irradiation

The samples (monocrystalline germanium discs, 21-mm diameter, *ca.* 1-mm

* Aspirant of the N.F.W.O.

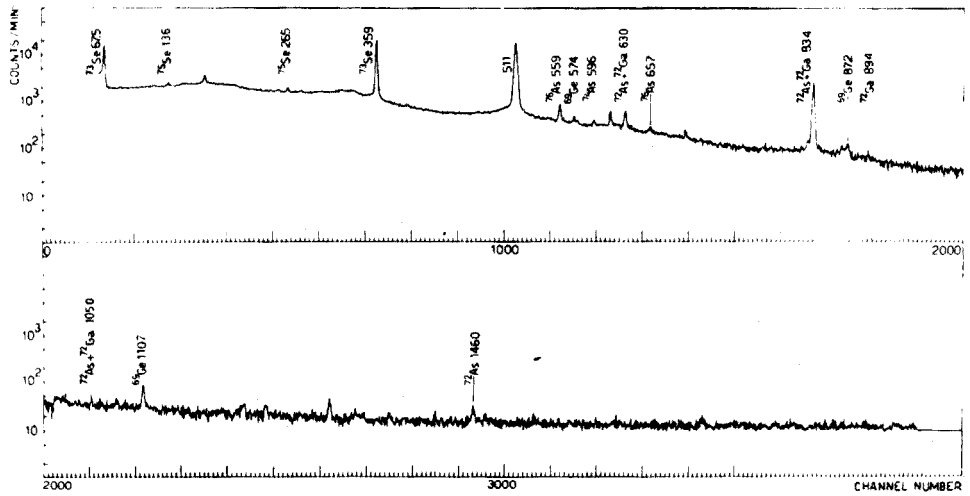

Fig. 1. Ge(Li) γ-ray spectrum of a germanium sample irradiated with 45-MeV α-particles. Irradiation time, 1 h; intensity, 2.00 μA; decay time, 3 h. The sample was counted with a geometry about 450 times less sensitive than that used for analysis.

TABLE I

REACTIONS OF GERMANIUM WITH 45-MeV ALPHA PARTICLES

Reaction	*Isotope formed*		
	$t_{\frac{1}{2}}$	*γ-Ray energy (keV)*	*% Annihilation radiation*
^{73}Ge(α,αp)^{72}Ga	14.1 h	601(8%); 630(27%); 834(96%); 894(10%); 1050(7%)	—
^{70}Ge(α,αn)^{69}Ge	39 h	574(13%); 872(10%); 1107(28%)	68
^{70}Ge(α,pn)^{72}As	26 h	630(8%); 834(78%); 1050(3%)	150
^{72}Ge(α,pn)^{74}As	17.9 d	596(61%); 635(14%)	59
^{73}Ge(α,p)^{76}As	26.4 h	559(43%); 657(6%); 1216(5%)	—
^{70}Ge(α,n)^{73}Se	7.1 h	67.5(65%); 359(99%)	130
^{72}Ge(α,n)^{75}Se	120.4 d	121(17%); 136(57%); 265(60%); 280(25%); 401(12%)	–

thick) were irradiated under vacuum ($<10^{-4}$ torr) in the external beam of the isochronous cyclotron at Louvain-La-Neuve, Belgium, with 45-MeV α-particles. They were placed in a water-cooled sample holder, on which an aluminium tube (18-mm diameter, 5 cm long) is mounted. This tube reduces the loss of secondary electrons. A copper collimator (16-mm diameter, 10 cm long) was placed in front of the sample. The current was measured with a digital voltmeter and kept constant during the irradiation, which was of 1–2 h duration at an intensity of between 1 and 2 μA.

As a standard, a pile of mica foils, thicker than the α-particle range, was irradiated for 10 min at 100-nA intensity, with the incident current determined in the same way.

Surface treatment

The surface treatment, both before and after irradiation, is very important. About 5 min before placing it in the irradiation position under vacuum, the sample was etched for 2 min in a mixture (v/v) of acetic (27.5%), nitric (45%) and hydrofluoric acids (27.5%) with a few drops of bromine added (CP_4), to remove surface oxygen.

After irradiation, a layer of *ca.* 100 μm was removed by etching the sample successively for about 5 min in two different baths containing the solution described above. The thickness removed was determined within ± 2 μm with a micrometer. Alternatively, a similar thickness was ground off with alumina powder slurry on a glass plate. The energy on the layer corresponding to the depth of etching or grinding is about 40 MeV.

Chemical separation

Dissolve the sample under reflux in a mixture of 20 ml of 12 *M* hydrochloric acid and 10 ml of 14 *M* nitric acid, with about 400 mg of sodium fluoride carrier and 20 mg of As_2O_3, H_2SeO_3 and Ga_2O_3 added as hold-back carriers. At the end of the dissolution, GeO_2 precipitates. Transfer the solution to a distillation flask connected to a steam generator and add 50 ml of 85% phosphoric acid. Increase the temperature to 115°C before introducing steam, then keep the temperature constant. Collect about 400 ml of the distillate to which add 100 ml of 85% phosphoric acid and 20 mg of H_2SeO_3. Distil once more under the same conditions, collecting 600 ml of distillate. Bring the distillate to pH 4–5 by adding 6 *M* ammonia. Add 10 ml of 2.75 *M* sodium chloride and 20 ml of 0.75 *M* lead nitrate solution to precipitate lead chlorofluoride. Filter the precipitate onto a 47-mm diameter, 5-μm membrane filter, and wash twice with 10 ml of the lead nitrate solution. Place the precipitate between two 2-mm thick aluminium annihilator discs in a plastic container.

The chemical yield is determined by irradiation in an ^{227}Ac–Be isotopic neutron source[10], with a total neutron output of about 10^8 n s^{-1}. Use is made of the $^{19}F(n, \alpha)^{16}N$ reaction, counting the ^{16}N γ-rays above 4.5 MeV. The precipitate is compared with a standard sodium fluoride sample.

Measurements

Measurements were made on a Ge(Li) detector with a relative detection efficiency of 15%, coupled to a 4000-channel analyser. This allowed the purity of the precipitate to be verified and corrections to be made for interferences. Measurements of 50 min were made every hour, for 10–15 h, starting immediately after the separations, 5–6 h after irradiation. One sample was also counted by means of the γ,γ-coincidence system[11]. The standard mica foils were counted for 1 min in geometrical conditions that were 80-fold less sensitive than used for the samples. The area of the 511-keV peaks in the spectra of the samples and the standards and of the 359-keV peaks in the spectra of the samples were determined by manual integration and linear background subtraction. The 511-keV peak in the natural background was subtracted later from that in the spectra of the sample.

RESULTS AND DISCUSSION

During the chemical separation, the activity of ^{73}Se decreased by a factor of

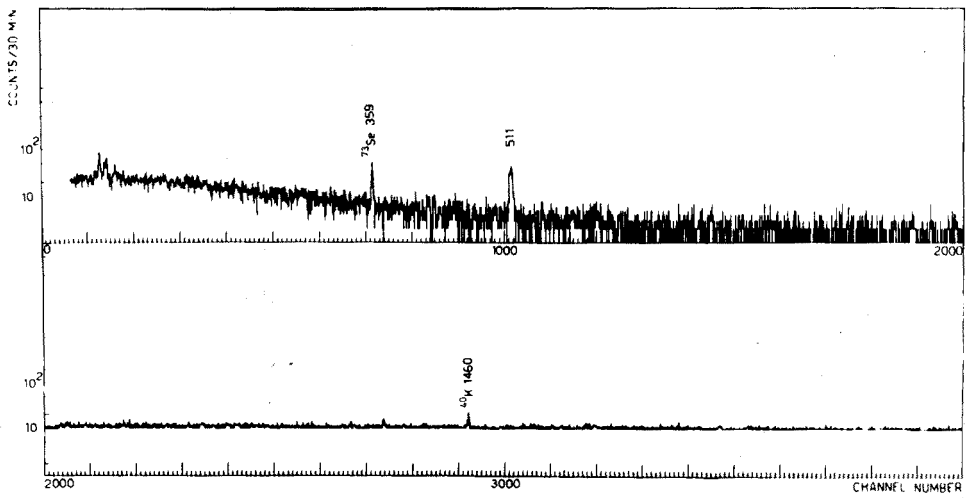

Fig. 2. Ge(Li) γ-ray spectrum of the final PbFCl precipitate obtained for the sample involved in Fig. 1. Counting was started 6 h after irradiation, and was made with the normal geometry for analysis. The chemical yield was 38%.

$4 \cdot 10^6$–$1 \cdot 10^7$, that of ^{76}As by more than $2 \cdot 10^6$, and that of ^{69}Ge by more than $2 \cdot 10^5$. The relatively low average chemical yield of about 40% is due mainly to the low distillation temperature selected; a higher distillation temperature increases the yield and allows the PbFCl to precipitate from a smaller volume, but a less pure distillate results. Indeed, when the temperature is increased to 135°C instead of 115°C, the ^{73}Se activity found in the distillate is *ca.* 30 times more intense.

The only peaks in the Ge(Li) γ-ray spectrum of the final precipitate are the annihilation peak and the 359-keV peak of ^{73}Se, as shown in Fig. 2. The ^{18}F contribution to the annihilation peak, which serves as the analytical signal for oxygen, is determined both by a γ-spectrometric method and by decay curve analysis. The former method uses the ratio of the annihilation peak of ^{73}Se to its 359-keV peak to correct the 511-keV activity for the contribution of ^{73}Se. This ratio is obtained from the measurement in an identical geometry of the sample of selenium precipitated from the residue of the first distillation. The latter is based on least-squares analysis of the decay curve by means of the CLSQ program[12], based on fixed half-lives of 109.8 min (^{18}F) and of 7.1 h (^{73}Se), followed by an iterative procedure to determine a best value for the half-life of the first component.

At an initial stage, an attempt was made to determine oxygen in high-purity germanium in a similar way to that described[11] for oxygen in silicon, *i.e.* by irradiating muscovite foils in front of the sample as flux monitors. This yielded an apparent oxygen content in the $\mu g\ g^{-1}$ range, independent of the method used for the post-irradiation removal of the surface layer. Either chemical etching or grinding, as described, were used to remove up to 100 μm of the front side of the sample, as measured by micrometer.

Later, the standardization method proposed by Ricci and Hahn[13], which consists of irradiating the standard and the sample separately while measuring the

beam intensity, and which assumes an "average cross-section" independent of the matrix, was applied. The ranges in mica and germanium were calculated from the tables of Williamson *et al.*[14]. Irreproducible results for oxygen, up to *ca.* 300 ng g^{-1}, were obtained.

When the etching before irradiation described above was included in the experimental procedure, the results in Table II were obtained. Figure 3B shows a decay curve for the PbFCl precipitate obtained from a high-purity germanium sample. For these samples it is impossible to determine the half-life of the first component precisely by the iterative procedure.

The standard deviations and detection limits indicated in Table II were obtained in different ways for decay curve analysis and for the spectrometric analysis.

For decay curve analysis, the standard deviations as calculated by the CLSQ program from the scattering around the fitted curve are indicated. When the 109.8-min component is not obtained, *i.e.* when all the activity is attributed to 7.1-h ^{73}Se, an upper limit, which depends on the ^{73}Se counting rate, is given. Actual decay curves with data scattered normally around the exact value were simulated. They were composed of the detector background, which is subtracted before the analysis, for 109.8-min and 7.1-h contributions. Analysing a series of such curves, with a given 109.8-min counting rate and a variable 7.1-h counting rate, allowed the standard deviation of the ^{18}F counting rate as a function of the ^{73}Se contribution to be obtained. When this was repeated for different ^{18}F contributions, the detection limit, defined as the 109.8-min counting rate corresponding to a standard deviation of 30%, could be determined as a function of the ^{73}Se counting rate.

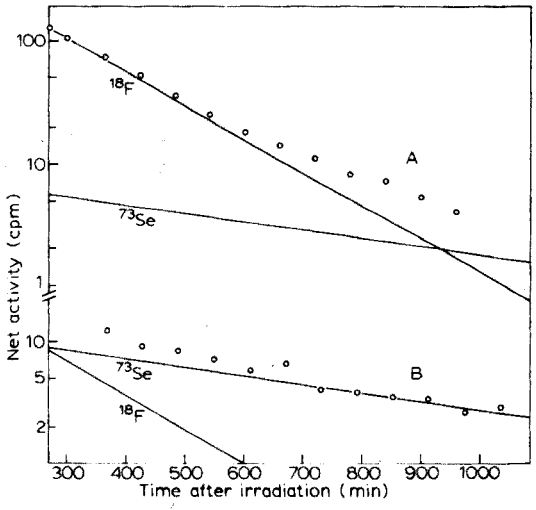

Fig. 3. Decay curves obtained for PbFCl precipitates from irradiated germanium samples. (A) Oxygen-doped germanium sample yielding 685 ng g^{-1} of oxygen. $T_{irr}=1.5$ h; intensity, 1.00 μA. After iteration, a half-life of 104 ± 3 min was obtained for the component attributed to ^{18}F. (B) High-purity sample No. 1A, yielding 29 ng g^{-1} of oxygen. $T_{irr}=2$ h; intensity, 1.00 μA. After iteration, a half-life of 107 ± 30 min was obtained for the component attributed to ^{18}F.

TABLE II

RESULTS FOR OXYGEN IN GERMANIUM

Sample	*Oxygen concentration (ng g^{-1})*	
	Decay curve	*γ-Ray spectrometry*
High-purity germanium		
1A	29±8	18±5
1B	19±5	<20
1C	18±12	23±6
1D	<43	<41
1E	<22	—
2	14±5	26±6
Oxygen-doped germanium		
1	685±15	690±10
2	385±9	413±11

For γ-ray spectrometry, the standard deviations are calculated from the counting statistics. When a significant contribution, *i.e.* greater than the critical level in Currie's definition[15], is not obtained, the limit of detection is indicated.

The different sensitivities obtained in different determinations arise from variations in the irradiation time and intensity, in the chemical yield, and in the decontamination obtained during chemical separation.

The results in Table II for the high-purity samples indicate concentrations of around 20 ng g^{-1}. It is probable that the high values obtained when the flux was monitored with the mica foils or when etching before the irradiation was not applied, should be attributed to the diffusion of recoil ^{18}F formed from the oxygen in the mica or in the superficial oxide layer. The diffusion should then extend behind the germanium layer which is removed after the irradiation. The effect should not be important when the pre-irradiation surface treatment is applied, as it reduces the surface oxygen level[16] to *ca.* 0.04 μg cm^{-2}. This figure corresponds to *ca.* 250 ng g^{-1}, when all the ^{18}F formed at the surface diffuses behind the removed layer. This is highly improbable since the presence of the mica foils (each *ca.* 4 mg cm^{-2}, containing about 50% oxygen) yields an apparent oxygen content which is only in the μg g^{-1} range, although a large part of the ^{18}F activity in the last of these recoils on the sample surface.

The results for the high-purity germanium samples agree with some previous data[5,7]. They disagree clearly with some previous determinations by helium-3 activation[8].

Two oxygen-doped samples were also analysed. A decay curve is given in Fig. 3A and the results are shown in Table II.

The sensitivity of the present method can be estimated at about 10 ng g^{-1} for a 2-h irradiation at 1-μA intensity. This takes into account a 3-h delay for the chemical treatment and a 2-h delay for the transport of the sample from the cyclotron to the radiochemical laboratory.

Grateful acknowledgement is made to R. Kieffer for valuable technical

assistance, to the "Comité de gestion du cyclotron" of Louvain-La-Neuve (U.C.L.) for the use of the cyclotron, to Dr. J. Pauwels (Eurisotop Office) and Dr. L. De Laet (Metallurgy Hoboken) for providing the samples, and to the "Nationaal Fonds voor Wetenschappelijk Onderzoek" for financial support.

SUMMARY

The determination of trace levels of oxygen in germanium by activation analysis with 45-MeV α-particles is described. The chemical separation of ^{18}F formed from oxygen consists of repeated distillation of fluorosilicic acid followed by precipitation of lead chlorofluoride and allows a reduction of the matrix radiation by a factor of $4 \cdot 10^6$. Oxygen concentrations of about 20 ng g^{-1} are found for high-purity germanium; for oxygen doped monocrystals, oxygen concentrations of 400 and 700 ng g^{-1} are found. The influence of surface contamination on the final results is studied.

REFERENCES

1 E. Pell, *J. Appl. Phys.*, 31 (1960) 291.
2 E. Pell, *J. Appl. Phys.*, 31 (1960) 1675.
3 E. Pell, *Solid State Physics—Semiconductors*, Academic Press, New York, 1960, p. 261.
4 R. Fox, *IEEE Trans. Nucl. Sci.*, NS 13 (3) (1966) 367.
5 G. Aleksandrova, A. Demidov, G. Kotelnikov, G. Plashakova, G. Sukhov, D. Choporov and G. Schmanenkova, *Sov. At. Energy*, (1967) 797.
6 C. Kim, *Radiochem. Radioanal. Lett.*, 2 (1969) 53.
7 E. Schweikert, J. Mc. Ginley, G. Francis and D. Swindle, *J. Radioanal. Chem.*, 19 (1974) 89.
8 D. Holm, W. Briscoe, J. Parker, W. Sanders and S. Parker, *Proc. of the 2nd Conf. on Practical Aspects of Activation Analysis with charged Particles*, EUR 3896 d-f-e, 1968, Brussels.
9 J. Giroux and J. Thomas, *J. Radioanal. Chem.*, 19 (1974) 129.
10 L. Alaerts, J. Op de Beeck and J. Hoste, *Anal. Chim. Acta*, 69 (1974) 1.
11 C. Vandecasteele, F. Adams and J. Hoste, *Anal. Chim. Acta*, 71 (1974) 67.
12 J. Cumming in G. O'Kelley (Ed.), *Applications of Computers to Nuclear and Radiochemistry*, Nuc. Sci. Ser. Rep. NAS-NS 3107, National Academy of Sciences - National Research Council, p. 25.
13 E. Ricci and R. Hahn, *Anal. Chem.*, 39 (1967) 794.
14 C. Williamson, J. Boujot and J. Picard, *Tables of Ranges and Stopping Power of Chemical Elements for Charged Particles of Energy 0.05 to 500 MeV*, Rapport CEA-R 3042, Paris, 1966.
15 L. Currie, *Anal. Chem.*, 40 (1968) 586.
16 G. Weber and L. Quaglia, private communication.

Analytica Chimica Acta, 78 (1975) 129–143

ANALYSE D'ECHANTILLONS DE COBALT PAR SPECTROMETRIE GAMMA DIRECTE APRES IRRADIATION AU MOYEN DE PROTONS DE 10 MeV

P. BENABEN, J. N. BARRANDON et J. L. DEBRUN

Groupe d'Application des Réactions Nucléaires à l'Analyse Chimique, C.N.R.S.—Service du Cyclotron, 45045 Orléans-La-Source (France)

(Reçu le 21 decembre 1974)

Ce travail a été entrepris dans le cadre d'une collaboration avec le laboratoire de Métallurgie de l'École Nationale Supérieure de Chimie de Paris, dont les chercheurs ont étudié les échantillons de cobalt avant analyse. Les résultats devaient permettre de relier entre elles la résistivité à basse température et la teneur en impuretés. Bien que la nature et la teneur en impuretés du cobalt ne soient pas les seules causes de la variation de la résistivité (influence du ferromagnétisme et de la structure du cobalt), des études faites sur différents métaux montrent, dans le cas des métaux ferromagnétiques, l'influence importante des impuretés.

Nous présentons ici une partie de nos recherches sur l'analyse de ce métal qui est l'objet d'études du fait de plusieurs caractéristiques intéressantes, comme sa dureté à haute température, sa résistance à la corrosion, son aimantation permanente et sa haute limite élastique.

Par ailleurs, le cobalt est utilisé pour l'obtention de sources radioactives bon marché (^{60}Co) qui ont de nombreuses applications dans le domaine médical et industriel (stérilisation des aliments). De même que l'étude métallurgique, ces applications exigent un métal dont les impuretés soient connues et l'analyse a donc, ici, un rôle important à jouer.

Après examen des différents modes d'activation utilisables, nous avons *à priori*, éliminé l'activation neutronique qui est habituellement employée; en effet, du fait de la forte section efficace du cobalt (18+19 barns) des séparations chimiques nécessitant des sorbonnes blindées, doivent être faites après irradiation pour éliminer ^{60}Co, et en outre l'absorption des neutrons entraîne une distorsion de flux non négligeable. L'activation au moyen des photons γ qui produit à partir du ^{59}Co du ^{58}Co par (γ, n), ne permet pas de dosage par spectrométrie-γ directe, ce qui était notre objectif.

Suite aux travaux précédents, qui ont déjà montré tout l'intérêt que présente l'activation au moyen des protons[1], nous présentons ici les résultats d'une étude plus complète sur l'analyse de traces d'impuretés dans des échantillons de cobalt par irradiation dans un flux de protons d'énergie 10 MeV et spectrométrie-γ directe.

Choix de la particule

De toutes les particules chargées, les protons de moyenne énergie (10 MeV)

sont celles qui semblent les plus intéressantes pour réaliser l'analyse instrumentale directe du cobalt. En effet, les réactions nucléaires (p, n) et (p, αn) sur le seul isotope stable du cobalt, conduisent à deux radioisotopes n'émettant pas de photons-γ, tandis que la réaction (p, α) conduit à un isotope stable du fer. Les seules réactions pouvant induire une activité gênante pour effectuer les dosages d'impuretés sans séparations chimiques, sont les réactions nucléaires: (p, d) et (p, pn) produisant du ^{58}Co.

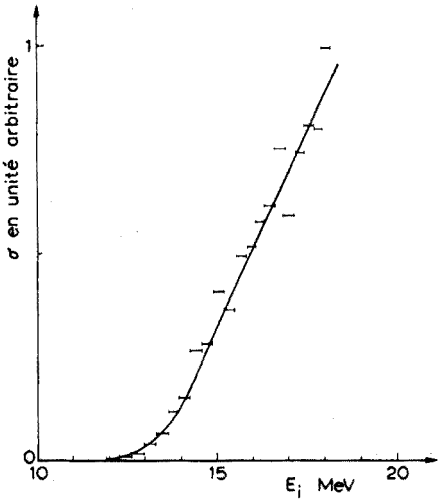

Fig. 1. Production de ^{58}Co à partir de ^{59}Co.

Les seuils théoriques des réactions (p, d) et (p, pn) sur le ^{59}Co sont respectivement de 8,35 MeV et 10,62 MeV[2]. Le seuil pratique de production du ^{58}Co par ces deux réactions, était de 12 MeV (Fig. 1). En irradiant les échantillons de cobalt dans un faisceau de protons de 10 MeV, on s'affranchit des réactions (p, d) et (p, pn) et ainsi on n'obtient aucun radioisotope gênant formé par réaction avec les protons sur la matrice. L'expérience confirme ces résultats et les seuls radioisotopes produits sur le cobalt sont ceux obtenus par réactions nucléaires avec les neutrons rapides secondaires émis par le porte-cible et l'échantillon lui-même. Nous avons ainsi constaté la présence de ^{56}Mn, ^{60}Co, ^{60m}Co et ^{59}Fe obtenus par les réactions: ^{59}Co (n, α) ^{56}Mn, ^{56}Co (n, γ) ^{60}Co, et ^{69m}Co ^{59}Co (n, p) ^{59}Fe.

Nous avons aussi détecté du ^{58}Co que nous attribuons à la réaction nucléaire ^{59}Co (n, 2n) ^{58}Co. Toutefois, la production des radioisotopes précédents n'est pas très importante et n'empêche pas la dosage de traces d'impuretés dans le cobalt.

Les protons ne permettent pas le dosage par spectrométrie-γ directe d'un certain nombre d'éléments intéressants tels que: C, N, O, F, Mg, Al, Si; en effet, les caractéristiques nucléaires des radioisotopes obtenus par activation protonique sur ces éléments ne sont pas favorables à un dosage instrumental. Lorsque l'on désire connaître les teneurs en ces éléments, il est nécessaire d'effectuer des séparations chimiques, ou d'utiliser d'autres méthodes. Pour notre part, nous avons

dosé l'oxygène[3] par irradiation dans les hélions-3, le carbone, le fluor par irradiation dans les photons-γ, et l'azote par irradiation dans les protons après séparations chimiques.

Au cours de recherches futures, nous nous proposons d'étudier la possibilité du dosage de Mg, Al, Si, par irradiation dans un faisceau de deutons et séparations chimiques.

PARTIE EXPERIMENTALE

Appareillage utilisé

Nous avons effectué les irradiations au cyclotron à énergie variable du Centre Hospitalier Frédéric Joliot à Orsay. Les échantillons de cobalt sont irradiés pendant 1 h avec un faisceau de protons dont l'énergie incidente est de 10 MeV. Suivant les expériences, l'intensité du courant était 1–4 μA. Durant l'irradiation, les échantillons de cobalt sont refroidis par un courant d'eau froide circulant dans le porte-échantillon et par un courant d'air comprimé circulant dans la chambre d'irradiation. Devant chaque échantillon de cobalt nous avons placé un moniteur de flux (feuille de Havar de 11 μm d'épaisseur) qui permet de déterminer l'intensité moyenne du courant de protons durant l'irradiation. Entre la feuille de Havar et l'échantillon, nous avons intercalé une feuille d'aluminium de 17 μm qui arrête les noyaux de recul pouvant provenir du moniteur de flux. Le dispositif d'irradiation que nous avons utilisé a été décrit précédemment[4]. Les protons, dont l'énergie initiale est de 10,7 MeV, sont ralentis, jusqu'à 10 MeV, par la traversée de ces différentes feuilles. Après irradiation, les échantillons sont très légèrement décapés à l'acide nitrique dilué afin d'éliminer les pollutions de surface.

Environ 15 min après irradiation, les mesures de radioactivité peuvent être effectuées. Nous utilisons un détecteur Ge(Li) de 2,5 keV de résolution pour le pic à 1332,5 keV du ^{60}Co et de 22% de rendement sur ce même pic par rapport à un NaI de 75 × 75 mm, avec un analyseur 4000-canaux, et une bande magnétique. Les spectres-γ sont traités grâce au programme SAMPO modifié[5]. Les calculs sont effectués au C.I.R.C.E. sur ordinateur I.B.M. 370/168.

Etalonnage et calcul de teneur

Toutes les fois où cela est possible, nous effectuons un étalonnage interne sur chaque spectre en utilisant les pics de radioisotopes bien connus, présents dans l'échantillon après irradiation. Nous avons utilisé dans le cas du cobalt, les radioisotopes produits par les neutrons secondaires sur la matrice: ^{56}Mn et β^+ pour les comptages effectués peu de temps après irradiation, ^{59}Fe–^{58}Co–^{60}Co pour les comptages de longue durée.

Grâce à la détermination précise des énergies et à la connaissance des périodes de décroissance, nous obtenons une grande sécurité pour la détermination des impuretés présentes.

L'analyse quantitative est réalisée par l'utilisation de la section efficace moyenne[6] et avec la méthode de calcul déjà exposée lors d'analyses antérieures[4].

Dans les mêmes conditions expérimentales que pour les échantillons de cobalt, nous avons déterminé les activités spécifiques des étalons (nombre d'impulsions détectées par minute de comptage, pour une p.p.m. de l'élément considéré,

à la fin d'une heure d'irradiation avec un faisceau de protons d'intensité 1 μA) pour chaque radioisotope produit par réaction protonique et pour chaque raie-γ émise par ce radioisotope[7].

Dans le cas où le dosage peut être effectué sur plusieurs raies-γ venant d'un ou de plusieurs radioisotopes, une teneur moyenne est calculée.

Pour les éléments non décelés, une limite de détection expérimentale a été calculée, en prenant comme quantité minimum détectable, 3 fois la racine carrée de l'activité mesurée dans la bande d'énergie située à l'emplacement théorique du pic utilisé pour un dosage éventuel.

RESULTATS

Nous donnons les résultats pour 9 échantillons d'origine et de pureté différentes. Cinq d'entre eux sont des cobalts industriels Ugine–Kulhmann; les quatre autres sont des cobalts de la firme Hoboken, dont certains ont subi une série de purifications au laboratoire de Métallurgie de l'E.N.S.C.P.

TABLEAU I

ELEMENTS DETECTES DANS LES COBALTS UGINE–KUHLMANN

(Teneurs donnees en p.p.m.)

	1	*3*	*4*	*5*	*2*[a]
Ca	—	4	—	4,3	$3,6 \pm 0.13$ (3)[b]
Fe	110	287	300	355	$252 \pm 9,4$ (12)
Ni	158	680	600	880	560 ± 19 (22)
Cu	14,2	—	9	9,5	$12 \pm 2,7$ (4)
Zn	0,9	—	7,3	—	—
As	0,55	0,75	—	—	0,5
Se	—	2,2	2,5	5,2	$2,5 \pm 0,2$ (17)
Mo	0,9	1,4	—	2,2	$1,3 \pm 0,2$ (4)

[a] Teneur a 95% de limite de confiance.
[b] Nombre de determinations.

Nous avons constaté une grande différence dans la teneur en impuretés dans les deux espèces de cobalts. Dans le Tableau I, sont rassemblés les résultats relatifs aux cinq échantillons Ugine–Kulhmann. Il est à constater la forte teneur en Fe et Ni, qui d'ailleurs se révèle quelque peu gênante pour la détermination des niveaux d'impuretés des autres éléments. Par irradiation dans les protons de 10 MeV, on observe sur le fer et le nickel, les réactions suivantes:

Réaction	*Période (h)*	*Principales raies-γ (keV)*
$^{56}Fe(p,n)^{56}Co$	1855,2	846,7; 1037,6; 1238,0; 1771,4
$^{57}Fe(p,n)^{57}Co$	6480	122,1; 136,4
$^{58}Fe(p,n)^{58}Co$	1711	810,6
$^{60}Ni(p,n)^{60}Cu$	0,39	826,2; 1332,5; 1792,0
$^{61}Ni(p,n)^{61}Cu$	3,41	283,0; 656,3; 1185,7
$^{58}Ni(p,\alpha)^{55}Co$	17,9	477,2; 931,5; 1408,3
$^{60}Ni(p,\alpha)^{57}Co$	6480	122,1; 136,4

Les caractéristiques nucléaires de ces radioisotopes montrent bien que leur activité est importante à quelque moment que la mesure soit effectuée, et par suite que la mesure de la radioactivité des autres éléments en est gênée. Malgré cela, nous avons pu doser dans certains de ces échantillons à forte teneur en fer et nickel 0,55 p.p.m., d'As et 0,9 p.p.m. de Zn et Mo, et déterminer des limites de détection pour les éléments que nous n'avons pu déceler. Les résultats donnés dans le Tableau II et qui concernent le cobalt no. 4, montrent que ces limites sont pour de nombreux éléments, inférieures ou égales à 10^{-6} g g^{-1}.

Pour les 4 échantillons de la firme Hoboken, les résultats sont rassemblés dans le Tableau III. L'analyse de ces échantillons porte sur quarante éléments dosés simultanément au cours d'une même irradiation. On peut remarquer sur les

TABLEAU II

LIMITES DE DETECTION POUR LES ELEMENTS NON DECELES DANS LE COBALT UGINE-KULHMANN No. 4

Elément dosé	*Radioisotope utilisé*	E_γ *(keV)*	*Limite obtenue (p.p.m.)*
B	^{7}Be	477,6	< 1,3
Li	^{7}Be	477,6	< 0,14
Ca	^{44}Sc	1157,0	< 0,28
Ti	^{48}V	1311,8	< 0,08
V	^{51}Cr	320,0	< 0,46
Cr	^{52}Mn	935,5	< 0,33
Ga	^{69}Ge	1106,6	< 0,06
Ge	^{72}As	834,0	< 0,07
As	^{75}Se	264,4	< 0,20
Br	^{79}Kr	261,4	< 0,12
Rb	^{85m}Sr	231,7	< 0,13
Sr	^{86}Y	1077,4	< 0,42
Y	^{89}Zr	909,1	< 0,02
Zr	^{90}Nb	1129,1	< 0,10
Nb	^{93m}Mo	1477,1	< 0,8
Mo	^{95}Tc	765,8	< 0,14
Ru	^{100}Rh	539,7	< 0,2
Rh	^{103}Pd	357,0	< 320
Pd	^{105}Ag	344,2	< 3,4
Ag	^{107}Cd	93,0	< 0,90
Cd	^{111}In	245,4	< 0,2
In	^{113}Sn	391,7	< 12
Sn	^{122}Sb	564,0	< 1,0
Sb	^{121}Te	573,2	< 0,5
Te	^{130}I	668,5	< 0,27
I	^{127}Xe	202,8	< 0,1
Ba	^{135}La	480,5	< 120
W	^{184}Re	903,2	< 20
Re	^{185}Os	645,9	< 5,3
Ir	^{191}Pt	538,8	< 8,9
Pt	^{194}Au	328,3	< 1,3
Au	^{197m}Hg	134,0	< 2,9
Hg	^{200}Tl	368,0	< 1,9
Tl	^{203}Pb	279,2	< 1,7
Pb	^{206}Bi	802,8	< 7,0

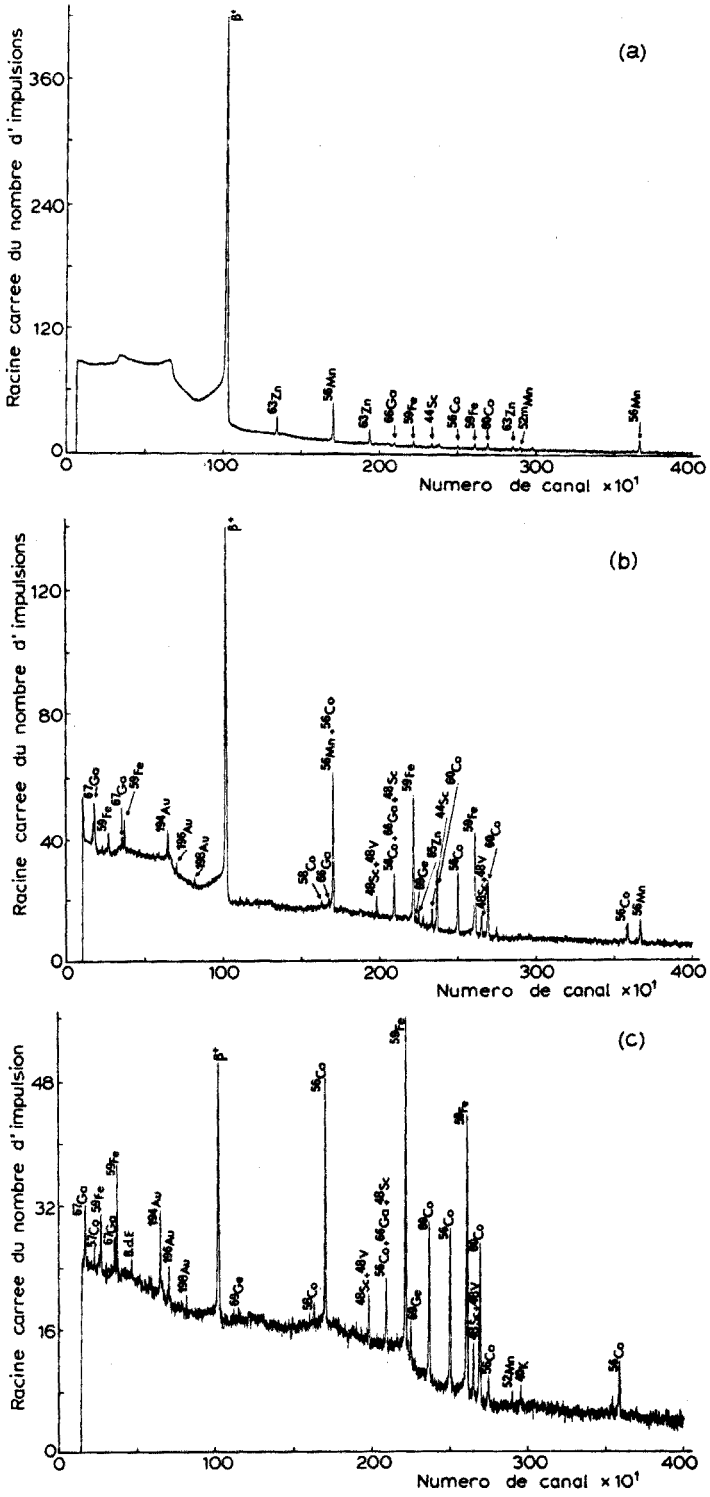
(a)
Racine carree du nombre d'impulsions
Numero de canal ×10¹
(b)
Racine carree du nombre d'impulsions
Numero de canal ×10¹
(c)
Racine carree du nombre d'impulsion
Numero de canal ×10¹

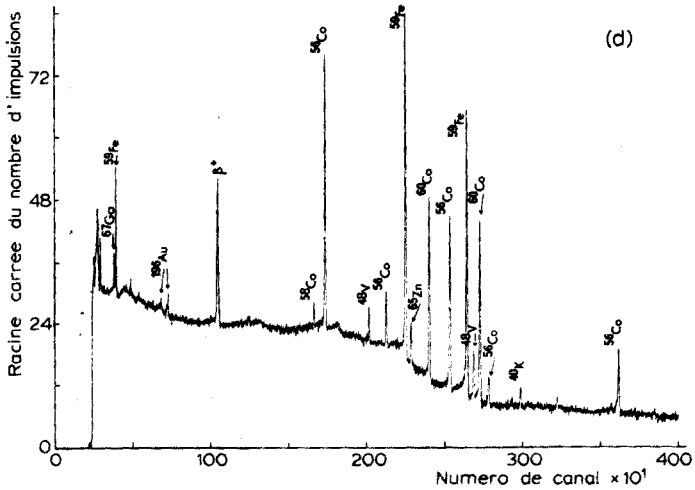

Fig. 2. Spectres-γ obtenus après irradiation du cobalt no. 7. (a) Temp de décroissance, 72 min. Temp de comptage, 30 min. (b) Temp de décroissance, 10 h. Temp de comptage, 11 h. (c) Temp de décroissance, 29 h. Temp de comptage, 15 h. (d) Temp de décroissance, 9 j. Temp de comptage, 42 h.

échantillons nos. 6 et 7, la contamination en platine due probablement à la présence de joints en platine dans l'installation de traitement thermique. Pour l'éprouvette no. 6, nous avons pu donner une limite de concentration inférieure ou égale à 0,1 p.p.m. pour 20 éléments, tandis que 8 sont à un niveau de teneur inférieur ou égal à 1 p.p.m. Les conditions d'études de cet échantillon ont été les suivantes: irradiation de 1 h dans un flux de protons d'énergie 10 MeV et d'intensité moyenne 1,2 μA. Nous avons fait sur cet échantillon, 9 mesures d'activité dont les caractéristiques ainsi que les résultats sont reportés dans le Tableau IV. Nous présentons dans la Fig. 2, les différents spectres obtenus à partir de l'échantillon no. 7 après irradiation.

DISCUSSION

Influence du niveau de pureté sur la sensibilité des dosages

Dans le cas des cobalts à haute teneur en fer et nickel (dépassant les 100 p.p.m.), l'activité induite à partir de la réaction (p,n) sur le ^{60}Ni ne permet pas de mesure immédiatement après irradiation. Nous avons dû, dans tous les cas, attendre la décroissance de l'activité du ^{60}Cu pour pouvoir effectuer les comptages dans de bonnes conditions, ce qui nécessite environ 2 h. Il est donc très difficile de doser le soufre dans ces échantillons en analyse par spectrométrie-γ directe à l'aide de la réaction ^{34}S(p,n)^{34m}Cl du fait de la courte période de ce radioisotope (32,2 min) et de l'énergie basse (146 keV) de son rayonnement-γ le plus intense (dans toutes ces mesures, nous avons exclu la possibilité d'effectuer les dosages grâce au rayonnement à 511 keV qui est la composante de beaucoup trop d'éléments de périodes voisines pour qu'il puisse être utilisable en analyse sans séparations chimiques). Lorsque l'on désire connaître la teneur en soufre d'un échantillon de cobalt de ce type, il est souhaitable de procéder à une séparation

chimique[8] de ^{34m}Cl; la sensibilité ainsi obtenue est bien améliorée.

Cas du Cr et du Cu. Du fait de leur courte période (21,1 et 38 min), il est difficile d'utiliser le ^{52m}Mn et le ^{63}Zn pour effectuer les dosages de Cr et de Cu dans des cobalts à forte teneur en Fe et Ni. Ce sont pourtant les radioisotopes pour lesquels la sensibilité la meilleure est obtenue.

Nous avons dû calculer ces teneurs sur les pics à 744,2; 935,6; 1434,3 keV

TABLEAU III

RESULTATS D'ANALYSE POUR 4 ECHANTILLONS DE COBALT "HOBOKEN" EN P.P.M.

Elément	*No. 6*	*No. 7*	*No. 8*	*No. 9*
B	< 0,6	< 0,7		
Li	< 0,06	< 0,07		
S	< 9,8	< 7,2		
Ca	< 0,08	1,4	<0,2	<0,03
Ti	< 0,02	0,38	<0,04	<0,2
V	< 0,1	< 0,1	<0,15	<0,15
Cr	< 0,04	0,2	0,06	0,13
Fe	5,0	28	1,2	2,3
Ni	< 0,3	< 0,5	<0,2	<0,25
Cu	3,3	7,5	2,4	1,5
Zn	< 0,03	1,4	<0,1	<0,04
Ga	< 0,02	< 0,11	<0,06	<0,03
Ge	< 0,02	< 0,03	<0,05	<0,03
As	< 0,09	< 0,1	<0,1	<0,08
Se	< 0,06	< 0,09	<0,15	<0,1
Br	< 0,05	< 0,08	<0,1	<0,08
Rb	< 0,04	< 0,1	<0,04	<0,01
Sr	< 0,08	< 0,05		
Y	< 0,01	< 0,01		
Zr	< 0,02	< 0,04	<0,1	<0,015
Nb	< 0,2	< 0,4	<0,7	<0,2
Mo	< 0,03	< 0,05	<0,15	<0,04
Ru	< 0,04	< 0,6	<0,3	<0,05
Rh	<90	<102		
Pd	< 0,35	< 0,45	<0,2	<0,3
Ag	< 0,06	< 0,4	<0,6	<0,2
Cd	< 0,06	< 0,7	<0,5	<0,3
In	< 6,7	< 8,2	<7	<9
Sn	< 0,4	< 0,7	<0,4	<0,9
Sb	< 0,2	< 0,2	<0,3	<0,3
Te	< 0,03	< 0,05	<0,1	<0,04
I	< 0,09	< 0,07	<0,15	<0,1
Ba	<13	< 29		
W	< 8	< 8,4	<8	<10,5
Re	< 2,2	< 2,6		
Ir	< 3,5	< 4		
Pt	5,2	5	<0,8	<0,5
Au	< 0,7	< 1,3		
Hg	< 0,5	< 0,8		
Tl	< 0,5	< 0,7	<0,5	<0,5
Pb	< 3,6	< 5	<6	<7

TABLEAU IV

ECHANTILLON No. 6 COBALT "HOBOKEN"—DETAIL DES MESURES DE RADIOACTIVITE

Nos.	*Temp de comptage (min)*	*Temp de décroissance (min)*	*Radio-isotope*	*Energie-γ (keV)*	*Eléments dosé*	*Teneur[a] (p.p.m.)*
1	5	40	^{63}Zn	669,8	Cu	3,4
			^{63}Zn	962,2	Cu	3,2
2	5	47	^{63}Zn	669,8	Cu	3,2
			^{63}Zn	962,2	Cu	3,5
3	5	59	^{63}Zn	669,8	Cu	3,1
			^{63}Zn	962,2	Cu	3,4
4	30	71	^{63}Zn	669,8	Cu	2,9
			^{63}Zn	962,2	Cu	3,3
5	60	102	^{63}Zn	669,8	Cu	3,2
			^{63}Zn	962,2	Cu	3,3
6	870	401	^{56}Co	846,7	Int. ^{56}Mn	
			^{56}Co	1238,0	Fe	4,8
			^{65}Zn	1115,5	Cu	3,6
			^{194}Au	293,5	Pt	4,0
			^{194}Au	328,3	Pt	4,9
			^{196}Au	355,7	Pt	5,3
			^{198}Au	411,8	Pt	5,7
7	1481	1140	^{56}Co	846,7	Fe	5,3
			^{56}Co	1238,0	Fe	4,8
			^{65}Zn	1115,5	Cu	3,1
			^{194}Au	293,5	Pt	5,9
			^{194}Au	328,3	Pt	5,4
			^{196}Au	355,7	Pt	5,5
			^{198}Au	411,8	Pt	5,8
8	900	2367	^{56}Co	846,7	Fe	4,9
			^{56}Co	1238,0	Fe	5,1
			^{65}Zn	1115,5	Cu	3,0
			^{194}Au	293,5	Pt	5,1
			^{194}Au	328,3	Pt	4,1
			^{196}Au	355,7	Pt	5,3
			^{198}Au	411,8	Pt	5,4
9	2400	11841	^{56}Co	846,7	Fe	4,9
				1037,6	Fe	5,5
				1238,0	Fe	4,9
				1771,4	Fe	4,7
			^{65}Zn	1115,5	Cu	3,6
			^{196}Au	355,7	Pt	5,4

[a] Résultats à 95% de L.C. Teneur Cu: 3,3±0,14. Teneur Fe: 5±0,2. Teneur Pt: 5,2±0,4.

du ^{52}Mn pour le chrome, et pour le cuivre nous avons effectué le dosage sur le pic à 1115.5 keV du ^{65}Zn, ce qui provoque une perte de sensibilité importante.

Cas des autres éléments à doser. A chaque pic photoélectrique, est associée une distribution Compton qui représente une activité gênante et diminue d'autant la sensibilité de certains dosages. De ce fait, dans le cas d'un cobalt à haute teneur en Fe et Ni (Tableau II), les limites obtenues sont nettement moins bonnes que dans le cas d'un cobalt pur.

Interférences possibles entre les raies-γ de plusieurs radioisotopes

Nous avons observé certaines interférences entre les raies-γ émises par différents radioisotopes, dans le cas où l'échantillon renferme Ca, Ti, Fe, Zn, As et Mo. En effet, par activation de ces différents éléments au moyen des protons de 10 MeV, on obtient des radioisotopes dont les caractéristiques nucléaires sont rassemblées dans le Tableau V (en même temps que les principales activités spécifiques). Les interférences sur les raies-γ pouvant se produire lors de la présence simultanée de ces éléments, apparaissent clairement:

Cas de la présence simultanée de Fe, Mo. Le pic photoélectrique à 847 keV environ est la somme des pics photoélectriques de ^{56}Co, ^{94}Tc et ^{96}Tc, car le pouvoir discriminateur de l'appareillage n'est pas assez grand pour les séparer. Pour effectuer le dosage du Mo, il faut alors utiliser les autres raies-γ et les autres radioisotopes.

Le dosage du fer peut s'effectuer sur les autres raies-γ du ^{56}Co et sur les raies-γ du ^{57}Co, mais il est souhaitable de confirmer ces résultats par un calcul de teneur sur le pic à 846,7 keV qui est le plus sensible. Pour cela, une estimation du rapport teneur en fer à teneur en molybdène doit être effectuée. Suivant la valeur de ce rapport nous avons étudié les deux cas suivants:

(a) Rapport supérieur à 100: C'est le cas de la plupart des échantillons que nous avons eu à analyser (exception faite des cobalts no. 7 et no. 8 pour lesquels les limites de détection obtenues pour le molybdène ne nous permettent pas de faire cette conclusion). Après 8 jours de décroissance de l'activité après irradiation, la contribution à 847 keV du ^{94}Tc est parfaitement négligeable (période du ^{94}Tc: 4,9 h), et les rendements respectifs des pics à 846,7 keV du ^{56}Co (période: 1855,2 h) et 849,9 keV du ^{96}Tc (période: 104,4 h) sont égaux. La contribution du Mo au pic à 847 keV n'excède donc pas 1%, ce qui permet avec une erreur inférieure à 1%, de calculer la teneur en fer à partir de ce pic. La comparaison des teneurs obtenues à partir des autres pics du ^{56}Co et de la teneur trouvée à cette énergie là, confirme les résultats.

(b) Rapport inférieur à 100: Nous avons vérifié les résultats obtenus sur les autres raies-γ du ^{56}Co, en attendant 30 jours de décroissance de l'activité de l'échantillon après irradiation, en calculant la teneur en fer sur le pic à 847 keV. A cette data là, et à teneur égale en Fe et Mo, la contribution du ^{96}Tc au pic à 847 keV est environ 30 fois plus faible que celle du ^{56}Co. Compte tenu des teneurs et limites trouvées, l'activité du ^{96}Tc à 847 keV est négligeable devant celle du ^{56}Co. L'expérience confirme les résultats; nous avons obtenu une bonne concordance entre les différents dosages.

Cas de la présence simultanée de Ca et Ti. Le calcium et le titane conduisent, entre autres radioisotopes, à ^{48}Sc, et ^{48}V qui, décroissant sur les niveaux excités du ^{48}Ti, par β^- pour le ^{48}Sc et β^+ pour le ^{48}V, donnent certaines raies-γ communes. Pour effectuer le dosage du calcium, on peut utiliser les autres radioisotopes obtenus par réaction (p,n) et en particulier le ^{44}Sc qui se révèle le plus sensible.

Le dosage du titane est plus délicat. Il faut soit utiliser le pic à 944,2 keV du ^{48}V quand la teneur le permet, soit attendre la décroissance du ^{48}Sc de 43,7 h de période. Dans le cas du cobalt no. 7 qui est le seul des échantillons analysés à contenir à la fois calcium et titane, la faible teneur ne nous permet pas

TABLEAU V

CARACTERISTIQUES NUCLEAIRES DES RADIOISOTOPES POUVANT DONNER LIEU A DES INTERFERENCES ENTRE LES DIFFERENTES RAIES-γ, OU GENANT A HAUTE TENEUR POUR LES DOSAGES

Eléments	*Radio-isotopes obtenus*	*Période (h)*	*Energie-γ (keV)*	*Activité spécifique (imp/min μA p.p.m.)*[a]
Ca	^{44}Sc	3,95	1157,0	10,33
	^{44m}Sc	58,6	271,2	0,10
	^{48}Sc	43,7	983,4	0,19
			1037,4	0,17
			1311,6	0,12
Ti	^{48}V	386,4	944,2	0,34
			983,5	4,0
			1311,8	3,0
Fe	^{56}Co	1855,2	846,7	0,61
			1037,6	0,063
			1238,0	0,26
			1771,4	0,048
	^{57}Co	6480	122,1	0,049
			136,4	0,0072
Ni	^{60}Cu	0,39	826,2	27,7
			1332,5	85,8
			1792	35,8
	^{61}Cu	3,41	283,0	2,7
			656,3	1,12
			1185,7	0,23
	^{55}Co	17,9	931,5	0,35
Zn	^{66}Ga	9,4	834,0	2,2
			1039,3	13,5
			1333,8	0,25
			1730,0	0,42
	^{67}Ga	78,1	93,1	2,7
			184,2	1,5
			300	0,8
As	^{75}Se	2880	121,2	0,77
			136,1	2,6
			264,4	1,7
			279,4	0,78
			400,5	0,57
Mo	^{94}Tc	4,9	702,9	3,0
			871,3	2,8
	^{95}Tc	20	765,8	12,4
			1074,0	0,36
	^{96}Tc	104,4	778,2	2,8
			812,6	2,1
			849,9	2,3
			1127,0	0,3
	^{99m}Tc	6,05	140,5	8,6

[a] Pour 1 h d'irradiation et à la fin de l'irradiation.

d'effectuer ce calcul sur le pic à 944,2 keV qui est en effet peu abondant.

Le rapport des activités spécifiques $A(^{48}V)/A(^{48}Sc)$ juste après la fin de l'irradiation sur les pics à 983,5 et 1311,8 keV, est légèrement supérieur à 20. Après 9 jours de décroissance de l'activité, ce rapport est de 400. Nous avons calculé pour le Co no. 7 et après 9 jours de décroissance, la teneur en Ti, en négligeant la contribution du ^{48}Sc. Cette teneur a été trouvée 4 fois plus faible que celle du calcium. À moins de 1% d'erreur, la teneur en titane est donc trouvée en négligeant la contribution du ^{48}Sc.

Cas de la présence simultanée de Zn, Ca, Fe. Cette interférence se situe à environ 1038 keV et se révèle gênante pour le dosage du Zn à faible teneur. Dans le cas où cette teneur est suffisante pour que les autres pics du ^{66}Ga et les pics du ^{67}Ga puissent être détectés, le dosage peut s'effectuer sur ces pics là, et il n'y a pas de problèmes. Si la teneur est trop faible, il est nécessaire de soustraire l'activité du ^{56}Co et du ^{48}Sc. Pour cela, il faut chiffrer la teneur en fer et calcium grâce aux possibilités, (comme il a été dit précédemment) et calculer ensuite leur contribution sur le pic à 1038 keV. L'activité restante est due au ^{66}Ga, et il est alors possible d'effectuer le dosage de Zn. Cette méthode introduit des incertitudes du fait de la double soustraction, mais elle est parfois la seule utilisable.

Sensibilité de la méthode

Nous avons rassemblé dans le Tableau VI les meilleures limites de détection obtenues dans les cobalts analysés. Dans tous les échantillons étudiés jusqu'à présent, nous avons détecté du fer et dans les cobalts les plus purs, du cuivre. Il ne nous était donc pas possible de déterminer la sensibilité pratique de la méthode pour ces 2 éléments. Nous avons calculé une valeur théorique de cette sensibilité en prenant comme quantité minimum détectable, 3 fois la racine carrée de l'activité mesurée à l'emplacement du pic, soustraction faite de l'aire du pic

TABLEAU VI

MEILLEURES LIMITES DE DETECTION OBTENUES DANS LES ECHANTILLONS DE COBALT

Eléments	*Meilleures limites (p.p.m.)*	*Numero échantillon*	*Eléments*	*Meilleures limites (p.p.m.)*	*Numero échantillon*	*Eléments*	*Meilleures limites (p.p.m.)*	*Numero échantillo*
B	0,6	6	As	0,08	9	In	6,7	6
Li	0,06	6	Se	0,06	6	Sn	0,4	6
S	7,2	7	Br	0,05	6	Sb	0,2	6
Ca	0,03	9	Rb	0,01	9	Te	0,03	6
Ti	0,02	6	Sr	0,05	7	I	0,07	7
V	0,1	6–7	Y	0,01	6–7	Ba	12,8	6
Cr	0,04	6	Zr	0,015	9	W	7,9	6
Fe	0,1	6	Nb	0,2	6–9	Re	2,2	6
Ni	0,2	8	Mo	0,03	6	Ir	3,5	6
Cu	0,3	6	Ru	0,04	6	Pt	0,5	9
Zn	0,03	6	Rh	90	6	Au	0,7	6
Ga	0,02	6	Pd	0,2	8	Hg	0,5	6
Ge	0,02	6	Ag	0,06	6	Tl	0,5	8–9
			Cd	0,06	6	Pb	3,6	6

correspondant. Nous avons obtenu dans le cas du cobalt no. 6, une limite de 0,1 p.p.m. pour le fer et 0,3 p.p.m. pour le cuivre.

Nous avons déjà signalé que la seule méthode d'activation permettant de doser le fer dans le cobalt avec sensibilité et sans interférence, était l'activation protonique, et qu'en utilisant des protons de 10 MeV, le dosage présente l'avantage d'être "non-destructif".

Nous venons de voir qu'une limite théorique de 100 p.p.b. peut être ainsi obtenue en irradiant 1 h avec 1,2 μA; cette limite peut être diminuée d'un facteur en $(It)^{\frac{1}{2}}$, en augmentant l'intensité (I) et le temps (t) d'irradiation puisque activité spécifique et activité parasite croissent proportionnellement à It (t devant la période de ^{56}Co).

La méthode récemment proposée [9] qui consiste à irradier à haute énergie (protons de 30 MeV) pour produire ^{53}Fe et le séparer ensuite radiochimiquement, semble donc peu intéressante puisque la sensibilité annoncée n'est que de 50 p.p.b. pour une irradiation de 20 min à 5 μA, et augmenter le temps d'irradiation serait ici peu profitable puisque la période du ^{53}Fe n'est que de 8,5 min.

CONCLUSION

Les méthodes présentées jusqu'ici dans diverses publications portent essentiellement sur le dosage d'un élément à la fois et sont souvent plus limitées en sensibilité que l'activation protonique. Citons cependant Lagrou et Verbeek[10] qui proposent une méthode permettant de doser simultanément le cuivre, le cadmium, et le plomb avec des limites de 0,02, 0,04, et 0,1 p.p.m. respectivement, et Speecke et Maes[11] qui, par activation neutronique, dosent dans un domaine de quelques p.p.m. à quelques centaines de p.p.m., Cu, Zn et Mn.

Notre travail montre que la spectrométrie-γ directe après irradiation avec des protons de 10 MeV, permet de déterminer facilement le niveau de pureté d'un cobalt donné en ce qui concerne les 41 éléments que nous avons étudiés. Suivant les échantillons, 3–6 éléments ont été détectés, une limite de détection a été calculée pour les éléments non décelables. Cette limite qui est très variable suivant les éléments, dépend en outre du niveau global de pureté des échantillons. Le tableau VII nous montre que pour 80% des éléments étudiés, la limite de détection est inférieure à 1 p.p.m.

TABLEAU VII

LIMITES DE DETECTION POUR LES IMPURETES DANS LE COBALT

X > 10 p.p.m.	*10 > X > 1 p.p.m.*	*1 > X > 0,1 p.p.m.*	*X < 0,1 p.p.m.*
Ba, Rh	S, In, W, Re, Ir, Pb	B, V Fe, Ni, Cu, Nb, Pd, Sn, Sb, Pt, Au, Hg, Tl	Li, Ca, Ti, Cr, Zn, Ga, Ge, As, Se, Br, Rb, Sr, Y, Zr, Mo, Ru, Ag, Cd, Te, I

D'après nos récentes expériences, cette méthode peut être étendue à la détermination dans le cobalt de certains éléments de la série des lanthanides, et en particulier La, Pr, Nd, Sm, Eu, Gd, Dy, Er et Yb qui, excepté pour l'europium et le dysprosium dont les limites de détections sont de quelques p.p.m., sont susceptibles d'être décelés à moins de 1 p.p.m.

Enfin, il est possible, après les comptages-γ, de récupérer les échantillons de cobalt pour effectuer des analyses par d'autres méthodes; dans notre cas, les échantillons ont été réactivés à l'aide de photons de haute énergie, d'hélions-3, et même de protons pour doser C, N, O et F.

En raison de tous ses avantages et considérant la grande sûreté avec laquelle les résultats sont obtenus, l'activation protonique appliquée à l'analyse du cobalt présente un grand intérêt.

Nous remercions le Laboratoire de Métallurgie de l'École Nationale Supérieure de Chimie de Paris, et plus particulièrement Monsieur B. Dubois qui a bien voulu nous fournir les échantillons. Nous tenons aussi à remercier le Service Hospitalier Frédéric Jolio d'Orsay de nous avoir accueillis dans son Laboratoire et d'avoir bien voulu mettre à notre disposition leur cyclotron.

RESUME

Nous avons mis au point l'analyse d'échantillons de cobalt, par activation au moyen de protons et spectrométrie-γ directe; 41 éléments sont recherchés simultanément, après irradiation avec des protons de 10 MeV. Des métaux industriels provenant de deux Compagnies différentes ont été analysés: Fe et Cu ont toujours été détectés, jandis que Ca, Ti, Cr, Zn, As, Se et Mo ne l'ont été qu'occasionnellement. Dans le cas des autres éléments, une limite de détection est calculée: pour 33 d'entre eux cette limite est inférieure à la partie par million.

SUMMARY

Proton activation is applied to the analysis of cobalt samples; 41 elements were only occassionally detected. For the other elements, detection limits were irradiation with 10-MeV protons. Samples from two commercial Companies were analysed: Fe and Cu were always detected, while Ca, Ti, Cr, Zn, As, Se and Mo were only occasionally detected. For the other elements, detection limits were calculated: 33 limits are below the part per million level.

BIBLIOGRAPHIE

1 J. L. Debrun et J. N. Barrandon, *J. Radional. Chem.*, 17 (1973).
2 R. J. Howerton, D. Braff, W. J. Cahill et N. Chazan, *Thresholds of Nuclear Reactions*, Lawrence Radiation Laboratory, Livermore, California.
3 A. Kohn, J. N. Barrandon, J. L. Debrun, M. Valladon et B. Vialatte, *Anal. Chem.*, 46 (12) (1974) 1737.
4 J. N. Barrandon, P. Benaben, J. L. Debrun et M. Valladon, *Anal. Chim. Acta*, 73 (1974) 39.
5 C. Rouxel, Rapport interne.
6 E. Ricci et R. L. Hahn, *Anal. Chem.*, 37 (1965) 742.
7 J. N. Barrandon, J. L. Debrun et P. Benaben, Soumis à *Anal. Chem.*

8 J. L. Debrun, J. N. Barrandon et Ph. Albert, *Modern Trends in Activation Analysis, N.B.S. Gaithersburg*, 7–11 octobre 1968.
9 D. L. Swindle, L. R. Novak et A. Schweikert, *Anal. Chem.*, 46 (6) (1974) 655.
10 A. Lagrou et F. Verbeek, *Anal. Lett.*, 4 (9) (1971) 573.
11 A. Speecke et K. Maes, *Radiochemical Methods of Analysis, Vol. I*, 51, International Atomic Energy Agency, Vienna, 1965.

Analytica Chimica Acta, 78 (1975) 145–157

FLOW INJECTION ANALYSES

PART I. A NEW CONCEPT OF FAST CONTINUOUS FLOW ANALYSIS

J. RŮŽIČKA and E. H. HANSEN

Chemistry Department A, The Technical University of Denmark, Building 207, Lyngby (Denmark)

(Received 10th February 1975)

The ever-increasing demand for analyses in clinical, agricultural, pharmaceutical, industrial and other types of analytical control has led to the development of a large number of different instruments for automated analysis[1]. Developments in this field have been further stimulated by the additional advantages of automation, such as increased precision, decreased cost of individual assay, and the satisfactory reliability of automated equipment. It has been estimated[2] that the market for automated instruments for wet chemistry will achieve an annual growth rate in excess of 15% up to 1980, compared with the growth rate of 9% for all other types of analytical instrumentation. The demand for the type, complexity, multiplicity and rate of analyses to be performed is very diversified; consequently, the major manufacturers tend to concentrate on specific areas, like clinical analysis, which offer a large market, and relatively similar types of material to be analysed. The present trend is aimed at increased sampling rates of both single and multipurpose analysers, which thus become more complex to devise and more expensive to manufacture. The numerous instruments manufactured and suggested for analysis of a large number of individual sample solutions can be divided into two groups: batch analysers and continuous flow analysers.

In the batch analyser, each sample is placed in its individual container in which it remains for at least most of the analytical procedure which comprises discrete additions of buffers and reagents dilution, heating, *etc.* at predetermined points of the analytical cycle until the treated sample reaches the colorimetric cell or other detector. Up to that point the individual character of each sample is strictly preserved as it moves within the instrument in an individual container. Therefore, cross-contamination is minimal, and this allows a high sampling rate, up to 150 samples per hour. Even higher sampling rates can be achieved in the so-called fast parallel analysers based on the transfer of samples and reagents by centrifugal force. This most interesting system, originally developed at the Oak Ridge National Laboratory[3], employs a rotor containing cavities to hold samples and reagents. By spinning at speeds of about 1200 rev min^{-1}, the solutions are mixed and transferred into set of fifteen cuvettes arranged radially; the cuvettes spin past the stationary beam of a light of a photometer and the absorbances are displayed as a series of peaks on an oscilloscope. To assist the transfer of liquids, a variable underpressure is applied at the rotor chamber. Thus, fifteen analyses are executed simultaneously, within 1–2 min, depending on the reaction rate, but the washing of

the rotor and pipetting of the samples and reagents into their cavities also take some time. Currently, at least three different manufacturers are marketing slightly different versions of this machine. The disadvantage of such machines, as well as of more conventional batch analysers, which contain moving belts to transport the sample containers, is the complexity of their moving parts, which eventually become worn during use and are expensive to manufacture. Yet, batch analysers find wide application, especially for one-component determinations in clinical laboratories.

Another type of system, the stop-flow analyser[4], is by concept and construction close to batch analysers. In this system, both sample and reagent are rapidly mixed by injection into a mixing chamber from which the reacting mixture is forced into an absorption cell. There the flow of solution is abruptly stopped and the absorbance of the idle solution is measured, before the cell is flushed out. Recently, these analysers have been successfully used in reaction-rate methods of analysis[5].

In the continuous flow analysers, the samples are successively aspirated from their individual containers into a tube through which they move until the whole analysis is completed. Thus the samples become a part of a continuously moving stream, into which, at predetermined points, reagents are added at fixed flow rates. The processed stream finally flows through the cell of a spectrophotometer (or another measuring device) where the quantitative measurement is executed and the signal continuously recorded. The movement of all liquids within the conduits of continuous flow analysers is controlled by a peristaltic pump which also takes care of aspiration of the samples. It is the versatility of continuous flow analysers which causes their widespread use: samples can be split for multiple analyses, and the flowing stream can be dialyzed, extracted, filtered, heated, decanted and even distilled. The greatest disadvantage of the continuous flow concept is that each sample is liable to contamination from the preceding sample; moreover, contamination increases as the rate of sampling is increased because of closer spacing of the samples. By alternate aspiration of sample solution and distilled water, cross-contamination can be suppressed, and in a simple module, sampling rates up to 10–15 samples per hour can be expected under laminar flow conditions. It was, however, the introduction of air-segmented streams by Skeggs[6] in 1957 which made continuous flow analysis practicable. Today, Autoanalysers, which are based on Skegg's idea and produced by Technicon, form an indispensable part of any clinical laboratory and find an increasing number of applications in all other types of routine laboratory. Over five thousand papers have been devoted to Autoanalyser techniques, but only about 1% of these deal with the theoretical aspects of the air-segmented, continuously moving stream.

Thiers *et al.*[7] were the first to make general observations on mutual sample interactions; their work, which was confirmed and extended by Walker *et al.*[8], remains the basis of quantitative considerations in determining the highest practicable sampling rate. To increase the sampling rate, which is usually around 60 samples per hour, two approaches have been used: (a) modification of the original Autoanalyser design; and (b) introduction of an appropriate correction factor[9] or even computer regeneration[10] of the recorded curve. The most significant changes in the design have been electronic rather than mechanical timing of the sampler, a rapidly moving sampling probe[11], a bubble-gating flow cell[12] or a computer-watched flow

cell through which the air bubbles are allowed to pass. These innovations, together with computerized curve regeneration[10], or even more recently rising curve slope computing techniques, lead to complex and inevitably more expensive instrumentation which may have only doubled or perhaps quadrupled output.

The purpose of the present work is to introduce a new concept of continuous flow analysis based on injecting the sample into a rapidly flowing carrier stream[13] which has not been segmented by air.

THEORY

The peaks recorded by a continuous flow analyser are made of rise and fall curves which represent the transition between different steady-state conditions[7,8] (A, B, Fig. 1). These curves are quantitatively described by two parameters, the half-wash time $W_{\frac{1}{2}}$ and the lag phase a. The half-wash time, which has been shown[8,14] to originate in non-segmented parts of the stream, describes the exponential part of the transition curve. The lag phase, which is said to be mainly due to air segmentation[14,15], precedes the exponential part. Thus, in the absence of lag phase, the rise curve is described by the equation $y=E(1-e^{-t/b})$, and the fall curve by the equation $y=Ee^{-t/b}$; here y is the absorbance at time t, E is the absorbance at the plateau (B, Fig. 1), and t is the time elapsed from the start of the rise curve or the fall curve. The half-wash time equals $0.69b$. In order to minimize irregularities in the sampling time, which are due to uneven pumping, different levels of sample liquid in the sampler cups, and slightly uneven timing of the sampler, 95% or better achievement of the plateau is used in AutoAnalyser methodologies. This obviously requires sampling times of 4.5 $W_{\frac{1}{2}}$ or $3b$. Consequently, with a typical lag phase of 20 s and a half-wash time of 10 s, a total of 65 s is needed to reach 95% of peaking. Thus

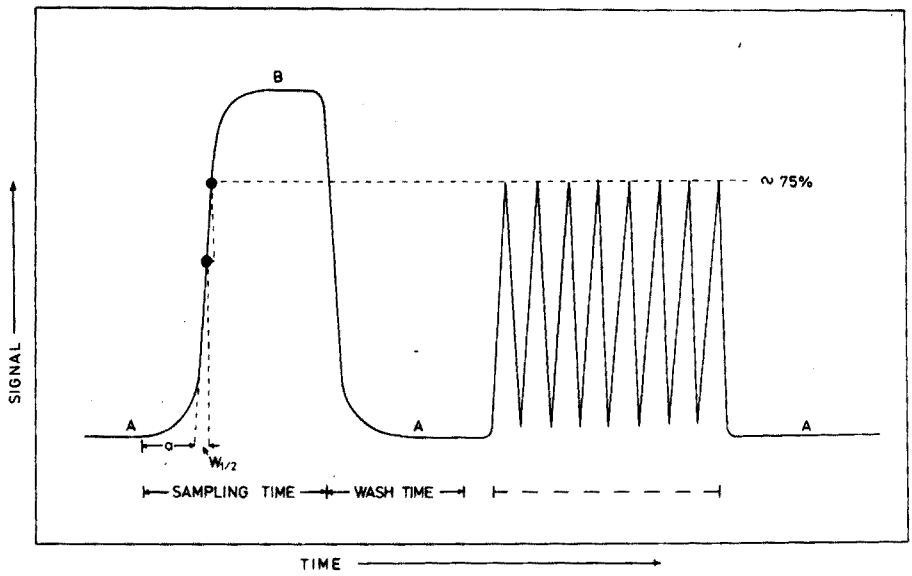

Fig. 1. Relation between the "steady-state" peak, as obtained in an AutoAnalyser, and a peak obtained by injecting the sample for two half-wash times. A and B are the steady states, a is the lag phase and $W_{\frac{1}{2}}$ is the half-wash time.

with a sampling/wash ratio of 2:1, 100 s are needed for one sampling cycle, which gives an analysis output of 40 samples/h. Higher sampling rates lead to significant carry-over, and unless some sort of correction factor can be worked out, the precision and accuracy of the determination deteriorate.

It is, however, known[7,8] that: (a) the rise and fall curves are almost identical reversals of each other; (b) the lag phase and half-wash time are independent of E; (c) any peak which does not reach E is the arithmetic mean of the rise and fall curve.

Therefore, provided that the Lambert–Beer law holds, the y value for any given time t is as good a measure of the concentration of the analyte as the final steady state reached. For optimal sensitivity and readability, y should be read at the top of a peak resulting from a partial rise and fall curve (Fig. 1). The peak height, rather than its area, would have analytical significance, provided that the timing of sample introduction is sufficiently reproducible. However, the timing must be the more precise, the shorter the sampling period, because the rate of change of the absorbance, $dy/dt = -b^{-1}Ee^{-t/b}$, is faster at the beginning of the rise (and fall) curve. Provided that exact instant sampling can be achieved, sampling times of one or two $W_{\frac{1}{2}}$ should allow a substantial increase in the sampling rate (Fig. 1).

The beneficial effects of air segmentation have been so obvious that the necessity of introducing air bubbles was never really doubted, although the drawbacks of its presence in the flowing stream are well known: (a) because of the compressibility of air, the stream tends to pulsate rather than flow regularly; (b) streams have to be debubbled before they enter the flow cell or before repumping; (c) the size of the air bubbles has to be controlled for faster sampling rates; (d) the pressure drop—and flow velocities—vary in the presence of air for different tubing materials[16]. Although it might appear that the role of the bubble is to divide the stream into a number of slugs which then do not mix, the main function of the air segments is in fact to cause wall friction with resulting turbulent, rather than laminar flow even at low pumping velocities[17]. Yet it is known that at higher pumping rates, and with decreased diameters of tubing, sufficient turbulence will be produced to avoid the laminar flow which is responsible for carry-over. At conventional sampling rates, however, the consumption of the sample may exceed its availability, and the consumption of the reagents would become uneconomical. Instant discrete sampling, however, with five-fold higher rates of analysis would still give the same reagent consumption even at five-fold faster reagent flows.

It is therefore suggested here that a small volume of sample be injected rapidly into a turbulently flowing carrier stream of reagent. Thus, at the point of injection, the reagent solution would be pushed aside and in this manner a slug or zone of sample would be formed, which would then be further processed and carried into the flow cell of a detector. The feasibility of this idea would depend on the following factors: (a) reproducibility of the volume of the sample and of the speed of the injection; (b) a reproducible movement of the sample zone within the conduits of the analyser, and a reproducible degree of disturbance arising from travel and addition of further reagents downstream; and (c) sufficient and reproducible mixing of each sample with the reagent contained in the carrier stream, yet minimum carry-over between samples.

While the first requirement is not difficult to fulfil, as the piston-type devices deliver easily reproducible volumes, the last two requirements are, to some extent,

contradictory. Therefore, all the test experiments described here were devised so that they involved a chemical reaction between the carrier solution and the reagent stream.

EXPERIMENTAL

Sample injection

Samples were injected from 1-ml disposable plastic syringes (B-D-Plastipac, Ireland) supplied with a standard hypodermic needle (thickness 0.5 mm, length 10 mm). The sample solution (0.7–0.6 ml) was aspirated into the syringe, care being taken to avoid air bubbles, and then the piston was pressed so that its edge reached exactly the 0.5-ml mark. The actual injection was done manually, at maximum, but still convenient, rate. The early experiments were made with an injector which was made of a rubber tube (wall thickness 3 mm) situated in a perspex block, furnished with precisely bored holes, which allowed controlled piercing of the wall of the rubber tube with an hypodermic needle. As the tube had a tendency to bleed after multiple piercing, an injection block (Fig. 2) was made of two perspex blocks, screwed together by two screws (not shown) which passed through the top block freely and fitted a threaded hole in the bottom one; a silicone rubber disc (Beckman spare part no. 567026, for Gas Chromatograph 65) was squeezed between the blocks and served as a septum. The dimensions of the needle guide in the top block were chosen so that the orifice of the inserted hypodermic needle was situated in the carrier stream at the moment of injection. As the septum is compressed, and can be easily repositioned, several hundred injections can be made through one disc before the carrier liquid starts to bleed through or air leaks into the system.

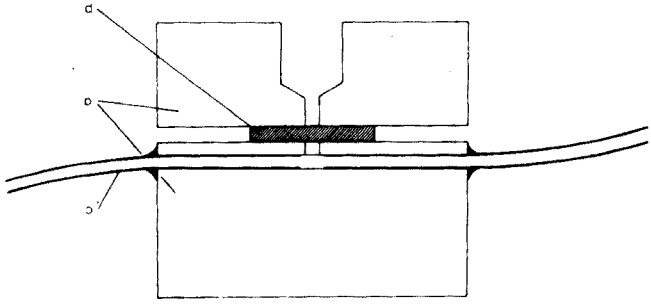

Fig. 2. Injection block. (a) Perspex blocks; (b) silicone rubber septum; (c) polyethylene tubing. (For details, see text).

Pumping system

The carrier stream was pumped at a rate of 18 ml min^{-1}, and additional reagents were added downstream, by peristaltic pump. Two types of pump were used: a standard Technicon AutoAnalyser pump Mark II (where several pumping tubes were joined to pump the carrier stream) and a Polymetron (CH-8634, Hombrechtikon, Switzerland) pump model 8511 (60 r.p.m.) in which 3-mm silicone rubber tube was used to pump the carrier stream. Unlike the Technicon pump, the Polymetron pump does not use rollers to squeeze the pump tube, but a series of

closely spaced plungers, located on the same crankshaft. As the plungers press the plastic tubing and do not pull it at the same time, the pump tubes withstand two months of full-time operation before they have to be renewed. Moreover, the absence of friction during pumping avoids any build-up of static electricity, which is undesirable when ion-selective electrodes are used as detectors.

Manifold and mixing coils

The manifold was made entirely from polyethylene tubing (diameter 1.5 mm, wall thickness *ca.* 0.25 mm). The pumping tubes of the Polymetron pump, which is supplied with 1.0, 2.0 and 3.0-mm internal diameter tubing (wall thickness *ca.* 2.5 mm), served not only as the pumping tube but also in short pieces as elastic connectors between mixing coils, T-fittings, flow cell inlets and polyethylene transmission tubings.

Mixing coils were made of the above polyethylene tubing by winding an appropriate length of it round a glass tube (length 10 cm, diameter 5 cm) and securing it at the ends with tape. T-pieces were made from perspex blocks ($3 \times 3 \times 1.5$ cm) into which T (or Y)-shape connections were drilled (1.9-mm bore). Short pieces of polyethylene tubing were glued into the holes by "araldite" so that their ends within the block left practically no dead space.

Flow-through cells

The flow-through cell for the spectrophotometer (Hellma type 178-QS) had a light path of 10 mm and a volume of 0.080 ml. The flow-through cell for the air-gap electrode[18] was made of perspex and was cylindrical in shape with an internal diameter of 2 cm and a height of 2 cm. The inlet to the cell situated close to its bottom was made as described for the T-piece, while the outlet (internal diameter 3 mm) was situated *ca.* 6 mm above the bottom on the opposite side of the cell. The air-gap electrode body served as a lid, and the electrode itself protruded from it so that its gas-sensitive surface was *ca.* 5 mm above the level of the streaming liquid. The level of the liquid in the cell was maintained by differential pumping, *i.e.* the input was kept at 10 ml min^{-1} and the output at 12 ml min^{-1}. Air was let into the cell by a vent (diameter 1.5 mm), the orifice of which was situated as close as possible to the cell outlet. To avoid condensation of water vapours on the electrode surface (which would eventually form a drop and thus cause a sluggish response), the electrode was always kept at least 2°C warmer than the solution passing through the cell.

Instrumentation

A Beckman Model DB or Model DB-GT Spectrophotometer was used. In both cases, a dual-beam mode was used, the carrier stream liquid serving as a blank in a 10-mm stationary cuvette. In the DB model, a mask with a 3-mm aperture had to be used in the reference beam to compensate for the small window of the flow cuvette, but in the DB-GT model this compensation was made electronically.

The pH meter used in conjunction with the air-gap electrode was a digital one (PHM 64, Radiometer) with a readibility of 0.001 pH.

The recorders used were the Servograph REA 310 (Radiometer), Beckman Ten Inch Laboratory Recorder (Model 1005) or Servogor RE 511 (Goertz, Austria). It is important that the full scale response of the recorder be less than 0.5 s, as

otherwise the high readings would be distorted. For this reason, the Servogor recorder was used only in potentiometric measurements, where the larger dead volume of the flow-through cell allowed the use of a slower responding recorder.

RESULTS AND DISCUSSION

Model system

A model system based on spectrophotometric determination of the red acidic form of methyl orange was chosen to investigate the reproducibility and maximum sampling rates achievable by Flow Injection Analysis. It was decided to inject the yellow basic form of this indicator into an acidic carrier stream, so that the streaming liquid not only provided the transport but also served as a reagent for colour development. Therefore, samples of methyl orange (25.0, 12.5, 6.25, 3.125 and $1.563 \cdot 10^{-4}$%) in $1 \cdot 10^{-3}$ *M* sodium hydroxide were injected into a carrier stream of 2.10^{-1} *M* hydrochloric acid. The volume of the samples was 0.50 ml, the carrier stream was pumped at a rate of 18 ml min^{-1}, and the wavelength of the spectrophotometer was adjusted to 510 nm. The total length of tubing between the injection point and the flow cell was approximately 2.5 m, of which *ca.* 1.5 m was the length of the mixing coil. The continuous recording of absorbance *versus* time is shown in Fig. 3; the calibration graph, obtained by plotting the height of the recorded peaks against the concentration of methyl orange in the samples, was rectilinear over the above-mentioned range. The maximum sampling rate that can be achieved with manual injection is seen in Fig. 4; this actually corresponding to an output of 270 samples per hour.

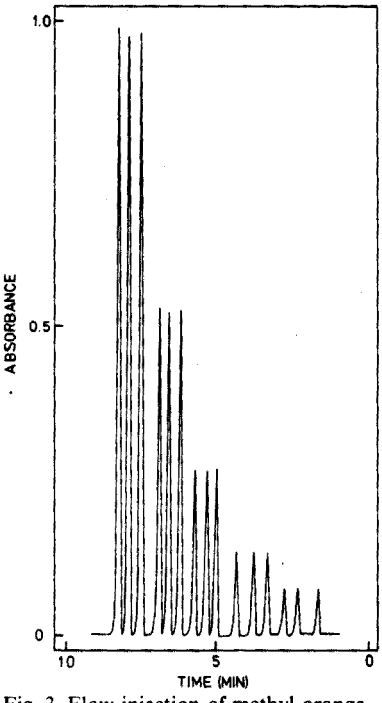

Fig. 3. Flow injection of methyl orange.

The results obtained on this model system confirmed that:

(a) the output of the instrument closely follows the Lambert–Beer law;

(b) manual injection allows a high precision, which in the case of measurement of the red form of methyl orange gave a regression coefficient of 0.9993 and a standard deviation of 0.05 absorbance unit, corresponding to *ca.* 1% in the concentration of methyl orange;

(c) there is no carry-over between samples even at a rate of 270 samples per hour as the signal still reaches the baseline.

As the change of the yellow colour to red was clearly visible, it was easy to follow the formation of the sample zone, the rate of the acid–base reaction and the transport of the sample within the system. At the point of injection, the carrier solution is pushed aside and the sample zone, during transport, changes colour from the sides towards the middle. Large volumes of sample and or too short a length of tubing, which may not give sufficient time for reaction or enough reagent to equilibrate across the full sample zone, yield a minimum, or valley, at the top of the peak. How-

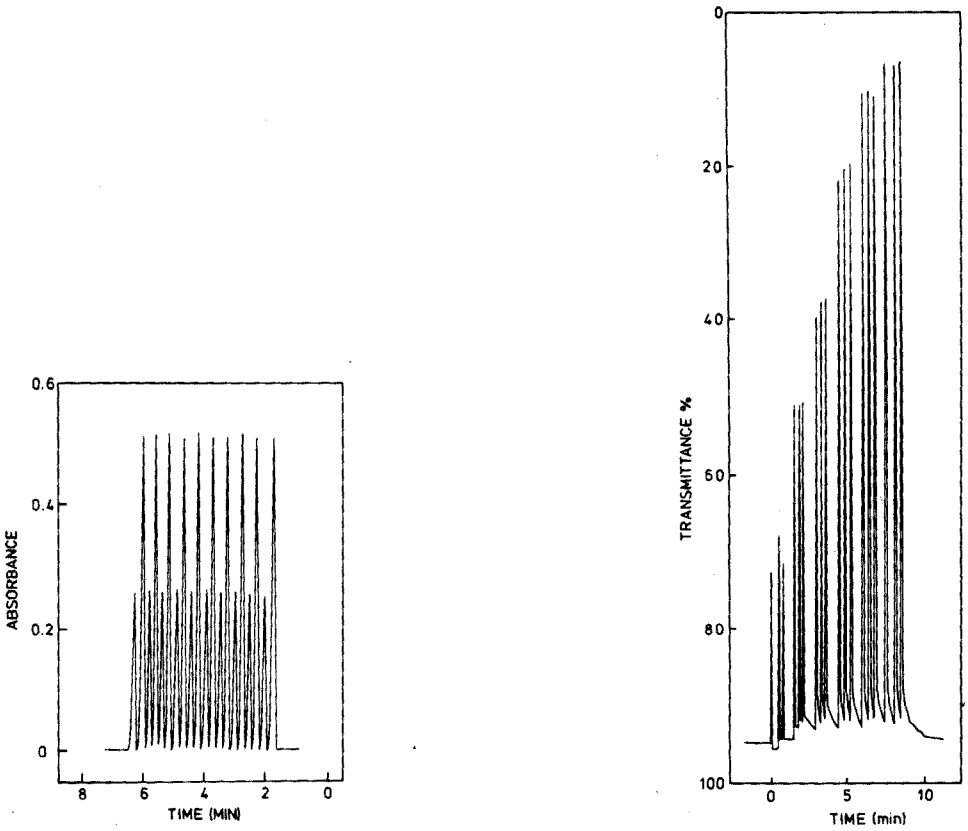

Fig. 4. Flow Injection of methyl orange at a rate of 285 samples per hour (6.25 and $12{,}50 \cdot 10^{-4}$% methyl orange samples).

Fig. 5. Flow Injection Analysis for phosphate by the molybdenum yellow method. Paper speed 0.2 inch min^{-1}. Sampling rate 120 samples h^{-1}. 5.0, 7.5, 10.0, 15.0, 20.0, 25.0 μg P ml^{-1}.

ever, it ought to be pointed out that in the model system, this valley formation occurred only at very extreme conditions.

Spectrophotometric determination of phosphate

The spectrophotometric determination of phosphate was based on the measurement of molybdenum yellow[19] as well as molybdenum blue[20]. This system was chosen because it could serve as a model for simple and fast colorimetric determinations (yellow method), as well as for a more complicated reaction which requires the use of additional reagent downstream and is said[21] to require a considerable reaction time (blue method).

The yellow phosphomolybdate was measured at 362 nm and the manifold was the same as that used in the methyl orange measurement. The carrier stream, pumped at the rate of 18 ml min^{-1}, was 0.005 *M* ammonium molybdate in 0.4 *M* nitric acid. The samples (0.50 ml) contained sodium orthophosphate in amounts of

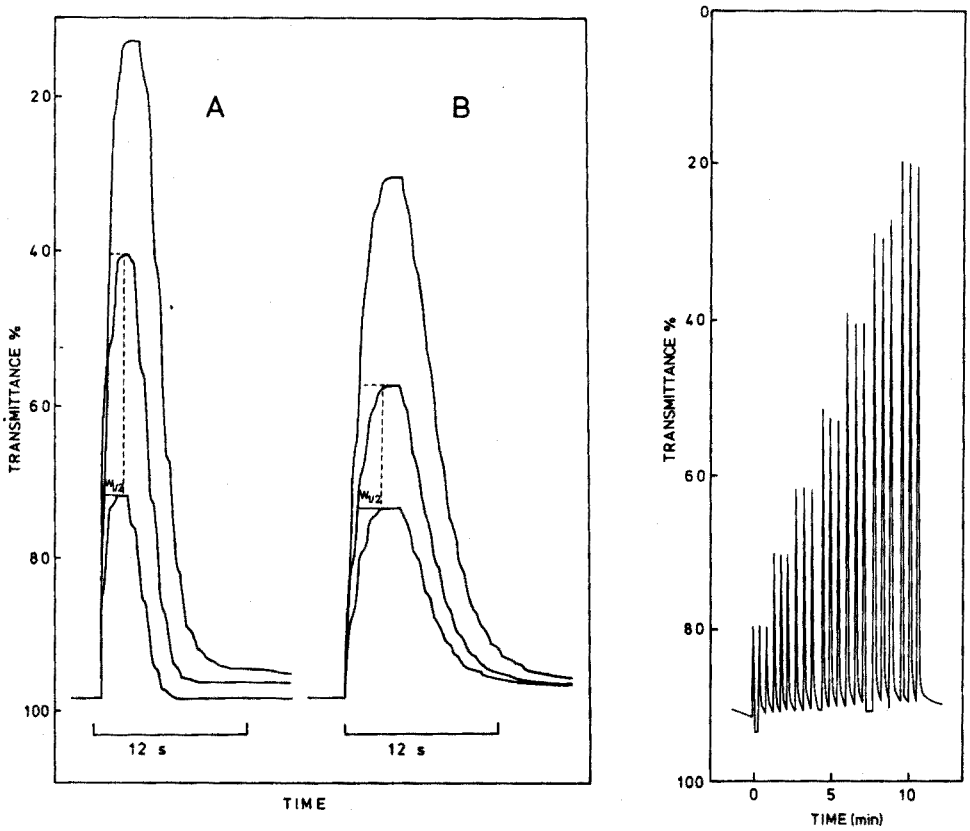

Fig. 6. Flow Injection Analysis for phosphate recorded at high paper speed (10 in. min^{-1}) for evaluation of flow parameters, 5.0, 10.0 and 20.0 μg of P. A. Molybdenum yellow method yielding $W_{\frac{1}{2}}$ of 1.5 s. B. Molybdenum blue method yielding $W_{\frac{1}{2}}$ of 1.9 s.

Fig. 7. Flow Injection Analysis for phosphate by the molybdenum blue method. Paper speed 0.2 in. min^{-1}. Sampling rate 120 samples h^{-1}. 2.5, 5.0, 7.5, 10.0, 15.0, 20.0, 25.0 μg P ml^{-1}.

5.0, 7.5, 10.0, 15.0, 20.0 and 30.0 μg P ml^{-1}. The continuous recording of the transmittance shown in Fig. 5 again demonstrates fair reproducibility and absence of carry-over even at high sampling rates; and when plotted as a calibration curve, $-\log T$ gave a rectilinear response with respect to the phosphate content ($r=0.998$). In order to evaluate the duration of lag phase and half-wash time, the peaks for 5, 10 and 20 μg of phosphorus were recorded at the fastest available (10 in min^{-1}) paper speed (Fig. 6A). The half-wash time estimated from the peak heights, corresponding to a doubled concentration of analyte, was 1.5 s while the lag phase was totally absent. The small undulations on the wave are due to irregularities in the pumping action.

The blue phosphomolybdate was measured at 660 nm and as this method involves the reduction of yellow phosphomolybdate, a reducing reagent had to be added downstream. Therefore another mixing coil (length 2.5 m) was added together with a T-piece. Here, the sample, injected into a carrier stream of 0.005 *M* ammonium molybdate–0.4 *M* nitric acid, passed through the first mixing coil (1.2 m) where the yellow phosphomolybdate was formed, and then an aqueous 1% solution of ascorbic acid was added at a rate of 1.5 ml min^{-1} through the T piece into the carrier stream, which further passed through the second (2.5 m) mixing coil into the detector. Surprisingly, the residence time of 6 s during which the reduction occurs in the second mixing coil was sufficient for colour development. Even more interesting was the observation that the substantial increase in the length of the tubing (more than 200%) and the addition of the second reagent downstream, did not create any lag phase and increased the half-wash time only by 0.3 s (Fig. 6B). The continuous record of the transmittance (Fig. 7) shows good reproducibility, and when plotted as a calibration graph gave a rectilinear response of $-\log T$ with respect to phosphate content ($r=0.998$). A study of flow injection analysis for phosphate in plant materials by the blue phosphomolybdate method showed that even with an average analysis rate of 200–250 samples per hour very precise measurements could be achieved (within 1–2%)[22].

In addition to the observations already made on the model system with methyl orange, which were confirmed by these phosphate determinations, it was learned that:

(a) the half-wash time is less than 2 s and the lag phase is negligible;

(b) neither the addition of a second reagent downstream nor additional tube length (of 2.5 m) significantly alters these parameters.

These results give reasonable grounds to suppose that the proposed system will find wide practical applications, as there are many spectrophotometric determinations which are fast and simple enough to be performed in similar manner, *i.e.*, by injecting the sample into a buffer and adding the second reagent downstream.

Potentiometric determination of ammonia

The potentiometric determination of ammonia was investigated as a model system with an ion-selective electrode as a detector. The carrier stream of 0.05 *M* sodium hydroxide was pumped at a rate of 10 ml min^{-1} through tubing with a total length of 1.5 m, two thirds of it made into a mixing coil. The aqueous samples of ammonium chloride (1.0, 5.0, and $10.0 \cdot 10^{-3}$ *M*) were injected in the usual way and were converted quantitatively into ammonia gas, which when trans-

ported into the flow cell, diffused across the air gap and caused an increase of pH at the gas-sensitive surface of the air-gap electrode[18]. The signal of this electrode, which is a special glass electrode in conjunction with a reference electrode, was continuously monitored by a pH meter and recorded. The recorded signal consisted of a series of peaks, each of which corresponded to one sample injection (Fig. 8). While the increase in pH was due to an increase in the ammonia partial pressure in the flow chamber, the fall part of the curve was caused by its decrease when the chamber was washed by the carrier stream and by the air which was entering the chamber by a side vent (see flow-cell). In this case, the digital readout at the top of a peak (readable to 0.001 pH unit) was used to obtain better precision. The resulting calibration curve had a regression coefficient of 0.99996 and a standard deviation of 0.0038 pH units, corresponding to a standard deviation of 0.9% in the concentration of ammonia.

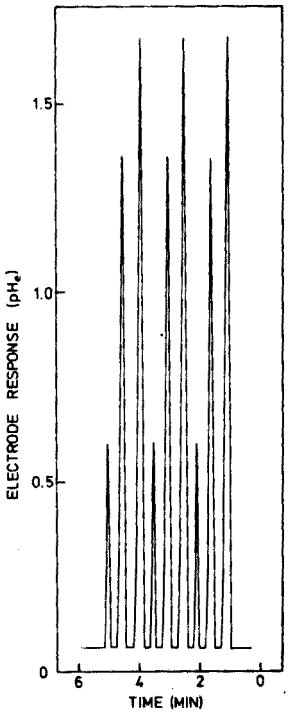

Fig. 8. Flow Injection Analysis for ammonia with the air-gap electrode as sensor ($1.0 \cdot 10^{-3}$, $5 \cdot 10^{-3}$ and $1 \cdot 10^{-2}$ *M* NH_4Cl).

These results confirm that a linear response with a Nernstian slope can be obtained in a Flow Injection Analyser furnished with a potentiometric sensor, and that the reproducibility of the determination can be as good as that obtained by a spectrophotometric measurement. The low sampling rate of *ca.* 60 samples per hour was due to a large dead volume of the flow cell (2.3 ml of solution and *ca.* 4 ml of air constituting the air gap), and to a slower pumping rate.

CONCLUSIONS

From the above results, it is evident that instant discrete sampling by injection into a carrier stream allows continuous analysis to be performed in a new, much simplified way. Because of the absence of lag phase, at a half-wash time of 2 s and a sample: wash ratio of 1:1.5, 360 samples per hour can be theoretically analysed (at 75% peaking). With manual injection, rates in the vicinity of 280 analyses per hour were actually achieved. The analyser is extremely simple to construct, and with a little practice even manual injection gives results with a standard deviation better than 1%. For larger numbers of analyses, however, the contruction of an automatic injector (similar to that used in stop-flow analysers[23]) must be undertaken to utilize the productivity of the system in full.

In contrast to the AutoAnalyser, where the sample and wash solutions are alternately aspirated, pumped, air-segmented and supplied with reagents, and thus form a continuously moving stream of air and solutions slugs, Flow Injection Analysis is based on the formation of well defined sample zones in a rapidly moving carrier stream of reagent. Because of the absence of air segmentation, the carrier stream of reagent flows more regularly as it is not compressible. Consequently, except for detector warm-up, the system is ready for instant operation immediately after the pump has been switched on. Thus, even a small number of samples can be conveniently assayed in a very short span of time in "computer-like" fashion with a good economy of reagent consumption. The new concept, and absence of air segmentation, allows the use of a simple manifold with fewer pumping tubes and easier programming.

The present stage of development leaves, however, a number of open questions. It is not yet known if the sample can be split for multiple analysis and it is doubtful that dialysis can be performed on the injected sample without distorting the flow parameters. The relationships between sampling rates, sample volumes and sensitivity as well as the influence of tube lengths and tube material wettability, has recently been investigated[22]. Obviously, over a certain length of tubing, the turbulent flow will become less effective than air segmentation, and will result in decreased peak height and loss of sensitivity. Thus it can be visualized that the continuous flow analysis will be eventually performed on:

(a) sample injected into a turbulently flowing stream,
(b) sample injected into an air-segmented stream, or
(c) sample aspirated and pumped into an air-segmented stream.

The last approach, represented by the AutoAnalyser design, will clearly remain useful for the more involved types of multiple analyses. The first possibility investigated and described here, may very well replace the AutoAnalyser method in numerous analyses involving fast reactions and the addition of one or two reagents downstream. Work is under way to test and adapt various analytical methods for this purpose. Injection of very small samples into the air-segmented stream remains an intriguing possibility.

The authors wish to express their thanks to Dr. J. W. B. Stewart, UNDP Expert, for discussion and reading of the manuscript; to the Centro de Energia Nuclear na Agricultura, Piracicaba, São Paulo, Brasil, for support in experiments

with phosphate analysis during J.R.'s leave of absence on U.N. Development Project BRA/71/556; to Polymetron A/S, Switzerland for a loan of the peristaltic pump; and to the Danish Natural Science Research Council for a partial financial support.

SUMMARY

The concept of a new continuous flow analyser system is described. Based on instant discrete sampling by injection into a carrier stream, the system allows continuous flow analysis to be performed in a fast, much simplified way. As the continuous flowing stream is characterized by a turbulent rather than a laminar flow, the discrete instant sampling creates geometrically well-defined segments of sample solution within the flowing stream. Because of the absence of lag phase, an unprecedented sampling rate for continuous flow analysis of well over 200 samples per hour can be achieved; and even manual injection of the samples allows a very high degree of accuracy and precision to be obtained ($\leqslant \pm 1\%$). Uses of the system in various analytical procedures are described and discussed. A potentiometric sensor (the air-gap electrode used in a flow-through unit) and a spectrophotometric arrangement with a flow-through cell have been used as detector units.

REFERENCES

1 J. T. van Gemert, *Talanta*, 20 (1973) 1045.
2 R. T. Knock, *Analytical Instruments, Stanford Research Institute, Report No. 447*, October 1971.
3 N. G. Anderson, *Anal. Biochem.*, 28 (1968) 207.
4 H. W. Malmstadt, E. A. Cordos and C. L. Delaney, *Anal. Chem.*, 44 (1972) 26A.
5 P. M. Beckwith and S. R. Crouch, *Anal. Chem.*, 44 (1972) 221.
6 L. T. Skeggs, *Amer. J. Clin. Pathol.*, 28 (1957) 311.
7 R. E. Thiers, R. R. Cole and W. J. Kirsch, *Clin. Chem.*, 13 (1967) 451.
8 W. H. C. Walker, C. A. Penncock and G. K. McGowan, *Clin. Chim. Acta*, 27 (1970) 1576.
9 H. S. Strickler, P. J. Stanchak and J. J. Maydak, *Anal. Chem.*, 42 (1970) 1576.
10 W. H. C. Walker, *Clin. Chim. Acta*, 32 (1971) 305.
11 R. E. Thiers, J. Bryan and K. Oglesby, *Clin. Chem.*, 12 (1966) 120.
12 R. L. Habig, B. W. Schlein, L. Walters and R. E. Thiers, *Clin. Chem.*, 15 (1963) 1047.
13 E. H. Hansen and J. Růžička, *Danish Pat. Appl. No. 4846/74.*
14 R. E. Thiers, A. H. Reed and K. Delander, *Clin. Chem.*, 17 (1971) 42.
15 R. D. Begg, *Anal. Chem.*, 44 (1972) 631.
16 A. L. Chaney, *Technicon Symp.*, 1 (1967) 115.
17 J. R. Gerke and A. Ferrari, *Technicon Symp.*, 1 (1967) 531.
18 E. H. Hansen and J. Růžička, *Anal. Chim. Acta*, 72 (1974) 353.
19 J. F. Kennedy and D. A. Weetman, *Anal. Chim. Acta*, 55 (1971) 448.
20 S. R. Dickman and R. H. Bray, *Ind. Eng. Chem., Anal. Ed.*, 12 (1940) 665.
21 D. F. Boltz and M. G. Mellon, *Ind. Eng. Chem. Anal. Ed.*, 19 (1947) 873.
22 J. Růžička and J. W. B. Stewart, *Anal. Chim. Acta*, in press.
23 H. W. Malmstadt and H. L. Pardue, *Anal. Chem.*, 34 (1962) 299.

Analytica Chimica Acta, 78 (1975) 159–169

REALISATION ET MISE AU POINT D'UN APPAREIL DE TITRAGE AUTOMATIQUE DE GRANDE PRECISION

E. MERCINY, J. M. GATEZ, L. SWENNEN et G. DUYCKAERTS

Laboratoire de Chimie Analytique et de Radiochimie, Université de Liège au Sart Tilman, B-4000 Liège (Belgique)

(Reçu le 21 février 1975)

Les acides aminoacétiques tels l'acide iminodiacétique (IMDA), l'acide nitrilotriacétique (NTA), l'acide hydroxyéthyléthylènediaminotriacétique (HEDTA), l'acide éthylènediaminotétraacétique (EDTA) peuvent former avec les cations à nombre de coordination élevé tels les lanthanides, outre des complexes binaires[1–7] de stoechiométrie 1:1, 1:2 et même 1:3, des complexes mixtes renfermant, autour d'un cation central, deux acides chélatants différents; on trouve dans la littérature de nombreux travaux relatifs à la détermination des constantes de formation de ces complexes[8–17].

Dans un précédent travail[18], nous avons montré que les complexes 1:2 des lanthanides avec le HEDTA (H_3Y) peuvent exister en solution, non seulement sous la forme LnY_2^{3-} mais également sous différentes formes protonées $LnY_2H_n^{(3-n)-}$; nous en avons déterminé les constantes d'acidité à partir des courbes de titrage par la soude de l'acide seul d'une part et de l'acide en présence de son complexe de stoechiométrie 1:1 LnY d'autre part.

Il nous a semblé intéressant d'appliquer cette méthode à toute une série d'autres complexes doubles et mixtes: en effet, la connaissance des constantes de formation de ces complexes protonés peut nous aider dans l'interprétation de certaines courbes d'extraction chromatographique d'une part[19] et d'autre part elle doit entraîner une meilleure connaissance du comportement des lanthanides en solution aqueuse (nombre de coordination, nombre de molécules d'eau d'hydratation du cation et de ses complexes)[20–25].

Au cours du travail mentionné ci-dessus[18], nous nous sommes heurtés à de sérieuses difficultés surtout dues au fait que les constantes d'acidité des complexes $LnY_2H_n^{(3-n)-}$ peuvent être très proches de celles de l'acide chélatant H_3Y; la méthode par titrage ne peut alors fournir des résultats significatifs que moyennant une très grande précision de mesure du pH. De plus, au voisinage des points équivalents, la cinétique de neutralisation devient fort lente; vingt à trente minutes sont requises pour atteindre l'équilibre entre deux injections de réactif titrant; l'obtention d'une seule courbe de titrage exige, dans ces conditions, un travail fastidieux et ininterrompu d'une vingtaine d'heures.

Ces raisons nous ont incité à construire un titrateur automatique de très grande précision, capable de fournir des résultats valables même dans le cas de cinétiques de neutralisation défavorables.

Nous nous proposons, dans cette publication, de donner une description de cet appareil et d'en évaluer les performances.

DESCRIPTION DU MONTAGE EXPÉRIMENTAL

Appareillage

La différence de potentiel entre l'électrode indicatrice de pH et l'électrode de référence est mesurée au moyen d'un voltmètre digital Tekelec Airtronic TE 370 à six chiffres fournissant sur l'échelle d'un volt une sensibilité de 10 μV soit $1{,}7 \cdot 10^{-4}$ unité pH. Afin de pouvoir utiliser le titrateur avec des électrodes indicatrices à résistance interne élevée, il est monté en série avec un électromètre de 10^{13} ohms d'impédance d'entrée.

Le titrant est introduit au moyen d'une burette à piston Gilson Digistrib qui permet de régler mécaniquement le volume d'une injection entre 0,01 et 0,5 ml. Nous avons fixé ce volume à 0,1 ml environ; le volume total de titrant introduit est obtenu à partir du nombre d'injections; l'étalonnage de la burette est vérifié par pesée avant chaque titrage: la reproductibilité de la mesure des volumes de titrant est très grande, l'erreur peut être estimée à 0,1%.

Ce type de burette, rarement utilisé pour des titrages, présente pourtant de nombreux avantages: l'erreur relative sur la mesure du volume total de titrant délivré est constante et fixée par l'erreur sur chaque injection; des variations de température ambiante n'affectent que légèrement la mesure de ce volume et enfin, l'enregistrement du volume est très simple.

Les informations fournies par le voltmètre et la burette à injection sont transmises à une imprimante S.E.S. "Printses" par l'intermédiaire d'une électronique adaptée; celle-ci réalisée dans nos ateliers constitue, en fait, le coeur de l'appareil: en effet, compte tenu de la variation de potentiel résultant du dernier ajout de titrant, elle décide du nombre d'injections à effectuer et du temps d'attente pour la mesure suivante; le nombre d'injections diminue et le temps d'attente augmente lorsque la variation de potentiel observée augmente; cela signifie que dans les zones tamponnées, où la solution subit des variations plus faibles de pH, les ajouts seront plus importants et plus rapprochés car l'équilibre s'établit plus rapidement. Lorsque le temps nécessaire à l'établissement de l'équilibre est écoulé, elle commande l'impression du potentiel et du nombre d'injections de titrant. Elle décide enfin de l'arrêt du titrage soit lorsqu'un certain volume de titrant a été ajouté, soit lorsqu'un certain pH a été atteint.

La cellule de titrage

La cellule de titrage à double paroi thermostatée par circulation d'eau a une contenance de 150 ml; elle comporte quatre tubulures rôdées destinées respectivement à l'électrode indicatrice, au pont de jonction ou à l'électrode de référence suivant les cas, à la burette et au barboteur à hydrogène; une tubulure supplémentaire fixée à sa partie supérieure permet l'évacuation du gaz.

Le pont de jonction du type "Wilhelm" est thermostaté par une circulation d'eau; il est replié à 180° pour minimiser les inductions parasites et pour faciliter la faradisation éventuelle de l'ensemble[26].

La régulation de la température de la cellule et du pont de jonction est

réalisée par un thermostat Haacke N.B.22 dont l'eau de refroidissement est elle-même thermostatée par un Thermomix Braun. Dans ces conditions, les fluctuations de température observées dans la cellule ou dans le compartiment du pont réservé à l'électrode de référence ne dépassent pas 0,01°C.

Un agitateur magnétique I.K. Combimag RCH assure une homogénéisation de la solution pendant les titrages.

Signalons enfin que le titrateur est installé dans un local thermostaté à ± 1°C et continuellement éclairé pour réduire au maximum les variations de potentiel de l'électrode de référence.

Electrode indicatrice de pH

On ne peut nier les avantages de l'électrode de verre pour les mesures de pH courantes: son utilisation est aisée, sa réponse rapide, sa précision suffisante pour des mesures de routine (0,01 unité pH). Pour des mesures très précises, elle présente certains défauts: tout d'abord sa réponse n'est pas linéaire en milieu relativement basique, surtout en présence de fortes concentrations en ions alcalins; elle nécessite un étalonnage à partir de tampons de pH dont la précision fixe finalement la précision de la mesure du pH et enfin, les très bonnes électrodes de verre fournissent une précision qui ne dépasse pas 0,005 unité pH[27]. Il faut également rappeler leur résistance interne très élevée et leur déterioration rapide et irréversible en milieu fort alcalin.

L'électrode à hydrogène, beaucoup moins maniable, présente par contre, pour des mesures très précises de pH, des avantages indéniables: sa réponse est parfaitement linéaire dans tout le domaine de concentration en ions H^+, elle permet d'obtenir une précision supérieure au millième d'unité pH. La connaissance du potentiel normal apparent de l'électrode de référence suffit pour calculer le pH sans étalonnage préalable à partir de la mesure de la force électromotrice et de la pression d'hydrogène.

Comme nous le montrerons par la suite, nous avons constaté que cette électrode est à la fois extrêmement stable et très reproductible. Sa vitesse de réponse, réputée lente[28,29] est en réalité fixée par la vitesse de saturation de la solution en hydrogène; une dispersion efficace du gaz dans la solution réduit considérablement la durée requise pour la saturation: dans ces conditions, la vitesse de réponse est aussi rapide que celle de l'électrode de verre.

Préparation. L'électrode est constituée d'un treillis de platine de forme cylindrique de 35 mm de hauteur et 13 mm de diamètre. Après nettoyage dans l'eau régale diluée et l'acide nitrique concentré et chaud, le platine est passé, après rinçage, dans la flamme oxydante d'un bec Bunsen.

Le dépôt de noir de platine est obtenu par électrolyse d'une solution à 2% d'acide chloroplatinique dans l'acide chlorhydrique 2 M[30]. L'homogénéité du dépôt est assurée par rotation de la cathode, la solution est désoxygénée par barbotage d'azote, l'électrolyse est réalisée avec une tension de 3,5 V sous un ampère pendant 35–45 min.

Etant donné les exigences draconiennes en ce qui concerne la stabilité et la reproductibilité des mesures de pH, l'électrode doit être retraitée après 15–20 titrages.

L'hydrogène. L'hydrogène employé pour saturer la solution est décarbonaté par passage sur pastilles de KOH, désoxygéné par passage à chaud sur un catalyseur

BASF et saturé en eau par barbotages dans trois laveurs consécutifs. Il pénètre dans la solution à titrer au travers d'un fritté G3 qui assure une bonne dispersion du gaz. Pour éviter toute rentrée d'oxygène dans la cellule pendant les titrages, on s'arrange pour maintenir une légère surpression d'hydrogène (environ 5 cm d'eau) dans la cellule.

Le potentiel de l'électrode à hydrogène dépend de la pression par le terme $RTF^{-1} \ln (pH_2)^{\frac{1}{2}}$; pH_2 étant la pression d'hydrogène sec, exprimée en atmosphère, en équilibre avec la solution.

$$pH_2 = P - pH_2O + \frac{0{,}4h}{1033{,}6} \tag{1}$$

avec P = pression totale du gaz au-dessus de la solution à titrer, pH_2O = tension de vapeur de l'eau à la température de travail, h = hauteur (cm) de liquide au dessus de l'admission du gaz; $0{,}4h/1033{,}6$ = produit de la pression hydrostatique par le facteur de sursaturation déterminé par Hills et Ives[30]. Tous les termes de la formule (1) sont exprimés en atm.

Dans notre cas, la distance entre le barboteur et la surface de la solution varie entre 3,8 et 5.8 cm entre le début et la fin du titrage; en prenant une valeur moyenne constante de 4,8 cm, on commet une erreur de 1,5 μV ($8 \cdot 10^{-5}$ unité pH) qui peut être négligée.

Le second terme de la formule (1) est constant par thermostatisation de la solution; à 25°C, il vaut 0,031 atm.

Le premier terme peut varier au cours d'un titrage notamment avec les variations de pression atmosphérique. Nous avons construit un système automatique de correction de pression qui ramène directement la tension mesurée à la valeur réduite à une atmosphère ce qui nous place, à tout moment, dans des conditions standard de pression. Ce système est constitué d'un baromètre de Toricelli, la hauteur du mercure étant mesurée par un pont à reluctance variable. Deux branches inductives du pont entourent l'une le tube de Toricelli au niveau supérieur du mercure, l'autre un noyau de cuivre ajustable qui sert de référence.

Electrode de référence

En raison de sa grande stabilité, de sa facilité de préparation et de manipulation et de la possibilité qu'elle offre de travailler, avec ou sans pont de jonction, dans des milieux de force ionique très variable, nous avons choisi comme référence l'électrode Ag/AgCl préparée suivant la méthode thermo-électrolytique décrite par Bates[27].

Nous avons déterminé son potential normal, à 25°C, par rapport à l'électrode à hydrogène dans une cellule sans jonction saline. Pour ce faire, nous mesurons la différence de potentiel (ΔE) entre ces deux électrodes plongées dans une solution de l'acide chlorhydrique 0,01 molale dont on connaît[31] avec précision le coefficient d'activité $\gamma_{HCl} = 0{,}9048$

$$\Delta E = E^{\circ}_{Ag/AgCl} - \frac{RT}{F} \ln a_{Cl^-} - \frac{RT}{F} \ln \frac{a_{H^+}}{(pH_2)^{\frac{1}{2}}} \tag{2}$$

$$= E^{\circ}_{Ag/AgCl} - \frac{RT}{F} \ln m_{Cl^-}\, m_{H^+} - \frac{RT}{F} \ln \gamma_{Cl^-}\, \gamma_{H^+} + \frac{RT}{F} \ln (pH_2)^{\frac{1}{2}} \tag{3}$$

avec $\gamma_{HCl} = (\gamma_{H^+}\, \gamma_{Cl^-})^{\frac{1}{2}}$

La préparation de la solution d'acide chlorhydrique 0,01 molale est très importante puisque, en fin de compte, elle va fixer la précision dans la connaissance de $E^{\circ}_{Ag/AgCl}$ c'est-à-dire finalement du pH. Elle est préparée à partir d'acide pour analyse bidistillé, préalablement dilué jusqu'à une molarité d'environ 0,1 par de l'eau tridistillée sur quartz. La molarité de cette solution-mère est déterminée par gravimétrie de AgCl réalisée en chambre noire pour éviter toute photolyse du précipité; elle est enfin diluée pour obtenir, par pesée, une solution exactement 0,01 molale.

Le dosage gravimétrique a été effectué une dizaine de fois sur cette solution de HCl ainsi que sur une solution étalon réalisée par pesée de KCl sec; on peut estimer à 0,05% l'erreur sur la normalité de la solution-mère.

La dilution suivie par pesée, en tenant compte de la correction de poussée d'Archimède n'entraîne aucune erreur supplémentaire mesurable.

La valeur de $E^{\circ}_{Ag/AgCl}$ que nous avons obtenue dans ces conditions est de 0,22230 V alors que la valeur proposée par Bates est de 0,22234 V. Quatre autres électrodes réalisées simultanément donnent les valeurs suivantes: 0,22228 V, 0.22230 V, 0,22230 V et 0,22236 V.

Signalons pour terminer que l'évolution du potentiel normal de cette électrode en fonction de la température nous fournit, dans la zone de 20 à 30°C un coefficient de température de 0,7 mV K^{-1} environ[27].

La stabilisation de la température à $\pm 0{,}01$°C donne lieu à des variations de potentiel de ± 7 μV ($\pm 0{,}0001$ unité pH) qui sont donc négligeables étant donné la sensibilité du voltmètre.

PERFORMANCES

Rapidité d'obtention du potentiel d'équilibre de l'électrode à hydrogène

Nous avons voulu nous rendre compte du temps nécessaire pour obtenir le potentiel d'équilibre avec une électrode à hydrogène; à cet effet, le potentiel est mesuré à partir du temps zéro pris au moment du début du barbotage d'hydrogène.

TABLEAU I

RAPIDITÉ D'OBTENTION DU POTENTIEL D'ÉQUILIBRE DE L'ÉLECTRODE À HYDROGÈNE

(Conditions expérimentales: voir fig. 1.)

Temps (min)	*ΔpH*	*Temps (min)*	*ΔpH*
0	12,526	4,0	0,101
0,5	10,159	5,0	0,051
1,0	5,426	6,0	0,034
1,5	2,722	7,0	0,017
2,0	0,524	8,0	0,008
2,5	0,237	9,0	0,003
3,0	0,169	12,0	Equilibre

Le Tableau I et la fig. 1 montrent l'évolution du pH en fonction du temps, ΔpH représente la différence entre le pH à l'équilibre et la valeur à l'instant *t*.

La même expérience réalisée sur une solution préalablement saturée en hydrogène demande moins de cinq minutes pour atteindre l'équilibre.

Stabilité à court terme

Nous entendons par là, la stabilité du système de mesure pendant le laps de temps requis par un titrage (15–20 h). A cet effet, nous nous plaçons dans la zone tampon (taux de titrage de 33%) de la courbe de titrage d'une solution 0.01 *M* en acide nitrilotriacétique (NTA) en milieu de force ionique égale à 1 (KCl). Les résultats sont repris dans le Tableau II et représentés sur la Fig. 2.

La stabilité à court terme du système est assez remarquable. En effet, si on représente l'évolution de la f.e.m. mesurée en fonction du temps par l'équation $Y = aX + b$, Y étant la tension et X le temps, et que l'on traite les données par la méthode des moindres carrés, on trouve une pente de $(0{,}0 \pm 0{,}7)$ μV h^{-1}; la valeur de ΔE est égale à $(0{,}38186 \pm 0{,}00004)$ V à 95% de confiance.

TABLEAU II

ÉVOLUTION DE LA F.E.M. MESURÉE EN FONCTION DU TEMPS

(Conditions expérimentales: voir Fig. 2. L'intervalle de temps entre deux mesures est de 15 min; le temps 0 est pris après 30 min d'équilibration.)

Temps (min)	*E(V)*	*Temps (min)*	*E(V)*
0	−0,38183	435	−0,38185
15	−0,38185	450	−0,38185
30	−0,38185	465	−0,38187
45	−0,38187	480 (8 h)	−0,38185
60 (1 h)	−0,38187	495	−0,38185
75	−0,38186	510	−0,38185
90	−0,38187	525	−0,38187
105	−0,38185	540 (9 h)	−0,38187
120 (2 h)	−0,38186	555	−0,38187
135	−0,38186	570	−0,38186
150	−0,38186	585	−0,38186
165	−0,38186	600 (10 h)	−0,38185
180 (3 h)	−0,38185	615	−0,38186
195	−0,38185	630	−0,38185
210	−0,38187	645	−0,38187
225	−0,38187	660 (11 h)	−0,38187
240 (4 h)	−0,38186	675	−0,38186
255	−0,38185	690	−0,38186
270	−0,38185	705	−0,38185
285	−0,38184	720 (12 h)	−0,38185
300 (5 h)	−0,38187	735	−0,38185
315	−0,38187	750	−0,38186
330	−0,38186	765	−0,38185
345	−0,38185	780 (13 h)	−0,38186
360 (6 h)	−0,38185	795	−0,38186
375	−0,38186	810	−0,38187
390	−0,38187	825	−0,38186
405	−0,38186	840 (14 h)	−0,38187
420 (7 h)	−0,38187		

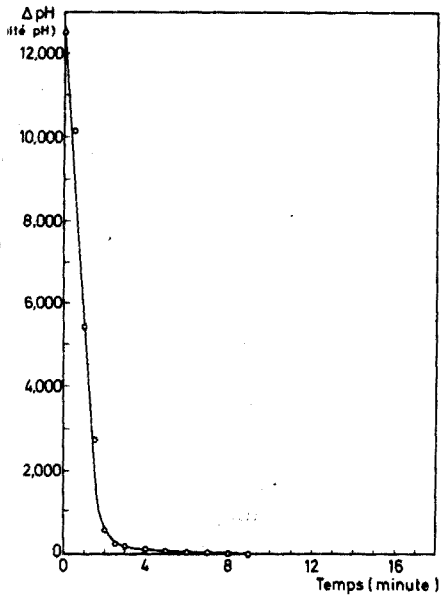

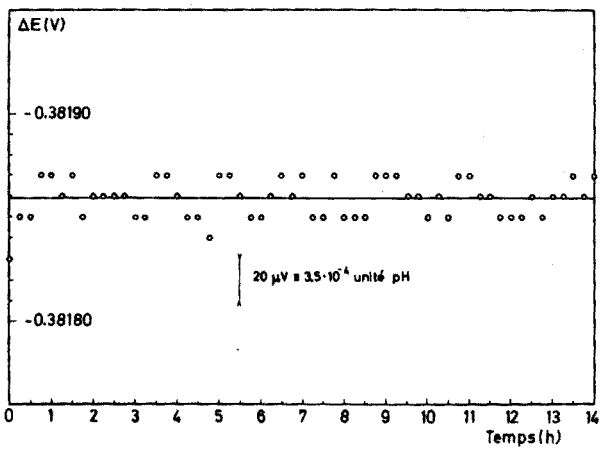

Fig. 1. Rapidité d'obtention du potentiel d'équilibre de l'électrode à hydrogène. Conditions expérimentales: Solution, 100 ml de HCl 0,01 *m*. Cellule sans pont de jonction. $t°$, (25,00±0,01)°C. Débit H_2, 100 ml min^{-1}, pH_2, 760 mm Hg.

Fig. 2. Evolution de la f.e.m. mesurée (ΔE) en fonction du temps. Conditions expérimentales: Solution, 100 ml de KH_2Y (avec H_3Y=NTA). t , (25,00±0,01)°C. Electrode de référence. Ag/AgCl dans KCl *m*, Pont de jonction, KCl *m*. Débit H_2, 100 ml min^{-1}, pH_2, 760 mm Hg.

Le traitement statistique des données permet donc de conclure à l'absence totale de dérive du système pendant le temps d'un titrage. La dispersion des points est très faible: le plus grand écart par rapport à la moyenne est de 20 μV ou $3{,}4 \cdot 10^{-4}$ unité pH.

Stabilité à long terme

L'absence de dérive et la stabilité du système à long terme ont été vérifiées en mesurant le pH de la solution choisie dans l'essai précédent après des intervalles de temps beaucoup plus longs. Les conditions expérimentales sont identiques à celles du test de stabilité à court terme; les résultats sont repris dans le Tableau III.

TABLEAU III

STABILITÉ À LONG TERME

Temps en mois	*ΔE(V)*
0	0,38200
1	0,38191
2	0,38186
3	0,38194
4	0,38190
5	0,38193
6	0,38182

Nous avons appliqué à ces données le même traitement statistique que dans le cas de la stabilité à court terme. On obtient une pente de (-16 ± 30) μV h^{-1} et la valeur de la tension à 95% de confiance est de (0.38196 ± 0.00010) V.

On peut donc conclure que le système n'a subi aucune dérive significative au cours de six mois d'utilisation. La dispersion des points peut paraître plus importante que dans l'essai précédent mais il ne faut pas oublier que dans ce cas ci, on doit tenir compte d'éventuelles erreurs expérimentales dans la préparation des solutions tampons. Quoi qu'il en soit, il est bon de souligner que le plus grand écart par rapport à la moyenne est de 90 μV ce qui représente $1{,}5\cdot10^{-3}$ unité pH.

Exactitude des mesures de pH

Avant d'aborder ce point important, il nous parait utile de mentionner les conditions dans lesquelles s'effectueront les titrages en vue de la détermination des constantes de formation des complexes de lanthanides; le choix de ces conditions sera discuté dans une publication ultérieure: la solution à titrer comprend une solution 10^{-2} *M* en agent complexant seul ou en présence d'un complexe de stoechiométrie 1:1 en concentration 10^{-2} *M*; la force ionique est réglée à 1 au moyen de KCl *M*; le pont de jonction est constitué par KCl *m*; le compartiment de référence comprend KCl *m*; $t^\circ=(25{,}00\pm0{,}01)^\circ$C; pH_2: 760 mm Hg.

Rappelons que le potentiel normal de l'électrode de référence (Ag/AgCl) a été déterminé à 25°C et trouvé égal à 0,22230 V; il est très proche de celui proposé par l'IUPAC (0,22234 V). Le coefficient d'activité des ions Cl^- en milieu KCl *m* à

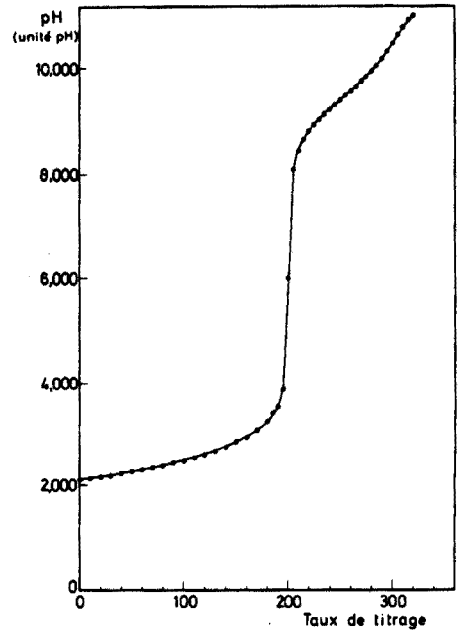

Fig. 3. Courbe de titrage de NTA par KOH. Conditions expérimentales: Solution, 100.08 ml de NTA 0,01 *M*. Force ionique, KCl *M*. Titrant, KOH 0,09851 *M*, $\mu=1$ (KCl). Volume d'une injection, 0,10092 ml. t°,$(25{,}00\pm0{,}01)^\circ$C. pH_2, 760 mm Hg. Débit H_2, 100 ml min^{-1}. Durée du titrage. 15 h.

TABLEAU IV

COMPARAISON DE DEUX COURBES DE TITRAGE

(Conditions expérimentales: voir Fig. 3.)

Taux de titrage	ΔE_1 *(V)*	ΔE_2 *(V)*	*ΔpH*	*Taux de titrage*[a]	ΔE_1 *(V)*	ΔE_2 *(V)*	*ΔpH*
0	0,35911	0,35908	0,0005	155	0,40541	0,40534	0,0012
5	0,35998	0,35997	0,0002	160	0,40874	0,40864	0,0020
10	0,36090	0,36087	0,0005	165	0,41240	0,41237	0,0005
15	0,36182	0,36180	0,0003	170	0,41675	0,41668	0,0012
20	0,36277	0,36276	0,0002	175	0,42177	0,42168	0,0019
25	0,36374	0,36374	0	180	0,42763	0,42763	0
30	0,36456	0,36453	0,0005	185	0,43570	0,43550	0,0034
35	0,36576	0,36574	0,0003	190	0,44659	0,44640	0,0032
40	0,36682	0,36678	0,0007	195	0,46569	0,46577	−0,0014
45	0,36787	0,36785	0,0003	200	0,58898	0,58401	0,084[b]
50	0,36897	0,36896	0,0002	205	0,71409	0,71350	0,01
55	0,37009	0,37007	0,0003	210	0,73410	0,73398	0,0020
60	0,37125	0,37123	0,0003	215	0,74622	0,74660	−0,0064
65	0,37242	0,37242	0	220	0,75542	0,75528	0,0024
70	0,37365	0,37364	0,0002	225	0,76271	0,76271	0
75	0,37491	0,37490	0,0002	230	0,76905	0,76910	−0,0008
80	0,37621	0,37620	0,0002	235	0,77507	0,77499	0,0014
85	0,37756	0,37755	0,0002	240	0,78050	0,78032	0,0031
90	0,37897	0,37894	0,0005	245	0,78562	0,78550	0,0020
95	0,38041	0,38039	0,0003	250	0,79063	0,79049	0,0024
100	0,38193	0,38190	0,0005	255	0,79550	0,79564	−0,0024
105	0,38351	0,38348	0,0005	260	0,80053	0,80039	0,0024
110	0,38515	0,38511	0,0007	265	0,80563	0,80549	0,0024
115	0,38689	0,38685	0,0007	270	0,81090	0,81076	0,0024
120	0,38872	0,38868	0,0007	275	0,81653	0,81633	0,0034
125	0,39062	0,39059	0,0005	280	0,82260	0,82269	−0,0015
130	0,39264	0,39263	0,0002	285	0,82930	0,82920	0,0017
135	0,39484	0,39482	0,0003	290	0,83698	0,83670	0,0030
140	0,39717	0,39715	0,0003	295	0,84551	0,84522	0,0049
145	0,39967	0,39964	0,0005	300	0,85500	0,85510	0,0017
150	0,40243	0,40234	0,0017	305	0,86489	0,86467	0,0037

[a] Un taux de titrage de 300 correspond à la neutralisation des 3 protons de l'acide nitrilotriacétique.

[b] Cette différence correspond, dans cette zone de la courbe de titrage, à une erreur de 0,004 ml sur les ajouts.

25°C est connu avec précision[31], il vaut 0,605; il est donc possible de calculer le potentiel de l'électrode de référence dans ces conditions expérimentales: on trouve $E'_0 = 0{,}23521$ V. Enfin, la similitude des solutions du pont de jonction, du compartiment de référence et de la cellule de titrage permet de négliger les potentiels de jonction.

Le pH peut ainsi être calculé à partir de l'expression suivante comprenant ΔE, la f.e.m. mesurée:

$$\mathrm{pH} = \frac{\Delta E - E'_0}{2{,}303\, RT/F} = \frac{\Delta E - 0{,}23521}{0{,}059157} \text{ à } 25°\mathrm{C}$$

Il était intéressant de vérifier l'exactitude de nos mesures de pH en utilisant l'un ou l'autre standard proposé par l'IUPAC; les seules données, dans un milieu de force ionique KCl *m* sont celles de Valensi[32] ainsi, pour le tampon KH_2PO_4/Na_2HPO_4 en milieu KCl *m*, l'auteur propose comme valeur du pH: 6.545; nous mesurons dans les mêmes conditions 6,544.

Reproductibilité

La reproductibilité des résultats fournis par notre titrateur automatique a été vérifiée en réalisant deux titrages successifs d'une même solution, dans les mêmes conditions expérimentales.

L'allure de la courbe de titrage apparaît sur le Fig. 3. Les valeurs de pH sont comparées, en fonction du taux de titrage, dans le Tableau IV.

En conclusion, les différents tests auxquels nous avons soumis le titrateur automatique, indiquent que du point de vue précision, stabilité, et exactitude, il réalise d'excellentes performances qui sont supérieures à ce que peuvent offrir les appareils commerciaux.

RÉSUMÉ

Les auteurs décrivent la construction et la mise au point d'un titrateur automatique de grande précision utilisant une électrode à hydrogène et une électrode de référence Ag/AgCl ainsi qu'une burette à injections répétées asservie à la mesure de potentiel. Les tests effectués en vue d'évaluer la stabilité, l'exactitude et la reproductibilité des mesures permettent d'affirmer que les mesures du pH sont obtenues en tout point de la courbe de titrage avec une erreur qui ne dépasse pas la millième d'unité de pH. Nous avons l'intention d'utiliser cet appareil pour la détermination des constantes de formation des complexes 1:1 et 1:2 ou des complexes mixtes des lanthanides avec les acides aminoacétiques.

SUMMARY

The development and design of a high-precision automatic titrator is described. This setup includes a hydrogen electrode, an Ag/AgCl reference electrode and a repeated injection burette which is controlled by the potential measurement. Tests performed in order to evaluate the stability, precision and reproducibility of the results lead to the conclusion that pH measurements are obtained at every titration curve point with an error not exceeding 0.001 pH unit. This apparatus will

be used to measure stability constants of 1:1, 1:2 or mixed complexes of lanthanides with aminoacetic acids.

BIBLIOGRAPHIE

1 L. C. Thompson, *Inorg. Chem.*, 1 (1962) 490.
2 G. N. Kupriyanova et L. I. Martynenko, *Russ. J. Inorg. Chem.*, 15 (7) (1970) 1024.
3 W. Noddak et G. Oertel, *Z. Electrochem.*, 61 (1957) 1216.
4 K. V. Astakov, V. B. Verenkin, V. I. Zinin et A. D. Zverkova, *Russ. J. Inorg. Chem.*, 6 (1961) 1057.
5 T. Moeller et R. Ferrus, *Inorg. Chem.*, 1 (1962) 49.
6 P. Zur Nedden, E. Merciny et G. Duyckaerts, *Anal. Chim. Acta*, 64 (1973) 197.
7 Y. P. Galaktionov et K. V. Astakhov, *Russ. J. Inorg. Chem.*, 8 (1963) 460.
8 T. V. Ternovaya et N. A. Kostromina, *Russ. J. Inorg. Chem.*, 16 (*11*) (1971) 1580.
9 T. V. Ternovaya, *Ukr. Khim. Zh.*, 36 (1970) 1203.
10 N. A. Kostromina, K. V. Yatsimirskii, T. V. Ternovaya et N. N. Tananaeva, *Proceedings of 3rd Symp. Coord. Chem.*, Vol. I, Beck, Debrecen, Hungary, 1970.
11 L. C. Thompson et J. A. Loraas, *Inorg. Chem.*, 2 (*1*) (1963) 89.
12 G. Geier, et U. Karlen, *Helv. Chim. Acta*, 54 (*1*) (1971) 135.
13 Y. P. Galaktionov et K. V. Astakov, *Russ. J. Inorg. Chem.*, 8 (1963) 1309; 11 (1966) 1216.
14 N. N. Tananaeva, N. A. Kostromina et L. B. Novikova, *Russ. J. Inorg. Chem.*, 16 (*6*) (1971) 824.
15 N. A. Kostromina et N. N. Tananaeva, *Zh. Teor. Éksperim. Khim.*, 7 (1971) 67.
16 N. N. Tananaeva et N. A. Kostromina, *Russ. J. Inorg. Chem.*, 17 (*9*) (1972) 1243; 16 (*6*) (1971) 824.
17 T. Taketatsu et S. Yoshida, *J. Inorg. Nucl. Chem.*, 35 (1973) 881.
18 E. Merciny et G. Duyckaerts, *J. Chromatogr.*, 35 (1968) 549.
19 F. Schoebrechts, E. Merciny et G. Duyckaerts, *J. Chromatogr.*, 79 (1973) 293.
20 R. H. Betts et O. F. Dahlinger, *Can. J. Chem.*, 37 (1959) 91.
21 J. L. Mackey, J. E. Powell et F. H. Spedding, *J. Amer. Chem. Soc.*, 84 (1962) 2047.
22 F. H. Spedding, S. A. Crejka et C. W. de Koch, *J. Phys. Chem.*, 70 (1966) 2423; F. H. Spedding et M. J. Pikal, *J. Phys. Chem.*, 70 (1966) 2430; F. H. Spedding, M. J. Pikal et B. O. Ayers, *J. Phys. Chem.*, 70 (1966) 2440; F. H. Spedding et K. C. Jones, *J. Phys. Chem.*, 70 (1966) 2450.
23 L. A. K. Staveley, D. R. Marklam et M. R. Jones, *Nature (London)*, 211 (1966) 1172.
24 S. L. Bertha et G. R. Choppin, *Inorg. Chem.*, 8 (1969) 613.
25 G. Anderegg et F. Wenk, *Helv. Chim. Acta*, 54 (1971) 216.
26 F. J. C. Rossotti, *Chemical Applications of Potentiometry*, Van Nostrand, London, 1969.
27 R. G. Bates, *Determination of pH*, Wiley, New York, 1964.
28 D. I. Hitchcock et A. C. Taylor, *J. Amer. Chem. Soc.*, 59 (1937) 1812.
29 G. A. Perley, *Trans. Electrochem. Soc.*, 92 (1947) 485.
30 G. J. Hills et D. J. G. Ives, *J. Chem. Soc., London*, (1951) 305.
31 H. S. Harned et B. B. Owen, *The Physical Chemistry of Electrolytic Solutions*, Reinhold, New York, 1958.
32 G. Valensi, *Pure Appl. Chem.*, 31 (1972) 547.

Analytica Chimica Acta, 78 (1975) 171–181

LINEAR TITRATION PLOTS FOR THE POTENTIOMETRIC DETERMINATION OF MIXTURES OF STRONG AND WEAK ACIDS

C. McCALLUM
Department of Chemistry, The University, Southampton (England)
D. MIDGLEY
Central Electricity Research Laboratories, Kelvin Avenue, Leatherhead, Surrey (England)
(Received 30th December 1974)

The potentiometric titration of a mixture of a strong and a weak acid with a strong base does not necessarily result in a two-step pH–titrant volume curve (Fig. 1); even when it does, the points of inflexion differ from the equivalence points by amounts determined by the dissociation constant of the weak acid and the relative concentrations of strong and weak acids. Ricci[1] has given an approximate treatment for the case of a mixture of a strong acid and a monobasic weak acid.

Johansson[2] has described an approximate solution, based on Gran plots[3], for resolving the components of the mixture, but this approach is limited in use,

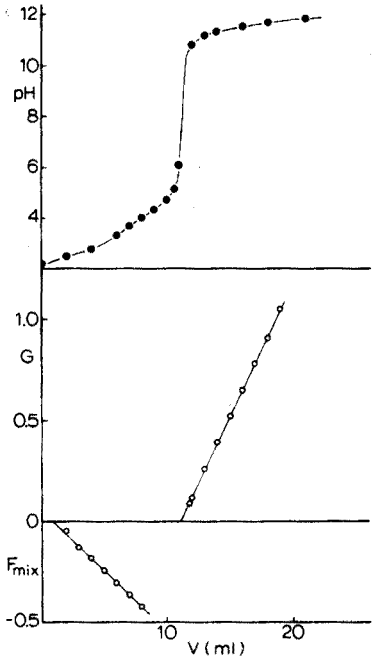

Fig. 1. Titration of 10 ml of 0.05 mol l^{-1} oxalic acid + 1 ml of 0.10 mol l^{-1} nitric acid + 100 ml of water with 0.09906 mol l^{-1} sodium hydroxide, showing pH, Gran and F_{mix} curves.

becoming less satisfactory as the relative fraction of strong acid decreases and the dissociation constant of the weak acid increases. It is possible to apply general error minimization techniques[4–6] to the problem, but these are complex and require considerable calculation.

By rigorous application of the charge- and mass-balance equations, together with the equilibrium constants of the system, linear titration plots have been obtained for titrations involving titrands of varying degrees of complexity[7–9]. In this paper, the same techniques are applied to a mixture of a strong acid and a weak acid, which may have any number of dissociation steps of any strength. The resultant linear titration plot is used, together with a Gran plot, to determine the strong and total acid concentrations of the mixture. When necessary, activity coefficients are calculated iteratively and applied to the function. The linear titration plot is far simpler than the error minimization methods and of more general application than approximate methods. The method has been applied to typical titrations, and its susceptibility to errors caused by the neglect of activity coefficients and by inaccuracies in the pH, in the dissociation constants of the weak acid and in the total acidity, has been examined.

THEORY

For convenience, charges have been dropped from ionic symbols: V is the volume of base added, V_e is the volume of base equivalent to the total acidity and V_s the volume of base equivalent to the strong acid. K_w is the thermodynamic autoprotolysis constant of water and, assuming $f_H = f_{OH} = f_1$, [OH] is given by $K_w/\{H\}f_H$, $\{H\}$ being the experimentally observed hydrogen ion activity. Any other assumption about activity coefficients can be accommodated, and titrations at constant ionic strength treated, by setting all activity coefficients equal to unity.

In order to resolve the mixture into its components by this method, it is necessary to know the total acidity of the solution. This value may be obtained in a separate experiment, by any suitable method, or by continuing the titration into the basic region and using either the S-shaped titration curve or the appropriate Gran[3] function $G = (V_0 + V)[OH]$; the latter method was used in the program described below.

V_0 ml of a solution of a mixture of a strong acid, HX, of concentration c_s mol l^{-1} and a weak acid H_hAY_j of concentration c_w mol l^{-1} are titrated with a strong base BOH of concentration m mol l^{-1}. Y is a univalent ion with the charge sign necessary to maintain electrical neutrality, h is the number of protons removable by titration, a is the negative charge on A, and $j = |h - a|$... The ith association constant of the weak acid is defined as:

$$K_i = \frac{[H_iA]f_i}{\{H\}^i[A]f_a} \tag{1}$$

where f_a and f_i are the activity coefficients of A and its i-th protonated form, respectively.

At any point in the titration, the mass-balance equations are as follows:

total strong acid $\quad T_s = [X] = mV_s/(V_0 + V)$ (2)

total weak acid $T_w = [A]+[HA]+...[H_iA]+[H_kA] = [A](1+\beta)$ (3)

total acid equivalent $T_A = T_s + hT_w = mV_e/(V_0+V)$ (4)

total base $T_B = [B] \quad = mV/(V_0+V)$ (5)

If charge q is assigned to Y, we can also write:

$$q[Y] = -(h-a)T_w \tag{6}$$

The charge-balance equation is:

$$[B]+[H]+q[Y] = [OH]+[X]+a[A]+ (a-1)[HA]+...(a-i)[H_iA]+...(a-k)[H_kA] \tag{7}$$

Substituting for [B], q[Y], [X] and all forms $[H_iA]$ in eqn. (7) gives

$$T_B+[H]-(h-a)T_w = [OH]+T_s+aT_w-[A]\alpha \tag{8}$$

In eqns. (8) and (3) respectively, α and β are defined by

$$\alpha = \sum_{i=1}^{k} iK_i\{H\}^i \frac{f_a}{f_i} \text{ and } \beta = \sum_{i=1}^{k} K_i\{H\}^i \frac{f^a}{f_i}$$

where k is the maximum number of protons that can combine with species A. Substituting for [A] in eqn. (8) followed by rearrangement gives

$$[H]-[OH]+T_B-T_A = -\frac{\alpha}{1+\beta}T_w = -\frac{\alpha}{h(1+\beta)}(T_A-T_s)$$

Thus

$$([H]-[OH])(1+\beta)+(T_B-T_A)\left(1+\beta-\frac{\alpha}{h}\right) = (T_s-T_B)\frac{\alpha}{h}$$

Dividing by α, expressing [H] and [OH] in terms of the experimental quantity $\{H\}$ and substituting for T_A, T_s and T_B gives:

$$\left\{\left(\frac{\{H\}}{f_1}-\frac{K_w}{\{H\}f_1}\right)(1+\beta)+m\frac{(V-V_e)}{V_0+V}\left(1+\beta-\frac{\alpha}{h}\right)\right\}\Big/\alpha = \frac{m}{h}\frac{(V_s-V)}{V_0+V}$$

Hence a function F_{mix} can be derived, and this can be calculated from the equilibrium constants K_w, K_i and the experimental data V_0, V, m, V_e and $\{H\}$. The function is linear when plotted against V, intercepting the V-axis at $V = V_s$.

$$F_{mix} = \left\{(V_0+V)\left(\frac{\{H\}}{f_1}-\frac{K_w}{\{H\}f_i}\right)(1+\beta)+m(V-V_e)\left(1+\beta-\frac{\alpha}{h}\right)\right\}/\alpha = \frac{m}{h}(V_s-V)$$

Thus, once the total acidity is known, the concentration of the strong acid can be calculated and hence the concentration of the weak acid found by difference Figure 1 shows the F_{mix} and Gran plots for a typical titration and for comparison the pH *vs.* V curve.

The effect of an error in the association constant

The accuracy of F_{mix} is clearly affected by the accuracy of the association constants contained in the terms α and β. In the following discussion of the

titration of a mixture of a strong acid and a monobasic weak acid, HA, with association constant K_A, activity coefficients have been neglected for convenience; the F_{mix} function therefore becomes

$$F'_{mix} = (V_0+V)\left([H] - \frac{K_w}{[H]}\right)\left(1 + \frac{1}{K_A[H]}\right) + \frac{m(V-V_e)}{K_A[H]} = m(V_s-V)$$

If ϕ_{mix} is taken as the value of the F_{mix} function calculated with an inaccurate constant $K'_A = rK_A$, then:

$$\phi_{mix} = (V_0+V)\left([H] - \frac{K_w}{[H]}\right)\left(1 + \frac{1}{K'_A[H]}\right) + \frac{m(V-V_e)}{K'_A[H]}$$

If $K_A[H]$ is large, $F'_{mix} \simeq \phi_{mix} \simeq (V_0+V)([H]-K_w/[H])$. This condition is most likely to be met at the beginning of a titration in which the proportion of strong acid is high and the weak acid has a large association constant, as can be seen in Fig. 2.

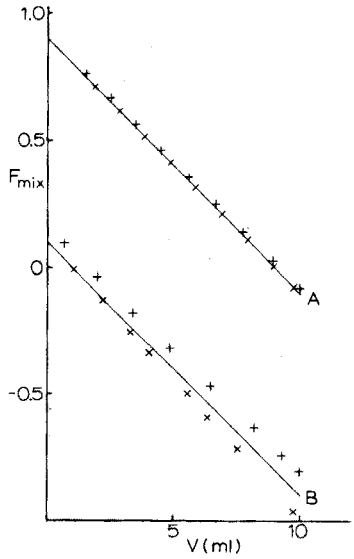

Fig. 2. The effect of errors in the acid association constant for theoretically generated titrations of: (A) 90 ml of 0.01 mol l^{-1} strong acid +10 ml of 0.01 mol l^{-1} weak acid; (B) 10 ml of 0.01 mol l^{-1} strong acid +90 ml of 0.01 mol l^{-1} weak acid with 0.1 mol l^{-1} strong base. ((+)$K = 10^2 + 10\%$, (×)$K = 10^6 - 10\%$, (−) theoretical lines).

In the general case,

$$\phi_{mix} - F'_{mix} = F'_{mix}\left(\frac{K_A}{K'_A} - 1\right) - (V_0+V)\left([H] - \frac{K_w}{[H]}\right)\left(\frac{K_A}{K'_A} - 1\right)$$

$$= \left(\frac{1}{r} - 1\right)\left\{(V_0+V)\left([H] - \frac{K_w}{[H]}\right)\frac{1}{K_A[H]} + \frac{m(V-V_e)}{K_A[H]}\right\}$$

If $[H] \gg K_w/[H]$, this can be simplified to:

$$\phi_{mix} - F'_{mix} = \frac{1-r}{rK_A}\left\{V_0 + V + \frac{m(V-V_e)}{[H]}\right\} \qquad (9)$$

When the strong acid has been neutralized, the following approximation holds[8]: where $[H]=(n-1)/K_A$, $n=(V_c-V_s)/(V-V_s)$.
Substituting for [H] in eqn. (9) gives:

$$\phi_{mix}-F'_{mix} = \frac{1-r}{rK_A}\{V_0+V+mK_A(V_s-V)\} \tag{10}$$

Substituting for F'_{mix}, and rearranging gives:

$$\phi_{mix} = \left\{\frac{1-r}{rK_A}(1-mK_A)-m\right\}V + \left\{\frac{mV_s}{r} + V_0\frac{(1-r)}{rK_A}\right\} \tag{11}$$

It can be seen from eqn. (10) that the difference between the two functions at any point in the titration after V_s is a function not only of the error in K_A but also of its absolute value and of the amount of strong acid in the mixture. Equation (11) shows that the inaccurate function is still a linear function of V, which will intercept the V-axis at

$$V'_s = \left\{\frac{mV_s}{r} + V_0\frac{(1-r)}{rK_A}\right\}\Big/\left\{m - \frac{1-r}{rK_A}(1-mK_A)\right\}$$

Since $V_0c_s=mV_s$,

$$V'_s = V_s\left\{\left(\frac{m}{r}+\frac{m}{c_s}\frac{1-r}{rK_A}\right)\right\}\Big/\left\{m - \frac{1-r}{rK_A}(1-mK_A)\right\} = V_s\left\{K_A+\frac{1-r}{c_s}\right\}\Big/\left\{K_A-\frac{1-r}{m}\right\}$$

If the value of K_A is overestimated ($r>1$), the equivalent volume for the strong acid will be underestimated and *vice versa.*

For the case $r>1$, the ratio V'_s/V_s should not be less than some arbitrary value $1-D$, where D is a small positive discrimination factor, thus:

$$\frac{V'_s}{V_s} \geqslant 1-D \text{ ; } i.e.\ K_A + \frac{1-r}{c_s} \geqslant (1-D)\left(K_A - \frac{1-r}{m}\right)$$

if $K_A>(1-r)/m$, which is the case for almost all titrations

$$i.e.\ r \leqslant 1+DK_Ac_s/\left[1+\frac{(1-D)}{m}c_s\right]$$

Similarly, for the case $r<1$, the condition $V'_s/V \leqslant 1+D$ is fulfilled if

$$r \geqslant 1-DK_Ac_s/\left[1+\frac{(1+D)}{m}c_s\right]$$

From the above it can be seen that greater errors in K_A can be tolerated, the weaker the weak acid and the more concentrated the strong acid, as is apparent from Fig. 2. Allowing for activity coefficients, the limits are:

$$1-\frac{DK_Ac_sf_1^2}{1+(1+D)c_s/m} \leqslant r \leqslant 1+\frac{DK_Ac_sf_1^2}{1+(1-D)c_s/m}$$

The effect of neglecting activity coefficients

If the calculations are simplified by omitting activity coefficients, the plot will give an underestimate of V_s. It can be shown that, for the case of a weak monobasic

acid with association constant K_A, the condition for obtaining an error δV_s no greater than DV_s, where D is a constant, is given by

$$\frac{K_A f^2}{1-f} \geqslant \frac{c_s+m-D}{Dmc_s} \tag{12}$$

where f is the univalent ion activity coefficient at the end-point. Because of the influence of K_A in relationship (12), the conditions are more suitable, the larger the association constant of the weak acid and the more concentrated the strong acid, as shown in Fig. 3 for some typical titrations, although the activity coefficients are more nearly constant when K_A is small.

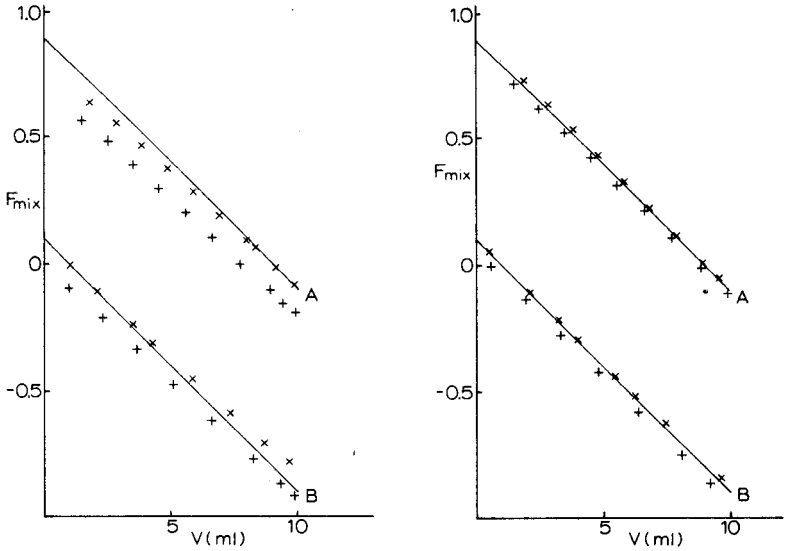

Fig. 3. Titrations (A) and (B) as in Fig. 2, showing the effect of neglecting activity coefficients for $K=10^2$ (+) and $K=10^6$ (×) compared with the true plots (——).

Fig. 4. Titrations (A) and (B) as in Fig. 2, showing the effect of a systematic error in pH. (+) $K=10^2$, Δ pH$=0.01$; (×) $K=10^6$, Δ pH$=-0.01$; (——) Δ pH$=0$.

The effect of neglecting activity coefficients in the Gran's plot part of the procedure has been discussed before[9].

The effect of an error in pH

Accuracy is lost if there is a bias in the measured pH. Figure 4 shows the effect of errors in pH on typical titrations. Since positive and negative errors have almost equal, if opposite, effects, deviations of only one sign are shown. A plot calculated with biased pH values will intercept the V-axis at a point giving an apparent equivalent volume with an error $\delta V_s = DV_s$ related to the bias, ΔpH, by the equation:

$$10^{-\Delta pH} = \frac{-D+(D^2+4(\theta-1-D)\psi)^{\frac{1}{2}}}{2(\theta-1-D)}$$

where $\theta = V_e/V_s$ and $\psi = \theta-1+D^2K_Am/(1+D+m/c_s)$.

Too high a pH gives an underestimate of V_s, and too low a pH an overestimate, the effect being symmetrical. The error is worse when the total cidity is low, the proportion of weak acid is high, and the weak acid has a small association constant. Random errors do not affect the accuracy, although the standard deviation of the fit will be increased.

The effect of an error in the total acidity

If the value of V_e used in the calculation of V_s is in error, there will be a deviation from the theoretical line which increases as the total acidity increases and the value of the association constant of the weak acid decreases, but the dominant effect is the increase with pH, *i.e.*, as the titration approaches the end-point. These trends are shown in Fig. 5 for a moderately strong acid ($K=10^2$), but are scarcely significant for weaker acids. This error is the only one to affect the linearity of the plot but, at the worst, a good extrapolation can be obtained from points in the low pH region. The error in V_s arising from an error δV_e can be calculated from eqn. (13) for a monobasic weak acid.

$$\delta V_s \simeq \frac{-\delta V_e (V_0+V_e)^{\frac{1}{2}}}{K_A^{\frac{1}{2}} V_s m^{\frac{1}{2}} (V_e-V_s)^{\frac{1}{2}}} \tag{13}$$

EXPERIMENTAL

A Pye 290 pH meter and an E.I.L. 33 1160 200 combination glass electrode were used. Deionized water (100 ml) was transferred by pipette to a 250-ml three-necked flask with a capillary inlet at the bottom, followed by the appropriate volumes of 0.1 mol l^{-1} nitric acid (B.D.H. concentrated volumetric solution) and 0.05 mol l^{-1} oxalic acid (B.D.H., Analar). The cell was immersed in a water bath at 25 ± 0.1°C and nitrogen, which had been presaturated with water by passage through a bubbler also in the water bath, was bubbled through the solution in order to mix the reagents and to prevent the absorption of carbon dioxide as the titration proceeded. The solution was titrated with standard sodium hydroxide

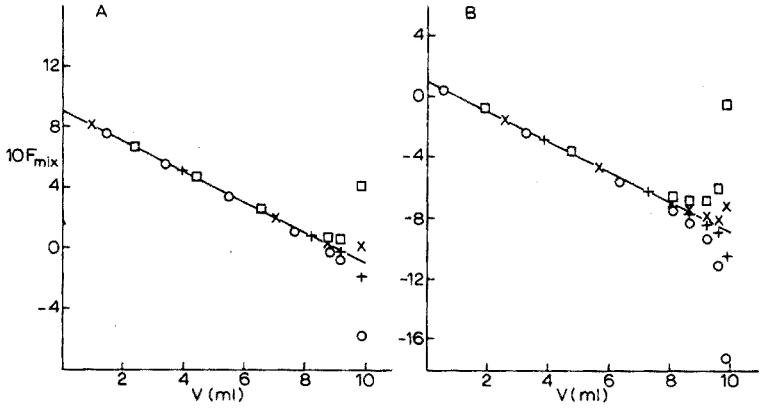

Fig. 5. Titrations (A) and (B) as in Fig. 2 for a weak acid with $K=10^2$, showing the effect of errors in V_e. r=fractional error in V_e: 0 (——), $5\cdot10^{-3}$ (○), $1\cdot10^{-3}$ (×), $-1\cdot10^{-3}$ (+), and $-5\cdot10^{-3}$ (□).

solution which was prepared, stored and dispensed with the usual precautions against the absorption of carbon dioxide. The portions of acids taken were 5 ml + 5 ml, 10 ml + 1 ml and 1 ml + 10 ml.

The calibration of the glass electrode was checked before and after each run by means of three buffer solutions; pH 4.01 and pH 7.00 (Corning buffer salts) and pH 9.24 (E.I.L. buffer powder).

RESULTS AND DISCUSSION

For each run the total acidity was calculated from data after the total equivalence point (pH > 10.7) by Gran's method and the strong acid concentration was calculated by the present method from data before the total equivalence point (pH < 5.5). The results are summarized in Table I.

TABLE I

DETERMINATION OF STRONG ACID IN MIXTURES

Strong acid[a]	*Weak acid*	*NaOH concn.* (*mol* l^{-1})	V_0 (*ml*)	*Source of K*	*Theoretical*		*Found*	
					V_s (*ml*)	V_e (*ml*)	V_s (*ml*)	V_e (*ml*)
HNO_3	Oxalic	0.09906	100	(14)	5.047	10.095	5.191	10.12
HNO_3	Oxalic	0.09906	111	(14)	10.095	11.104	10.178	11.118
HNO_3	Oxalic	0.09906	111	(14)	1.010	11.104	1.102	11.083
HCl[10]	Oxalic	0.1088	115	(15)	9.20	18.854	9.21	—
HCl[10]	Oxalic	0.1088	65	(15)	9.20	18.854	9.13	—
HCl[11]	Malic	0.1244	10	(16)	1.988	6.586	2.015	—
HCl[11]	Tartaric	0.1244	10	(14)	2.175	6.532	2.107	—
HCl[11]	Citric	0.1244	10	(14)	2.119	6.811	2.198	—
—[13]	Tartaric	0.0716	186.3	(13)	0.000	7.57	−0.01	—
—[13]	Tartaric	0.0716	188.5	(13)	0.000	12.45	0.01	—

[a] The reference numbers indicate the source of the data.

The procedure was also tested with data taken from other work. Titrations of mixtures of hydrochloric and oxalic acids with sodium hydroxide at constant ionic strength ($\mu = 0{,}1$; $NaClO_4$) have been performed by Armitage[10] using a glass electrode at 25°C; since data after the total equivalence point were not available, the volume of V_e was taken as given and not calculated from the same run. As the ionic strength was constant, activity coefficients were not calculated, and iteration in the procedure was unnecessary.

Auerbach and Smolczyk[11] titrated mixtures of hydrochloric and malic, tartaric or citric acids with sodium hydroxide at 20°C, using a quinhydrone electrode. Their pH data were recalculated with modern values[12] for the standard potentials of the quinhydrone and calomel electrodes. Because of the errors of the quinhydrone electrode in basic solutions, the value of V_e was not calculated from the data, but was assumed to be known.

Calculations were also done with data[13] from the titration of tartaric acid alone with tetramethylammonium hydroxide solution at 25°C; the value of V_e was assumed to be known. The results are summarized in Table I.

Calculation

Calculation of the function is greatly facilitated by the use of a computer and a FORTRAN program was written; copies of this are available on request. This program will calculate the values of V_e and V_s, if data from both acidic and basic sides of the titration are available, or V_s alone, if a value of V_e is supplied. Both procedures can be carried out with or without acitivity corrections.

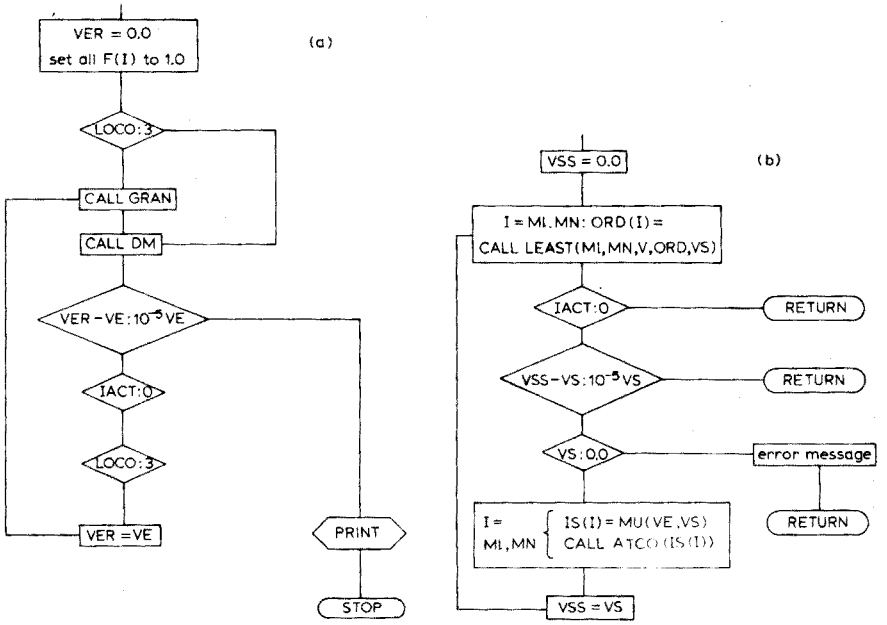

Fig. 6. Flow diagram for (a) the main part of the computer program, and (b) the subroutine DM.

The logic of the program is represented schematically in Fig. 6(a). The subroutines GRAN and DM calculate V_e and V_s, respectively. Their logic is essentially the same; that of DM is shown in Fig. 6(b). The subroutine LEAST is used to obtain the equivalent volumes from the appropriate functions and the volume of titrant by an unweighted least-squares method. The subroutine ACTCO calculates activity coefficients by means of the Davies equation[17] (although any other convention could easily be accommodated) from the ionic strength calculated by function subroutine MU. Iteration proceeds until V_e and V_s are reproduced simultaneously within 0.01%. The necessary input data are the pH and volume of titrant added, the original volume of sample and concentration of titrant and the stability constants of the weak acid.

The GRAN subroutine uses data taken after the total equivalence point. In theory, the DM subroutine uses data from all parts of the titration, but it was found that data after the total equivalence point produced distorted results because of rounding errors, even with theoretically generated data, and it is recommended that only data before the total equivalence point be used.

The standard deviations of V_e and V_s are derived from the fit of the points to the least-squares straight lines and through the usual formulae for combination

of errors. The calculated base concentration, BCALC, is obtained from the slope of the least-squares line in subroutine DM and serves as a check on the calculation. An error in pH or the equilibrium constants will be apparent both by the large standard deviation in V_s and a value of BCALC different from the known concentration of titrant.

Graphical solutions

It can be seen from Figs. 2–5 that even when a systematic error causes curvature in the F_{mix}-function, it still intercepts the V-axis at a good approximation to V_s. This feature can be used if some uncertainty in the parameters of the F_{mix}-function is unavoidable and as a means of detecting systematic errors. The standard derivation in V_s and the value of BCALC indicate when a graphical solution may be appropriate, and to facilitate this, the program prints the co-ordinates of each point in the titration and its deviation from the least-squares line.

Scope of the method

The program is written so as to deal with a general weak acid H_hAY_j, where h is the number of protons removable by titration, Y is a univalent ion and $j=|h-a|$. where a is the anionic charge on A, *e.g.* for citric acid, $h=a=3$; for monosodium citrate, $h=2$, $a=3$; for ammonium chloride $h=1$, $a=0$. The acid may have several dissociation steps, which may overlap, as with tartaric or citric acids, or be moderately strong, *e.g.* oxalic acid. The results in Table I show that the method works well in a variety of circumstances, including titrations at constant and variable ionic strengths and mixtures of varying proportions, including pure weak acid. If the weak acid is sufficiently weak, the method is relatively insensitive to errors in the parameters of the function, but if it is moderately strong more care must be taken. The simple form of the plot makes a visual assessment easy, and systematic errors can be detected by the appearance of curvature; even so a graphical solution should usually be possible.

We wish to thank Dr. G. M. Armitage for making his data available to us.

SUMMARY

A linear titration plot method is derived for determining the components in a mixture of a strong acid and a weak acid, which may be polybasic with overlapping dissociation steps, from pH titration data. A FORTRAN program for the calculations is described and the effects of errors in the parameters of the linear function on the accuracy of the method are discussed.

REFERENCES

1 J. E. Ricci, *Hydrogen Ion Concentration*, Princeton University Press, Princeton, U.S.A., 1952, p. 166.
2 A. Johansson, *Analyst (London)*, 95 (1970) 535.
3 G. Gran, *Analyst (London)*, 77 (1952) 661.
4 N. Purdie, M. B. Tomson and G. K. Cook, *Anal. Chem.*, 44 (1972) 1525.
5 F. Ingman, A. Johansson, S. Johansson and R. Karlsson, *Anal. Chim. Acta*, 64 (1973) 113.
6 T. Meites and L. Meites, *Talanta*, 19 (1972) 1131.

7 F. Ingman and E. Still, *Talanta*, 13 (1966) 1431.
8 D. Midgley and C. McCallum, *Talanta*, 21 (1974) 723.
9 C. McCallum and D. Midgley, *Anal. Chim. Acta*, 65 (1973) 155.
10 G. M. Armitage, unpublished results.
11 F. Auerbach and E. Smolczyk, *Z. Phys. Chem. Stoechiom. Verwandtschaftslehre*, 110 (1924) 65.
12 D. J. G. Ives and J. G. Janz, *Reference Electrodes, Theory and Practice*, Academic Press, New York, 1961.
13 H. S. Dunsmore and D. Midgley, *J. Chem. Soc. Dalton*, (1972) 64.
14 R. S. Robinson and R. A. Stokes, *Electrolyte Solutions*, Butterworths, London, 2nd edn., revised, 1965.
15 G. M. Armitage and H. S. Dunsmore, *J. Inorg. Nucl. Chem.*, 35 (1973) 817.
16 M. Eden and R. G. Bates, *J. Res. Nat. Bur. Stand.*, 62 (1959) 161.
17 C. W. Davies, *J. Chem. Soc., London*, (1938) 2093.

Analytica Chimica Acta, 78 (1975) 183–192

END-POINT CONSTRUCTION AND SYSTEMATIC TITRATION ERROR IN LINEAR TITRATION CURVES—COMPLEXATION REACTIONS

P. M. J. COENEGRACHT

Laboratory for Pharmaceutical and Analytical Chemistry, Antonius Deusinglaan 2, Groningen (The Netherlands)

A. J. M. DUISENBERG

Laboratorium voor Algemene Chemie, Transitorium 3, De Uithof, Utrecht (The Netherlands)

(Received 31st January 1975)

In a recent paper[1] an apparatus for precise, stepwise recording of amperometric titration curves has been described. The recorded curve is automatically corrected for dilution of the sample solution with the titrant. The end-point is found from the intersection of the extrapolated "linear" segments (ranges) on the two branches that form the titration curve. The automatic correction for changes in volume makes it possible to extrapolate such ranges at large distances after the end-point, where otherwise dilution effects would distort the curve. This possibility is particularly important if the titration reaction does not proceed completely; in such cases, the recorded titration curve deviates from the straight lines (Fig. 1, curve A), and the theoretical hyperbolic form is more apparent. The curvature in the vicinity of the end-point prevents accurate extrapolation.

Careful selection of the ranges of the titration parameter, f, which are used for extrapolation, makes it possible to minimize the systematic titration error. Rosenthal *et al.*[2] have reported a few ranges which result in a small systematic titration error, but no procedure for the selection of the ranges has been given. Moreover, the length of the range used for extrapolation before the end-point always equals the length of the range used after the end-point. However, practical reasons, *e.g.*

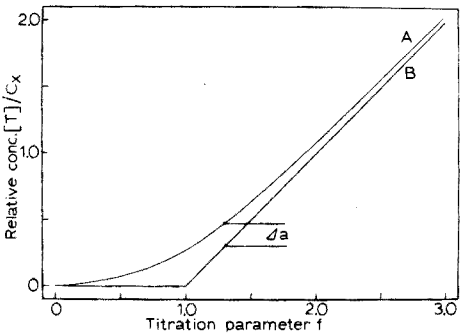

Fig. 1. Calculated normalized titration curves for the reaction X+T⇄XT. (A) Incomplete reaction, $Kc_x = 10$. (B) Complete reaction, $Kc_x = \infty$.

a limited number of data points and partial deformation of the curve, make it desirable to be able to choose various combinations of ranges of different lengths.

In the present paper, a graphical method is proposed for the selection of these ranges, when the end-point is constructed by the intersection of tangents to the titration curve. The selection of the ranges is based on minimizing the systematic titration error. Measurement errors are not considered. First, the systematic titration error is calculated; subsequently, one can select two collections of tangents to ranges before and after the end-point, which result in a given maximum absolute titration error. As the exact selection of ranges requires that the end-point be known, ranges can only be estimated. Although the estimation has been performed with reasonable accuracy[2], it remains difficult to determine the ranges on strongly bent titration curves. If the titration is continued far beyond the end-point ($f > 2$), the second branch of the curve better approximates a straight line and can be extrapolated more easily than the first branch. Thus the construction of an end-point by the intersection of the volume axis with the tangent to the second branch of the titration curve is considered for titration curves of a reversed-L shape (Fig. 1).

THEORETICAL CONSIDERATIONS

The titration reaction of a component X with a titrant T to yield a soluble 1:1 product XT can be represented by

$$X + T \rightleftharpoons XT \tag{1}$$

for which the conditional formation constant is

$$K = [XT]/[X][T] \tag{2}$$

For precipitation reactions eqn. (2) does not apply. Work on this case is in progress and leads to different results. Charges are omitted and concentrations are used instead of activities. Dilution effects can be neglected because of the automatic correction. The analytical concentrations of the component and the titrant are c_x and c_t. The titration parameter, f, is defined by

$$f = c_t/c_x \tag{3}$$

and the following equations are valid

$$[X] + [XT] = c_x \tag{4}$$

$$[T] + [XT] = c_t = fc_x \tag{5}$$

It is assumed that the titration curve is recorded by monitoring the concentration of only one compound involved in the reaction. The relationship between the titration parameter and the concentration of this compound is found by elimination of the other variables from eqns. (2), (4) and (5).

The relationship between f and [T] is represented by

$$f = \frac{[T]}{c_x} + \frac{K[T]}{1 + K[T]} \tag{6}$$

and the titration curve has a reversed-L shape. Analogous expressions can be derived for the relation between f and the concentration of X and XT [3].

Calculation of the systematic titration error

Case A. The end-point is found by the intersection of two tangents to the titration curve, one at a point $[T]_b$, f_b, before the end-point, and another at a point $[T]_a$, f_a, after the end-point. The equation of a tangent to the titration curve at point $[T]_a$, f_a, is

$$[T] = \left(\frac{d[T]}{df}\right)_a (f - f_a) + [T]_a \tag{7}$$

Elimination of [T] from eqn. (7) and the similar equation of the tangent at point $[T]_b$, f_b, results after rearrangement in a general expression for the titration parameter in the point of intersection f_i,

$$f_i = \frac{[T]_a - [T]_b + \left(\frac{d[T]}{df}\right)_b f_b - \left(\frac{d[T]}{df}\right)_a f_a}{\left(\frac{d[T]}{df}\right)_b - \left(\frac{d[T]}{df}\right)_a} \tag{8}$$

The value of f_i can be calculated for given values of Kc_x, f_a and f_b as follows. First, all terms of the right-hand side of eqn. (8) are multiplied by K. When the products are calculated, eqn. (6) can be rewritten as

$$K[T]^2 - (fKc_x - Kc_x - 1)[T] - fc_x = 0 \tag{9}$$

Solving the quadratic equation, one obtains

$$[T] = \{fKc_x - Kc_x - 1 + ((-fKc_x + Kc_x + 1)^2 + 4fKc_x)^{\frac{1}{2}}\}/2K \tag{10}$$

The other root of the quadratic is physically meaningless. $K[T]_a$ and $K[T]_b$ are calculated from eqn. (10) for given values of Kc_x, f_a and f_b. Differentiation of eqn. (6) with respect to [T] and inversion of the resulting expression yields

$$\frac{d[T]}{df} = \frac{c_x(1 + K[T])^2}{Kc_x + (1 + K[T])^2} \tag{11}$$

For given values of Kc_x, f_a and f_b, one calulates $K(d[T]/df)_a$ and $K(d[T]/df)_b$ by substitution of the values of $K[T]_a$ and $K[T]_b$ calculated above in eqn. (11). Subsequently f_i is calculated by means of eqn. 8. At the equivalence point $f_i = 1$ and the systematic titration error E_i is given by

$$E_i = f_i - 1 \tag{12}$$

Freese[4] has shown that the systematic titration error is the same for f–[T], f–[X] and f–[XT] curves.

Case B. The end-point is found by the intersection of the volume axis with the tangent at point $[T]_a$, f_a, when the titration curve is of the reversed-L type. Even for low values of Kc_x, the titration curve approaches a straight line at high values of the titration parameter ($f > 2$). Graphical extrapolation of this almost linear part of the curve is more convenient than extrapolation of any range before the end-point ($0 \leqslant f < 1$). Intersection with the volume axis eliminates the practically difficult extrapolation of a more or less bent part of the titration curve before the end-point.

The relation between the point of intersection, f_s, and the ordinate of the point of contact, $[T]_a$, is found by substitution of $[T]=0$ in eqn. (7). From the resulting expression, f_a and $(d[T]/df)_a$ are eliminated by means of eqns. (6) and (11), and after simplification the titration parameter at the point of intersection, f_s, is given by

$$f_s = \frac{K^2[T]_a^2}{(K[T]_a+1)^2} \tag{13}$$

$$f_s = 1+E_s = 1 - \frac{2K[T]_a+1}{(K[T]_a+1)^2} \tag{13a}$$

For $K[T]_a \gg 1$ the titration error is approximately equal to

$$E_s \approx -\frac{2}{K[T]_a} \tag{14}$$

The titration error may be expressed in terms of Kc_x, f_a and the fractional deviation from complete reaction. The fractional deviation (after the end-point), Δ_a, is defined as the difference between the real and the "ideal" concentration of the titrant, normalized to the analytical concentration, c_x, of the component (see Fig. 1):

$$\Delta_a = \frac{[T]_a-(f_a-1)c_x}{c_x} = [T]_a/c_x-(f_a-1) \tag{15}$$

Combination of eqns. (14) and (15) gives:

$$E_s \approx -2/\{Kc_x(f_a-1+\Delta_a)\} \tag{16}$$

For increasing values of f_a, the systematic titration error decreases, but remains negative. For $f_a=3$, the error is approximately equal to $-1/Kc_x$, which is the systematic titration error when the end-point is constructed[4] by the intersection of the tangents at $f_b=0$ and $f_a=2$.

RESULTS

Case A

The end-point was constructed by the intersection of the tangent to the curve at the points $f_b=0.0$, 0.1, 0.2, 0.3, 0.4 and 0.5 with tangents at points f_a varying from 1.0 to 4.0. Systematic titration errors, E_t, were calculated for $Kc_x=50$, 100, 500 and 1000 with a programmable desk calculator (Compucorp 142E).

The results are presented in Fig. 2. Several combinations of ranges of f_b with ranges of f_a can be selected; these are determined by a given maximum absolute titration error and by the value of Kc_x. The length of the range (interval) before the end-point may be increased by increments of $0.1f$, whereas the interval of f_a may be varied continuously.

An example will illustrate the use of the graphs. If for $Kc_x=100$, ranges are to be found which give a maximum titration error of $\pm 1\%$, then it can be seen from Fig. 2(a), curve B, that the intersection of the tangent at $f_b=0.0$ with the tangent at $f_a=2.0$ results in a titration error of -1%. The intersection of the same tangent at $f_b=0.0$ with a tangent at $f_a=4.0$ gives a titration error of $+0.3\%$.

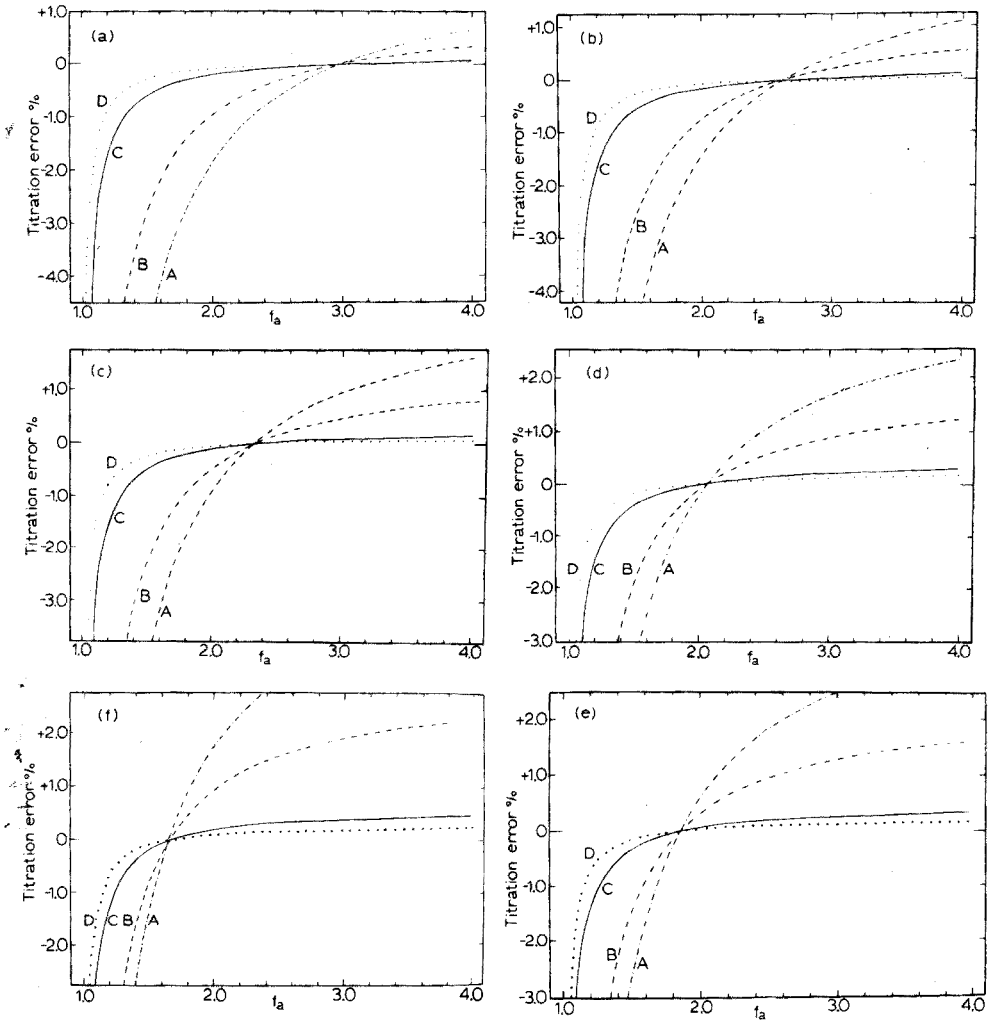

Figs. 2a–f. Plots of the systematic titration error, E_t, as a function of f_a at discrete values of f_b for different values of Kc_x: (A) $Kc_x = 50$; (B) $Kc_x = 100$; (C) $Kc_x = 500$; (D) $Kc_x = 1000$. Fig. 2a, $f_b = 0.0$. Fig. 2b, $f_b = 0.1$. Fig. 2c, $f_b = 0.2$. Fig. 2d, $f_b = 0.3$. Fig. 2e, $f_b = 0.4$. Fig. 2f, $f_b = 0.5$.

TABLE I

RANGES OF f_a WHICH GIVE A MAXIMUM ABSOLUTE TITRATION ERROR OF 1% ON INTERSECTION BY TANGENTS AT DIFFERENT VALUES OF f_b FOR $Kc_x = 100$

Fig. 2	f_b	f_a *range*
a	0.0	2.0–4.0
b	0.1	1.9–4.0
c	0.2	1.8–4.0
d	0.3	1.7–3.4
e	0.4	1.6–2.6
f	0.5	1.5–2.0

It is obvious that the intersection of the tangent at $f_b = 0.0$ with any tangent at f_a between 2.0 and 4.0 gives an absolute titration error equal to or smaller than 1%. This procedure can be repeated for the tangents at $f_b = 0.1$, 0.2, 0.3, 0.4 and 0.5 (Fig. 2(b–f)). The results are given in Table I, and have been rounded off to the first number after the decimal point.

Ranges of f_b are chosen from the data from Table I and combined with ranges of f_a. Each value of f_b determines a range of f_a. When a range of f_b has been chosen, then both the lower and the upper limiting value of this f_b range defines a range of f_a. The overlapping part of the two f_a ranges forms the useful range of f_a, which must be combined with the chosen range of f_b. A few examples are given: 0.0–0.2 with 2.0–4.0; 0.0–0.3 with 2.0–3.4; 0.1–0.4 with 1.9–2.6; or 0.2–0.4 with 1.8–2.6. For the range 0.0–0.5 no suitable range of f_a can be found. Each range is limited by two tangents. The intersection of the tangent at the beginning of the range of f_b with the tangent at the beginning of the range of f_a gives the maximum negative titration error, -1%. Likewise, the intersection of the tangents at the end of each range gives the maximum positive titration error, $+1\%$.

In the same manner, the titration error can be represented, when the end-point is constructed by the intersection of the tangent at discrete values of f_a with tangents at f_b values varying from 0.0–1.0. This is shown in Fig. 3(a–d) for $f_a = 1.5$, 2.0, 2.5 and 3.0. Although it is possible to cover the whole titration curve by extension of Fig. 2(a–f) for the remaining values of f_b, Fig. 3(a–d) is given in order to show clearly the variation of the titration error with f_b for a constant value of f_a. The part of the titration curve that is the most important for the construction of the end-point is covered sufficiently with Figs. 2 and 3.

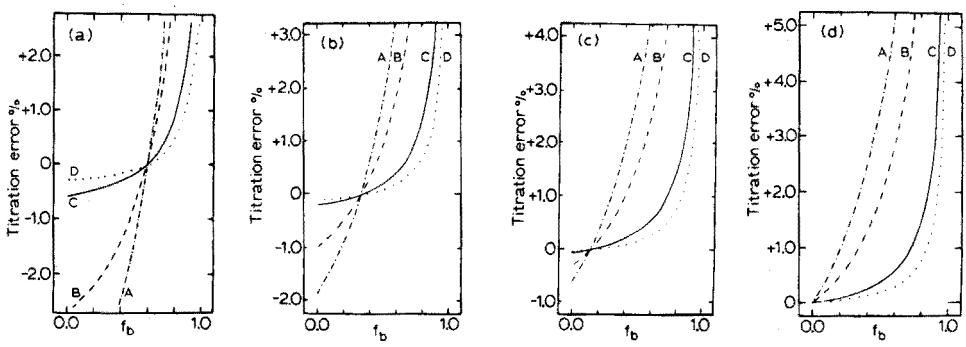

Figs. 3a–d. Plots of the systematic titration error, E_i, as a function of f_b at discrete values of f_a for different values of Kc_x. (A) $Kc_x = 50$; (B) $Kc_x = 100$; (C) $Kc_x = 500$; (D) $Kc_x = 1000$. Fig. 3a, $f_a = 1.5$. Fig. 3b, $f_a = 2.0$. Fig. 3c, $f_a = 2.5$. Fig. 3d, $f_a = 3.0$.

It is obvious from Fig. 3(d) that the combination of any range of f_b with a range of f_a starting at 3.0 always results in a positive titration error. Figure 4 was constructed from Figs. 2 and 3 and some additional calculations. This nomogram shows the $\pm 1\%$ error limits for $Kc_x = 50$, 100, 500 and 1000. It permits a selection of combinations of ranges that give a maximum absolute titration error of 1%. First, a range of f_b can be selected by departing from the negative error limit for a given value of Kc_x at the lower limiting value of the desired f_b range in the vertical

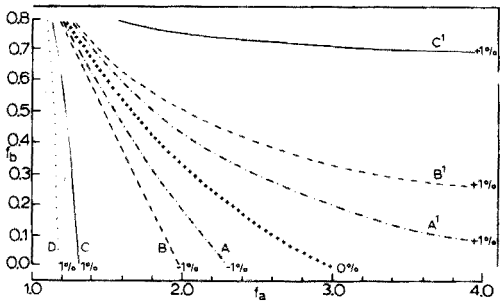

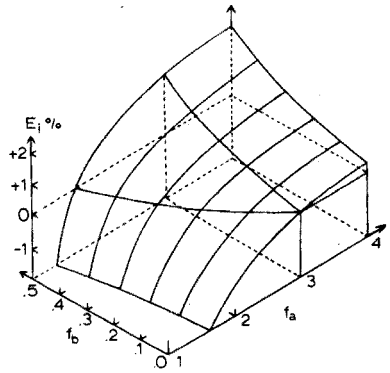

Fig. 4. Nomogram giving $\pm 1\%$ limits of the systematic titration error, E_i, as a function of f_b and f_a for different values of Kc_x. (A, A') $Kc_x = 50$; (B, B') $Kc_x = 100$; (C, C') $Kc_x = 500$; (D) $Kc_x = 1000$. D' lies outside the figure. The crossed curve is the zero error limit for all values of Kc_x.

Fig. 5. Model showing interrelationships between the systematic titration error, E_i, and f_b and f_a.

direction until the desired upper limiting value of this range is reached. From this point, which also indicates the lower limiting value of the f_a range, one goes in horizontal direction until the positive error limit for the same value of Kc_x is reached. This point indicates the upper limiting value of the range of f_a. The central crossed curve in Fig. 4 indicates the pair of tangents at f_b and f_a, which intersect in $f = 1$ and give zero titration error; this curve applies for every investigated value of Kc_x.

The titration error as a function of both points of contact f_b and f_a is depicted as the curved surface of Fig. 5 for $Kc_x = 100$. The curves B in Fig. 2(a–f) and in Fig. 3(a–d) are the secants of the error surface with planes perpendicular to the f_b- and the f_a-axis respectively. In Fig. 4, curve B, B' and the central crossed curve are secants of the error surface with planes perpendicular to the E_i-axis for $E_i = -1\%$, $+1\%$ and 0%.

The ranges found from the Figs. are based on the intersection of tangents, whereas the end-point is actually constructed by the intersection of linearly extrapolated ranges of the titration curve. A computer program was written in order to obtain an estimate of the systematic titration error that results from the extrapolation method compared with the error from the tangent method. The program calculates a number of NP points of the normalized titration curve, *i.e.* $[T]/c_x$ is calculated for f values between 0.0 and 4.0 for $Kc_x = 50$, 100, 500 and 1000 by means of eqn. (10), with NP = 40, 120, 400. Subsequently, two ranges are chosen on the titration curve, one beginning at $f_b = 0.0$ and another at $f_a = 1.0$. Both ranges have equal lengths of $0.1f$, $0.2f$ or $0.3f$; $\bar{f}_b$ and $\bar{f}_a$ are the respective central values of the ranges: $\bar{f}_b$ and $\bar{f}_a$ are moved along the titration curve in steps equal to half the interval ($0.05f$, $0.1f$ or $0.15f$). The best lines through the points belonging to the ranges are calculated by a least-squares method and the systematic titration error which results from the intersection of the $\bar{f}_b$ lines with the $\bar{f}_a$ lines is tabulated. These data show that the number of points has almost no influence on the systematic titration error, provided that at least three points per interval are used for the calculation of the

line. This result is not too surprising because no measurement errors and only small intervals are considered.

The ranges found by extrapolation are longer than the ranges found by the tangent method in the analogous case. For intervals of $0.1f$ and $0.2f$, graphs can be constructed which are almost identical with the curves of Figs. 2–4, when f_b is replaced by $\bar{f}_b$, and f_a by $\bar{f}_a$. Graphical comparison of the data for the interval of $0.3f$ with the Figs. is not possible for all cases, but no important differences are found, and the ranges are longer than the ranges found by the tangent method. It can be concluded that the tangent method provides a cautious estimation of the desired ranges and has an inherent safety margin against a poor estimate of the end-point.

Case B

The end-point was constructed by intersection of the volume axis with tangents at f_a values varying from 1.0 to 4.0 for a reversed-L shaped titration curve. Systematic titration errors, E_s, were calculated for $Kc_x = 50$, 100, 500 and 1000. The results are presented in Fig. 6. The last term of eqn. (13(a)) was used for the calculation. The dashed line in Fig. 6 was calculated from eqn. (14). It can be seen from Fig. 6 that the titration error at $f_a = 2.0$ is twice the titration error at $f_a = 3.0$. The titration error at $f_a = 3.0$ is indeed equal to $-1/Kc_x$ and it can be concluded that this construction of the end-point, which is simple to perform, results in an error no larger than the error of the conventional method, provided that the titration is continued to higher values of the titration parameter.

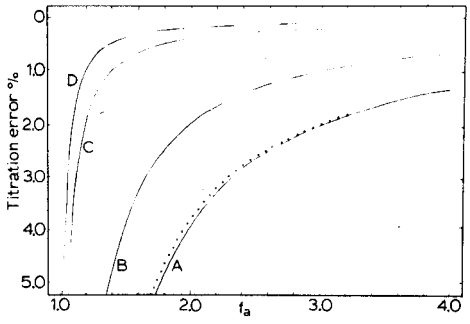

Fig. 6. Plots of the systematic titration error, E_s, as a function of f_a for different values of Kc_x. (A) $Kc_x = 50$; (B) $Kc_x = 100$; (C) $Kc_x = 500$; (D) $Kc_x = 1000$.

DISCUSSION

The exact selection of ranges yielding a given titration error for a given value of Kc_x requires that the conditional formation constant and the stoichiometric end-point be known. Conditional formation constants can often be found or calculated from published data[5,6], and the end-point can be estimated from the titration curve. If the conditional formation constant is unknown, one can find couples of ranges which result in small titration errors for Kc_x values of 50 (or more) from Figs. 2–4. For the selection, it is useful to have a rule of thumb, which can be

found from Figs. 2 and 3: the titration error is approximately inversely proportional to Kc_x for titration errors smaller than about 5%. Curves B and B′ in Fig. 4 can be used as the $\pm 2\%$ error limits for $Kc_x = 50$. Now two combinations of ranges, 0.0–0.2 with 2.3–3.0, or 0.0–0.4 with 2.0–2.6, can be found from the curves A, A′ and B, B′ of Fig. 4, which result in a titration error of $\pm 1\%$ and of $\pm 2\%$, resepctively, for $Kc_x = 50$. The useful ranges of f_b usually start at $f_b = 0.0$. If this is the case, and if the f_b range must be smaller than about $0.4f$ because of strong curvature of the titration curve, then the f_a range must begin at high values of the titration parameter, usually at values greater than about $f_a = 2.0$. A large excess of titrant must be added. The smaller the range of f_b, the higher the values of f_a which must be chosen. If the f_a range is selected at too high values of the titration parameter, then a positive titration error is introduced. The negative titration error made by selecting the f_a range at too low values of the titration parameter is usually larger, because the negative error varies more with f_a than the positive error. From the examples given above, it is clear that with Figs. 2–4, various couples of ranges can be chosen for a given titration error and for a given value of Kc_x. The ranges may have different intervals before and after the end-point and the f_b range need not begin at $f_b = 0.0$. This may be advantageous if there are experimental difficulties that cause the first measurements of the titration curve to deviate. The effort of carefully selecting ranges will be worthwhile if one wishes fully to exploit the advantages of linear methods in the titration of very dilute solutions. Then the linear segments of the titration curve are short and difficult to extrapolate.

Careful selection of ranges will not only give more accurate results, but will also help to improve precision and to shorten the time necessary for duplicate titrations. Ranges can be estimated from the first titration, which must be plotted entirely; for subsequent titrations, measurements are made only within the estimated ranges. Precision is improved by taking sufficient, *i.e.* 6–8, data points per range[7,8]. Time is gained because no measurements are done outside the ranges. Usually fewer measurements than the number needed to plot the complete titration curve will suffice. Moreover, the time per measurement can be shorter, because no measurements are made in the vicinity of the end-point, where the equilibrium is established slowly.

If the titration curve has a reversed-L shape the end-point can be easily constructed by taking 6–8 measurements starting from $f_a = 3.0$ and by intersecting the least-squares line of the points with the volume axis. It is important that only the titrant contributes to the measured quantity. For example, in amperometric titrations the residual current must be neglible, otherwise the intersection of the least-squares line with the volume axis will introduce a larger negative error. If the residual current is constant, the least-squares line must be intersected by the residual current line.

SUMMARY

The systematic titration error which is introduced by the intersection of tangents to hyperbolic titration curves is discussed. The effects of the apparent (conditional) formation constant, of the concentration of the unknown component and of the ranges used for the end-point construction are considered. A graphical

method is presented for the selection of pairs of ranges which result in small systematic titration errors. The method permits the selection of pairs of ranges with equal or unequal intervals before and after the end-point. For titration curves with a reversed-L shape, the error is calculated when the end-point is constructed by the intersection of the tangent to the second branch of the curve with the volume axis. The systematic titration error is equal to $-1/Kc_x$ when the tangent to the curve is taken at $f_a = 3.0$.

REFERENCES

1 P. M. J. Coenegracht, *Anal. Chem.*, 45 (1973) 1675.
2 D. Rosenthal, G. L. Jones Jr. and R. Megargle, *Anal. Chim. Acta*, 53 (1971) 141.
3 G. den Boef, *Grondslagen van de analyse in waterige oplossingen*, Agon Elsevier, Amsterdam, 1968, p. 62.
4 F. Freese, Ph.D. Thesis, Amsterdam, 1971.
5 L. G. Sillen and E. Martell, *Stability Constants of Metal Ion Complexes*, The Chemical Society, London, 1964.
6 A. Ringbom, *Complexation in analytical chemistry*, Interscience, New York, 1963.
7 C. Liteanu and D. Cörmös, *Rev. Roum. Chim.*, 10 (1965) 361.
8 J. Vrestal and S. Kotrly, *Talanta*, 17 (1970) 151.

Analytica Chimica Acta, 78 (1975) 193–200

THE USE OF GEL FILTRATION IN THE STUDY OF METAL BINDING BY HUMIC ACIDS AND RELATED COMPOUNDS

R. F. C. MANTOURA and J. P. RILEY

Department of Oceanography, University of Liverpool, P.O. Box 147, Liverpool L 69 3 BX (England)

(Received 6th February 1975)

There is a growing realization of the important part that humic acids and related compounds play as metal binding agents, not only in soils[1], but also in natural waters[2–6]. However, little quantitative information is available about the nature and stability of the complexes formed[6]. Most of the data have been obtained for soil humic and fulvic acids by potentiometric, continuous variation or ion-exchange methods[1,7], Inherent drawbacks of such methods are that measurements of stability constants must be made (i) by assuming a knowledge of the metal binding stoichiometry; (ii) within restricted pH values (1.5–4.0), and (iii) at unrealistically high metal concentration, with the resulting risk of precipitation of the complex. Furthermore, since the pK_a values of humic acids are not clearly defined, it is not possible to extrapolate these stability constants accurately to those applicable under the pH conditions prevailing in most natural waters. Thus, in computer simulation of trace metal speciation, aquatic chemists have been forced to base their models on synthetic chelating agents such as quinoline-2-carboxylic acid[8] and nitrilotriacetic acid[9].

An alternative approach is to use a modified gel filtration technique; this was first suggested by Hummel and Dreyer[10] and has been subsequently employed for estimation of the stability constants of reversible metal complexes of biochemical macromolecules including copper–deoxyribonucleic acid[11], manganese–nucleotides[12], and zinc–plasma[13]. The method, which is a form of zonal analysis, is a dynamic equilibration technique based on the fact that complexes formed between metals and the macromolecules are excluded to a greater or lesser extent from the gel whereas the free metal ions completely permeate the gel, thus permitting a separation of the two.

A Sephadex G-15 column is equilibrated with a flowing buffered solution containing a known concentration of the metal ion of interest. A similar solution which has been equilibrated with a known amount of the complexing agent is injected into the flow system. As the organic complex traverses the column, it continuously binds further metal until it comes to equilibrium with the free metal ion concentration in the solution. The resulting metal deficiency travels more slowly than the band of the metal complex. Monitoring of the metal content of the effluent from the column shows first a peak at the void volume, the area of which corresponds to the amount of bound metal (Fig. 1). This is followed by a trough of the same area at the salt volume, corresponding to the resultant metal deficiency. In this way it is possible to determine the concentration of complexed

metal at equilibrium with a known concentration of free metal ion, and thence the overall stability constant. It should be noted that almost all workers have disregarded the fact that the pH buffers used do, in fact, themselves form complexes with metals, thus reducing the free metal concentration in the system[11,12]. Low ($< 10^{-5}$ *M*) concentrations of free metal ions in the solution are liable to be unstable and are difficult to determine accurately. It was thought that the technique could be considerably improved by the use of a metal buffer system, to obtain stable known concentrations of free metal ions. This paper describes the use of one such buffer system, employing tris-(hydroxymethyl)-amino methane (TRIS), which for some metals enables work to be carried out at free metal ion concentrations down to 10^{-8} *M*, and which also serves as a hydrogen ion buffer. Thus, it is possible to simulate the pH and pM conditions encountered in natural waters.

EXPERIMENTAL

Reagents

TRIS buffer. Dissolve 0.58 g of sodium chloride in 800 ml of redistilled water, add 1.21 g of TRIS and titrate to pH 8.0 with 0.5 *M* hydrochloric acid prepared from redistilled constant-boiling hydrochloric acid. Add a sufficient volume of a standard solution of the chloride of the metal under investigation to give the required concentration of free metal ion. Dilute to 1 l with redistilled water. The resultant solution is 0.01 *M* with respect to both NaCl and TRIS.

Sephadex G-15. Before use treat the Sephadex gel with a large excess of degassed TRIS buffer and allow it to swell overnight. Excess of buffer along with entrained "fines" should be decanted before the column is packed.

Humic acids

Samples of humic and fulvic acids were obtained from garden peat by the method described previously[14]. Fresh-water fulvic acid was isolated from 50 l of filtered (Whatman GF/F) water from Lake Celyn, North Wales, by adsorption at pH 2.2 onto Amberlite XAD-2 resin and elution with 1:1 methanol–2 *M* ammonium hydroxide mixture[14]. The eluate was evaporated to dryness at 35°C in a rotary evaporator. The residue (0.591 g) was dissolved in 2 l of silica-distilled water and passed through a column of the ammonium form of Chelex-100 in order to render it free from trace metals. The ammonium salt of the fulvic acid was recovered by rotary evaporation of the column effluent; its weight average molecular weight was found to be 5000 ± 350 by gel filtration.

Apparatus

The apparatus used is shown diagrammatically in Fig. 2. The heart of the system is the column (A) of 95–105 ml of swollen Sephadex gel which is contained in a 24-cm length of 2.5-cm bore chemical pipeline. Fine nylon meshes mounted on PTFE pistons retain the gel in the column, liquid-tight sealing being achieved by the use of silicone piston rings. In use, the upper piston is pressed firmly down on the top of the settled gel bed in such a way as to exclude air and to leave no dead volume at the top of the column. TRIS buffer is introduced into the top of the column from the polyethylene reservoir (B) via a 3-way stopcock (C) and capillary

tubing. The remaining arm of the stopcock is connected to a glass reservoir (D) which serves to contain the buffered solution of the humic acid. A Watson–Marlow peristaltic pump (E) is used to induce an effluent flow rate of 30 ml h^{-1} from the column to a recording u.v.–visible spectrophotometer (F) and thence to a fraction collector (G). The absorbance is recorded with a 2-channel variable-speed recorder (J).

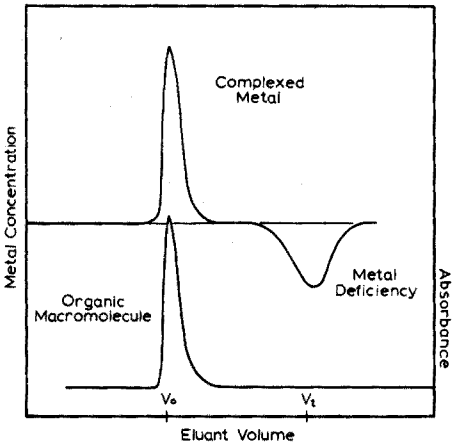

Fig. 1. Theoretical gel filtration chromatogram for the interaction of organic macromolecules with metal ions.

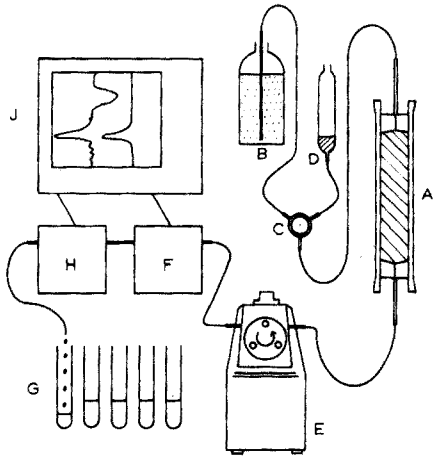

Fig. 2. Diagrammatic representation of the gel filtration apparatus for the determination of stability constants. (A) Gel column, (B) pH-pM buffer reservoir, (C) 3-way stopcock, (D) sample reservoir, (E) peristaltic pump, (F) u.v.-visible spectrophotometer, (G) fraction collector, (H) γ-scintillation counter, (J) 2-channel recorder.

Procedure

Weigh out 5–15 mg of the humic acid sample into a 5-ml calibrated flask, dissolve it in TRIS buffer containing the required concentration of free metal ion and dilute to volume with the same reagent. Allow to equilibrate overnight at room temperature. Place 1 ml of the equilibrated solution into reservoir D, and inject it into the gel column which has been previously equilibrated by passage of 250–300 ml of the metal–TRIS buffer. Rinse the reservoir with 2 ml of this buffer and allow the washings to flow through the column. Turn the stopcock C so as to connect the column to the main reservoir B containing 500 ml of the metal–buffer solution. Monitor the absorbance of the effluent from the column at a wavelength appropriate to the concentration of humic acid expected in the effluent (usually 250–420 nm).

Using a fraction collector with an automatic system shut-down facility, collect 100 fractions of 1.30 ml. Analyze these for the appropriate metal ion by atomic absorption spectrometry, using calibration graphs prepared with standard metal ion solutions made up in the same concentration of TRIS buffer as that used in the column. Alternatively, if a suitable γ-emitting radio-isotope of the metal under investigation is available, the assay of the metal can be carried out by passing the

column effluent through a glass helix mounted within the well crystal of a scintillation counter connected to a recording ratemeter (see (H) in Fig. 2).

Calculation of stability constants

Plot the concentrations of trace metals found in the various fractions as a function of elution volume, as shown in Fig. 3. With a calibrated planimeter, measure the bound metal and the metal deficiency corresponding to the peak and trough, respectively. These should be practically identical; their average is taken to be the number of moles (M_b) of metal bound by the number of moles of humic acid (M_{HA}) taken. Repeat the experiment using a range of concentrations of free metal (corresponding typically to a total metal concentration of $3 \cdot 10^{-6}$–$1.5 \cdot 10^{-3}$ M). Calculate $\bar{\nu} = M_b/M_{HA}$.

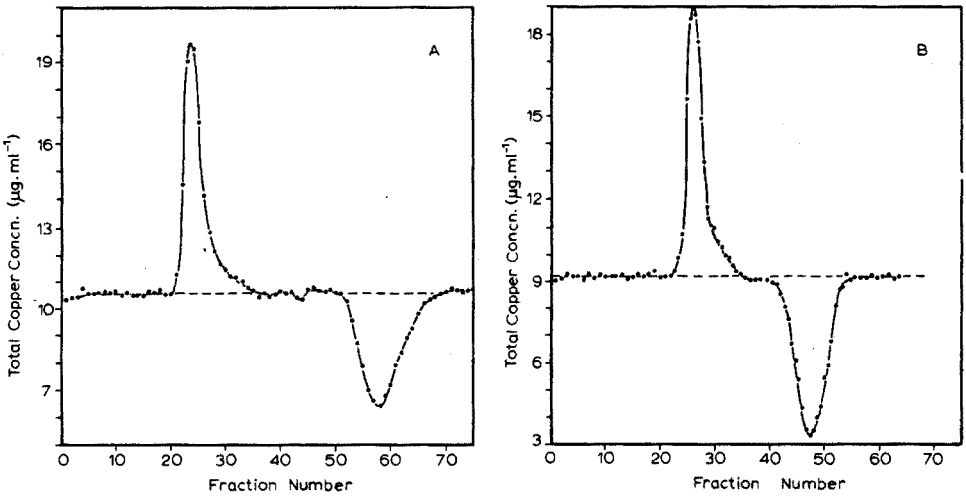

Fig. 3. Gel filtration chromatograms for the interaction of *ca.* 10 μg ml^{-1} copper (at pH 8.0 and $\mu = 0.02$) with (A) 2.73 mg of lake water fulvic acid and (B) 9.37 mg of peat fulvic acid. Total copper was determined by atomic absorption spectrometry. Volumes of fractions were 1.95 ml.

The calculation of the stability constant of the metal–humic acid complex is carried out in three stages.

(i) Using the Henderson–Hasselbach equation[15], calculate the concentration of TRIS which is in the unprotonated state and thus free to complex with the metal.

$$\mathrm{pH} = \mathrm{p}K_a + \log \frac{[T_f]}{[T_t] - [T_f]} \tag{1}$$

where pK_a is the negative logarithm of the acid dissociation constant of TRIS[16] (8.06 at 20°C and $\mu = 0.01$); $[T_t]$ is the total concentration of TRIS in the buffer (0.01 M); and $[T_f]$ is the concentration of unprotonated TRIS (which equals 0.00454 M at 20°C and pH 8.00).

(ii) Calculate the concentration of the free metal ion $[M_f]$ in the TRIS buffer medium using the expression

$$[M_f] = \frac{[M_t]}{1 + \Sigma \beta_n [T_f]^n} \tag{2}$$

where $[M_t]$ is the total concentration of the metal in the TRIS buffer medium, and $\beta_1, \beta_2, \ldots, \beta_n$ are the successive stability constants of TRIS–metal complex. Values of these constants for a number of metal–TRIS interactions have been published by Hanlon *et al.*[17].

It should be noted that eqn. (2) is valid only if $[T_f] \gg [M_t]$. Thus, in the presence of 10 m*M* TRIS at pH 8.0, the total metal concentration must not exceed 0.1 m*M*, corresponding to a minimum $[T_f]:[M_t]$ ratio of 45:1.

(iii) Although it is possible to calculate the overall association constant (K_0) of the metal–humic acid complex from a single run, by the use of eqn. (3)[18]:

$$K_0 = \frac{M_b}{[M_f] \cdot (M_{HA} - M_b)} \tag{3}$$

much more information on the nature of the binding can be obtained by carrying out chromatographic runs at a variety of metal concentrations. These results can then be treated by the method of Scatchard[19] in which it is assumed that

$$\frac{\bar{\nu}}{[M_f]} = K_i (n_i - \bar{\nu}) \tag{4}$$

where $\bar{\nu} = M_b/M_{HA}$, K_i is the stability constant of the metal–humic acid complex; and n_i is the number of metal binding sites per molecule of humic acid. The subscript $i = 1, 2 \ldots$ denotes the type of metal binding site on the humic acid molecules. Using the values of $\bar{\nu}$ obtained from a series of runs carried out over a range of free metal concentrations, plot $\bar{\nu}/[M_f]$ against $\bar{\nu}$ (Fig. 4). It is clear from the Scatchard equation that the slope of the line is equal to $-K_i$ and that the intercept on the $\bar{\nu}$ axis corresponds with n_i.

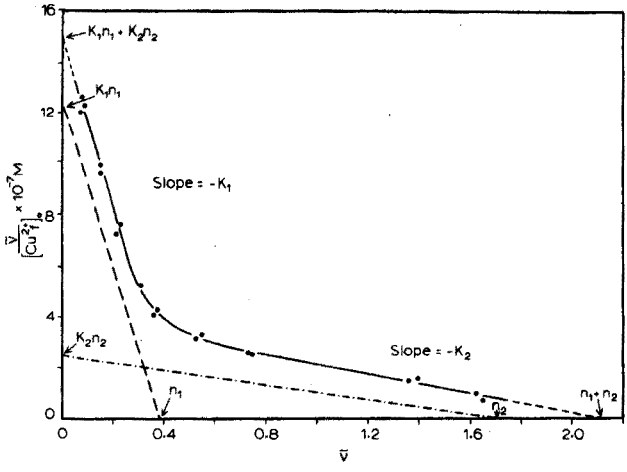

Fig. 4. Scatchard plot for the binding of copper(II) by peat fulvic acid at pH 8.0 and $\mu = 0.02$. The linear components of the curve are the resolved contributions from the "strong" sites (----) and the "weak" sites (-·-·).

RESULTS AND DISCUSSION

The use of the proposed method can be conveniently illustrated by reference to the complexation of copper by fulvic acids derived from lake water and peat. The application of the gel filtration technique to these systems in the presence of *ca.* 10 μg of total copper per ml is illustrated diagrammatically in Fig. 3. In both instances the amounts of complexed copper found from the areas of the peak corresponded to within 1.5% of those computed from the areas of their respective troughs. The reproducibility of the method was assessed by carrying out five identical runs on peat fulvic acid at pH 8.0. These showed an average K_0 value of $4.41 \cdot 10^7$ with a relative standard deviation of 5.8%. Data obtained when the above experiments were repeated with peat fulvic acid for a range of copper concentrations (corresponding to $[M_f] = 7.5 \cdot 10^{-10}$–$3.6 \cdot 10^{-7}$ M) were incorporated into a Scatchard plot (Fig. 4). The resultant curve may be resolved into two linear portions; these are obviously the result of the presence of two different types of binding sites in the fulvic acid polymer. Analysis of the linear components, as indicated by the two dotted lines in the Fig., showed the presence of an average per fulvic acid molecule of 0.39 sites of the more strongly binding ligand (log $K_1 = 8.51$). It also showed the existence of

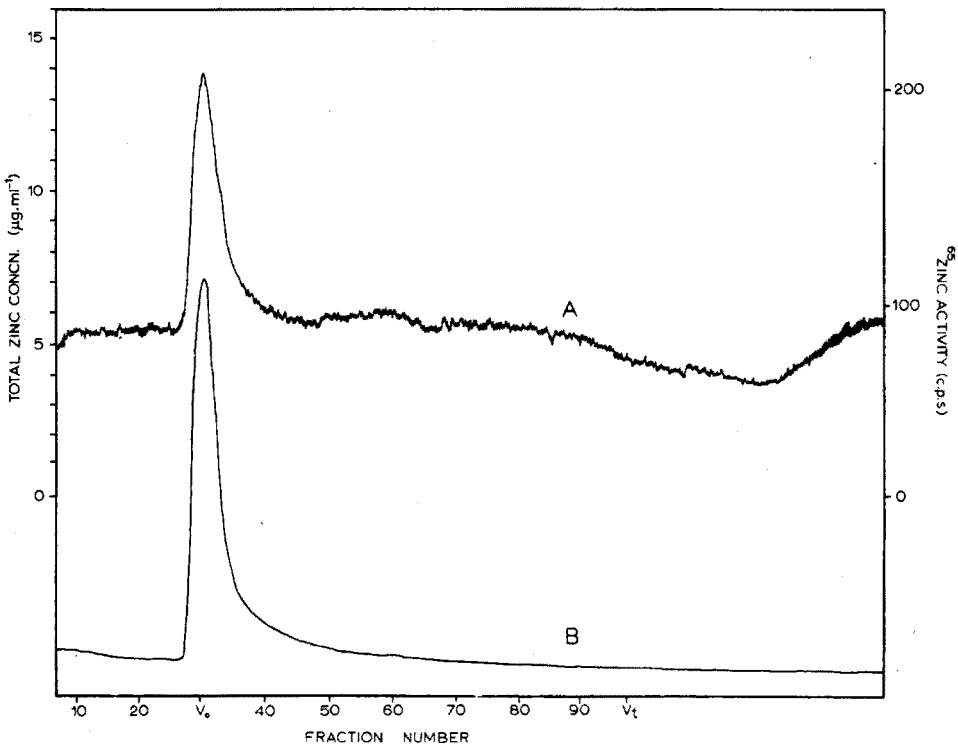

Fig. 5. Gel filtration chromatogram for the binding of zinc by lake-water fulvic acid with zinc-65 as tracer. Measurements were made with a γ-scintillation counter (curve A) and a visible spectrophotometer (curve B) attached to a 2-channel recorder. Curve B shows the absorbance of the eluate measured in a 2-mm flow cell; the peak of the curve corresponds to an absorbance of 0.255 at 460 nm. Volumes of fractions were 1.95 ml; 2.78 mg of fulvic acid was used.

1.73 sites per molecule of the weaker ligand ($\log K_2 = 7.16$). These binding sites are probably respectively the phenolic and carboxylic groups which are known to be the metal-complexing sites in fulvic acids[1].

The above technique was also used to study the interaction of copper with peat fulvic acid and the complexation of nickel and zinc (Fig. 5) by lake-water fulvic acids; the results (Table I) indicate that the values obtained for the number of different binding sites n_1 and n_2 per molecule of the same sample of fulvic acid did not vary significantly from one metal to another. Thus the sites involved in the complexation of the various metals are identical. It is noteworthy that once n_1 and n_2 are known for a given humic or fulvic acid, it is possible to make a reasonable estimate of the intrinsic stability constants K_1 and K_2 for any metal by carrying out two runs at both very low and high concentrations of the free metal ion.

TABLE I

STABILITY CONSTANTS AT 20°C AND BINDING STOICHIOMETRIES FOR COPPER(II), NICKEL(II) AND ZINC(II) WITH LAKE-WATER FULVIC ACID, PEAT FULVIC ACID, AND SOIL FULVIC ACID

Metal	*Fulvic acid*	i[a]	n_i[b]	K_i	*Log* K_i
Cu(II)	Lake water	1	1.10	$6.25 \cdot 10^8$	8.80
		2	2.55	$1.11 \cdot 10^8$	8.05
		0	3.65	$2.66 \cdot 10^8$	8.42
	Peat	1	0.39	$3.23 \cdot 10^8$	8.51
		2	1.73	$1.44 \cdot 10^7$	7.16
		0	2.12	$7.06 \cdot 10^7$	7.85
	Soil[c]	0	1.0	$2.0 \cdot 10^3$	3.3
Ni(II)	Lake water	0	3.65	$1.38 \cdot 10^5$	5.14
	Peat	1	0.41	$4.38 \cdot 10^5$	5.64
		2	1.85	$2.08 \cdot 10^4$	4.32
		0	2.26	$9.45 \cdot 10^4$	4.98
	Soil[c]	0	1.0	$1.26 \cdot 10^3$	3.1
Zn(II)	Lake water	0	3.65	$1.38 \cdot 10^5$	5.14
	Peat	0	2.26	$6.76 \cdot 10^4$	4.83
	Soil[c]	0	1.0	$2.24 \cdot 10^2$	2.35

[a] i denotes the type of binding site; $i = 0$ denotes the overall binding.
[b] n_i signifies the average number of binding sites of type i per molecule of fulvic acid.
[c] Result obtained by Schnitzer and Khan[1] for determinations carried out at pH 3.0, $\mu = 0.1$.

The data in Table I also indicate that there is a considerable difference between the complexing ability of the fulvic acids from peat and fresh water. Thus, the latter contains approximately 1.5 times more complexing sites, and the complexes which they form have stability constants nearly half an order of magnitude greater. As would be expected, the stability constants obtained at pH 8 by the gel filtration method are several orders of magnitude greater than those quoted by Schnitzer and Khan[1] who used a method of continuous variations and a pH of 3.0. Our preliminary findings suggest that the degree of trace element–fulvic acid interaction in natural waters is very much greater than has been previously suspected[9].

The basic requirements of the procedure are that the peak of the complex must be separated from the metal deficiency trough and that the complexation reaction must have reached equilibrium before the peak containing the organometallic complex leaves the column. Attainment of equilibrium is indicated in the metal chromatogram by the return of the metal concentration to its initial value between the peak and the trough. In principle the method may be applied to the examination of complexation at other pH values by the use of any suitable combination of hydrogen ion and metal ion buffers[16]. In conclusion, the advantage of the method is that it is possible to obtain detailed information about numbers of binding sites and stability constants of metal chelates at realistic values of pH and metal concentrations.

SUMMARY

A gel filtration technique is described for the study of the complexation of dissolved metals by humic and fulvic acids. Measurements can be made under realistic conditions of pH and free metal ion concentrations, both of which can be maintained by the use of TRIS as a buffer. The procedure permits the determination not only of the overall stability constant, but of the binding stoichiometries and the intrinsic stability constants associated with the various types of metal binding sites. The procedure has been applied to the investigation of the interaction of fresh-water fulvic acids with Cu, Zn and Ni, and has provided evidence for the existence of two different types of binding sites in the fulvic acid molecule.

REFERENCES

1 M. Schnitzer and S. U. Khan, *Humic Substances in the Environment*, M. Dekker, New York, 1972.
2 K. M. Khailov and Z. Z. Finenko in J. H. Steele (Ed.), *Marine Food Chain*, Oliver and Boyd, Edinburgh, 1970.
3 R. M. Ingle and D. F. Martin, *Environ. Lett.*, 1 (1) (1971) 69.
4 H. de Haan, *Verh. Internat. Verein. Limnol.*, 18 (1972) 685.
5 R. Johnston, *J. Mar. Biol. Ass. U.K.*, 43 (1963) 427.
6 A. Siegel in S. F. Faust and J. V. Hunter (Eds.), *Organic Compounds in Aquatic Environments*, M. Dekker, New York, 1971.
7 V. Cheam, *Can. J. Soil. Sci.*, 53 (1973) 377.
8 E. K. Duursma in D. W. Hood (Ed.), *Symposium on Organic Matter in Natural Waters*, University of Alaska, 1970.
9 W. Stumm and J. J. Morgan, *Aquatic Chemistry*, Wiley-Interscience, New York, 1970.
10 J. P. Hummel and W. J. Dreyer, *Biochim. Biophys. Acta*, 63 (1962) 530.
11 S. E. Bryan and E. Friedan, *Biochemistry*, 6 (1967) 2728.
12 R. F. Colman, *Anal. Biochem.*, 46 (1972) 358.
13 F. A. Suso and H. M. Edwards, Jr., *Proc. Soc. Exp. Biol. Med.*, 138 (1971) 157.
14 R. F. C. Mantoura and J. P. Riley, *Anal. Chim. Acta*, 76 (1975) 97.
15 V. R. Williams and H. B. Williams, *Basic Physical Chemistry for the Life Sciences*, Freeman, San Francisco, 1967.
16 D. D. Perrin and B. Dempsey, *Buffers for pH and Metal Ion Control*, Chapman and Hall, London, 1974.
17 D. P. Hanlon, D. S. Watt and E. W. Westhead, *Anal. Biochem.*, 16 (1966) 225.
18 N. Yoza, *J. Chromatogr.*, 86 (1973) 325.
19 G. Scatchard, *Ann. N.Y. Acad. Sci.*, 51 (1949) 660.

Analytica Chimica Acta, 78 (1975) 201–209

CHELATES DU MANGANESE(II) AVEC DES COORDINATS PHENOLIQUES

PARTIE I. COMPLEXES SIMPLES BINAIRES

J. P. SCHARFF et R. GENIN

Laboratoire de Chimie Minérale, U.E.R. de Chimie–Biochimie, Université Claude Bernard Lyon I, 43 Boulevard du 11 Novembre, 69621-Villeurbanne (France)

(Reçu le 14 janvier 1975)

Le manganèse étant un métal important parmi les constituants minéraux des végétaux, il nous a semblé intéressant d'étudier les interactions des ions manganèse-(II) avec quelques acides-phénols dont la présence constante dans les plantes a été reconnue[1].

Dès 1956, Jurd et Geissman[2] faisaient remarquer que de nombreux composés phénoliques naturels contiennent certains groups structuraux susceptibles de former des complexes avec les métaux: *o*-dihydroxyphénols, hydroxy-3 et hydroxy-5 chromones, groupements *o*-hydroxycarbonylés, etc.

D'autre part on sait que les acides humiques et fulviques qui constituent (avec l'humine et les acides hymatomélaniques) la matière organique, stabilisée et non vivante du sol (humus), sont capables de former des complexes métalliques[3,4]. Bien que les structures de ces acides polymères ne soient pas encore totalement élucidées, quelques travaux ont permis d'évaluer la stabilité ionique de leurs complexes avec quelques ions métalliques et de montrer dans certains cas une coordination du type "salicylate"[4–9]. Enfin les investigations structurales des substances humiques ont montré que les essais de dégradation de ces acides[10] conduisent notamment à de nombreux polyphénols tels que les acides 3,5; 3,4; 2,4; 2,3; et 2,6-dihydroxybenzoïques.

Nous avons choisi pour cette étude des coordinats comportant au moins un groupement hydroxyle aromatique. Ces coordinats phénoliques sont les suivants: acide sulfo-5 salicylique, acide hydroxy-8-sulfo-5 quinoléïne, acide pyrocatéchol-disulfonique-3,5, acide dihydroxy-3,4 benzoïque (protocatéchique) et acide dihydroxy-2,4 benzoïque (β-résorcylique). Ce sont donc des molécules relativement simples mais dont les sites de coordination sont des modèles applicables aux cas des composés phénoliques naturels décrits ci-dessus.

Liste des symboles

c_M, c_A: concentrations totales des constituants M et A.
c_H: concentration totale en protons neutralisables.
m, a, h: concentration des constituants libres et des protons.
β_{pqr}: constante de stabilité ionique globale de l'espèce $M_pH_qA_r$ formée d'après l'équilibre $pM+qH+rA \rightleftarrows M_pH_qA_r$; $\beta_{pqr}=[M_pH_qA_r]/m^p h^q a^r$.

$\bar{r}$: nombre moyen de coordinats A fixés par atome métallique M.
$\bar{q}=(c_H-h+oh)/c_A$: nombre moyen de protons fixés par mole de coordinat A.
$K_q^H=[H_{q-1}A]\cdot h/[H_qA]$: constante de dissociation du coordinat H_qA.

PARTIE EXPÉRIMENTALE

Technique expérimentale

L'étude des complexes formés a été réalisée par une méthode protométrique. Les mesures de pH ont été effectuées à l'aide d'un compensateur Metrohm type E 388 en milieu de force ionique 1 *M* maintenue constante par du perchlorate de sodium (Fluka puriss) et à la température de $25\pm0{,}1°C$ suivant le processus déjà décrit[11]. Toutes les solutions ont été préparées avec de l'eau distillée désaérée et les mesures effectuées en cellule étanche sous atmosphère d'azote désoxygéné par barbotage préalable au sein de solutions réductrices (V^{2+}).

Réactifs

Nous avons utilisé l'acide sulfo-5 salicylique (Merck p.a.), l'acide hydroxy-8 sulfo-5 quinoléïne (Merck) après recristallisation à partir d'une solution chlorhydrique (3% en HCl), l'acide pyrocatécholdisulfonique-3,5 (Merck p.a.) sous forme de son sel disodique (Tiron), l'acide dihydroxy-3,4 benzoïque (Serlabo) et l'acide dihydroxy-2,4 benzoïque (Fluka puriss). Pour les trois derniers coordinats nous avons constaté que les solutions étaient peu stables au cours du temps. D'autre part il est bien connu que les diphénols (en particulier les dérivés *ortho* et *para*) s'altèrent rapidement à l'air et à la lumière en milieu alcalin. Nous avons donc pour chaque manipulation pesé la quantité nécessaire de réactif qui était introduite en solution juste avant le début des mesures.

Les solutions de perchlorate manganeux (Fluka, purum) peuvent être stabilisées par addition d'une faible quantité d'acide perchlorique. L'acidité libre est déterminée par la méthode de Gran[12]. Le titre en manganèse(II) est obtenu par titrage à l'EDTA, soit en milieu ammoniacal en présence de chlorhydrate d'hydroxylamine, avec détection visuelle (noir ériochrome T)[13]; soit en milieu acétique (pH 4,6) avec détection potentiométrique à l'électrode de mercure[14].

INTERACTIONS PROTON-COORDINAT

Les constantes de dissociation K_q^H des cinq coordinats utilisés ont été reprécisées pour les conditions expérimentales de cette étude ($NaClO_4$ 1 *M*, 25°C). Les déterminations potentiométriques classiques conduisent au tracé des courbes de titrage normalisées $\bar{q}_0=f(-\log h)$ (*cf.* Fig. 2 et 5 par exemple) dont l'exploitation conduit aux résultats rassemblés dans le Tableau I. Les valeurs obtenues sont généralement conformes aux travaux antérieurs. Cependant quelques remarques sont nécessaires, notamment en ce qui concerne les coordinats "*o*-diphénoliques" (Tiron, acide protocatéchique) pour lesquels nous obtenons des valeurs de pK_1^H assez nettement différentes de celles habituellement indiquées. En effet, du fait de l'oxydation de ces diphénols en milieu alcalin, ces valeurs sont souvent entachées d'erreurs importantes. C'est ainsi que Murakami *et al.*[15] indiquent les résultats suivants:

catéchol $pK_1^H = 11{,}59$
acide protocatéchique $pK_1^H = 11{,}94$
acide pyrocatécholsulfonique-4 $pK_1^H = 12{,}16$
acide pyrocatécholdisulfonique-3,5 (Tiron) $pK_1^H = 12{,}26$

Ces valeurs et l'ordre de croissance des pK_1^H sont à notre avis inexacts. En effet elles conduisent les auteurs à proposer, pour la dissociation des groupements phénoliques, le schéma suivant:

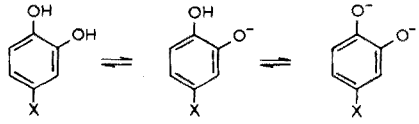

qui est en contradiction avec le fait que l'effet inductif attracteur d'électrons d'un substituant X est plus important en position *para*, qu'en position *méta* comme ceci est d'ailleurs vérifié[16] par les pK respectifs du phénol (9,80) et des acides *m*-hydroxybenzoïque (9,61) et *p*-hydroxybenzoïque (8,985). Murakami *et al.* sont d'ailleurs amenés à constater, sans l'expliquer, que l'ordre indiqué est en contradiction avec celui des fréquences de vibrations longitudinales intramoléculaires déterminé par spectroscopie infra-rouge. La bonne concordance des résultats est obtenue avec nos valeurs où pK_1^H pour le Tiron (11,83) est inférieur à celui de l'acide protocatéchique (12,8) qui doit être lui-même inférieur à celui du pyrocatéchol (ceci a été montré également par Harada[17]). Enfin notre valeur pour le Tiron est confirmée par les travaux de Nasanen[18] effectués à force ionique identique (pK_1^H = 11,6; $NaClO_4$ 1 *M*).

En ce qui concerne l'acide *β*-résorcylique, la valeur élevée de pK_1^H est expliquée par la formation d'une liaison hydrogène intramoléculaire.

TABLEAU I

CONSTANTES DE DISSOCIATION DES COORDINATS

(T=25°C, $NaClO_4$ 1 *M*)

Coordinat	pK_1^H	pK_2^H	pK_3^H
Acide sulfo-5 salicylique	11,57	2,33	
Acide hydroxy-8 sulfo-5 quinoléïne	8,30	4,19	
Acide pyrocatécholdisulfonique-3,5	11,83	7,25	
Acide protocatéchique	12,80	8,68	4,34
Acide *β*-résorcylique	>13	8,69	3,19

INTERACTIONS MANGANÈSE(II)-COORDINAT

Méthode d'investigation

Les complexes formés dans les différents systèmes ont été étudiés par le tracé des courbes de formation $\bar{r} = f(-\log a)$ suivi de l'exploitation de ces courbes par la méthode des moindres carrés suivant un processus déjà décrit[11]. Pour

chaque système un grand nombre de titrages protométriques ont été effectués pour différents rapports $R = c_A/c_M$ de réactifs engagés. Dans tous les cas nous avons également tracé les courbes normalisées $\bar{q} = f(-\log h)$ qui permettent de suivre qualitativement et quantitativement les phénomènes de complexation[19,20].

Résultats

Dans un travail préliminaire[20] nous avions traité le cas du système manganèse(II)–acide pyrocatécholdisulfonique-3,5 (H_4A) où les espèces MHA, MA, MA_2 et MA_3 avaient été détectées. Nous rappelons dans le Tableau II les valeurs des constantes de stabilité ionique obtenues pour les quatre espèces complexes afin de pouvoir les comparer à celles déterminées pour les autres systèmes envisagés. Un point important de cette étude était la mise en évidence de la formation à l'air et en milieu alcalin d'un complexe du manganèse(III) stable d'où la nécessité de travailler en atmosphère inerte.

Dans le cas des acides sulfo-5 salicylique (H_3A), hydroxy-8 sulfo-5 quinoléïne (H_2A) et protocatéchique (H_3A) les courbes de formation $\bar{r} = f(-\log a)$ (Fig. 1, 3 et 4) obtenues pour différents rapports $R = c_A/c_M$ sont confondues ce qui montre que les seules espèces formées sont du type MA_r.

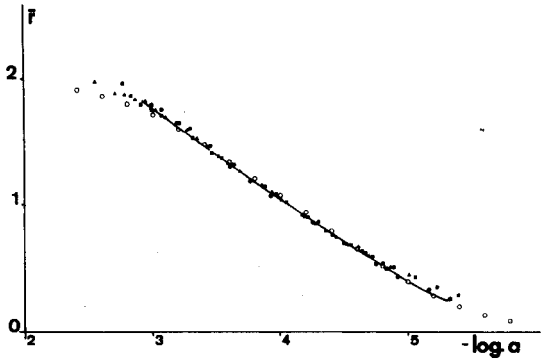

Fig. 1. Courbe de formation du système Mn(II)–acide sulfo-5 salicylique. $(c_M) = 0.992 \cdot 10^{-3}$ *M*. (●) $R = 10$; $c_A = 0{,}998 \cdot 10^{-2}$ *M*; (■) $R = 20$; $c_A = 1{,}997 \cdot 10^{-2}$ *M*. (▲) $R = 30$; $c_A = 2{,}995 \cdot 10^{-2}$ *M*. (○) Point recalculés.

Il faut noter que dans le cas de l'acide sulfo-5 salicylique, la plupart des travaux antérieurs[26–28] ont été effectués en milieu d'ion chlorure qui est un anion complexant et que d'autre part les auteurs n'ont examiné que des solutions où R était constant (généralement $R = 10$), les méthodes de calcul restant assez grossières. Dans ce travail, malgré l'utilisation de rapports R élevés ($R = 10$; 20; 30), $\bar{r}$ n'est jamais supérieur à 2 (Fig. 1) et nous n'avons donc considéré que les espèces MA et MA_2 lors du traitement des couples ($\bar{r}$; $-\log a$) par la méthode des moindres carrés. Nous n'excluons pas la formation d'une espèce MA_3, cependant la précipitation simultanée d'hydroxyde de manganèse(II) en interdit la mise en évidence.

En ce qui concerne le système manganèse(II)–acide hydroxy-8 sulfo-5 quinoléïne, nous montrons (Fig. 2) le faisceau de courbes normalisées $\bar{q} = f(-\log h)$ tracé pour $R = 2{,}5$; 4 et 5. On constate que les courbes correspondantes

s'écartent de la courbe $\bar{q}_0$ (neutralisation du coordinat seul) dès pH 4 ce qui montre que la complexation a lieu en milieu plus acide que dans les autres systèmes où la complexation débute pour des pH > 6. Ce fait est évidemment en relation avec la valeur de $pK_1^H = 8{,}30$ relativement faible par rapport aux pK_1^H des autres coordinats. D'autre part en milieu basique (pH > 9) on constate la précipitation d'hydroxyde manganèse(II).

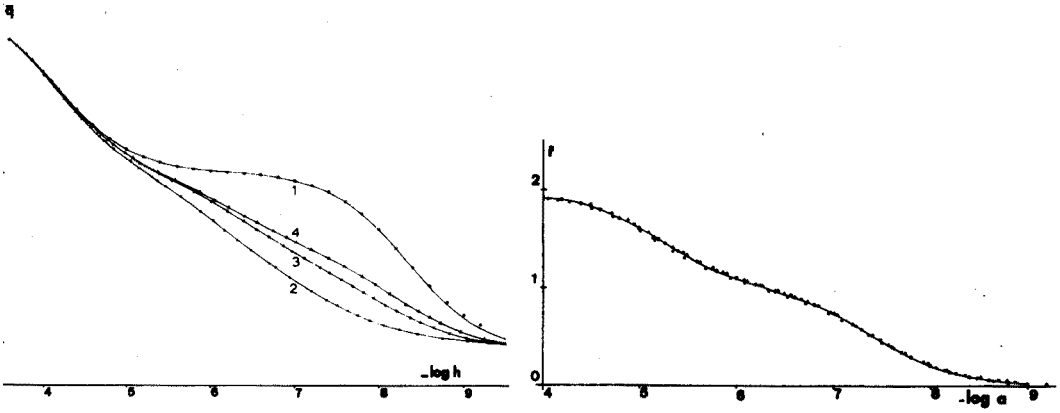

Fig. 2. Courbes de titrage normalisées du système Mn(II)–acide hydroxy-8 sulfo-5 quinoléïne. (1) $\bar{q}_0$ ($c_M = 0$). (2) $\bar{q}_{2.5}$ ($R = 2{,}5$). (3) $\bar{q}_4$ ($R = 4$). (4) $\bar{q}_5$ ($R = 5$).

Fig. 3. Courbe de formation du système Mn(II)–acide hydroxy-8 sulfo-5 quinoléïne. (●) $R = 2{,}5$; $c_M = 3{,}968 \cdot 10^{-4}$ M; $c_A = 0{,}991 \cdot 10^{-3}$ M. (*) $R = 4$; $c_M = 1{,}984 \cdot 10^{-4}$ M; $c_A = 0{,}743 \cdot 10^{-3}$ M. (■) $R = 5$; $c_M = 1{,}984 \cdot 10^{-4}$ M; $c_A = 0{,}991 \cdot 10^{-3}$ M. (▲) $R = 8$; $c_M = 1{,}190 \cdot 10^{-4}$ M: $c_A = 0{,}991 \cdot 10^{-3}$ M. (○) Points recalculés.

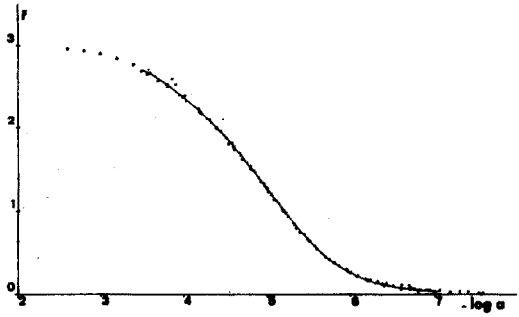

Fig. 4. Courbe de formation du système Mn(II)–acide protocatéchique. (●) $R = 3$; $c_M = 3{,}962 \cdot 10^{-3}$ M; $c_A = 1{,}188 \cdot 10^{-2}$ M. (■) $R = 4$; $c_M = 3{,}962 \cdot 10^{-3}$ M; $c_A = 1{,}585 \cdot 10^{-2}$ M. (▲) $R = 7$; $c_M = 1{,}981 \cdot 10^{-3}$ M; $c_A = 1{,}387 \cdot 10^{-2}$ M. (○) Points recalculés.

La courbe $\bar{r} = f(-\log a)$ est représentée sur la Fig. 3; on constate que l'on atteint facilement des valeurs de $\bar{r}$ supérieures à 2 lorsque R augmente. Il est donc possible de mettre en évidence l'espèce MA_3 non encore signalée et de calculer sa constante de stabilité: $\log \beta_{103} = 14{,}30$.

Pour le système manganèse(II)–acide protocatéchique la courbe de formation (Fig. 4) montre la formation successive des chélates MA et MA_2. La complexation a lieu pour des pH > 7 c'est à dire après la dissociation complète du groupement

carboxylique ce qui exclut la formation d'espèces protonées du type I, envisagées par Migal et Ivanov[21] dans le cas de fer(III).

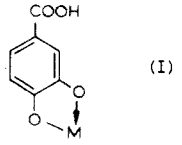

(I)

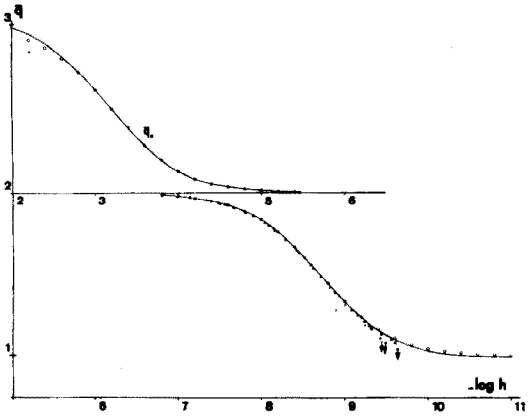

Fig. 5. Courbes de titrage normalisées du système Mn(II)–acide β-résorcylique $\bar{q}_0$ ($c_M = 0$). (*) $R = 5$; $c_M = 0{,}992 \cdot 10^{-3}$ M; $c_A = 0{,}496 \cdot 10^{-2}$ M. (■) $R = 10$; $c_M = 0{,}992 \cdot 10^{-3}$ M; $c_A = 0{,}993 \cdot 10^{-2}$ M. (▲) $R = 20$; $c_M = 0{,}992 \cdot 10^{-3}$ M; $c_A = 1{,}986 \cdot 10^{-2}$ M. Les flèches indiquent le début de précipitation.

Comme dans le cas du Tiron on constate en milieu alcalin une oxydation importante par formation de complexes manganèse(IV). Cette oxydation difficilement évitable pour des pH > 11 interdit la mise en évidence de l'espèce MA_3.

Enfin nous avons examiné le système manganiques(II)–acide β-résorcylique pour lequel les courbes $\bar{q} = f(-\log h)$ résultant de la neutralisation de solutions où $R = 5$; 10 et 20 (Fig. 5) sont confondues avec la courbe $\bar{q}_0$ (neutralisation du coordinat seul) jusqu'à pH 9,5. Au delà de cette valeur on observe d'ailleurs le début de la précipitation d'hydroxyde manganèse(II). Nous pouvons donc penser qu'il n'y a pas de phénomène de complexation dans ce cas. Ceci peut s'expliquer par le fait que pour ce coordinat seule la chélation du type "salicylate" peut conduire à la formation d'un complexe stable. Mais étant donné la forte valeur de $pK_1^H > 13$, la dissociation du groupement phénolique n'est pas possible. Il faut d'ailleurs noter qu'aucune formation de complexe n'a jamais été signalée pour ce système[22].

Le Tableau II rassemble nos résultats que l'on peut comparer avec les travaux antérieurs.

DISCUSSION

Pour les cinq systèmes simples binaires étudiés nous avons soit amélioré les travaux antérieurs, soit obtenu dans certains cas des données originales concernant des espèces non encore signalées.

TABLEAU II

CONSTANTES DE STABILITÉ IONIQUE

Espèces	*Constantes*	*log* β_{pqr}			
		Nos valeurs 25°C, 1 M $NaClO_4$	*Autres références*		
A = Acide sulfo-5 salicylique			*25°C*	*20°C*	*25°C*
			0,1 M $NaClO_4$[26]	*0,1–0,15 M KCl*[27]	*0,1 M KCl*[28]
MA	β_{101}	4,77	5,24	5,10	5,25
MA_2	β_{102}	8,19	8,24	8,00	8,65
A = Acide hydroxy-8 sulfo-5 quinoléïne			*25°C*	*25°C*	*20°C*
			0,1 M KNO_3[29]	*0,01 M KNO_3*[30]	*→0 M KNO_3*[31]
MA	β_{101}	5,47	5,67	6,94	6,6
MA_2	β_{102}	10,36	10,72		11,5
MA_3	β_{103}	14,30			
A = Tiron			*25°C*		
			0,1 M KNO_3[32]		
MHA	β_{111}	13,88			
MA	β_{101}	7,20	8,60		
MA_2	β_{102}	12,75			
MA_3	β_{103}	16,28			
A = Acide protocatéchique			*30°C*		
			0,1 M KNO_3[15]		
MA	β_{101}	7,43	7,22		
MA_2	β_{102}	12,64	12,28		
A = Acide β-résorcylique					
MA_r	Espèces non détectées				

C'est ainsi que la courbe de formation complète du système manganèse(II)–acide hydroxy-8 sulfo-5 quinoléïne est décrite pour la première fois ainsi que la stabilité ionique de l'espèce MA_3. Il faut noter que la stabilité est assez forte et nettement supérieure au cas de l'acide sulfo-5 salicylique où une telle espèce ne se forme pas.

Des résultats intéressants ont été également obtenus pour les systèmes Mn(II)–Tiron[20] et Mn(II)–acide protocatéchique. Dans les deux cas nous avons mis en évidence l'oxydation extrêmement importante de manganèse(II) en manganèse(III) en présence de coordinat et en milieu alcalin. Nous pensions que cette observation est intéressante pour l'explication du mécanisme de l'oxydation catalytique des pyrocatéchols en *o*-quinones par les ions métalliques. Bien que Tyson et Martell[23,24] aient proposé un mécanisme où le manganèse reste à l'état divalent, d'autres auteurs[25] avaient envisagé la possibilité d'un complexe manganèse-(III) intermédiaire. Il est d'ailleurs curieux de constater que l'action catalytique des ions métalliques décroît suivant la séquence: Mn(II) > Co(II) > Fe(II) > Cu(II) > Ni(II), Zn(II), et que par conséquent, les ions les plus "actifs" (Mn(II), Co(II),

Fe(II)) sont ceux qui, on le sait passent facilement, à l'état complexé, au degré d'oxydation +3.

Notons que dans le cas du système manganèse(II)–acide protocatéchique, l'oxydation des ions manganèse(II) apparaît encore plus importante que dans le cas du Tiron et de ce fait nous n'avons pu obtenir l'espèce MA_3. Avec l'acide β-résorcylique aucune chélation avec libération de proton n'a été mise en évidence.

Enfin l'ensemble de nos résultats montre que les complexes avec le Tiron et l'acide protocatéchique sont parmi les plus stables que forment les ions manganèse(II) avec des coordinats bidentés[22].

RÉSUMÉ

La formation des complexes simples binaires du manganèse(II) avec cinq coordinats phénoliques bidentés est étudiée par potentiométrie à 25°C et à force ionique 1 *M* $NaClO_4$. Les manipulations sont effectuées en atmosphère inerte de façon à éviter toute oxydation des ions manganèse(II) en ions manganèse(III), notamment dans le cas des *o*-diphénols. Des résultats originaux sont obtenus pour certains systèmes et les constantes de stabilité ionique de tous les complexes formés sont calculées. Les valeurs obtenues montrent que les chélates avec le Tiron et l'acide dihydroxy-3,4 benzoïque sont parmi les complexes les plus stables formés par l'ion manganèse(II) avec des coordinats bidentés.

SUMMARY

The complex formation of simple binary species of manganese(II) with five phenolic ligands has been studied by a potentiometric method at 25°C and at ionic strength of 1 *M* $NaClO_4$. Experiments were carried out in an inert atmosphere to avoid any oxidation to manganese(III), especially in the case of *o*-diphenolic ligands. New results are reported for some systems and the stability constants of all the species formed are computed. The data show that the Tiron and 3,4-dihydroxybenzoic acid–manganese(II) chelates are among the most stable complexes formed by bidentate ligands with manganese(II).

BIBLIOGRAPHIE

1 P. Ribereau-Gayon, *Les Composés Phénoliques des Végétaux*, Dunod, Paris, 1968.
2 L. Jurd et T. A. Geissman, *J. Org. Chem.*, 21 (1956) 1395.
3 J. L. Mortensen, *Soil Sci. Soc. Amer., Proc.*, 27 (1963) 179.
4 M. Schnitzer et E. H. Hansen, *Soil Sci.*, 109 (1970) 333.
5 D. Gamble, M. Schnitzer et I. Hoffman, *Can. J. Chem.*, 48 (1970) 3197.
6 P. G. Manning et S. Ramamoorthy, *J. Inorg. Nucl. Chem.*, 35 (1973) 1577.
7 S. Ramamoorthy et P. G. Manning, *J. Inorg. Nucl. Chem.*, 36 (1974) 695.
8 M. Schnitzer, *Soil Sci. Soc. Amer., Proc.*, 33 (1969) 75.
9 M. Schnitzer et S. I. M. Skinner, *Soil. Sci.*, 103 (1967) 247.
10 M. Schnitzer et S. U. Khan, *Humic Substances in the Environment*, M. Dekker, New York, 1972.
11 M. Morin, M. R. Pâris et J. P. Scharff, *Anal. Chim. Acta*, 57 (1971) 123.
12 G. Gran, *Analyst (London)*, 77 (1952) 661.
13 H. A. Flaschka, *EDTA Titrations*, Pergamon, London, 1964.
14 C. N. Reilley, R. W. Schmid et D. W. Lawson, *Anal. Chem.*, 30 (1958) 953.

15 Y. Murakami, K. Nakamura et M. Tokunaga, *Bull. Chem. Soc. Jap.*, 36 (1963) 669.
16 A. V. Willi et J. F. Stocker, *Helv. Chim. Acta*, 38 (1955) 1279.
17 H. Harada, *Nippon Kagaku Zasshi*, 90 (1969) 267.
18 R. Nasanen, *Suom. Kemistilehti*, 33B (1960) 111.
19 M. Morin et J. P. Scharff, *Anal. Chim. Acta*, 66 (1973) 113.
20 R. Genin et J. P. Scharff, *Bull. Chem. Soc. Fr.*, 7–8 (1974) 1307.
21 P. K. Migal et V. A. Ivanov, *Russ. J. Inorg. Chem.*, 18 (1973) 536.
22 L. G. Sillen et A. E. Martell, *Stability Constants of Metal Ion Complexes*, The Chemical Society, London, 1964 et 1971.
23 A. E. Martell, *Proceedings of the 3rd Symposium of Coordination Chemistry*, Akademiai Kiado, Budapest, 1971.
24 C. A. Tyson et A. E. Martell, *J. Amer. Chem. Soc.*, 94 (1972) 939.
25 R. R. Grinstead, *Biochemistry*, 3 (1964) 1308.
26 C. V. Banks et R. S. Singh, *J. Inorg. Nucl. Chem.*, 15 (1960) 125.
27 D. D. Perrin, *Nature (London)*, 182 (1958) 741.
28 V. S. K. Nair, *Talanta*, 9 (1962) 27.
29 C. F. Richard, R. L. Gustafson et A. E. Martell, *J. Amer. Chem. Soc.*, 81 (1959) 1033.
30 R. Nasanen et E. Uisitalo, *Acta Chem. Scand.*, 8 (1954) 835.
31 A. Albert, *Biochem. J.*, 54 (1953) 646.
32 R. C. Courtney, R. L. Gustafson, S. Chaberek et A. E. Martell, *J. Amer. Chem. Soc.*, 80 (1958) 2121.

Analytica Chimica Acta, 78 (1975) 211–218

CHELATES DU MANGANESE(II) AVEC DES COORDINATS PHENOLIQUES

PARTIE II. COMPLEXES MIXTES TERNAIRES

J. P. SCHARFF et R. GENIN

Laboratoire de Chimie Minérale, U.E.R. de Chimie–Biochimie, Université Claude Bernard Lyon I, 43 Boulevard du 11 Novembre, 69621-Villeurbanne (France)

(Reçu le 14 janvier 1975)

Depuis 1960 de très nombreuses déterminations ont été effectuées sur les complexes mixtes ternaires (deux coordinats différents fixés sur le même ion métallique). Cependant l'examen de diverses compilations rassemblant plusieurs centaines de données[1–3] montre que les complexes mixtes du manganèse ont été peu étudiés et les quelques exemples traités portent sur des complexes mixtes d'intérêt biologique. C'est ainsi que l'on peut citer les travaux concernant les systèmes: — Mn(II)–acide nitrilotriacétique–B où B = glycine[4 5], arginine[6], histidine[7], acide aspartique[8], éthylvalinate[4]; — (Mn(II)–glycine–B où B = acide pyruvique[9] et salicylaldéhyde[10]; — (Mn(II)–histidine–EDTA[7].

En effet l'étude de la chélation mixte est d'une importance fondamentale lorsqu'on désire connaitre le comportement des mélanges de cations métalliques et de coordinats différents comme c'est le cas général dans les milieux biologiques. D'autre part, dans de très nombreux cas, certains cations métalliques (dont les ions manganèse) activent les enzymes par formation d'un complexe mixte métal–enzyme–substrat[11]. L'existence d'espèces mixtes ternaires est également déterminante dans les phénomènes de transport de cations métalliques ou de groupements coordinés. L'importance biologique de la chélation mixte est donc bien établie et ce point sera développé par l'un de nous dans un prochain travail[12].

D'une manière générale il est admis que l'existence de complexes mixtes est prépondérante dans certains phénomènes tels que: la cinétique de formation des complexes, les effets catalytiques dans certaines réactions d'oxydo–réduction (par exemple l'oxydation des phénols[13]), les effets de synergisme dans les techniques d'extraction[14], etc.

Poursuivant notre étude des interactions manganèse(II)–coordinats phénoliques, nous abordons dans ce travail l'étude des complexes mixtes susceptibles de se former dans les systèmes manganèse(II)–acide sulfo-5 salicylique–acide hydroxy-8 sulfo-5 quinoléïne et manganèse(II)–acide pyrocatécholdisulfonique-3,5–acide hydroxy-8 sulfo-5 quinoléïne.

Liste des symboles

c_M, c_A, c_B:	concentrations totales des constituants M, A, B.
c_H:	concentration totale en protons neutralisables.
m, a, b, h:	concentrations des constituants libres et des protons.

β_{pqrs}: constante de stabilité ionique globale de l'espèce $M_pH_qA_rB_s$ formée d'après l'équilibre: $pM+qH+rA+sB \rightleftarrows M_pH_qA_rB_s$;
$\beta_{pqrs}=[M_pH_qA_rB_s]/m^p h^q a^r b^s$.

$\bar{r}$, $\bar{s}$: nombre moyen de coordinats A ou B fixés par atome métallique M.

$\bar{q}=(c_H-h+oh)/(c_A+c_B)$: nombre moyen de protons fixés par mole de coordinats.

PARTIE EXPÉRIMENTALE

Tous les détails expérimentaux sont indiqués dans le mémoire précédent[15]. Toutes les mesures furent effectuées à la température de $25\pm0{,}1°C$, en milieu de force ionique 1 M maintenue constante par du perchlorate de sodium.

Traitement des données expérimentales

Au cours de titrages protométriques par un acide fort ou une base forte, à température et pression constantes, l'état d'un système chimique contenant les quatre constituants M, H, A et B est défini par les équations suivantes:

$$c_M = m+\Sigma p\cdot\beta_{pqrs}\cdot m^p h^q a^r b^s \quad (1)$$

$$c_A = a+\Sigma r\cdot\beta_{pqrs}\cdot m^p h^q a^r b^s \quad (2)$$

$$c_B = b+\Sigma s\cdot\beta_{pqrs}\cdot m^p h^q a^r b^s \quad (3)$$

$$c_H = h-oh+\Sigma q\cdot\beta_{pqrs}\cdot m^p h^q a^r b^s \quad (4)$$

Les données expérimentales brutes: quantités des réactifs, potentiels d'électrodes peuvent être transformées en courbes normalisées $\bar{q}_{exp}=f(-\log h)$. Le principe de l'affinement des constantes de stabilité ionique β_{pqrs} déjà décrit en détail[16-18] et récemment étendu au cas des complexes mixtes quaternaires[19] consiste à rendre minimum la somme $U=\Sigma(\bar{q}_{exp}-\bar{q}_{calc})^2$ par la méthode du "pit-mapping".

Pour cela des valeurs initiales approchées des constantes β_{pqrs} peuvent être estimées par divers moyens (calcul approché, considérations statistiques, etc.). À l'aide de ces valeurs grossières le système des quatre éqns. (1)–(4) permet le calcul de m, a, b et $\bar{q}_{calc}$ que l'on compare à $\bar{q}_{exp}$. L'opération est alors répétée pour différentes valeurs de β_{pqrs} déduites des valeurs initiales par des variations systématiques fixées par un "pas" choisi au préalable. Il reste alors à extrapoler les valeurs des constantes β_{pqrs} vers des valeurs voisines de celles rendant minimum l'expression de U.

SYSTÈME Mn(II)–ACIDE SULFO-5 SALICYLIQUE–ACIDE HYDROXY-8 SULFO-5 QUINOLÉÏNE

Dans ce système où coexistent un ion métallique hexacoordiné et deux coordinats bidentés: H_3A (acide sulfo-5 salicylique) et H_2B (acide hydroxy-8 sulfo-5 quinoléïne), les espèces mixtes susceptibles de se former doivent être du type MAB, MA_2B et MAB_2.

Afin de déterminer les combinaisons des concentrations c_M, c_A et c_B les plus favorables à l'étude des complexes mixtes, il importe de pouvoir estimer des valeurs approchées des constantes β_{1011}, β_{1021} et β_{1012}. C'est ce que nous avons fait en nous

appuyant sur des considérations statistiques qui ont été discutées notamment par Sharma et Schubert[20]. On peut en effet calculer une constante statistique d'après la relation:

$$\log \beta_{10rs(\text{calc})} = \log S + \frac{r}{r+s} \log \beta_{10(r+s)0} + \frac{s}{r+s} \log \beta_{100(r+s)} \tag{5}$$

où S facteur statistique est défini par

$$S = \frac{(r+s)!}{r!\,s!} \tag{6}$$

On peut donc calculer la valeur probable de $\log \beta_{1011} = 9{,}58$. Cependant l'estimation de β_{1021} et β_{1012} ne peut être effectuée par cette méthode car l'on ne connait pas la valeur de β_{1030} correspondant à l'espèce MA_3 que nous n'avons pas détectée[15]. Nous avons donc utilisé la formule (7) établie par Sigel et McCormick[21]:

$$\log K_{rs} = \log \beta_{10rs} - (\log \beta_{10r0} + \log \beta_{100s}) \tag{7}$$

où $\log K_{rs}$ est considéré comme étant nul (approximation valable[21 22] pour obtenir une valeur indicative de $\log \beta_{10rs}$.)

Dans ces conditions les valeurs approchées retenues sont:

$$\log \beta_{1011} = 9{,}58;\ \log \beta_{1021} = 13{,}66;\ \log \beta_{1012} = 15{,}13$$

On peut alors déterminer les conditions d'étude les plus favorables et nous avons choisi de travailler sur les solutions a,b,c dont les compositions sont indiquées dans le Tableau I. Ces calculs préliminaires permettent aussi de constater qu'il sera difficile d'étudier les espèces MA_2B et MAB_2 dont les concentrations ne dépassent jamais quelques pour-cents de la concentration totale en ion métallique.

TABLEAU I

CONDITIONS D'ÉTUDE DU SYSTÈME Mn(II)-A-B

(A = acide sulfo-5 salicylique (ASS); B = acide hydroxy-8 sulfo-5 quinoléïne (HQS))

	Solution a	*Solution b*	*Solution c*
c_M	$1{,}981 \cdot 10^{-4}$ *M*	$1{,}981 \cdot 10^{-4}$ *M*	$1{,}981 \cdot 10^{-4}$ *M*
c_A	$4{,}915 \cdot 10^{-4}$ *M*	$9{,}831 \cdot 10^{-4}$ *M*	$4{,}915 \cdot 10^{-4}$ *M*
c_B	$2{,}460 \cdot 10^{-4}$ *M*	$2{,}460 \cdot 10^{-4}$ *M*	$3{,}690 \cdot 10^{-4}$ *M*
$[HClO_4]_T$	$2{,}000 \cdot 10^{-5}$ *M*	$2{,}000 \cdot 10^{-5}$ *M*	$2{,}000 \cdot 10^{-5}$ *M*

Les courbes de neutralisation par la soude des solutions a,b et c ont été transformées en courbes normalisées $\bar{q} = f(-\log h)$ et nous avons calculé $\bar{q}$ pour chaque point expérimental en supposant la seule existence des complexes simples binaires. La courbe calculée dans cette hypothèse n'est plus confondue avec la courbe expérimentale à partir de pH 8 (Fig. 1) ce qui indique la formation d'espèces complexes mixtes.

L'introduction dans les données de la valeur approchée $\log \beta_{1011} = 9{,}58$ conduit à une réduction de l'écart entre $\bar{q}_{\text{exp}}$ et $\bar{q}_{\text{calc}}$ et après affinement à l'aide de notre programme de calcul, la valeur $\log \beta_{1011} = 10{,}88$ sera retenue. On constate alors

(Fig. 1) la bonne concordance entre valeurs expérimentales et calculées compte tenu de la précision des mesures. L'introduction des constantes approchées des complexes MA_2B et MAB_2 n'apporte pas une amélioration sensible de l'affinement; aussi nous admettrons l'existence dans ce système d'une seule espèce mixte MAB ($\log \beta_{1011} = 10{,}88$).

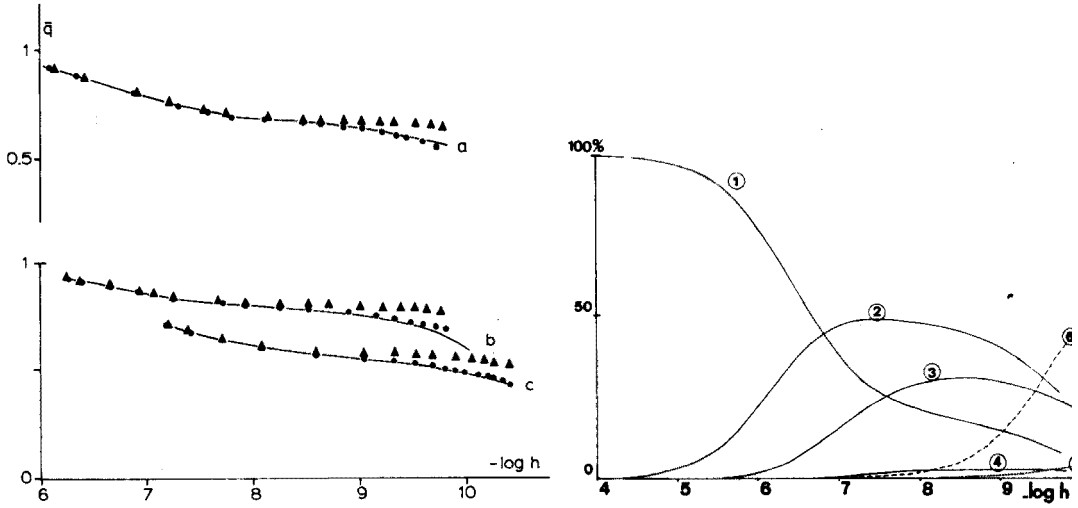

Fig. 1. Courbes de titrage normalisées du système Mn(II)–ASS–HQS (solutions a,b,c): (—) courbe expérimentale; (▲) points calculés dans l'hypothèse de la formation exclusive d'espèces simples; (●) points obtenus après affinement.

Fig. 2. Courbes de répartition du système Mn(II)–ASS–HQS (solution a): (1) métal libre; (2) MB; (3) MB_2; (4) MB_3; (5) MA; (6) MAB.

Les courbes de répartition des espèces en fonction du pH (Fig. 2) tracées pour la solution a montrent que la formation de l'espèce MAB est notable dès pH 8. On constate également la prépondérance des espèces simples MB_s par rapport aux espèces simples MA_r pratiquement inexistantes.

SYSTÈME Mn(II)–TIRON–ACIDE HYDROXY-8 SULFO-5 QUINOLÉÏNE

Comme dans le cas précédent, nous avons estimé à l'aide de l'éqn. (5) les valeurs probables des constantes de stabilité des espèces MAB, MA_2B et MAB_2. On obtient:

$$\log \beta_{1011} = 11{,}86;\ \log \beta_{1021} = 16{,}10;\ \log \beta_{1012} = 15{,}44$$

Les concentrations les plus favorables pour l'expérimentation sont indiquées dans le Tableau II.

Comme précédemment, nous avons tracé (Fig. 3) les courbes $\bar{q} = f(-\log h)$ expérimentales et celles calculées dans l'hypothèse de la seule existence des complexes simples binaires. Dès pH 5,5 ces courbes ne sont plus confondues. L'introduction dans les données des constantes des espèces mixtes MAB, MA_2B et MAB_2

TABLEAU II

CONDITIONS D'ÉTUDE DU SYSTÈME Mn(II)–A–B

(A = Tiron; B = acide hydroxy-8 sulfo-5 quinoléïne)

	Solution a	*Solution b*	*Solution c*	*Solution d*
c_M	$3{,}962 \cdot 10^{-4}$ *M*	$1{,}981 \cdot 10^{-4}$ *M*	$3{,}962 \cdot 10^{-4}$ *M*	$3{,}962 \cdot 10^{-4}$ *M*
c_A	$1{,}200 \cdot 10^{-3}$ *M*	$0{,}600 \cdot 10^{-3}$ *M*	$1{,}200 \cdot 10^{-3}$ *M*	$0{,}800 \cdot 10^{-3}$ *M*
c_B	$4{,}920 \cdot 10^{-4}$ *M*	$3{,}690 \cdot 10^{-4}$ *M*	$3{,}690 \cdot 10^{-4}$ *M*	$7{,}381 \cdot 10^{-4}$ *M*
$[HClO_4]_T$	$4{,}000 \cdot 10^{-5}$ *M*	$2{,}000 \cdot 10^{-5}$ *M*	$4{,}000 \cdot 10^{-5}$ *M*	$4{,}000 \cdot 10^{-5}$ *M*

améliore les résultats pour des pH > 7 mais reste sans effet en milieu plus acide. Nous sommes donc amenés à envisager l'hypothèse d'une espèce protonée MHAB (espèce probable étant donné l'existence signalée de MHA pour le système Mn(II)–Tiron[23]). Effectivement cette introduction réduit sensiblement la somme *U* manganeux du Tiron et de l'acide hydroxy-8 sulfo-5 quinoléïne[15] peut donc être détectée et l'affinement global conduit aux résultats définitifs:

$$\log \beta_{1011} = 12{,}00;\ \log \beta_{1021} = 17{,}30;\ \log \beta_{1012} = 15{,}93;$$
$$\log \beta_{1111} = 20{,}60;\ \log \beta_{1112} = 24{,}90$$

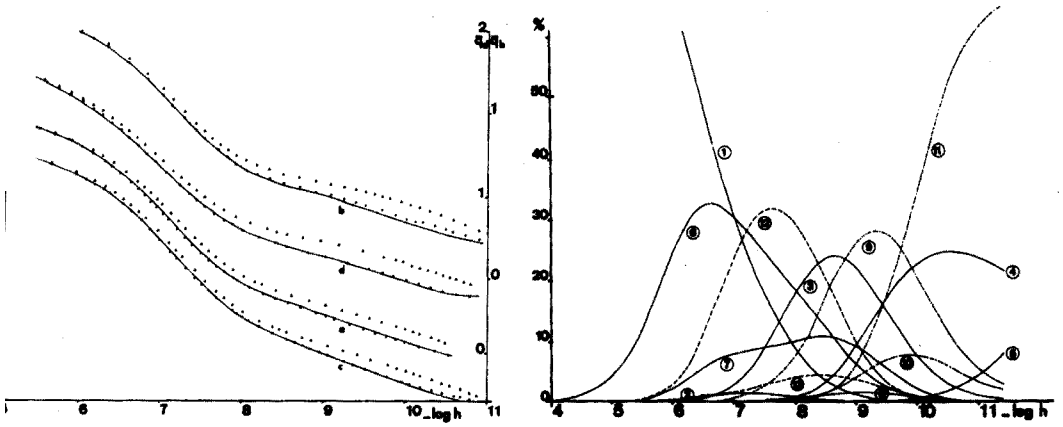

Fig. 3. Courbes de titrage normalisées du système Mn(II)–Tiron–HQS (solutions a,b,c,d): (—) courbe expérimentale; (▲) points calculés dans l'hypothèse de la formation exclusive d'espèces simples; (●) points obtenus après affinement.

Fig. 4. Courbes de répartition du système Mn(II)–Tiron–HQS (solution c): (1) métal libre; (2) MHA; (3) MA; (4) MA_2; (5) MA_3; (6) MB; (7) MB_2; (8) MB_3; (9) MAB; (10) MAB_2; (11) MA_2B; (12) MHAB; (13) $MHAB_2$.

Nous avons tracé (Fig. 4) les courbes de répartition des espèces dans le cas de la solution c. On constate la forte concentration de l'espèce MA_2B par rapport à celles des autres chélates mixtes. Ce fait est à rapprocher de l'importante stabilisation observée pour cette espèce et qui est chiffrée ci-dessous de manière plus précise.

DISCUSSION

En accord avec la plupart des travaux antérieurs sur la chélation mixte[1,2,24] on observe que la stabilité des espèces mixtes est supérieure à celle des complexes simples correspondants. Nous avons caractérisé ce renforcement de stabilité par trois méthodes différentes.

(a) Calcul des constantes log χ_{rs} suivant la méthode de Bonnet et Pâris[24] correspondant aux équilibres suivants:

$$MA_2 + MB_2 \leftrightarrows 2\ MAB$$

$$\log \chi_{11} = 2 \log \beta_{1011} - (\log \beta_{1020} + \log \beta_{1002}) \quad (8)$$

$$MA_3 + 2\ MB_3 \leftrightarrows 3\ MAB_2$$

$$\log \chi_{12} = 3 \log \beta_{1012} - (\log \beta_{1030} + 2 \log \beta_{1003}) \quad (9)$$

$$2\ MA_3 + MB_3 \rightleftarrows 3\ MA_2B$$

$$\log \chi_{21} = 3 \log \beta_{1021} - (2 \log \beta_{1030} + \log \beta_{1003}) \quad (10)$$

Ces paramètres log χ_{rs} représentent le renforcement global de stabilité.

(b) Calcul du renforcement de stabilité Δ_{rs} compte tenu de l'effet statistique

$$\Delta_{rs} = \log \beta_{10rs(\text{exp})} - \log \beta_{10rs(\text{calc})} \quad (11)$$

où log $\beta_{10rs(\text{calc})}$ est obtenu à l'aide de l'éqn. (5).

(c) Enfin on peut appliquer la méthode de Sigel et McCormick[21] en calculant les constantes

$$\Delta \log K_{rs} = \log \beta_{10rs} - (\log \beta_{10r0} + \log \beta_{100s}) \quad (12)$$

Les valeurs probables de $\Delta \log K_{rs}$ sont négatives[21,22]. Pour une série de complexes du même type, lorsque le renforcement de stabilité croit, les valeurs de $\Delta \log K_{rs}$ augmentent et dans certains cas deviennent positives.

TABLEAU III

LA STABILITÉ DES ESPÈCES MIXTES

Système	*Espèces*	$\Delta \log K_{rs}$			$\log \chi_{rs}$			Δ_{rs}		
		1,1	*1,2*	*2,1*	*1,1*	*1,2*	*2,1*	*1,1*	*1,2*	*2,1*
Mn(II)–ASS–HQS	MAB	+0,64			3,21			1,30		
Mn(II)–Tiron–HQS	MAB	−0,67			0,89			0,14		
	MAB_2			−1,63		2,91			0,49	
	MA_2B			−0,92			5,04			1,20
	M(HA)B	+1,25								
	$M(HA)B_2$	+0,66								

Les résultats sont rassemblés dans le Tableau III. Tous les chiffres obtenus confirment la stabilisation des espèces mixtes vis-à-vis des espèces simples. Ces résultats ne portant que sur deux systèmes, nous nous bornerons à constater la forte

stabilisation mise en évidence d'une part pour l'espèce MAB dans le système manganèse(II)–acide sulfo-5 salicylique–acide hydroxy-8 sulfo-5 quinoléïne, et d'autre part des espèces MAB_2 et MA_2B dans le système manganèse(II)–Tiron–acide hydroxy-8 sulfo-5 quinoléïne. La stabilité déjà importante des complexes manganeux du Tiron et de l'acide hydroxy-8 sulfo-5 quinoléïne[15] peut donc être encore accrue par la chélation mixte.

Les valeurs positives de Δ_{rs} montrent que l'effet entropique ou statistique rend partiellement compte du renforcement de stabilité observé. D'autres facteurs (intra ou extra-moléculaires) discutés récemment par l'un d'entre nous[2] doivent être alors considérés pour expliquer cette stabilisation.

Nous remercions vivement le Professeur R. A. Pâris pour les conseils et l'aide précieuse qu'il nous a apportés dans la réalisation de ce travail.

RÉSUMÉ

Les auteurs présentent une étude détaillée de la formation de complexes mixtes ternaires dans les systèmes contenant des ions manganèse(II), l'acide hydroxy-8 sulfo-5 quinoléïne et l'acide sulfo-5 salicylique ou l'acide pyrocatéchol-disulfonique-3,5 (Tiron) en milieu $NaClO_4$ (1 *M*) et à la température de 25°C. Les données potentiométriques permettent la détection des complexes mixtes dont les constantes de stabilité ionique sont affinées par la méthode du "pit-mapping". La chélation mixte conduit dans tous les cas à un renforcement de la stabilité des complexes et cette stabilisation est exprimée suivant divers paramètres.

SUMMARY

A detailed examination of mixed-ligand chelate formation in systems containing manganese(II), 8-hydroxyquinoline-5-sulphonic acid and 5-sulphosalicylic acid or 3,5-pyrocatecholdisulphonic acid (Tiron), has been made at 25°C (1 *M* $NaClO_4$). Potentiometric data were used to detect mixed complexes (including protonated species) and their stability constants were refined by the "pit-mapping" treatment. Mixed coordination enhances the stability of complexes and the stabilization is expressed in terms of various parameters.

BIBLIOGRAPHIE

1 Y. Marcus et I. Eliezer, *Coord. Chem. Rev.*, 4 (1969) 273.
2 R. P. Martin, M. M. Petit-Ramel et J. P. Scharff in H. Sigel (Ed.), *Metal Ions in Biological Systems, Vol. 2*, M. Dekker, New York, 1973.
3 L. G. Sillen et A. E. Martell, *Stability Constants of Metal Ion Complexes*, The Chemical Society, London, 1964 et 1971.
4 D. Hopgood et R. J. Angelici, *J. Amer. Chem. Soc.*, 90 (1968) 2508.
5 J. Israeli et J. R. Çayouette, *Can. J. Chem.*, 49 (1971) 199.
6 J. Israeli et M. Cecchetti, *Can. J. Chem.*, 46 (1968) 3821.
7 J. Israeli et M. Cecchetti, *J. Inorg. Nucl. Chem.*, 30 (1968) 2709.
8 J. Israeli et M. Cecchetti, *Talanta*, 15 (1968) 1031.
9 D. L. Leussing et D. C. Shultz, *J. Amer. Chem. Soc.*, 86 (1964) 4846.
10 D. L. Leussing et K. Sunbai, *Anal. Chem.*, 40 (1968) 575.

11 A. S. Mildvan et M. Cohn, *Advan. Enzymol.*, 33 (1970) 1.
12 R. P. Martin et J. P. Scharff in D. R. Williams (Ed.), *An Introduction to Bioinorganic Chemistry*, C. C. Thomas, Springfield, 1975.
13 C. A. Tyson et A. E. Martell, *J. Amer. Chem. Soc.*, 94 (1972) 939.
14 M. T. Beck, *Chemistry of Complex Equilibria*, Van Nostrand, London, 1970.
15 J. P. Scharff et R. Genin, *Anal. Chim. Acta*, 78 (1975) 201.
16 L. G. Sillen, *Acta Chem. Scand.*, 16 (1962) 159.
17 N. Ingri et L. G. Sillen, *Ark, Kemi*, 23 (1964) 97.
18 R. P. Martin et M. Blanc, *Bull. Soc. Chim. Fr.*, 6 (1969) 1866.
19 M. Cromer-Morin, R. P. Martin et J. P. Scharff, *C.R. Acad. Sci. Paris*, 277 (1974) 1339.
20 V. S. Sharma et J. Schubert, *J. Chem. Educ.*, 46 (1969) 506.
21 H. Sigel et D. B. McCormick, *Chim. (Aarau)*, 21 (1967) 489.
22 H. Sigel et D. B. McCormick, *Accounts Chem. Res.*, 3 (1970) 201.
23 R. Genin et J. P. Scharff, *Bull. Soc. Chim. Fr.*, 7–8 (1974) 1307.
24 M. C. Bonnet et R. A. Pâris, *Bull. Soc. Chim. Fr.*, 2 (1966) 747.

Analytica Chimica Acta, 78 (1975) 219–223

SHORT COMMUNICATION

References standards for the electrometric determination, with ion-selective electrodes, of potassium and calcium in blood serum

A. K. COVINGTON and R. A. ROBINSON

Department of Physical Chemistry, University of Newcastle-upon-Tyne, Newcastle-upon-Tyne NE1 7RU (England)

(Received 19th February 1975)

The principal ionic constituents of blood plasma are[1] (in mol l^{-1}) 0.145 Na^+, 0.0042 K^+, 0.00125 Ca^{2+}, 0.0008 Mg^{2+} as cations with 0.103 Cl^- and 0.027 HCO_3^- as the principal anions. An exact ion balance is not indicated by these figures because of the presence of small amounts of sulphate, phosphate and ions of biological material. The pH of normal blood is 7.3–7.4 and its ionic strength is about 0.15 mol l^{-1}. Essentially it is a buffered, near neutral, solution of sodium chloride containing small amounts of K^+, Ca^{2+}, Mg^{2+} and HCO_3^-.

Most importance medically attaches to the potassium and calcium ion concentrations and their variations. Ion-selective electrodes responsive to either of these ions, with high selectivities for these ions over sodium ions, would be an important means of monitoring their concentrations (or activities) for medical or biochemical purposes. There are some indications[2] that electrodes with adequate selectivity over sodium ions can now be made, *e.g.* the tetrakis(chlorophenyl)borate[3] electrode for potassium and the alkyl calcium phosphonate electrode[4] for calcium ions. As in pH measurements, the analogous quantities $pK = -\log m_K \gamma_K$ and $pCa = -\log m_{Ca} \gamma_{Ca}$ could be determined electrochemically using the cells

K^+ electrode | X or S || ref. electrode

Ca^{2+} electrode | X or S || ref. electrode

if standards (S) for pK and pCa were established[5]. This cannot be done in a precisely similar manner to that adopted for pH standards for two principal reasons, one being the unique nature of the hydrogen ion and its relation to hydroxide ions and water, and the second being that a higher ionic strength is involved than the value of 0.1 which is reckoned to be the upper limit of applicability of the Bates–Guggenheim convention[6].

The standard solutions must conform to three criteria: (i) values of m_K and γ_{KCl} or of m_{Ca} and γ_{CaCl_2} must be readily measurable or capable of calculation from already available data; (ii) an extrathermodynamic convention is applicable to obtain γ_K and γ_{Ca} from the respective mean ionic activity coefficients; (iii) the residual liquid junction potential from the cells involving X and S must be negligible.

Blood plasma is a fairly complicated electrolyte and, to make progress, some

simplification is necessary. It seems reasonable to a first approximation to regard blood plasma as a three cation– one anion mixture (Na^+, K^+, Ca^{2+}, Cl^-), whose principal component is NaCl. It is then necessary to ask what information is available about the specific interactions of ions in such a mixture, and whether these are important to the problem of establishing pH and pCa standards.

The binary salt systems NaCl+KCl, NaCl+$CaCl_2$, KCl+$CaCl_2$ have been studied[7–10]. The last two are very similar in behaviour and, because of the low concentrations of potassium and calcium ions involved, it is justifiable to neglect K^+–Ca^{2+} interactions, and to treat the problem of pK and pCa standards separately in terms of the two first mentioned systems at an ionic strength rounded to 0.15 mol kg^{-1}.

From the Guggenheim–Scatchard–Robinson treatment[11] of mixed electrolyte solutions, we have for the activity coefficient of KCl in the presence of NaCl (γ_{KCl}) compared with its value in pure KCl solutions (γ^0_{KCl}):

$$2\ln(\gamma_{KCl}/\gamma^0_{KCl}) = [2(\phi^0_{NaCl}-\phi^0_{KCl})+b_{01}I+b_{02}I^2]y-\tfrac{1}{2}b_{02}I^2y^2$$

where b_{01}, b_{02} are interaction parameters, ϕ^0_{NaCl}, ϕ^0_{KCl} are osmotic coefficients for the pure electrolytes at the same ionic strength as the mixture (I), and $y=m_{Na}/I$ is a mixture fraction.

Values of $b_{01}=-0.0253$, and $b_{02}=-0.0030$ have been calculated by Rush[12] from the data of Robinson[7]. Also[13], $\phi^0_{NaCl}-\phi^0_{KCl}=0.0086$. Thus for a solution containing 0.1462 mol NaCl kg^{-1} and 0.0042 mol KCl kg^{-1} with $y=0.9720$, *i.e.* the same as in blood serum, we have

$$\log \gamma_{KCl}/\gamma^0_{KCl} = 0.0028$$

It can be concluded from this that only a small error would ensue from taking for γ_{KCl} in blood plasma that for KCl in a solution of molality equal to the ionic strength (0.15) of blood plasma.

Similarly for a solution of 0.1462 mol NaCl kg^{-1} and 0.00126 mol $CaCl_2$ kg^{-1}

$$\ln(\gamma_{CaCl_2}/\gamma^0_{CaCl_2}) = [2(\phi_{NaCl}-1)-(\phi_{CaCl_2}-1)+b_{01}I+b_{02}I^2]y-\tfrac{1}{2}b_{02}I^2y^2$$

This equation has a slightly different form from the previous one because of the different valence types of the ions concerned. Values of $b_{01}=0.0703$ and $b_{02}=-0.0225$ are available from the analysis of Rush[9] of the data of Bower and Robinson[8]; and[14] $\phi^0_{NaCl}=0.928$, $\phi^0_{CaCl_2}=0.863$; and $y=m_{Na}/I=0.9747$.

Then,

$$\log \gamma_{CaCl_2}/\gamma^0_{CaCl_2} = 0.0017$$

and again little error would ensue from taking the activity coefficient of calcium chloride in blood plasma as equal to $\gamma^0_{CaCl_2}$ in pure calcium chloride at an ionic strength of 0.15 mol kg^{-1}. These conclusions are a result, not of the fact that the specific ion interactions are small, but of the fact that the ionic strength is low and the mixture fraction high; the solution is effectively 0.15 mol NaCl kg^{-1}.

To proceed requires a convention for single ionic activity coefficients. For solutions of single electrolytes, this problem has been treated by Bates, Staples and Robinson[15] who utilised the Stokes–Robinson hydration approach[16]. Values

for pCa and pK at 25°C for single electrolytes have been tabulated by Covington[2] but these are not appropriate here.

At $I=0.15$ mol kg^{-1}, for pure NaCl solution, we have[15]

$$\log \gamma_{Cl} = \log \gamma_{NaCl} - 0.00782\, hm\phi = -0.1251$$

where h is the hydration number ($=3.5$) of sodium chloride. It is interesting to note that if the Bates–Guggenheim convention[6] is adopted instead, the value is identical. If this value for γ_{Cl} is taken as appropriate for the mixed electrolyte at $I=0.15$ mol kg^{-1}, and

$$\log \gamma_K = 2 \log \gamma_{KCl} - \log \gamma_{Cl} = -0.1267$$

is calculated using an interpolated value for $I=0.15$ of $\log \gamma_{KCl} = -0.1287$, and

$$\log \gamma_{Ca} = 3 \log \gamma_{CaCl_2} - 2 \log \gamma_{KCl} = -0.4596$$

is calculated using an interpolated value for $I=0.15$ of $\log \gamma_{CaCl_2} = -0.2365$, then

$$pK = -\log m_K \gamma_K = 2.377 + 0.127 = 2.504$$

and

$$pCa = -\log m_{Ca} \gamma_{Ca} = 2.900 + 0.460 = 3.360\,.$$

The error from taking γ^0_{KCl}, $\gamma^0_{CaCl_2}$ instead of γ_{KCl} or γ_{CaCl_2} is not more than 0.003 in pK or pCa.

A second approach is to explore the possibility of using a single standard solution for both pK and pCa containing 0.1422 mol NaCl kg^{-1}, 0.0041 mol KCl kg^{-1} and 0.00122 mol $CaCl_2$ kg^{-1}. Such a solution has the three cations present in the same ratio as they are present in blood serum and the total ionic strength is again 0.15 mol kg^{-1}. For the activity coefficient of KCl in the mixture, the treatment of Reilly, Wood and Robinson[17] yields the equation:

$$\ln \gamma_{KCl}/\gamma^0_{KCl} = 0.9480(1-\phi^0_{NaCl}) + 0.0122(1-\phi^0_{CaCl_2}) - 0.9727(1-\phi^0_{KCl})$$

The numerical factors arise from the relative amounts of Na^+, K^+ and Ca^{2+} in the solution and the charges on the ions (mixture fractions taking valence differences into account). When the osmotic coefficients given above are used, then:

$$\ln \gamma_{KCl}/\gamma^0_{KCl} = 0.0084\,.$$

The corresponding equation for $CaCl_2$ is

$$\ln \gamma_{CaCl_2}/\gamma^0_{CaCl_2} = 0.9756(1-\phi^0_{CaCl_2}) - 1.896(1-\phi^0_{NaCl}) - 0.0546(1-\phi^0_{KCl}) = -0.0061$$

But these equations omit the effect of specific ionic interactions. Again all but the Na–K^+ and Na^+–Ca^{2+} interactions, respectively, can be ignored in calculating γ_{KCl} and γ_{CaCl_2}. Interpolation from the available data[8,9] yields:

$$\ln \gamma_{KCl}/\gamma^0_{KCl} = 0.0084 - 0.0019 = 0.0065$$

$$\ln \gamma_{CaCl_2}/\gamma^0_{CaCl_2} = -0.0061 + 0.0100 = 0.0039$$

If it is assumed again, since the concentration of NaCl is relatively high, that the single ion activity coefficient γ_{Cl} in this mixture is equal to that in a pure NaCl solution of 0.15 mol kg^{-1} ionic strength, then the equation of Bates, Staples and Robinson[15] yields:

$$\log \gamma_{Cl} = -0.1251$$

Hence

$$\log \gamma_{K} = -0.1259$$

using the same interpolated value for $\log \gamma_{KCl}$ as before, so

$$pK = 2.514$$

and $\log \gamma_{Ca} = -0.4596$

using the previously interpolated value for $\log \gamma_{CaCl_2}$ at $I = 0.15$ mol kg^{-1}, so

$$pCa = 3.373$$

Conclusions

The following solutions are proposed for the electrometric determination of potassium and calcium ions in blood serum, each having an ionic strength of 0.15 mol kg^{-1}:

(1) 0.1458 mol NaCl kg^{-1} + 0.0042 mol KCl kg^{-1} (or on a molarity basis 0.1450 mol NaCl l^{-1} + 0.0042 mol KCl l^{-1}) with pK = 2.504;

(2) 0.1462 mol NaCl kg^{-1} + 0.00126 mol $CaCl_2$ kg^{-1} (or on a molarity basis 0.1454 mol NaCl l^{-1} + 0.00126 mol $CaCl_2$ l^{-1}) with pCa = 3.360;

(3) 0.1422 mol NaCl kg^{-1} + 0.0041 mol KCl kg^{-1} + 0.00122 mol $CaCl_2$ kg^{-1} (on a molarity basis 0.1414 mol NaCl l^{-1} + 0.0041 mol KCl l^{-1} + 0.00121 mol $CaCl_2$ l^{-1}), with pK = 2.514 and pCa = 3.373 (also pNa = 0.966).

These solutions all meet the criteria laid down earlier in this communication, and in particular (iii) is likely to be accurately met since the ionic strength of the standards is closely matched to that of blood serum. This is especially important since for the measurement of potassium ions the usual saturated KCl–calomel reference electrode system cannot be employed without the use of an intermediate salt bridge for fear of leakage of potassium ions into the sample. Ammonium nitrate is not an acceptable intermediate bridge as electrodes may show poor selectivity for K^+ over NH_4^+. It may therefore not be possible to find an equitransferent bridge electrolyte, hence, unless the ionic strength is closely matched, residual liquid junction potentials could be sizeable.

It remains to be seen whether these solutions are useful standards in practice, and whether it is justifiable to ignore, as has been done here the effects of the hydrogen carbonate and magnesium ion contents of blood plasma.

REFERENCES

1 S. P. Datta and J. H. Ottaway, *Biochemistry*, Boulliere, Tindall and Cassell, London, 2nd edn., 1969, p. 282.
2 A. K. Covington, *CRC Crit. Rev. Anal. Chem.*, 3 (1973) 356.
3 W. M. Wise, M. J. Kurey and G. Baum, *Clin. Chem.*, 16 (1970) 103.
4 E. W. Moore in R. A. Durst (Ed.), *Ion Selective Electrodes*, NBS Spec. Publ. 314, 1969.
5 R. G. Bates and M. Alfenaar in R. A. Durst (Ed.), *Ion Selective Electrodes*, NBS Spec. Publ. 314, 1969.
6 R. G. Bates and E. A. Guggenheim, *Pure Appl. Chem.*, 1 (1960) 163.
7 R. A. Robinson, *J. Phys. Chem.*, 65 (1961) 662.

8 V. E. Bower and R. A. Robinson, *J. Res. Nat. Bur. Stand.*, 70A (1966) 313.
9 R. M. Rush, *ORNL Report 4402*, 1969.
10 R. A. Robinson and A. K. Covington, *J. Res. Nat. Bur. Stand.*, 72A (1968) 239.
11 H. S. Harned and R. A. Robinson, *Multicomponent Electrolyte Solutions*, Pergamon, Oxford, 1968, pp. 17–22.
12 R. M. Rush and R. A. Robinson, *J. Tenn. Acad. Sci.*, 45 (1968) 22.
13 R. A. Robinson and R. H. Stokes, *Electrolyte Solutions*, Butterworths, 1965, 2nd edn., App. 8.3.
14 H. G. McLeod and A. R. Gordon, *J. Amer. Chem. Soc.*, 68 (1946) 58.
15 R. G. Bates, B. R. Staples and R. A. Robinson, *Anal. Chem.*, 42 (1970) 867.
16 R. H. Stokes and R. A. Robinson, *J. Amer. Chem. Soc.*, 70 (1948) 1870.
17 P. J. Reilly, R. H. Wood and R. A. Robinson, *J. Phys. Chem.*, 75 (1971) 1305 (eqn. A-9).

Analytica Chimica Acta, 78 (1975) 224–226

SHORT COMMUNICATION

The colorimetric determination of titanium in chromites

A. J. EASTON

Department of Mineralogy, British Museum (Natural History) London SW7 5BD (England)

(Received 10th January 1975)

Colorimetric methods for the determination of titanium have been based on the complexes with hydrogen peroxide and tiron (1,2-dihydroxybenzene-3,5-disulphonic acid)[1,2], the latter being more sensitive. Chromium also forms a coloured complex with tiron and so interferes with the determination of titanium[2,3]. The ratio of chromium (as Cr_2O_3) to titanium (as TiO_2) in chromite is[4] of the order of 100:1. Several schemes for the separation of titanium from chromium before the determination of titanium have been proposed including electrolysis and precipitation[5], but these separations are lengthy.

The quantity of titanium suitable for measurement in chromites corresponds to 0.5–2.0 p.p.m. of TiO_2 in a solution which would also contain about 100 p.p.m. iron (as Fe_2O_3) and up to 250 p.p.m. chromium (as Cr_2O_3). Titanium forms[6] two distinct yellow complexes with tiron in the pH ranges 2.0–4.0 and 4.3–9.6. The latter range is most frequently used when titanium is determined in silicates[7] and has a slightly higher molar absorptivity; the interference of small quantities of the iron(III)–tiron complex (purple) is almost eliminated by addition of some sodium dithionite to the final solution, but when larger amounts of iron (*e.g.* 300 p.p.m.) are present, it is necessary to add EDTA (disodium salt) to the acid solution before the pH adjustment and addition of sodium dithionite[8]. If more than 3 p.p.m. chromium(III) is present in solution[9], a greenish-blue coloration is produced which the addition of EDTA does not prevent.

It was found that the interference caused by 250 p.p.m. chromium was much less in the pH range 2.0–4.0 than in the pH range 4.3–9.6. That of 100 p.p.m. iron was almost eliminated by adding ascorbic acid to the aliquot before the tiron. The spectral curves of the complexes formed by iron, chromium and titanium with tiron at pH 3.0 are shown in Fig. 1: the absorbances are additive. It can be seen that the best wavelength for measuring the titanium–tiron complex is 360 nm (near maximum absorption) where the absorption of the chromium–tiron complex is at a minimum; iron shows only a minor variation over the spectral scan. A pH value of 3.0 ± 0.2 has been recommended for development of the titanium–tiron complex[6]; at this pH the absorbance of the chromium–tiron complex was found to increase on standing, almost doubling during the first 30 min of development. It is therefore advantageous to measure the absorbance of the solution after the minimal time required to adjust the pH and volume. The absorbance of the complex increased rapidly with pH, hence strict adherence to the pH value 3.0 ± 0.2 is necessary. The pH was adjusted with a solution of ammonium acetate, which had to be added

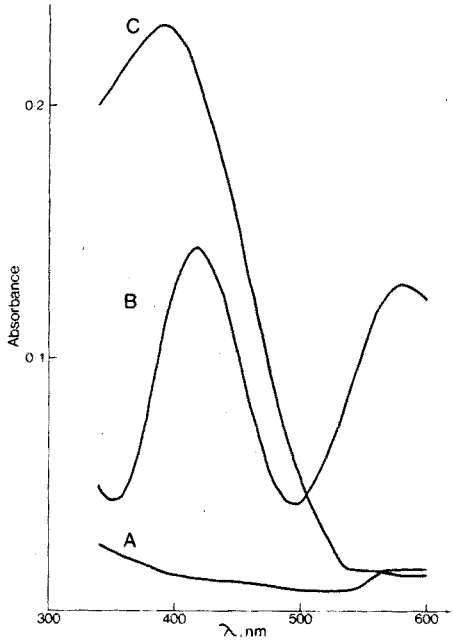

Fig. 1. Spectral curves for tiron complexes at pH 3.0 (with ascorbic acid): A, 100 p.p.m. iron (Fe_2O_3); B, 300 p.p.m. chromium (Cr_2O_3); C, titanium 0.6 p.p.m. (TiO_2).

dropwise while swirling, in order to avoid local formation of the chromium–tiron complex at higher pH. Consistent absorbance readings were obtained provided that the above conditions were observed, and correction curves were constructed for iron and chromium under similar conditions. When the titanium content of a chromite sample was 0.5%, the combined correction for iron and chromium was only about 5% of the total absorbance reading.

Experimental

Potassium hydrogensulphate solution. 20% (w/v) solution of potassium hydrogensulphate in 2.4 *M* hydrochloric cid.

Standard titanium solution (0.01 mg TiO_2 ml^{-1}). Fuse 0.01 g ±0.0001 of Specpure titanium dioxide with 2 g of analytical reagent potassium hydrogensulphate in a 50-ml platinum crucible, cool and dissolve the fusion cake in 200 ml of 0.5 *M* sulphuric acid, heating until a clear solution is obtained. Adjust the volume to 1 l.

Standard chromium solution (2.5 mg Cr_2O_3 ml^{-1}) and iron solution (5.0 mg Fe_2O_3 ml^{-1}) are also needed.

Procedure. Fuse 100 mg of chromite or chrome ore with 4 g of potassium hydrogensulphate in a platinum crucible, cool and dissolve the fusion cake in 4 ml of 11 *M* hydrochloric acid and hot water. Transfer the solution to a 50-ml volumetric flask and adjust to volume with water. Place a 5-ml aliquot in a 40-ml beaker, add 2 ml of freshly prepared and filtered aqueous 5% (w/v) ascorbic acid solution, swirl to mix and add 2 ml of filtered aqueous 5% (w/v) tiron solution. Using a pH meter, adjust the pH to 3.0±0.2 by dropwise addition of aqueous 8% (w/v)

ammonium acetate solution. Rinse the glass electrode with a little water, transfer the solution to a 25-ml volumetric flask, and adjust to volume with water. Measure the absorbance at 360 nm against a reagent blank in 20-mm cells after a fixed interval, *e.g.* 5 min from the addition of the tiron.

Prepare correction curves for the interferences of iron (0–100 p.p.m. Fe_2O_3) and chromium (0–300 p.p.m. Cr_2O_3) by mixing aliquots of the standard solutions with 2 ml of a 20% (w/v) potassium hydrogensulphate solution in 2.4 *M* hydrochloric acid, and proceeding as above, starting with the addition of ascorbic acid. Read the absorbances corresponding to the quantities of iron and chromium in the sample aliquot from the correction curves and deduct this from the total absorbance of the sample. Compare the remaining absorbance with the absorbances obtained by similar treatment of aliquots of the standard titanium solution mixed with 2 ml of the potassium hydrogensulphate solution.

Conclusion

The method given for the determination of titanium in the presence of iron and chromium allows the development of the titanium–tiron complex under conditions which reduce interferences to a minimum. Corrections can be applied to eliminate the interferences entirely.

REFERENCES

1 J. H. Yoe and A. R. Armstrong, *Anal. Chem.*, 19 (1947) 100.
2 E. B. Sandell, *Colorimetric Determination of Traces of Metals*, Interscience, New York, 3rd edn., 1959, p. 875.
3 A. J. Easton, *Chemical Analysis of Silicate Rocks*, Elsevier, Amsterdam, 1st edn., 1972, p. 114.
4 R. E. Stevens, *Amer. Mineral.*, 29 (1944) 1.
5 S. A. Bilgrami and C. O. Ingamells, *Amer. Mineral.*, 45 (1960) 576.
6 P. N. R. Nichols, *Analyst (London)*, 85 (1960) 452.
7 L. Shapiro and W. W. Brannock, *U.S. Geol. Surv., Bull.*, 1036-C (1956) 36.
8 A. J. Easton, *Anal. Chim. Acta*, 29 (1963) 52.
9 A. A. Moss, unpublished results.

Analytica Chimica Acta, 78 (1975) 227–230

SHORT COMMUNICATION

Kinetic spectrophotometric determination of chloride and bromide at low concentrations

E. MENTASTI and E. PELIZZETTI
Istituto di Chimica Analitica, Università di Torino, Torino (Italy)
(Received 21st January 1975)

Thallium(III) has not received much attention as an analytical reagent, although several equilibrium and kinetic studies have been reported[1,2]. The formal reduction potential of the Tl(III)/Tl(I) couple is 1.25 V (in 1 *M* perchloric acid) and its behaviour as an oxidant for inorganic and organic substrates suggests the possibility of analytical applications because of the high rates of reaction. Thallium(III) oxidations have been compared with the oxidations effected by Hg(II) and Pb(II), and both selectivity and speed show a trend favourable to thallium(III)[3].

Thallium(III) oxidizes 4,4′-dihydroxydiphenyl (DHDP) quantitatively to diphenoquinone (DPQ) with assessed kinetics and a known stoichiometry[4] according to the reaction:

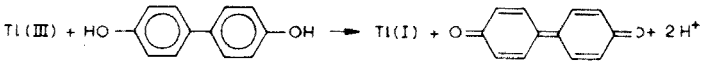

(1)

Reaction (1) is now proposed for the determination of chloride and/or bromide at low concentrations (10^{-4}–10^{-6} *M*). Chloride and bromide give with thallium(III) in excess a strong 1:1 complex[5], which does not oxidize DHDP to DPQ; this gives the basis for a kinetic and a simple spectrophotometric method for the determination of these anions.

Kinetic method

When a solution of DHDP is mixed with a solution of thallium(III) in excess, both at the same acidity (0.10 *M* perchloric acid) and temperature (25.0°C), in a stopped-flow spectrophotometer, an increase of absorbance at 399 nm (maximal absorption of DPQ, $\varepsilon = 3.47 \cdot 10^4$ l mol^{-1} cm^{-1}, the only absorbing species at this wavelength) can be observed and equilibrium is reached in about 1 min. If thallium(III) is in large excess with respect to DHDP, a pseudo-first-order kinetic dependence is observed:

$$\ln\left(\frac{A_{eq} - A}{A_{eq}}\right) = k_{obs} \cdot t \qquad (2)$$

where A is the absorbance at time t, and A_{eq} is the absorbance at equilibrium ($A_{eq} = \varepsilon_{DPQ}[DPQ] = \varepsilon_{DPQ}[DHDP]_{init}$). A plot of the left-hand side of eqn. (2) as a function of time gives k_{obs}, which depends linearly (at constant acidity and temperature) on the concentration of thallium(III) in excess. If chloride or bromide ions are added to thallium(III), k_{obs} decreases linearly through subtraction of the oxidizing species. Figure 1 shows the results of kinetic determinations of chloride and bromide obtained from a series of kinetic runs performed with constant thallium(III) and DHDP concentration and increasing amounts of chloride or bromide; extrapolation to zero rate corresponds to an anion addition equivalent $[Tl(III)]_{tot}$, thus determining the units on the X-axis.

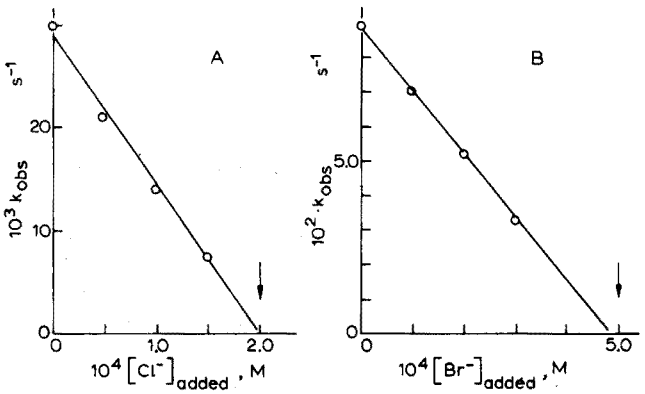

Fig. 1. Plots of k_{obs} as a function of $[X^-]_{added}$ (see text) for the reaction Tl(III)–DHDP. $[HClO_4] = 0.10$ M, $t = 25.0°C$. (A) $[Tl(III)]_{tot} = 2.0 \cdot 10^{-4}$, $[DHDP] = 1.0 \cdot 10^{-5}$ M; (B) $[Tl(III)]_{tot} = 5.0 \cdot 10^{-4}$, $[DHDP] = 1.0 \cdot 10^{-5}$ M.

Spectrophotometric method

The high molar absorptivity of DPQ and the inhibition of the oxidation of DHDP by the halide–Tl(III) complex gives an indirect spectrophotometric determination of chloride and/or bromide. A known amount of thallium(III) is added to a volumetric flask together with an aliquot of chloride or bromide solution; DHDP is then added in excess with respect to thallium(III). (The DHDP and standard thallium(III) solutions are acidified previously with perchloric acid so that they contain not less than 0.1 M). Again a rapid increase in absorbance at 399 nm is observed; the absorbance is read when equilibrium is attained (maximum absorbance), *i.e.* about 1 min after mixing at $[H^+] = 0.1$ M (acidity depresses the rate) and $[DHDP] \simeq 5 \cdot 10^{-4}$ M. Some results are given in Table I. The decomposition of DPQ is much slower and has no influence on the results. The unknown anion concentration $[X^-]$ is given by: $[X^-] = [Ti(III)]_{tot} - A/\varepsilon_{DPQ}$.

In both methods, $[X^-]$ must be less than $[Tl(III)]$ which, in turn in the spectrophotometric method is less than [DHDP]. Thus the spectrophotometric method is more sensitive (10 ml containing $5 \cdot 10^{-4}$ mg ml^{-1} of chloride can be easily detected), whereas the kinetic method gives more accurate determinations which are not influenced by the instability of DPQ. The standard deviation of the single k_{obs} values, calculated by a weighted least-squares method[6], was 1–2%.

TABLE I

SPECTROPHOTOMETRIC DETERMINATION OF CHLORIDE AND BROMIDE WITH THE Tl(III)–DHDP REACTION

([DHDP] = $5 \cdot 10^{-4}$ *M*; [$HClO_4$] = 0.1 *M*; methanol, 25% (v/v); pathlength, 1.00 cm.)

Total Tl(III) added ($\cdot 10^{-5}$ *M*)	X^- *added* ($\cdot 10^{-5}$ *M*)	A_{399} *nm*	X^- *found* ($\cdot 10^{-5}$ *M*)	*Error (%)*
Chloride				
3.0	1.0	0.67	1.07	+ 7
4.0	2.0	0.75	1.84	− 8
3.0	2.0	0.31	2.11	+ 6
4.0	1.5	0.89	1.44	− 4
2.0	0.50	0.50	0.56	+12
2.0	1.0	0.37	0.94	− 6
2.0	1.5	0.22	1.37	− 4
5.0	2.5	0.85	2.56	+ 2
5.0	3.0	0.62	3.22	+ 7
5.0	3.5	0.55	3.42	− 2
1.5	0.50	0.35	0.50	—
1.5	1.0	0.20	0.92	− 8
Bromide				
3.0	1.0	0.72	0.92	− 8
3.0	2.0	0.32	2.08	+ 4
4.0	2.0	0.68	2.08	+ 4
4.0	2.5	0.52	2.50	—
4.0	3.0	0.37	2.93	− 2
5.0	3.0	0.74	2.86	− 5
5.0	4.0	0.40	3.84	− 4

The weights were taken to be inversely proportional to the error in $(A_{eq} - A)$ (about ten $A = f(t)$ readings were taken for each run). The error in the determination, arising from the uncertainty in k_{obs}, was within ±4% for a kinetic determination (four runs); in the spectrophotometric method, the standard deviation was calculated as ±6%.

Reagents

Thallium(III) perchlorate was prepared by dissolution of Tl_2O_3 in hot 60% perchloric acid, and standardized either iodimetrically or by EDTA titration (PAN indicator, acetate buffer). Thallium perchlorate is stable in light and air, and is easily crystallized from aqueous acid solution. DHDP solutions were prepared by dissolving weighed amounts in a few drops of dilute sodium hydroxide, to which was added aqueous perchloric acid (0.10 *M*). Such solutions were stable for several weeks. More concentrated acidic stock solutions, for the spectrophotometric method, were prepared with 50% (v/v) methanol which was shown to have no effect on the absorption or the determination.

Interferences

Nitrate and sulphate (100-fold) do not interfere, but iodide, thiocyanate,

sulphite, thiosulphate, and species which oxidize DHDP or reduce thallium(III) interfere seriously.

REFERENCES

1 T. J. Kemp in C. H. Bamford and C. F. H. Tipper (Eds.), *Comprehensive Chemical Kinetics, Vol. 7*, Elsevier, New York, 1972, pp. 329–353.
2 E. Mentasti, E. Pelizzetti and E. Pramauro, *J. Inorg. Nucl. Chem.*, in the press; E. Pelizzetti, E. Mentasti and E. Pramauro, *Gazz. Chim. Ital.*, 105 (1975) 403.
3 R. J. Ouelette, D. Miller, A. South Jr. and R. D. Robins, *J. Amer. Chem. Soc.*, 91 (1969) 971.
4 E. Pelizzetti, E. Mentasti, C. Baiocchi and M. E. Carlotti, *Atti Accad. Sci. Torino*, 108 (1973–1974).
5 S. Ahrland and L. Johansson, *Acta Chem. Scand.*, 18 (1964) 2125.
6 G. Giraudi, E. Mentasti and E. Pelizzetti, *Atti Accad. Sci. Torino*, 108 (1973–1974).

Analytica Chimica Acta, 78 (1975) 231–233

SHORT COMMUNICATION

The extraction of osmium with tributyl phosphate and photometric determination with thiourea

S. KALYANARAMAN and S. M. KHOPKAR
Department of Chemistry, Indian Institute of Technology, Bombay-400076 (India)
(Received 18th December 1974)

Methods for the solvent extraction of osmium have been summarized recently[1,2]. In later work, methyl isobutyl ketone has been used for the separation of osmium from ruthenium in bromide media[3]; this extraction has been followed by a colorimetric determination with thiourea[4]. Of the chromogenic reagents for osmium, thiourea[5,6] is usually preferred, the complex, $[Os(NH_2CSNH_2)_6]^{3+}$, being extracted[7] into chloroform and measured at 480 nm.

Attempts have been made to extract osmium with tributyl phosphate (TBP) and other solvents from highly acidic media[8], but the extraction has not been systematically studied. The method proposed below is relatively simple, and allows a separation of osmium from some other platinum group elements. Osmium is extracted with TBP from 1–2 *M* hydrochloric acid, and determined photometrically as its complex with thiourea at 480 nm.

Experimental

Apparatus. A type FEK-57 filter photometer and a Perkin-Elmer 402 spectrophotometer with matched 10-mm quartz cells were used.

Stock solution of osmium. A solution of osmic acid (Arora–Matthew, India) in distilled water, was standardized[9] and suitable diluted. The working solution contained 138.3 μg Os ml^{-1}.

General procedure. To an aliquot of solution containing 0.12–1.2 mg of osmium, add *ca.* 1 ml of 5% (w/v) sodium sulphite to reduce osmium to the quadrivalent state, and enough hydrochloric acid to give a 1.5 *M* concentration in a final volume of 25.0 ml. Leave for 10 min to ensure complete reduction. Transfer to a separatory funnel, add 10 ml of 100% TBP (3.66 *M*), and shake vigorously for 5 min. Allow the phases to settle, withdraw the aqueous phase, and shake again with 10 ml of TBP. Combine the organic phases and shake with 10 ml of water containing 1 ml of perchloric acid (60%) and 1 ml of 5% (w/v) thiourea for 3 min. Carefully withdraw the organic phase, heat for 10 min in a boiling water bath to ensure complete colour development, and cool. Measure the absorbance of the violet osmium–thiourea complex against a reagent blank at 480 nm.

Results and discussion

The absorption spectrum of the solution of osmium–thiourea complex in tributyl phosphate showed a broad absorption band at 480 nm where the reagent blank did not absorb. The molar absorptivity was $1.8 \cdot 10^3$ at 480 nm on the basis of osmium content.

The effects of varying the hydrochloric acid concentration from 0.25 to 2 *M* and the concentration of TBP from 25 to 100% (0.915–3.66 *M*) with toluene as the diluent, were studied. Quantitative extraction of osmium was possible only from 1–2 *M* hydrochloric acid with 100% TBP, the distribution ratios exceeded $2.5 \cdot 10^3$); with 75% TBP from 1–2 *M* acid, the extraction was only 61%, and with 100% TBP from 0.8 *M* acid, extraction was only 80%. The volume of perchloric acid added was not critical.

An attempt was made to ascertain the probable composition of the extractable species from the plot of log *D* *vs.* log[TBP]; the slope at 1.5 *M* hydrochloric acid was 1.88, hence the extracted species is probably $H_2[OsCl_6(TBP)_2]$.

The chlorides of lithium, magnesium, ammonium and aluminium (0.5–2 *M*) were examined as salting-out agents in 1.5 *M* hydrochloric acid solutions, but caused no significant improvement in the extraction.

The period of equilibration during the extraction with TBP and during colour development with thiourea was varied from 1 min to 20 min; in both cases the optimal time was 5 min.

The concentration of the thiourea solution was varied between 1 and 20%; 1 ml of aqueous 5% (w/v) thiourea solution in a total volume of 10 ml was adequate for full colour development. The effect of varying time (10–30 min) and temperature (25–100°C) on the colour development was studied. Complete development was obtained at 60°C after 10 min, or at 100°C after 5 min. The absorbance of the coloured complex was stable for at least 96 h at room temperature.

When the general procedure was applied, Beer's law was obeyed over the concentration range 5–48 μg Os ml^{-1} at 480 or 540 nm, the latter wavelength providing lower sensitivity. At 480 nm, the Sandell sensitivity index was 0.1 μg cm^{-2}. The standard deviation at the 20 μg Os ml^{-1} level was 1.1% (20 determinations).

Effect of diverse ions. The tolerance limit was taken as the amount of ion which caused an error of less than ± 10%. The amount of osmium used for all tests was 415 μg. Calcium, potassium, magnesium, lithium, nitrate and sulphate ions were tolerated in weight ratios of 1 : 1000. Rubidium and chloride were tolerated at ratios of 1 : 500; acetate, oxalate, tartrate and EDTA at ratios of 1 : 250; beryllium, copper, chromium(III) or (VI) strontium, thorium, citrate, and malonate at ratios of 1 : 25; and aluminium, bismuth, cadmium, cobalt, caesium, iron(III), germanium, mercury (II), manganese, nickel, lead, titanium (IV), uranium (VI), zinc, zirconium, arsenate, molybdate, perrhenate, vanadate, tungstate, fluoride and phosphate at ratios of 1 : 10. Strong interferences were found from ruthenium, palladium, antimony, tellurite, ascorbic acid, bromide, iodide, nitrite, thiocyanate and thiosulphate. Interferences of larger amounts of some of the ions were eliminated by masking; e.g. vanadium, molybdenum and copper were masked with tartaric acid, iron with EDTA, and manganese with oxalate.

Separation from other platinum metals. Although palladium (II) and ruthenium (III) interfered at all levels, it was possible to separate osmium from rhodium, iridium

and platinum. The separation of osmium from other elements at ratios of 1 : 2 to 1 : 10 is shown in Table I. The procedure for separation was the same as the general procedure described for osmium. Platinum and rhodium were determined in the aqueous phase by the tin (II) chloride procedure[10]; iridium was determined by the TTA method[11]. It was possible to analyze binary and quaternary mixtures.

TABLE I

SEPARATION OF OSMIUM FROM IRIDIUM, RHODIUM AND PLATINUM

Taken (μg)				*Found (μg)*			
Os	*Ir*	*Rh*	*Pt*	*Os*	*Ir*	*Rh*	*Pt*
415	3860	3000	4400	414	3783	2940	4307
415	1930	1500	3080	414	1914	1462	2987
415	865	750	1056	411	856	742	1013

REFERENCES

1 A. K. De, S. M. Khopkar and R. A. Chalmers, *Solvent Extraction of Metals*, Van Nostrand-Reinhold, London, 1970, pp. 88, 98.
2 A. V. Rangnekar and S. M. Khopkar, *Bull. Chem. Soc. Jap.*, 41 (1968) 600.
3 E. W. Berg and H. E. Moselay, *Anal. Chim. Acta*, 47 (1969) 360.
4 K. Hayashi, Y. Sakaki and M. Masuda, *Jap. Anal.*, 21 (6) (1972) 793.
5 E. B. Sandell, *Ind. Eng. Chem., Anal. Ed.*, 9 (1937) 421.
6 G. H. Ayres and W. N. Wells, *Anal. Chem.*, 22 (1950) 317.
7 R. D. Sauerbrunn and E. B. Sandell, *J. Amer. Chem. Soc.*, 75 (1953) 3554.
8 H. Meier, F. Zimmerhacke, W. Albrecht, D. Bosche, W. Hecker, P. Menge, A. Ruckdeschel, E. Unger and G. Zeitler, *Mikrochim. Acta*, (1969) 557.
9 A. K. De, *Separation of Heavy Metals*, Pergamon, London, 1961, p. 237.
10 E. B. Sandell, *Colorimetric Determination of Traces of Metals*, Interscience, London, 1959, pp. 726, 769.
11 A. V. Rangnekar and S. M. Khopkar, *Chemist-Analyst*, 56 (1967) 84.

Analytica Chimica Acta, 78 (1975) 234–237

SHORT COMMUNICATION

The determination of sulphur in organic compounds. A reinvestigation of the potassium fusion method

A. D. CAMPBELL, M. J. BROWN and D. J. HANNAH
Department of Chemistry, University of Otago, Dunedin (New Zeland)
(Received 17th February 1975)

Although decomposition in an oxygen flask is now used extensively for the routine determination of sulphur in organic compounds[1], unsatisfactory results are given in the presence of many metals which occur in metal–organic complexes; ion exchange clean-up procedures are tedious and not always appropriate. After a preliminary investigation of several alternative procedures, the Bürger–Zimmermann potassium fusion method[2,3] was selected for detailed study as it incorporates a distillation stage which could separate the sulphur from interfering elements. The sample is decomposed by fusion with potassium in a sealed tube; the hydrogen sulphide obtained on acidification of the fusion mixture is distilled into buffered cadmium acetate, and determined by reaction with an excess of iodine.

Preliminary investigations

Accurate analyses require quantitative conversion of sulphur to sulphide, and methods[3,4] in which the sample is fused with potassium in a flame require considerable skill and judgement. To ensure that the fusion process was reproducible, samples were heated with potassium in a sealed tube at 480 ± 20°C for 20 h in a metal block. Prolonged heating at higher temperatures, *e.g.* 520°C, gave low results, probably through fusion of the sulphide into the pyrex sample tubes. Although short fusion times, *e.g.* 2 h, were unsatisfactory, particularly with inorganic samples, satisfactory results were obtained when a continuous mirror of metallic potassium formed completely over the inside of the fusion tube. Slightly low results were obtained initially for inorganic salts *e.g.* copper sulphate, but the addition of *ca.* 5 mg of anthracene or indulin base rectified this. Small amounts of sucrose were unsatisfactory, probably because the resulting char occluded sulphide.

The distillation process was investigated using weighed amounts of silver sulphide as the sample. Oxygen-free nitrogen, as suggested by Debal and Lévy[4], was a satisfactory carrier gas. The absorption and titration of hydrogen sulphide has been the subject of several investigations[5,6]. Although Zimmermann[3] obtained satisfactory results with buffered cadmium acetate as the absorbent, its use has been criticized[7] because cadmium sulphide is insoluble and light-sensitive. Sodium hydroxide, recommended by Bethge[6], readily absorbs sulphide and oxidation to sulphate does not occur if oxygen is excluded and the solution is strongly

alkaline. Ellison's technique[5] of running the absorbent solution into acid in an evacuated flask avoids loss of hydrogen sulphide and the reaction with iodine in the same flask is quantitative.

Experimental

Decomposition mixture. Prepare a mixture of 6 *M* hydrochloric acid (200 cm^3) and 20% (w/v) titanium(III) chloride (20 cm^3).

Nitrogen gas. Remove traces of oxygen with BASF Katalysator R 2-11 or with hot copper.

Fusion tubes. 80 mm × 10 mm, from Pyrex glass tubing.

Heating block. Constructed from aluminium, 10 cm high and 9 cm in diameter. The block contains 8 holes, 8 cm deep and 15 mm in diameter, for sample tubes and one central hole, 8 cm deep and 5 mm in diameter, for a thermocouple. The block, insulated with a layer of asbestos cord covered with aluminium foil, is heated on a hot-plate controlled by a simmerstat and is covered with a cap fabricated from layers of aluminium foil.

Distillation apparatus. The apparatus (Fig. 1) is similar to that described by Zimmermann[3], with a receiver as modified by Ellison[5]. Tube A (18 mm × 120 mm) is attached by a B14 ground glass joint, above which concentric tubes permit addition of solution from funnel B (50 cm^3) and carrier gas. Condenser C leads

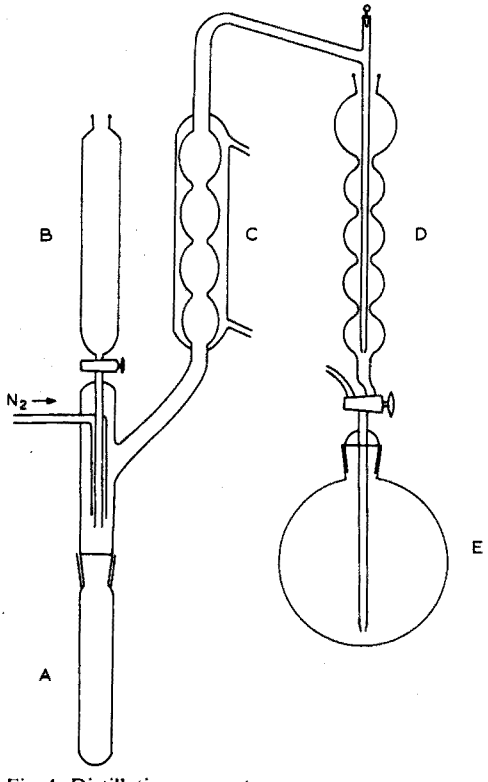

Fig. 1. Distillation apparatus.

to a tube (5 mm o.d., 2-mm jet) about 15 cm long which fits into the absorption column D, consisting of four bulbs *ca.* 20 mm in diameter surmounted by one bulb *ca.* 40 mm in diameter, and terminating in a two-way stopcock and B24 ground glass joint which is attached to a 250-cm^3 round-bottom flask (E).

Procedure. By long-handled weighing tube, accurately weigh the sample into a fusion tube. The sample (5–7 mg) should contain *ca.* 1 mg of sulphur; if it contains little or no organic material, add *ca.* 5 mg of indulin base. Carefully clean a piece of potassium, *ca.* 5 mm^3, in hexane containing a few drops of amyl alcohol. Pierce the potassium with a thin glass rod (about 20 mm long) and add the potassium (rod first) to the fusion tube. Seal the tube immediately in an oxygen–coal gas flame, drawing the tube out to form a neck 2–3 cm long. Place the sealed fusion tubes in the heating block, cover with the aluminium cap, and heat at $480 \pm 20°C$ for at least 20 h. When cold, the inside of the fusion tubes will be coated completely with a potassium mirror.

To open the cold, fusion tube, heat the tip in a gas flame and apply a bead of hot glass to a moistened file mark about 45 mm from the bottom. Invert the top of the tube into the bottom portion, transfer both into the distillation tube, and attach it with springs to the distillation apparatus. Add 10 *M* phosphoric acid (10 cm^3) to the 250-cm^3 flask, attach it to the absorption column, and evacuate by means of a water pump. Add 5 *M* sodium hydroxide (15 cm^3) to the absorption column and place it in position. Adjust the nitrogen flow-rate to give *ca.* 3 bubbles s^{-1} ascending the absorption column.

Add the decomposition mixture from the funnel until it covers the two sections of fusion tube completely. Heat the tube with a micro-burner as soon as any vigorous reaction subsides, and boil for *ca.* 15 min. Discontinue the gas flow after a further 2–3 min and allow the absorbent solution to flow into the flask, but do not allow air to enter. Wash down the tube and bubbler with distilled water (2×10 cm^3) and run the washings into the flask without allowing air to enter. Add potassium iodide (*ca.* 0.1 g) to the column and 0.00333 *M* potassium iodate (8.00 cm^3) followed by a few drops of 6 *M* hydrochloric acid, and run the resulting iodine solution into the flask. Rinse the absorption column (2×10 cm^3) into the flask and swirl for 1 min. Release any residual vacuum, detach the absorption column, and rinse it into the flask with water. Titrate the residual iodine with 0.02 *M* sodium thiosulphate to a pale straw colour, add fresh starch indicator, and complete the titration

$$[\%\ S = 32.06\ (8.00 - \text{volume of thiosulphate used})/\text{sample weight}]$$

If necessary, standardize the thiosulphate against the iodate solution in the usual way, and amend the factor.

Discussion

The method described gave good results for standard and research samples in the hands of several operators, as shown in Table I. Although the procedure is more tedious than both the oxygen flask technique and Zimmermann's modification of the Bürger method, it may be applied with confidence to a wide range of metal–organic complexes. The controlled fusion procedure ensures that reproducible conditions are used and eliminates one of the less satisfactory aspects of

the Zimmermann method. Although the fusion temperature appears to be fairly critical, satisfactory results are obtained when a continuous potassium mirror forms on the inside of the fusion tube.

TABLE I

ANALYSIS OF STANDARD SAMPLES

Sample	*Weight taken (mg)*	*Sulphur, (%)*			
		Theoretical	*Found*		
Sulphanilic acid	5–6	18.48	18.65	18.69	18.67
Dibenzyldisulphide	4–6	26.03	26.36	26.13	26.06
S-Benzylthiuronium chloride	4–6	15.82	15.98	15.84	15.68
Sulphamic acid	2–4	33.03	33.33	33.31	
Copper sulphate[a]	4–7	12.84	12.99	12.89	13.09
Sodium thiosulphate[a]	4–5	25.78	26.17	26.17	
Sulphonal	5–6	28.09	28.24	28.21	

[a] See text.

REFERENCES

1 H. Wagner, *Mikrochim. Acta*, (1957) 19.
2 K. Bürger, *Angew. Chem.*, 54 (1941) 479.
3 W. Zimmermann, *Mikrochemie*, 31 (1943) 15; 40 (1952) 162.
4 E. Debal and R. Lévy, *Mikrochim. Acta*, (1966) 202.
5 M. Ellison, *Analyst (London)*, 87 (1962) 389.
6 P. O. Bethge, *Anal. Chim. Acta*, 9 (1953) 129.
7 J. F. Alicino, A. I. Cohen and M. E. Everhard in I. M. Kolthoff and P. J. Elving (Eds.), *Treatise on Analytical Chemistry, Part II, Vol. 12*, Interscience, New York, 1965, p. 57.

Analytica Chimica Acta, 78 (1975) 238–239

BOOK REVIEWS

N. M. Atherton, *Electron Spin Resonance, (Ellis Horwood Series in Physical Chemistry)*, Edited by T. M. Sugden, Ellis Horwood, Chichester (distributed by Wiley, Chichester), 1973, x+438 pp., price £11.50.

This book, the first to be published by Ellis Horwood Ltd., and an excellent production in every respect, is a sound, scholarly piece of work that gives a comprehensive account of the fundamentals of the underlying theory and the interpretation of e.s.r. spectra. The treatment, unashamedly physical and mathematical, is intended for postgraduate chemists, following the author's beliefs that "most people are most easily able to cope with sophisticated mathematical techniques when they already have a feeling for the physics" (which is debatable), and "many undergraduate chemistry courses do not prepare people very well for reading the electron spin resonance literature" (which is, like it or not, entirely justified).

The author, wisely, did not attempt to produce a catalogue of all the applications of e.s.r. published up to the time of completion of his manuscript; what he has succeeded in doing is of much more permanent value. This book is not for the light in heart, nor for the frivolous modern button-basher; this book gives chemists concerned with the restricted range of systems amenable to investigation by e.s.r. spectroscopy, a chance of finding out precisely what it is all about and what is involved. There is then at least a chance that meaningful analytical results will be obtained: there is, after all, no other way.

D. M. W. Anderson

D. D. Perrin and Boyd Dempsey, *Buffers for pH and Metal Ion Control*, Chapman and Hall, London, 1974, viii+176 pp., price £3.50.

Although this excellent book is published in a series of Laboratory Manuals in Physical Chemistry and Biochemistry, it contains a lot of interesting information and useful data for analytical chemists. The authors cover all aspects of the theory, applications and limitations of buffers of every conceivable type—natural buffers, pseudo buffers, self buffers, volatile buffers, metal-ion buffers, anion buffers, buffers for electrophoresis, for complexometric titrations, for chromatography, for polarography, for non-aqueous systems, heavy water systems, etc. There are clear instructions for the purification of reagents and preparation of buffer formulations; the final 40 pages of this concise book are occupied by Appendices giving the composition-pH tables and other data for commonly used buffer systems. Good value this—Perrin and Dempsey have succeeded in putting a quart into a pint pot.

Donald J. Cook, *Elements of Chemistry*, Van Nostrand Reinhold, New York, 1974, xv+450 pp., price £4.80.

This book contains nothing of interest for analytical chemists. It was written to introduce American liberal-arts students to the study of science; by European standards it ranks as a secondary school text. Nevertheless it is quite an interesting book of its kind; there are novel ideas, a reasonable selection of topics, and thought-provoking questions—a compendium resulting from the author's 30 years experience of teaching "non-science majors". There is a Prologue and an Epilogue (both headed by quotations from The Prophet), and some ridiculously dramatic, even lurid, titles to Chapters, e.g. "The Magna Carta" (Periodic Table), "Shadows at Noon" (Atomic Structure), and "The Gathering Storm" (Society, Technology and Science). A few years ago this book would not have found a place in European tertiary education, but now that attempts are being made to "broaden education" by the introduction of popular science classes for Arts and Social Science students, perhaps this type of elementary text will yet find a market over here. Is educational progress really being made, however, when the author finds it desirable to give an Appendix entitled "Some Arithmetic", in which he gives examples of "The Proportion" and "The Percentage", explains indices, and shows in full how to solve for x in such a difficult example as $35/x=4/10$?

Analytica Chimica Acta, 78 (1975) 240

ANNOUNCEMENTS

Calendar of Events of Gesellschaft Deutscher Chemiker for 1975 and 1976

1975

8–10 September

6th European Food Symposium: "Engineering and Food Quality", Cambridge (U.K.), organized by the Food Working Party of the European Federation of Chemical Engineering, Food Engineering Panel, Food Group, Society of Chemical Industry and the Institution of Chemical Engineers. Secretariat of the Food Working Party: Gesellschaft Deutscher Chemiker.

8–13 September

General Assembly of Gesellschaft Deutscher Chemiker, Köln.

The following GDCh-Divisions will take part in the General Assembly:
Analytical Chemistry; Chemical education on the secondary level; Pigments and Dyes; Solid State Chemistry; History of Chemistry; Industrial Judicial Protection Division; Nuclear-, Radio- and Radiation Chemistry; Food and Forensic Chemistry; Macromolecular Chemistry; Medicinal Chemistry; Photochemistry; Detergent Chemistry.

24–27 September

GDCh-Division; Chemical education on the secondary level, Göttingen.

9–10 October

GDCh-Division "Applied Electrochemistry", Trier.

19–25 October

EUCHEM Conference "Organic Free Radicals", Schloss Elmau near Mittenwald.

The dates for the meetings of the GDCh-Divisions "Independent Chemists" and "Water Chemistry" are not yet known.

1976

4–9 April

EUCHEM Conference "Organic Liquids: Structures, Dynamics and Chemical Properties", Schloss Elmau near Mittenwald.

23 June

Chemistry Day of GDCh, on the occasion of the ACHEMA, taking place on 20–26 June, 1976, at Frankfurt/M.

12–16 July

VII International Symposium on Organic Sulphur Chemistry, Hamburg.

25–31 July

Tenth International Congress of Biochemistry, Hamburg.

6–10 September

XVIIth International Conference on Coordination Chemistry - I.C.C.C., Hamburg.

Details of the meetings listed above may be obtained from the Gesellschaft Deutscher Chemiker, D-6000 Frankfurt/M 90, Postfach 90 04 40, Federal Republic of Germany.

(Continued from page 4 of cover)

VOL. 78 NO. 1 ANALYTICA CHIMICA ACTA AUGUST 1975

CONTENTS

(Continued on inside page of cover)